THE UNIVERSITY
of EDINBURGH

Investigating the Influence of CDK11 in Developmental and Cancer Phenotypes

Roland Christopher Aldridge

Thesis submitted for the degree of Doctor of Philosophy

The University of Edinburgh
2018

This thesis has been composed solely by myself and has not been submitted, in whole or in part, in any previous application for a degree. The work presented is entirely my own.

Roland Christopher Aldridge, July 2017

Acknowledgements

I wish to thank my supervisor Professor Margaret Frame for her help, guidance and encouragement throughout this thesis project. In addition, my thanks also extend to Professor David Fitzpatrick, who supervised the work undertaken on the CdLS cohort. I received much advice and assistance from many people within the Edinburgh Cancer Centre and the Human Genetics Unit, I would like to thank them but particularly Simon Wilkinson, Hitesh Patel and Morad Ansari. Furthermore, I wish to thank Alex von Kriegsheim, who undertook the mass spectrometry at University College Dublin, and Adam Byron, who with Alex von Kreigsheim, provided advice regarding analysis of the mass spectrometry data. The work would not have been possible without the support given by the Wellcome Trust who provided funding. Most importantly, none of this would have been possible except for the support and tolerance of my wife, Kishan.

To Alexander and Eloise

Abstract

Cyclin-Dependent Kinase 11 (CDK11) is a serine/threonine kinase encoded at human locus 1p36.3 by two paralogous genes *CDK11A* and *CDK11B*. CDK11 has diverse roles in the regulation of transcription, splicing, apoptosis and mitosis. In proliferating cells, two predominant isoforms are expressed: CDK11p58 and CDK11p110. CDK11p110 is expressed throughout the cell cycle and regulates transcription and splicing. CDK11p58 is expressed at mitosis via IRES-dependent translation; it mediates mitotic progression and faithful chromosome segregation.

Loss of *Cdk11* in murine models causes early embryonic lethality, demonstrating that CDK11 is essential for normal development. Furthermore, dysregulated *CDK11* expression is associated with numerous late-onset disease states, indicating its importance in adult life. In cancer, abnormal expression of CDK11 correlates with poor prognosis in a variety of tumours. Moreover, deletion of the chromosomal region 1p36.3, containing the *CDK11* locus, is frequently observed in cancer and has recently been identified in a case of the development disorder, Cornelia de Lange Syndrome (CdLS). This thesis aimed to examine the functions of CDK11 and the impact of their dysregulation in cancer and developmental phenotypes.

The initial aim was to investigate the novel role for CDK11 in regulating autophagy in cancer cells; CDK11 depletion causes a marked autophagy phenotype, with accumulation of autophagy protein LC3. I demonstrate that this CDK11-mediated autophagy occurs as a consequence of mitotic dysregulation. Subsequently, I examined the role of autophagy following aberrant mitosis and chromosome missegregation. I show that autophagy is important in the maintenance of aneuploid karyotypes, with loss of autophagy impairing the survival of aneuploid cell populations.

I then investigated the effects of CDK11 in regulating cancer cell motility and determined that CDK11 depletion retards cancer cell migration. However, I

was unable to identify any failure in cell adhesion or cell polarization to explain this migration phenotype. Subsequently, I interrogated the CDK11 interactome to further characterize the mechanisms through which CDK11 regulates both novel and established functions. This work indicated the involvement of the distinct CDK11 isoforms in pathways that have not previously been reported. This included the interaction of CDK11p110 with ribosomal and spliceosomal proteins during mitosis and the interaction of CDK11p58 with spliceosomal and proteosomal constituents also during mitosis. These findings may provide the foundation for further study.

Finally I describe work undertaken to sequence the *CDK11* locus in a cohort of CdLS patients, with no known causative genetic mutation, to investigate *CDK11A*/*CDK11B* as candidate disease-associated genes. Although no causative mutation in *CDK11A* or *CDK11B* was identifying, sequencing of this region indicated NCBI and UCSC genome assemblies of this locus were inaccurate due to the genomic duplication. This has been confirmed by others and corrected in the most recent genome assemblies.

Lay Abstract

Cyclin Dependent Kinase 11 (CDK11) is a cell protein that performs many essential functions; these include regulating cell division and regulating processes that generate proteins from their DNA code. CDK11 is required both during embryonic development and for health in later life. Mice that lose CDK11 are predisposed to developing tumours and certain human cancers also appear to lose CDK11. Furthermore, abnormal levels of CDK11 are linked to poor outcomes in various forms of cancer, while several recent studies have identified CDK11 as a potential target for cancer treatment. Therefore understanding how CDK11 functions in both cancer and development is important.

This work set out to examine different effects that are observed in cancer cells, when CDK11 is depleted. Initially I examined the effects of CDK11 depletion on a process called autophagy. Autophagy is a 'self-eating' process whereby a cell can engulf its unwanted or harmful components and break these down to provide an energy source; this enables it to survive in stressful conditions. Defective autophagy may contribute to cancer development. However the role of autophagy in cancer cells themselves is less clear. This appears to be due to the multiple different mechanisms by which autophagy is activated and regulated in these cells; consequently autophagy may have either positive or negative effects on cancer cells depending on the signal that activates it and the components it engulfs. Autophagy has also been identified as a potential target in the treatment of cancer but due to the different effects of autophagy, it is important to understand more about the pathways that regulate it in each circumstance.

Depletion of CDK11 causes the accumulation of autophagy proteins in cancer cells. In this work, I have demonstrated that the changes in autophagy observed after CDK11 depletion occur due to abnormal cell division. This abnormal cell division leads to failure of cells to evenly divide their chromosomes between their 'daughter' cells resulting in an abnormal number of chromosomes within the divided cells. This abnormal number of

chromosomes is termed aneuploidy and is a common finding in cancer. Aneuploidy itself can harm cells and my work indicates that autophagy can aid cells to survive the damaging effects of aneuploidy.

I have also demonstrated that CDK11 depletion affects the ability of cancer cells to migrate; migration is fundamental to the ability of cancer to spread. Partial loss of CDK11 impaired the movement of breast cancer cells. In order to better understand how CDK11 regulates this cell migration and its other functions, I examined the proteins that interact with CDK11. This work identified many proteins known to interact with CDK11 but also many proteins with which CDK11 was not known to interact. These novel CDK11 interacting proteins indicate new mechanism through which CDK11 may perform its functions. Further work is required to confirm these interactions and to determine their significance.

Abbreviations

aCGH	Array Comparative Genomic Hybridisation
ATG5	Autophagy-related Protein 5
ATG7	Autophagy-related Protein 7
APC/C	Anaphase Promoting Complex/Cyclosome
β-1,4-GT 1	Beta-1,4-galactosyltransferase 1
BSA	Bovine Serum Albumin
bp	Base Pairs
BrdU	Bromodeoxyuridine
cDNA	Single Stranded Complimentary Deoxyribonucleic Acid
CdLS	Cornelia de Lange Syndrome
CDK	Cyclin Dependent Kinase
CK2	Casein Kinase 2
CSK	C-terminal Src Kinase
DAPI	6-diamidino-2-phenylindole dihydrochloride
DMSO	Dimethyl Sulphoxide
DMEM	Dulbecco Modified Eagle Medium
DNA	Deoxyribonucleic Acid
dNTP	Deoxynucleotide Triphosphate
EDTA	Ethylenediaminetetraacetic Acid
EIF3F	Eukaryotic Initiation Factor 3 Subunit F
FAK	Focal Adhesion Kinase
FCS	Foetal Calf Serum
FISH	Fluorescence in situ hybridisation
GST	Glutathione S-transferase
GFP	Green fluorescent protein
HDAC	Histone Deacetylase

HIV	Human Immunodeficiency Virus
HSP70	Heat Shock Protein 70
HSP90	Heat Shock Protein 90
IPTG	Isopropyl β-D-thiogalactopyranoside
Ig	Immunoglobulin
IRES	Internal Ribosomal Entry Site
Kb	Kilobases
KD	Kilodalton
mg	Milligrams
ml	Millilitres
mM	Millimolar
MMP	Metalloproteinase
MTOR	Mammalian Target of Rapamycin protein kinase
NCBI	National Centre for Biotechnology Information
NGS	Next Generation Sequencing
NIPBL	Nipped-B-like Protein
NP40	Nonidet P-40 Detergent
PAK1	p21 Activated Kinase 1
PBS	Phosphate Buffered Saline
PBS-T	Phosphate Buffered Saline-Tween-20
PCR	Polymerase Chain Reaction
PFA	Paraformaldehyde
PLK1	Polo-Like Kinase 1
pTEFB	Positive Transcription Elongation Factor B
RIPA	Radioimmunoprecipitation Assay Buffer
RNA	Ribonucleic Acid
RNA Pol II	RNA Polymerase II
ROS	Reactive Oxygen Species

SAC	Spindle Assembly Checkpoint
SDS PAGE	Sodium Dodecyl Sulfate-Polyacrylamide Gel Electrophoresis
SH2 Domain	Src Homology 2 Domain
SH3 Domain	Src Homology 3 Domain
SMC Proteins	Structural Maintenance of Chromosomes Proteins
snRNP	Small Nuclear Ribonucleoproteins
SNP	Single Nucleotide Polymorphisms
SRSF1-10	SR (Serine/Arginine) Splicing Factors 1-10
TFIIA-H	Transcription Factor II A-H
TBE	Tris/Borate/EDTA
TBS	Tris Buffered Saline
TBST	Tris Buffered Saline-Tween-20
UCSC	University of California, Santa Cruz
µl	Microlitres
µM	Micromolar
µg	Micrograms
UTR	Untranslated Region
WES	Whole Exome Sequencing
WGS	Whole Genome Sequencing
WT	Wild Type

Table of Contents

CHAPTER 1

CDK11

1.1 The Human Kinome

The evolution of increasingly sophisticated regulatory mechanisms to govern the panoply of cellular processes permits increased cellular and organismal complexity. Phosphorylation is a ubiquitous regulatory mechanism that has major roles in virtually every aspect of cellular physiology [1]. The phosphorylation of substrates by protein kinases regulates diverse processes including growth, differentiation, metabolism, cell cycle progression and cell death. Protein kinases share a conserved catalytic domain, which catalyses the transfer of the gamma-phosphate of ATP to a serine, threonine, or tyrosine residue in the protein substrate [1]. On account of the integral role phosphorylation plays, it is unsurprising that the protein kinase super family is one of the largest of eukaryotic proteins. The human kinome comprises 518 protein kinases that represent 1.7% of human genes [2]. Eukaryotic protein kinases may be assigned to 1 of 7 major groups on the basis of characteristic sequence identification features; the CMGC (CDK, MAPK, GSK, CDK-like related) group comprises 61 members [3]. The Cyclin-Dependent Kinase (CDK) family is classified within this group and comprises 20 human CDKs [4].

1.2 Cyclin-Dependent Kinases (CDKs)

CDKs are the catalytic subunits of heterodimeric serine/threonine protein kinases, generated by the association of each CDK with its regulatory cyclin partner [4]. CDKs are characterised by the presence of a kinase domain, the activity of which is modulated by cyclin binding. This conserved catalytic core comprises an ATP-binding pocket, a cyclin-binding domain and an activating T-loop motif [5]. This family of proteins participates in many cellular signaling pathways. The original member of the CDK family, designated CDK1, was identified through genetic screens of yeast species

examining for mutants unable to complete the cell division cycle [6]. CDKs play a major role in the regulation of the cell cycle but other important functions such as the regulation of gene expression, through mediation of co-transcriptional events, are well established [7]. The unifying CDK nomenclature was adopted in 1991 but prior to this members were often designated on the basis of the amino acid sequence within the conserved cyclin-binding domain of the kinase [4]. On account of this, CDK11 was previously termed PITSLRE. To be formally designated a CDK requires the identification of the activating cyclin subunit. The cyclins represent a diverse group of proteins characterised by a domain, termed the cyclin box, that mediates binding to the CDK [5]. Expression of cyclins often follows an oscillatory pattern through the cell cycle, to enable temporal CDK regulation. However, this is less frequently observed among the more recently identified members of the cyclin family, with their expression frequently regulated through signaling pathways activated by external stimuli [5]. The activity of these CDK/cyclin complexes is not only regulated by their co-expression but also by numerous CDK inhibitors (CKIs) [8]. CKIs are subdivided into two classes based on structure and CDK specificity; these constitute the INK4 family members, such as p16INK4A (CDKN2A) and p19INK4D (CDKN2D), and the CIP/KIP family, comprising p21CIP1 (CDKN1A), p27KIP1 (CDKN1B) and p57KIP2 (CDKN1C) [8]. The INK4 family members primarily target CDK4 and CDK6 while the CIP/KIP family members are more promiscuous and restrict the activities of a greater range of cyclin-dependent complexes [8]. In addition, there is evidence to suggest individual CDK, CKI or cyclin subunits may perform certain functions in isolation [5].

1.3 Cyclin-Dependent Kinase 11 (CDK11)

CDK11, a member of the CDK family, is a serine/threonine kinase encoded at human locus 1p36.3. This locus on human Chromosome 1 encodes two duplicate and tandemly linked *CDK11* genes; these are *CDK11A* (*CDC2L2*) and *CDK11B* (*CDC2L1*) [9]. Both genes are transcribed and both are ubiquitously expressed in all human cells, although their level of expression is reported to differ in certain tissues [10, 11]. The genes together span approximately 100kb on Chromosome 1, with each individual gene

comprising 20 exons and spanning approximately 30kb. In conjunction with the *CDK11* genes, the metalloprotease (MMP) genes, *MMP21* and *MMP22* are also duplicated [11]. This duplication is present in humans but absent in chimpanzees and other vertebrates, indicating this event has occurred late in evolution [12].

1.3.1 CDK11A and CDK11B Homology

The two *CDK11* genes encode proteins with a high degree of similarity and only a total of 15 amino acids of the 773-786 residues in the CDK11 protein are unique to either CDK11A or CDK11B [9]. The majority of these 15 amino acid alterations are located within the amino-terminal domain, with only four located in the protein kinase catalytic and carboxy-terminal domains [9]. This high degree of homology between the two gene products has made the study of each protein challenging; indeed, in all published work interrogating protein function, there is no differentiation of CDK11A and CDK11B, with the proteins considered to have indistinguishable functions. Although this has not been definitely established, given the homology and co-expression, a degree of functional redundancy is highly probable. It is reported that functional redundancy between duplicate genes can be actively maintained through evolution and speciation, over a period of more than 80 million years [13]. The duplication at the *CDK11* locus is a comparatively recent event in evolution and therefore some redundancy is expected. The *CDK11* sequence is highly conserved across vertebrates, with *CDK11B* most closely resembling these homologues [9]. This may indicate that *CDK11A* is either subject to positive selection or is potentially degenerating into a pseudogene.

1.3.2 CDK11 Gene Promoters

Although the expression of both genes is ubiquitous within human tissues, characterisation of the gene promoters reveals not only similarities but differences. The promoter regions of both genes are found to be GC-rich but lack both TATA and CAAT boxes [14, 15]. *CDK11A* and *CDK11B* contain ETS-1 binding motifs; ETS-1 is a member of the ETS (E26 Transforming-Specific) family of transcription factors. Expression of *CDK11B* is mediated

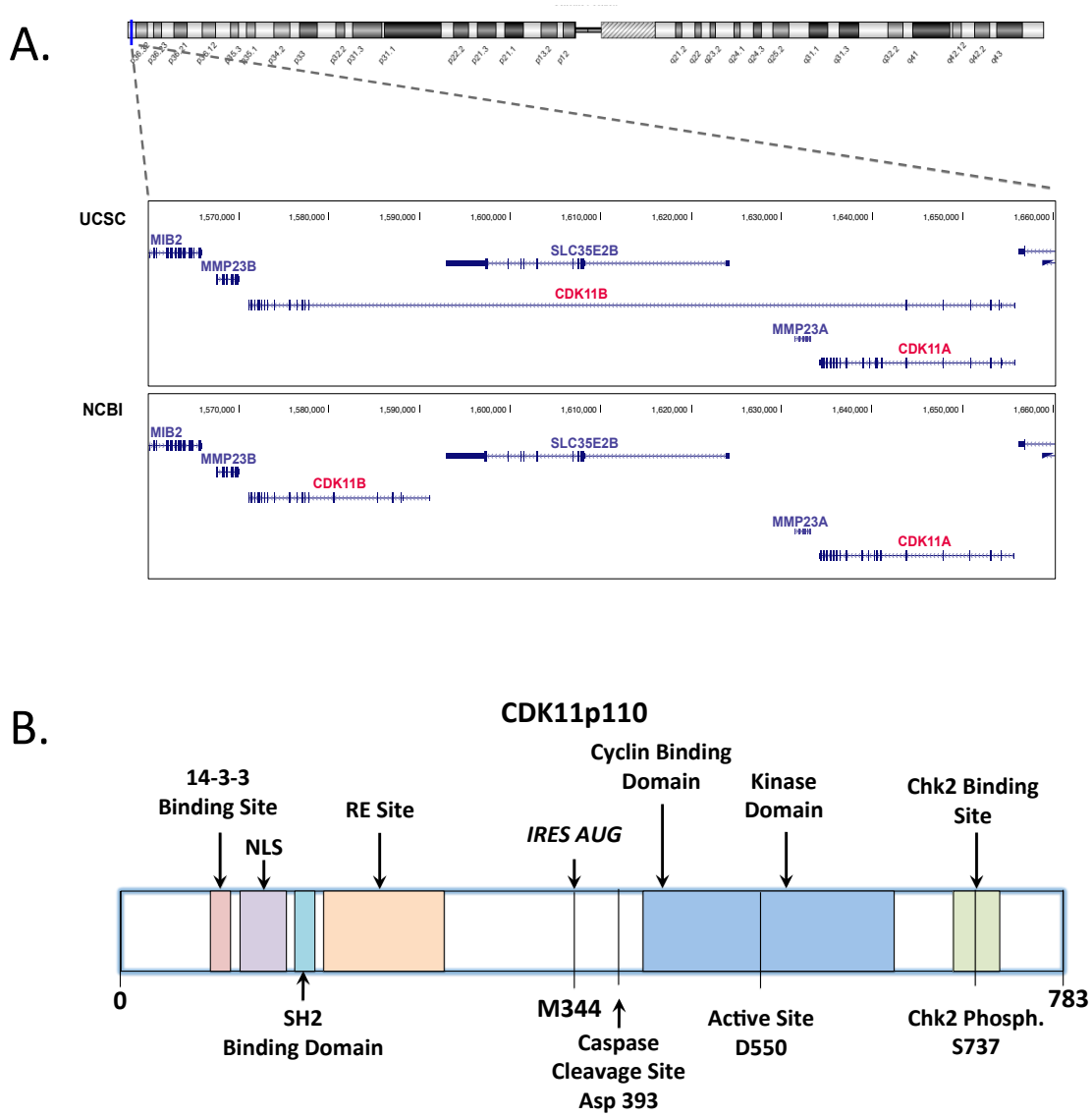

Fig 1.1 *CDK11* 1p36.33 Locus and CDK11 Protein. ***1.1A*** shows the NCBI and UCSC genome assemblies for the *CDK11* locus at the outset of the project. Due to gene duplication, there was noted to be sequence ambiguity within the region. This occurred due the absence of Exon 4 and Exon 5 in the *CDK11B* reference sequence. This was considered to be an alignment error but as a result UCSC overlapped *CDK11A* and *CDK11B*, suggesting that the Exons 4 and 5 were shared. In contrast, *CDK11B* in the NCBI assembly lacked Exon 4 and 5. This has now been corrected in most recent assemblies. ***1.1B*** is a diagrammatic representation of the CDK11p110 protein, with key protein domains included. CDK11p58 shares the C Terminus from the *IRES AUG* (M344).

by the binding of both ETS-1 and SKN-1, with both transcription factors obligate for basal transcription of the gene [15]. In contrast, the *CDK11A* promoter lacks the SKN-1 binding motif but contains CREB and TCF11/NRF2 sites. CREB and ETS-1 are required to sustain transcriptional activity of the *CDK11A* gene [16]. This demonstrates discrete mechanisms of transcriptional regulation, which may enable differential transcription of the genes.

1.3.3 CDK11 Isoforms

Transcription of the *CDK11* genes was initially reported to generate more than 20 distinct mRNA isoforms and this was assumed secondary to extensive alternate splicing [10, 17]. It is now established that a number of these supposed transcript isoforms undergo non-sense mediated decay. In total, 8 alternate CDK11 transcripts are now described [18]. These transcripts encode two predominant cellular protein isoforms, termed CDK11p110 and CDK11p58 on account of their molecular weights. CDK11p58 was the first isoform to be described. It was identified through purification of β -1,4 Galactosyltransferase 1, with which it was found to associate [19] [20]. The CDK11p110 isoform was subsequently identified from alternate CDK11 transcripts. Originally, translation of the two isoforms was reported to occur from distinct transcripts but it is now established that this is not the case [21]. The CDK11p110 isoform is expressed constitutively throughout the cell cycle, without significant fluctuation in protein levels. In contrast, the CDK11p58 protein is expressed predominantly, if not exclusively, at mitosis [21]. This observation led to the identification of an internal ribosomal entry site (IRES) within the CDK11 transcript [21]. This IRES sequence mediates the expression of the shorter p58 isoform at mitosis.

CDK11p110 regulates both transcription and splicing [22, 23]. In contrast, consistent with its mitotic expression, CDK11p58 regulates mitotic events [24, 25]. A third CDK11 isoform is also described, with CDK11p46 generated through cleavage of the longer isoforms on induction of apoptosis [26]. This chapter aims to provide an appraisal of published literature on CDK11, its roles in cellular processes and its contribution to health and disease. This will

provide a basis for the discussion of functions and interactions of CDK11 in later chapters.

1.4 CDK11, Transcription and Splicing

The regulation of gene expression is fundamental to the normal growth, development and survival of all organisms. Within eukaryotes, gene expression is highly complex and tightly controlled [27]. The transcription of DNA template to RNA, and associated RNA processing, represents the predominant stage regulating gene expression [28]. The major steps in mRNA biogenesis constitute transcription, 5' capping, splicing, and cleavage/polyadenylation [28]. Although all can be reconstituted independently *in vitro*, *in vivo* they occur synchronously and are termed co-transcriptional [29]. The regulation of these processes is mediated by analogous events [29, 30].

1.4.1 Transcription

Transcription is established to occur in three principal phases, termed initiation, elongation and termination [28]. At initiation, binding of activators to enhancer DNA elements, located upstream or downstream of the target gene promoter, causes sequential recruitment of general transcription factors and RNA polymerase II (RNA Pol II) to the promoter elements [31]. Proteins such as cohesin are reported to facilitate chromatin looping and thereby contact between enhancers and promoters [32]. The assembly of the pre-initiation complex (PIC), comprising general transcription factors TFIIA, TFIIB, TFIID, TFIIE, TFIIF, and TFIIH in association with the Mediator complex and RNA polymerase, is necessary for initiation to occur [33]. Within eukaryotes, all mRNA is synthesised by RNA Pol II. RNA Pol II is distinguished from other polymerases by the presence of the C-terminal domain (CTD) of its largest polypeptide constituent RPB1 [34]. The CTD comprises tandem heptad repeats that undergo extensive post-translational modifications, most notably phosphorylation, which regulate co-transcriptional events. On recruitment to the pre-initiation complex, serine 2 and serine 5 of the RNA Pol II CTD are unphosphorylated [31]. The canonical model of CTD phosphorylation

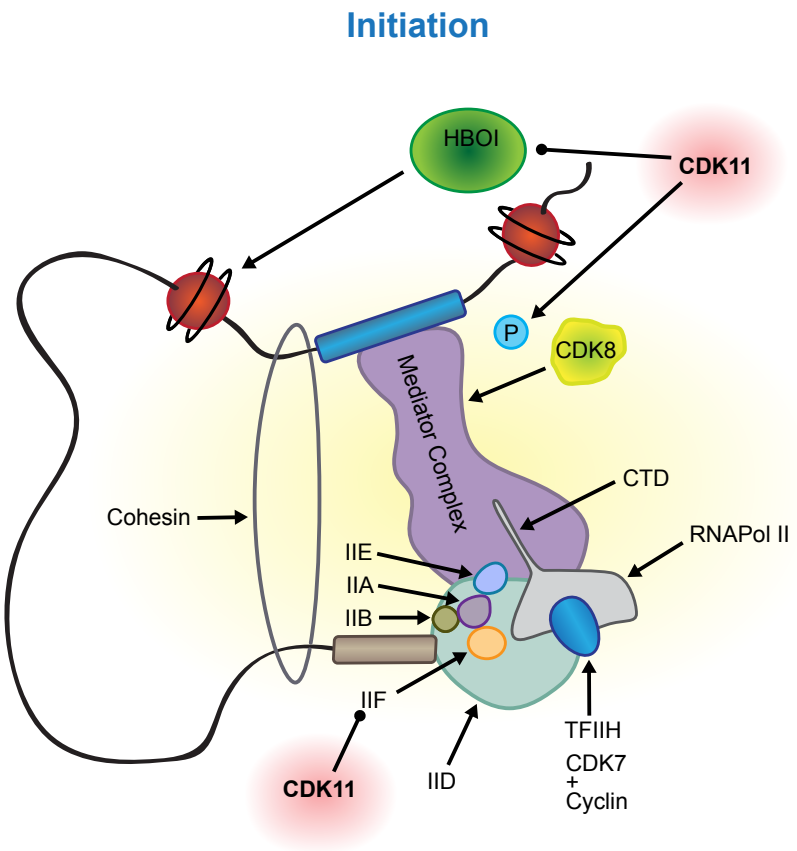

Fig 1.2 CDK11 at Transcription Initiation. The figure illustrates important proteins and complexes involved in transcription initiation. CDK11 interacts with TFIIF, a component of the Pre-Initiation Complex. Furthermore, in yeast, CDK11 regulates the interaction of CDK8 with the Mediator complex; this has not been demonstrated in metazoan species.

describes the phosphorylation of serine 5 by CDK7 near the transcription start site. On elongation, serine 2 is phosphorylated by Positive Transcription Elongation Factor b (P-TEFb), comprising CDK9 and one of its cyclin partners [31].

Previously, transcription was thought to be regulated predominantly by the recruitment of RNA polymerase to the promoter at transcription initiation [28]. It is now evident, however, that transcription elongation also plays a significant role in the regulation of gene expression. Transcriptional elongation by RNA Pol II is categorised into three distinct stages; these are promoter escape, promoter-proximal pausing and productive elongation. During promoter escape, RNA Pol II undergoes maturation and breaks contact with the promoter element [28]. Promoter-proximal pausing, or transcriptional stalling, occurs when the immature transcriptional complex pauses, approximately 20 to 40 bases from the transcriptional start site. This pausing plays an important regulatory role *in vivo*, with escape enabling productive elongation [28]. Numerous heat shock inducible genes and genes that modulate response to cellular stress are regulated through this mechanism, enabling more rapid induction of transcription [35]. Numerous elements mediate proximal pausing including DRB Sensitivity-Inducing Factor (DSIF) and Negative Elongation Factor (NELF) [28]. Proteins, including P-TEFb, TFIIS, and Elongator, allow transition to productive elongation. Other proteins have been implicated in this process, with the cohesin complex found to selectively bind and regulate genes with paused RNA polymerase in Drosophila [36]. Following progression to productive elongation, proteins such as Elongin and TFIIF are described to mediate elongation rate. In addition, epigenomic modifications to the chromatin structure such as histone acetylation or methylation are able to influence transcription rate [28]. The rate of transcription is noted to affect co-transcriptional processes including splicing, with it reported to determine alternative splicing decisions [37].

1.4.2 Splicing

RNA splicing is one of three major processing events in the production of mature messenger RNA, the two other processes being RNA capping and polyadenylation [29]. The removal of introns and congression of exons through the splicing of pre-mRNA is integral to eukaryotic gene expression. The splicing process is catalysed primarily by the spliceosome, which constitutes a large multimodular, highly dynamic complex [38]. It comprises five small nuclear ribonucleoproteins (snRNPs). Each snRNP is composed of a small nuclear RNA (U1, U2, U4, U5 or U6) in addition to a group of seven proteins termed the Sm ribonucleoproteins [38]. In addition to this snRNP, the spliceosome contains multiple non-snRNP protein components. Many RNA binding proteins mediate splicing regulation but the two predominant families of regulators are the SR proteins and heterogeneous nuclear ribonuleoproteins (hnRNPs) [39]. Classically, the SR proteins promote splicing, whilst the hnRNPs have the opposite effect [39]. The SR proteins are named on account of the RS protein domain, present within all family members, which comprises long repeats of serine and arginine residues [40]. This domain enables bindings with other members of the spliceosome complex. In addition, SR proteins contain an RNA recognition motif (RRM) domain, which facilitates binding to RNA [40].

The co-transcriptional regulation of transcription and RNA biogenesis is both dynamic and complex, with a large cohort of proteins required to mediate precise gene expression [29]. The modulation of proteins by phosphorylation is fundamental to this process and phosphorylation of the RNA Pol II CTD represents an influential and well-established mechanism of control [34]. Several CDKs and their respective cyclin partners are involved in the regulation of this intricate network [34].

1.4.3 CDK11 Interacts with Splicing Components

The involvement of CDK11p110 in splicing was first proposed on account of the RD (arginine and aspartate) and RE (arginine and glutamate) motifs within its N-terminal domain [41]. These motifs are important in the localisation of splicing components to nuclear speckles, also termed

interchromatin granules (ICGs), which contain numerous pre-mRNA splicing factors [42]. CDK11p110 co-localises with SR protein and splicing component SC35, also termed SR Splicing Factor 2 (SRSF2), at these ICGs [41]. In addition, RNA binding proteins RNPS1 and SS-A/Ro were identified as novel CDK11 binding partners using a yeast two-hybrid assay [41]. The interaction with RNPS1 is specific to the longer CDK11p110 isoform. Overexpression of RNPS1 causes the aggregation of nuclear speckles into fewer but larger clusters, with altered localisation of both CDK11p110 and SC35. Similar results are obtained on subjecting cells to transcriptional inhibition with H8 inhibitor [41]. The localisation of CDK11p110 with splicing components and its altered localisation on transcriptional inhibition were considered the first evidence of the involvement of CDK11 in transcription or splicing [41].

1.4.4 CDK11, Cyclin L and RNA Polymerase II

1.4.4.1 CDK11p110 and Transcriptional Elongation

CDK11p110 co-purifies with transcription elongation complexes, using fast protein liquid chromatography [23]. CDK11p110 co-elutes with both hypophosphorylated and hyperphosphorylated forms of RNA Pol II; proteins SPT16 and SSRP1, members of the FAcilitates Chromatin Transcription (FACT) heterodimeric complex, along with RAP30 and RAP74, constituents of TFIIF, also co-purify [23]. In addition, a yeast two-hybrid assay and subsequent co-immunoprecipitation assay identified transcription elongation factor ELL2 and TFIIS as novel binding partners of CDK11p110 [23]. Transcription elongation complexes have been classified into three distinct classes, based on their roles [43]. The first class comprises those that inhibit RNA polymerase arrest and includes TFIIS. The second class prevents transient pausing of RNA Pol II and comprises proteins such as ELL, ELL2 and TFIIF. The third class promotes transcription elongation through modification of chromatin structure and includes the FACT complex. CDK11p110 therefore interacts with members of all three classes of elongation complexes [23]. Consistent with these observations, inhibition of CDK11p110 kinase activity by addition of CDK11 monoclonal antibody, reduces transcription from both TATA and GC promoters in a standard *in*

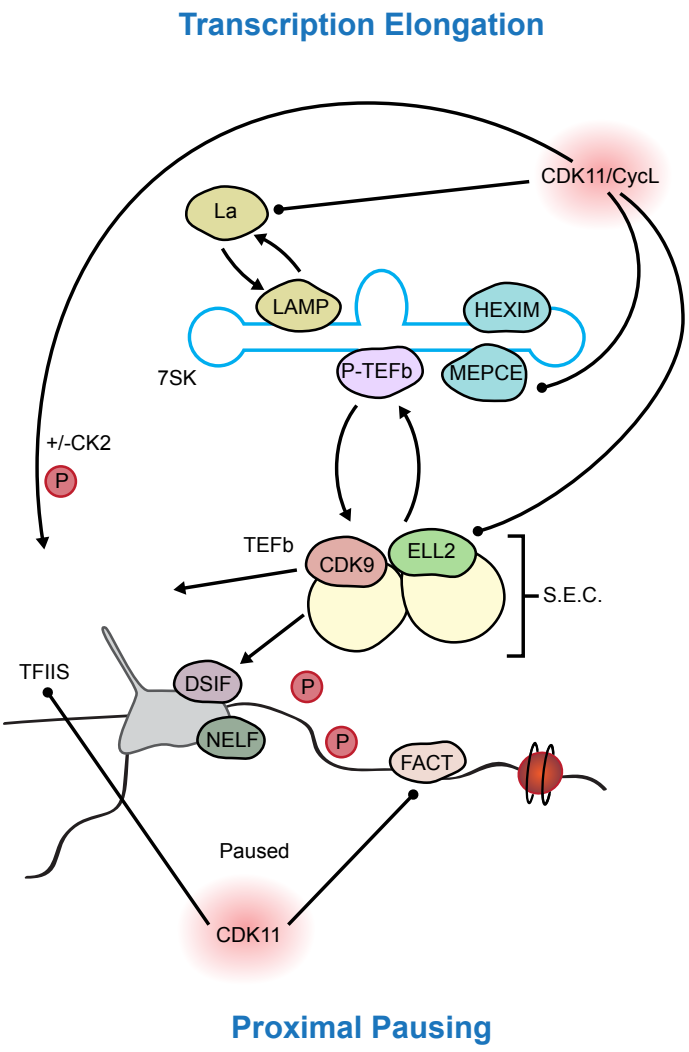

Fig 1.3 CDK11 at Trancription Elongation. The figure illustrates important proteins and complexes involved in transcription elongation. CDK11 interacts with FACT and TFIIS. In addition, in combination with CK2, CDK11 may have a role in phosphorylation of the RNA Pol II CTD. Furthermore CDK11 interacts with protein constituents of the Super Elongation Complex (SEC) and 7SK snRNA; these regulate CTD phosphorylation and transcription elongation.

vitro transcription assays. Re-addition of purified CDK11p110 to the reaction restores transcriptional activity [23]. This demonstrates the association of CDK11 with transcription elongation complexes and its ability to regulate transcription.

1.4.4.2 CDK11 and RNA Pol II CTD

Dickson et al. (2002) subsequently reported a possible role for CDK11 in the phosphorylation of RNA Pol II CTD [44]. The authors found that Cyclin L co-immunoprecipitate was able to phosphorylate both the RNA Pol II CTD and splicing factor SC35. CDK11p110 was assumed to be responsible on account of its interaction with Cyclin L and this was supported by the observation that addition of CDK inhibitor p21 ablated both phosphorylation events. The study subsequently interrogated the consequence of Cyclin L inhibition, utilising anti-Cyclin L antibody, on *in vitro* splicing. This found inhibition of splicing with the accumulation of intermediate products [44]. Again, CDK11p110 was considered the partner catalytic domain responsible for splicing regulation in this assay.

Although subsequent work has confirmed the importance of CDK11 to splicing, Trembley et al. (2003) demonstrated that CDK11p110 was not responsible for RNA Pol II CTD phosphorylation [45]. Instead, Casein Kinase-2 (CK2) was responsible for the CTD phosphorylation, with CK2 found to co-immunoprecipitate with both Cyclin L and CDK11. In addition, CK2 is found to phosphorylate CDK11p110, with the RE domain of CDK11 required for this phosphorylation [45].

The identification of CK2 as the kinase responsible for both RNA Pol II and CDK11p110 phosphorylation was corroborated in a subsequent paper by Sachs et al. (2003) [46]. This work confirmed that purified CDK11p110 was unable to phosphorylate the CTD in the absence of CK2. In addition, it reported phosphorylation of CDK11p110 by CK2 at serine 227. Serine 227 lies within the SH2 binding domain contained in the N-terminus of CDK11p110. The significance of this phosphorylation was not explored but the original paper that identified the SH2 binding domain within CDK11 reported enhanced SH2 binding with adjacent phosphorylation [47]. Although at that

time the precise site of phosphorylation was not identified, CK2 was again implicated in CDK11p110 phosphorylation [47].

1.4.4.3 CDK11 and 9G8

CDK11p110 interacts with splicing factor and SR protein 9G8 (SRSF7) [22]. 9G8 is a general splicing factor that is involved not only in splicing but also in mediating the nucleocytoplasmic export of mRNA. The interaction with CDK11p110 is dependent on the RE motif within the p110 isoform, but not the poly(E) domain or the CK2 phosphorylation site [22]. CDK11p110 phosphorylates 9G8 both *in vitro* and *in vivo*, with the phosphorylation of 9G8 required for both its splicing and export functions [48]. 9G8 contains a long RS domain similar to that found both in SC35 and Cyclin L; the RS domain has been implicated in determining the specificity of protein-protein interactions and these similarities may explain their common interactors [44]. Hu et al. (2003) directly interrogated the role of both CDK11p110 and 9G8 in splicing, with the use of standard *in vitro* splicing assays. As expected, 9G8 promoted *in vitro* splicing activity, while immunodepletion of CDK11p110 caused abrogation of splicing in this assay; this was reversed by the re-addition of immunoprecipitated CDK11p110 complexes [22].

1.4.4.4 CDK11 and HIV

This CDK11-9G8 interaction has also been reported to regulate the 3′ end processing of HIV-1 mRNA [49]. 9G8 is observed to bind upstream of the HIV-1 poly(A) site and promotes its cleavage in a sequence-specific manner [49]. Eukaryotic initiation factor 3f (eIF3f) is a component of the multi-subunit eIF3 translation factor that facilitates the formation of the ribosomal 43S preinitiation complex and has previously been identified as a substrate of the apoptosis-associated CDK11p46 isoform [50]. Interaction of eIF3f and CDK11p110 with 9G8 disrupts its mediation of 3′ end processing of the HIV-1 pre-mRNA, with the resulting degradation of unprocessed RNA in the nucleus [49]. Consistent with this, overexpression of either eIF3f or CDK11 reduced susceptibility to VSV-HIV viral transduction [49]. This work indicates a role for CDK11 not only in regulating HIV-1 infectivity but also in the 3′ end processing of pre-mRNA.

Yu et al. (2008) also suggested a role for CDK11 in HIV-1 replication [51]. HIV-1 infection targets both T-cells and macrophages, with T-cell activation necessary to enable high viral replication. Cyclin T1, a constituent of P-TEFb, is directly targeted by the viral Tat protein to activate proviral transcription. Yu et al. (2008) examined genes dependent on Cyclin T1 for expression following T-cell activation, to identify putative HIV-1 cofactors. CDK11 was identified in this assay and CDK11 knockdown was observed to inhibit HIV-1 luciferase reporter expression. This is paradoxical to the reduction in HIV-1 expression observed on CDK11 overexpression [49]. The reason for this remains unclear but may result from the different assays employed. In addition, Yu et al. (2008) reported reduction in CDK9 and HEXIM1 expression on CDK11 knockdown but with no effect on CDK8 [51]. Again, this indicates a role for CDK11 in the regulation of proteins integral to transcriptional elongation.

1.4.5 CDK11 and Cyclin L Regulatory Partners

Cyclin L1, previously termed Ania-6, was identified in murine cells as the first regulatory cyclin to associate with CDK11 [52]. Cyclin L1 co-localises with CDK11 to nuclear speckles and is able to co-immunoprecipitate both hyperphosphorylated RNA Pol II and CDK11p110, consistent with the p110 isoforms roles in transcription and splicing [52]. Two studies, published simultaneously, identified a distinct novel RNA Pol II-associated cyclin, which in similarity to Cyclin L1, contained an RS repeat domain [53, 54]. This novel cyclin, designated as Cyclin L2, was also observed to associate with CDK11p110, SC35, 9G8, and RNA Pol II [53, 54]. Cyclin L2 co-localises with splicing factors to nuclear speckles, indicating a role in splicing regulation. Corroborating this, recombinant Cyclin L2 stimulates *in vitro* mRNA splicing [54].

It is established that both Cyclin L1 and Cyclin L2 engage CDK11 as alternate cyclin regulatory partners. Both Cyclin L members contain similar domains, including both the cyclin box and RS domain. In addition, both *Cyclin L* genes generate numerous alternative transcripts that give rise to two predominant protein isoforms from each gene [55]. These constitute a long and short isoform, with both isoforms comprising equivalent N-terminal

sequences containing the cyclin box domain. The sequences diverge at their C-termini, with the longer or alpha isoforms containing the RS dipeptide repeat sequence. The significance of the similarity in protein biology between Cyclin L and CDK11 remains uncertain.

1.4.5.1 CDK11 and Cyclin L1 and L2 Interaction

Both *Cyclin L* genes are expressed ubiquitously, although their relative abundance differs in discrete tissues [54]. All the major Cyclin L isoforms bind all major CDK11 isoforms, including CDK11p46, although the observed binding affinity varies between isoforms. In addition, all major Cyclin L1 and L2 isoforms are reported to enhance splicing activity as assessed by both *in vivo* and *in vitro* splicing assays [55]. Loyer et al. (2008) also demonstrated that wild-type CDK11p110 enhanced splicing, whilst the kinase-dead CDK11p110 and CDK11p110, lacking the RE domain, inhibit splicing activity. Furthermore, constitutive expression of both CDK11p58 and CDK11p46 inhibited splicing in this assay [55].

Although the similarities between Cyclin L1 and Cyclin L2 are noted, it has been demonstrated that their cellular distribution and mobility differ [53]. Under physiological conditions both localise to nuclear speckles, however, GFP.Cyclin L1 is found to be immobile compared to GFP.Cyclin L2, using photo-bleaching techniques [56]. The relevance of the difference in the mobility remains unclear but Herrman et al. (2007) proposed it may indicate that Cyclin L1 is not directly involved in transcriptional regulation [56].

1.4.5.2 Cyclin L2 and DYRK1A

De Graff et al. (2004) identified interaction of Cyclin L2 with nuclear protein kinase DYRK1A [53]. *DYRK1A* is located on chromosome 21 in a locus termed the 'Down syndrome-critical region'. Overexpression of the protein in transgenic mice causes learning deficits and altered neurodevelopment [57]. The contribution of DYRK1A to human development has been confirmed with the recent description of *DYRK1A* gene mutations causing a syndromic intellectual disability with severe microcephaly and epilepsy [58]. DYRK1A was found to phosphorylate Cyclin L2, suggesting a putative role in splicing regulation.

1.4.5.3 Cyclin L Proteins and Alternate Splicing

In addition to the global effects on splicing activity mediated by Cyclin L proteins, enforced Cyclin L expression alone or in combination with CDK11p110 strongly mediates alternative splicing *in vivo* [55]. This was demonstrated using an E1A minigene reporter construct, with Cyclin L proteins influencing alternate splicing selection and the protein synthesised [55]. Published studies therefore demonstrate the influential role of CDK11 and its Cyclin L regulatory partners in both splicing activity and alternative splicing [55] [54].

The novel CDK11 binding protein RNA binding motif protein 15B (RBM15B) has been shown to regulate the CDK11p110-Cyclin L2 complex in its mediation of splicing [59]. RBM15B is an established cofactor of the nuclear export receptor NXF1 and is engaged in mRNA export but Loyer et al. (2011) established RBM15B is also a functional competitor of specific SR proteins [59]. This antagonism of SR proteins by RBM15B inhibits the formation of functional spliceosomal complexes and suppresses the stimulatory effect of the CDK11p110-Cyclin L2 complex on splicing both *in vitro* and *in vivo*. The authors confirmed that this was not due to the protein's influence on mRNA export, with this therefore providing insight into the mechanisms regulating CDK11 splicing activity [59].

1.4.6 CDK11 and Chk2

The recent identification of Checkpoint Kinase 2 (Chk2) as a novel CDK11p110 interacting protein further characterizes the mechanisms regulating CDK11 and splicing [60, 61]. Chk2 phosphorylates CDK11p110 at serine 737, with phosphorylation of this residue indispensible for homodimerisation of CDK11p110. While homodimerisation of CDK11p58 had been previously described [57], this represented the first report of it occurring with CDK11p110 [60, 61]. Phosphorylation of CDK11p110 at serine 737 had no influence on kinase activity but ablation of phosphorylation at this site, via introduction of a phospho-refractory mutant, abrogated CDK11p110 mediated splicing. This regulation of pre-mRNA splicing by

Chk2 was found to be constitutive and not associated with the DNA damage response, which regulates other Chk2 functions [60, 61].

1.4.7 CDK11 and Mediator Complex Assembly

This chapter provides a synopsis of the evidence establishing a role for CDK11 in splicing and transcription. Whilst these functions are evident, the mechanisms by which CDK11 regulates these processes require characterisation. As discussed, CDK11 interacts with RNA Pol II and proteins involved in transcriptional elongation, with its influence in transcription demonstrated by *in vitro* transcription assays [23]. A recent study identified a putative mechanism through which CDK11-cyclin L may mediate transcription [62]. This demonstrated that the fission yeast homologues of CDK11 and Cyclin L phosphorylate yeast mediator subunits, Med27 and Med4. This phosphorylation regulates the association of the CDK8 kinase module with the S-mediator complex [62]. Consistent with its role in regulating the association of a kinase-competent mediator complex, CDK11 depletion altered gene expression in a similar manner to CDK8 knockout [62]. Furthermore, CDK11 was observed in ChIP assays to distribute throughout the genome with bimodal enhancement at the 5′ and 3′ end of genes. Although the fission yeast CDK11 homologue differs substantially from metazoan CDK11p110, it does resemble the CDK11p58 isoform more closely. Drogat et al. (2012) therefore describe a novel mechanism through which CDK11 may regulate transcription [62]. However, no interaction with the mediator complex has been reported with human CDK11.

The report of a novel interaction between CDK11p58 and the histone acetyltransferase HBO1, a MYST family protein, demonstrates additional mechanisms through which CDK11 may regulate eukaryotic transcription [63]. Histone modification is established to influence transcription, with acetylation characteristically linked to euchromatin and transcriptional activation [28]. This may be due to both the reduction in the affinity of histones to DNA and the generation of binding sites that recruit proteins to facilitate gene expression. CDK11p58 enhances the histone acetyltransferase

activity of HBO1, however, CDK11p58 is primarily expressed at mitosis and this study did not examine interaction with the CDK11p110 [63]. Therefore, the relevance of this finding to interphase transcription remains unclear.

1.4.8 CDK11 and Steroid Hormone Receptors

In addition to its roles in transcription and splicing, CDK11 mediates transcriptional activation associated with the nuclear steroid receptor family [64-66]. In three papers by Gu and coworkers, CDK11p58 represses transcriptional activation associated with oestrogen receptor alpha, androgen receptor and vitamin D receptor [64-66]. This did not occur through modulation of translation or transcription of the receptors, as there was no associated repression of androgen receptor protein expression or oestrogen receptor / vitamin D receptor transcript levels. The repression of transcription mediated by both oestrogen receptor alpha and vitamin D receptor occurred through their ubiquitin-proteasome degradation, promoted by CDK11p58 [64, 65]. Both the interaction with CDK11p58 and its kinase activity are required for the receptors' polyubiquitination and subsequent degradation. In contrast, CDK11p110 enhances oestrogen receptor alpha-mediated transcriptional activation. Paradoxically, although CDK11p110 is the predominant constitutive isoform, CDK11 depletion also enhances oestrogen-driven transcription [65]. This dichotomy has not satisfactorily been explained.

In contrast, repression of the androgen receptor transcriptional activity required phosphorylation of its transcriptional activation unit 1 (TAU1) motif by CDK11p58 and a kinase-dead CDK11p58 mutant was unable to repress androgen receptor activity [66]. These papers therefore describe mechanisms through which CDK11 may modulate the transcriptional activity of nuclear receptors. These interactions and their effects were observed using constitutively expressed CDK11p58 but no interaction with these signaling pathways has been demonstrated with endogenous CDK11p58, expressed primarily during mitosis.

1.5 CDK11 and Mitosis

1.5.1 Mitosis

The faithful replication and subsequent accurate division of the genome is integral to the maintenance of orthodox cellular physiology. Aberrations in these processes have deleterious consequences and are frequently associated with cancer [67]. Mitosis describes the segregation of the replicated genome into two daughter cells. It comprises the stages prophase, prometaphase, metaphase, anaphase and telophase [68]. At prophase, chromatin within the nucleus condenses, with the loss of nucleoli. The centrosome comprising two centrioles, duplicated during S phase divides and the centrioles migrate to opposing cell poles [68]. Dissolution of the nuclear membrane marks the onset of prometaphase. During this period, kinetochore complexes form at the chromosome centromeres. Microtubules extending from the opposing centrosomes attach at kinetochores to form the mitotic spindle. The spindle fibres align the chromosomes at the cellular equator to form the metaphase plate that designates metaphase [68]. The separation of sister chromatids is delayed until the accurate alignment and attachment of bi-orientated sister kinetochore has occurred. The prevention of precocious sister chromatic dissociation is mediated by the mitotic checkpoint, termed the Spindle Assembly Checkpoint (SAC) [69]. Conserved across eukaryotes, the SAC comprises serine/threonine kinases Monopolar Spindle (MPS1) and Budding Uninhibited by Benomyl 1 (BUB1) in addition to non-kinase components Mitotic Arrest Deficient 1 (MAD1), MAD2, BUB3 and BUB1-related 1 (BUBR1) [69]. This protein complex inactivates Cell Division Cycle 20 (CDC20), a co-factor of the E3 ubiquitin ligase Anaphase Promoting Complex/Cyclosome (APC/C). APC/C enables sister chromatid segregation and mitotic exit via the ubiquitylation and subsequent proteasome-dependent destruction of both Cyclin B, a regulator of mitotic progression, and Securin, an inhibitor of Separase, to promote cleavage of the Cohesin complex [69]. Unattached kinetochores activate SAC signaling, causing inhibition of CDC20 and therefore APC/C, which delays mitotic exit. On kinetochore attachment and fulfillment of this mitotic checkpoint, sister chromatids separate, marking the onset of anaphase, and move to opposing poles [69]. At telophase, chromosomes disperse and novel nuclear

membranes are assembled around the daughter nuclei [68]. Cytokinesis describes the division of the residual single cytoplasm to form two daughter cells [70]. Following sister chromatid separation, a contractile ring comprising actin filaments assembles equatorially at the cell cortex [70]. This constricts the cell membrane to form a cleavage furrow, with ingression progressing until a midbody structure is formed. Abscission cleaves this midbody to enable completion of cytokinesis and separation of daughter cells [70]. Numerous proteins are reported to mediate cytokinesis and abscission, including RhoA [71].

1.5.2 CDK11p58 and Mitotic IRES Translation

The influence of CDK11 on mitotic regulation is well established. One of the first papers interrogating CDK11 function found that apposite levels of the kinase were required for successful completion of mitosis [24]. This study found that expression of CDK11p58 in Chinese Hamster Ovary (CHO) cells, with resultant overexpression of the kinase, resulted in mitotic aberrations [24]. These abnormalities comprised mitotic delay with prolonged telophase, an aberrant increase in tubulin midbodies and increased aneuploidy within the cells. It was subsequently determined that overexpression of CDK11p58 resulted in reduced growth rates in the same CHO cell line, with this reduction reported to occur secondary to apoptosis [72]. The mitotic role of CDK11 was further characterised by the identification of a novel cell cycle-regulated internal ribosome entry site (IRES) [21]. This work was predicated by the identification of the strong cell cycle regulation of the p58 isoform, which was predominantly expressed during mitosis, in contrast to the constitutively expressed p110 isoform. Cornelis et al. (2000) undertook the study using Ba/F3 cells, which represent interleukin 3-dependent pre-B-cells [21]. These cells show marked upregulation of CDK11p58 at mitosis; although this finding was subsequently confirmed in other cell types, the upregulation of CDK11p58 in Ba/F3 cells appears proportionately greater at mitosis [21, 25]. Cornelis et al. (2000) demonstrated the presence of an IRES sequence, which unusually was contained within the coding mRNA [21]. In contrast, the majority of described IRES sequences lie within the 5'UTR of the mRNA transcript. This study demonstrated that translation could be

initiated from the IRES sequence through an internal AUG codon, despite the introduction of frameshift mutations within the 5' sequence of the p110 coding mRNA [21]. This finding excluded the generation of CDK11p58 through the proteolytic cleavage of CDK11p110. In addition, no evidence of the alternative splicing was identified on analysis of mRNA transcripts. Translation at this IRES region was found to be exceptionally cell cycle dependent [21]. The mechanism of this mitotic regulation of the CDK11 IRES was subsequently characterized, with work demonstrating the importance of Upstream of N-ras (Unr) and hnRNP C1/C2 proteins [73, 74]. Unr itself is translated through IRES-mediated mechanisms at G2/M under strict regulation by hnRNP C1/C2 [73, 74]. hnRNP C1/C2 stimulates Unr translation, while polypyrimidine tract-binding protein (PTB) and Unr together suppress Unr translation[73, 75]. Subsequently, Unr regulates translation at the CDK11 IRES in this mitotic IRES-dependent cascade [73, 74]. Interestingly, subsequent work in embryonic stem cells demonstrates the importance of PTB in regulating CDK11 IRES activity [76] independent of Unr in stem cells, with PTB inhibiting CDK11 IRES activity. PTB depletion resulted in significant mitotic delay and aberrant chromosome segregation, considered a consequence of CDK11p58 overexpression and proposed to explain the embryonic lethality of PTB-deficient mice [76].

1.5.3 Mitotic Suppression of Cap-Dependent Translation

The importance of translation through IRES-mediated mechanisms has become evident [77]. This mechanism of translation is integral to maintaining cellular regulation during periods of physiological and pathological stress in eukaryote cells, when cap-dependent translation is compromised [77]. Protein biosynthesis consists of three principal stages, constituting initiation, elongation and termination. In canonical cap-dependent translation, initiation occurs with the binding of the cap-binding complex (eIF4F) 5' m7G cap-structure of mRNA [78]. This binding of eIF4F to the mRNA leads to the subsequent recruitment of the 40S ribosomal subunit and its associated initiation factors to form the 43S initiation complex. The 43S complex, when assembled on the 5'UTR, moves 3' in search of the initiation codon [78]. On recognition of the initiation AUG

codon, the 40S subunit is joined by the 60S subunit to form an elongation-competent 80S ribosome. This was once considered to be the only mode of translation initiation in eukaryote. However, study of viral RNA genomes identified alternative mechanisms that subjugated the requirement for cap-dependent scanning and resulted in the direct recruitment of the 40S ribosome to the initiating codon [78], with subsequent work identifying cellular transcripts that also undergo IRES-mediated translation. IRES-mediated translation enables continued translation during periods of cellular stress, when cap-dependent mechanisms are suppressed; many of the cellular mRNAs that contain IRES elements encode proteins mediating responses to cellular stress [77]. The importance of cap-independent translation in mitosis has been established, with 14-3-3σ found to regulate of mitotic translation [79, 80]. 14-3-3σ binds numerous translation initiation factors including eukaryotic initiation factor 4B in mitosis [80], enabling the suppression of cap-dependent translation and resultant stimulation of cap-independent mechanisms. Depletion of 14-3-3σ causes mitotic dysregulation, which is ascribed to the inability to inhibit cap-dependent translation and consequential reduction in CDK11p58 [80]. Forced expression of CDK11p58 rescues the mitotic phenotype caused by 14-3-3σ depletion [80]. Subsequently, Barna et al. (2008) attributed the mitotic dysregulation caused by hyperactivation of the oncogene Myc on the failure to undergo the translational switch to cap-independent mechanisms and the subsequent mitotic dysregulation of CDK11 expression [79]. Again, rescue of the mitotic phenotype by CDK11p58 expression was demonstrated [79]. These works demonstrate both the importance of cap-independent translation in mitosis and the consequential translational control of CDK11p58 expression.

1.5.4 CDK11, the Mitotic Centrosome and Spindle

The importance of CDK11 in the faithful regulation of mitosis has been demonstrated *in vivo* [81]. Li et al. (2004) generated a *CDK11*-null mouse model through targeted disruption of the gene using homologous recombination [81]. In this model, heterozygous *CDK11*$^{+/-}$ mice demonstrate normal development but loss of both alleles results in early embryonic lethality, with apoptosis of blastocyst cells at four days post-coitus. These

cells exhibit both proliferative defects and mitotic arrest, consistent with the role of CDK11 in mitosis [81]. Subsequent work has confirmed that it is the shorter p58 isoform that mediates mitotic regulation, as is expected given its primarily mitotic expression [25]. It was demonstrated that expression of GFP-tagged CDK11p58 could rescue the mitotic dysregulation caused by CDK11 depletion in HeLa cells [25]. However, expression of GFP-tagged CDK11p110, with mutation of the IRES region to prevent translation of the shorter isoform, failed to rescue the aberrant mitotic phenotype [25]. Petretti et al. (2006) were the first to demonstrate localisation of either CDK11 isoform to the centrosome; CDK11 was found to localise to the centrosome throughout the cell cycle, with enhanced signal at mitosis [25]. CDK11 knockdown resulted in the aberrant localisation of Aurora A and Plk1, with abrogation of Aurora A recruitment to the centrosome. Furthermore, there was also a reduction in Plk1 recruitment to both the centrosome and kinetochore [25]. The centrosomal localisation of gamma tubulin at was also decreased, with microtubule regrowth assays demonstrating a diminished capacity for microtubule nucleation following CDK11 depletion. Moreover, using an in vitro H1 histone kinase assay, Petretti et al. (2006) demonstrated enhanced kinase activity of CDK11p58 following precipitation from mitotic cells, whilst the mitotic activity of CDK11p110 was diminished compared to interphase [25]. This work established that GFP.CDK11p58, but not GFP.CDK11p110, localised to the centrosome consistent with its role in mitosis. However, if it is the p58 isoform that localises to the centrosome, then the reported CDK11 centrosomal localisation at interphase is discrepant as there is little CDK11p58 expression during interphase [25]. In addition, although this paper was fundamental in determining the differential roles of CDK11 isoforms at mitosis, the p110 isoform used in these rescue experiments lacked the 14-3-3 binding site [25], with binding of 14-3-3 proteins to CDK11p110 maximal at mitosis [82]. It remains unclear whether this may have influenced the findings observed.

1.5.5 CDK11 and Centrosome Duplication

The role of CDK11 at the mitotic centrosome was further characterised in a subsequent paper by Hotchin et al. (2011) [83]. This demonstrated CDK11

depletion caused defective centrosomal recruitment of proteins essential to centriole biogenesis, with reduction of both Plk4 and centrosomal protein CEP192. The mislocalisation of these proteins was considered to cause the failure of centriole amplification after CDK11 knockdown [83]. CDK11p58 and Plk4 were found to interact both *in vitro* and *in vivo*, using tagged expression constructs of both proteins. However, there was no evidence of CDK11 phosphorylation by Plk4 and the reverse kinase assay to determine whether Plk4 was a substrate of CDK11 could not be undertaken due to inactivity of precipitated recombinant CDK11p58 [83]. Interestingly, in this work, there was no localisation of CDK11 to the centrosome but instead it located to the mitotic spindle, although this was only observed on initial expression of the TET-regulated CDK11 fusion protein [83].

CDK11 recruitment to the mitotic spindle had been previously reported in work, which established a role for the CDK11 in mediating microtubule stabilization [84]. This study by Yokoyama et al. (2008) was based on the discovery that RanGTP supported local nucleation and plus-end stabilisation of microtubules at chromosomes during mitosis. Nuclear protein TPX2 was requisite for this nucleation and in order to identify other proteins integral to microtubule stabilisation, a complex affinity purification protocol was devised [84]. This identified both CDK11 and Cyclin L1 within the active fraction and an assay using mitotic Xenopus egg extracts established that CDK11 mediated this microtubule stabilisation. Paradoxically, this work suggested that it was CDK11p110 isoform and not the p58 isoform that was responsible for stabilization [84]. This was determined by the production of specific antibodies that distinguished the two isoforms; however, it is unclear how the antibody specific to the p58 isoform was derived given the identical peptide sequence of the proteins [84]. This work again demonstrated localisation of CDK11 (although CDK11p110 on this assay) to the mitotic centrosome and spindle. Following immunodepletion of CDK11, restitution of normal spindle assembly was observed following re-addition of recombinant, full-length CDK11p110 [84]. If these findings are valid, it indicates that both isoforms of CDK11 may engage in the regulation of mitosis, although this is not the accepted paradigm.

1.5.6 CDK11 and Sister Chromatid Cohesion

The cohesion of sister chromatids is integral to the accurate segregation of chromosomes at mitosis [85]. Sister chromatid cohesion is mediated by the Cohesin complex, a ring-shaped protein complex that is believed to encircle the DNA helices of sister chromatids following DNA replication and hold them adjacent [85]. In vertebrates, cohesin is loaded onto chromatin from late telophase, with the reformation of the nuclear envelope [86]. It is maintained on the chromatin through interphase and DNA replication, to be removed in distinct stages at mitosis [85]. During prophase, the majority of cohesin is removed from the chromosome arms, while cohesin remains bound at the centromeres. This process is regulated by Plk1, which is activated in early mitosis and translocates from the cytoplasm into the nucleus. Plk1 phosphorylates the cohesin SA2 subunit, which in combination with phosphorylation of pro-cohesion factor Sororin by CDK1 and Aurora B, leads to displacement of cohesin and loss of chromosome arm cohesion [86]. Cohesion at the centromere is maintained until the metaphase-anaphase transition, at which time all kinetochores are attached to spindle microtubules and the Spindle Assembly Checkpoint (SAC) is satisfied. The SAC then promotes release of activated separase, a proteolytic enzyme that cleaves the cohesin subunit Rad21, causing dissociation of the remaining centromeric cohesin [86]. For this to occur, the centromeric cohesin must be protected through the early mitosis until the metaphase-anaphase transition. Shugoshin 1 (Sgo1) mediates the protection of the centromeric cohesion. Sgo1 is recruited to the inner centromere at early mitosis following Bub1-mediated phosphorylation of histone H2A [86]. Sgo1 acts in conjunction with protein phosphatase 2A to oppose phosphorylation of SA2 and Sororin. The premature loss of sister chromatid cohesion engenders aberrant mitotic progression, with a propensity for chromosome mis-segregation. CDK11p58 is requisite for the maintenance of sister chromatid cohesion [87, 88]. CDK11 depletion impairs the recruitment of both BUB1 and Sgo1 to the inner centromere during prophase [88]. This causes a failure in the protection of centromeric cohesin and the subsequent premature sister chromatid separation. The precise mechanisms mediating this function remain unclear

but the kinase function of CDK11p58 is necessary for this role [88]. Following CDK11 knockdown, no aberrant cohesion is noted prior to prophase to indicate anomalous loading of cohesin [87]. In addition, Hu et al. (2007) confirmed that sister chromatid separation was not merely a consequence of precocious mitotic exit via staining for phosphorylated Histone H3 and Cyclin B1, which are both lost on transition to anaphase [87]. These studies characterize the mechanisms through which CDK11 depletion causes mitotic dysregulation and chromosome mis-segregation.

1.5.7 CDK11p58 and Pak1

CDK11p58 is reported to bind p21-activated kinase 1 (Pak1) during mitosis [89]. In the original study by Chen et al. (2003), the CDK11–Pak1 interaction was described only with CDK11p46 during apoptosis and no interaction with either CDK11p58 or CDK11p110 was detected [90]. However, subsequent work by Kong et al. (2009) found interaction of Pak1 with CDK11p58 during mitosis, using tagged fusion proteins [89]. The authors established that CDK11p58 phosphorylated Pak1 at Ser174; Pak1 representing the only described substrate of CDK11p58 [90]. Phosphorylation of Pak1 enabled its recruitment to the myosin V motor complex, through binding to dynein light chain 2 (DLC2), and this interaction was reported to be fundamental to mitosis [89]. Pak1 mutants that mimicked the phosphorylated and dephosphorylated protein were generated, with the phospho-mimetic Pak1 enabling mitotic progression following nocodazole block while the phospho-refractory mutant exhibited mitotic arrest [89]. Kong et al. (2009) therefore proposed Pak1 to be the predominant downstream effector of CDK11p58 during mitosis.

1.5.8 CDK11p58 and Cyclin D3

Although CDK11 is established to interact with Cyclin L1 and Cyclin L2, Zhang et al. (2002) demonstrated that CDK11p58 also interacts with Cyclin D3 [91]. This interaction was identified in the yeast two-hybrid system but was subsequently confirmed in human hepatocellular carcinoma cells. This interaction was exclusive to the G2/M phase of the cell cycle, with Cyclin D3 binding enhancing the activity of CDK11p58 in a histone H1 kinase assay.

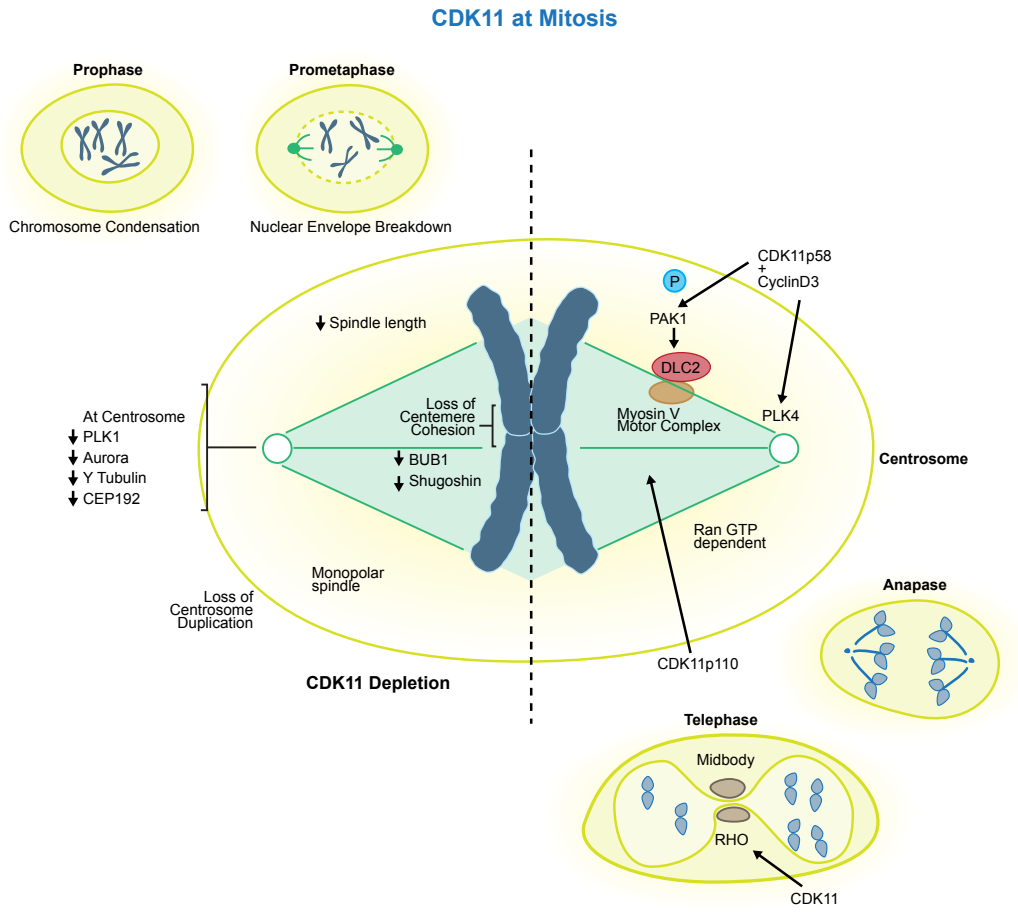

Fig 1.4 CDK11 at Mitosis. At mitosis CDK11 is reported to interact with CyclinD3 to phosphorylate PAK1; this interaction regulates Dynein Light Chain 2. CDK11p110 is reported to stabilise microtubules via RAN GTP dependent mechanisms. Following CDK11 depletion (left half of metaphase nucleus), there is loss of centrosome duplication, loss of centromere cohesion and the formation of shortened monopolar spindles. CDK11 may also engage in the mediation of anaphase and cytokinesis through regulation of Rho, although no direct interaction has been identified.

This interaction was specific to both the p58 isoform and the D3 Cyclin, with no Cyclin D1 or Cyclin D2 interaction demonstrated [91]. This work therefore identified an alternative cyclin regulator of CDK11p58 in mitosis.

1.5.9 CDK11 and Meiosis

The role of CDK11 in mitotic regulation is established, although the precise mechanisms require further characterisation. A recent study by Zeng et al. (2014) indicates a role for the Arabidopsis CDK11 homolog, CDKG1, in the regulation of synapsis and recombination during male meiosis [92]. Insertion of a mutation within the *cdkg1* gene leads to temperature-sensitive failure of meiosis in the late Pachytene and this is associated with defective formation of the synaptonemal complex, reduced bivalent formation and crossing over with resultant aneuploid gametes [92]. Disruption of the *Cyclin L* gene homologue strongly enhances the phenotype of these *cdkg1* mutants. Although no interrogation of members of the cohesin complex was undertaken in this study, the phenotype of *cdkg1* mutants, with partial asynapsis, is similar to that reported in other species on loss of cohesin complex proteins [93, 94]. The possible engagement of CDK11 in mediating meiosis is interesting and CDK11 may mediate this phenotype though mediation of Cohesin, as observed in mitosis [87]. Furthermore, the putative requirement for CDK11 at meiosis may explain the observation of discrete *CDK11* testis-specific transcripts [95, 96]. Several studies have identified the presence of these alternate *CDK11* transcripts, with one transcript generated via a trans-splicing event with non-coding RNA originating on the Y chromosome [97]. This non-coding RNA was spliced to the 5'UTR of *CDK11A* mRNA and Jehan et al. (2007) proposed that this alteration in the UTR may differentially regulate the expression of CDK11 within the testis [97]. In addition, work has demonstrated the expression of CDK11 within proliferating germ cells of the developing testis [98]. Furthermore, the protein is expressed in Pachytene primary spermatocytes during stage 7 to stage 11 of spermatogenesis, which is when synaptonemal complex formation and homologous chromosome crossover occurs [95, 96].

1.6 CDK11 and Apoptosis

Programmed cell death or apoptosis is a highly regulated process that plays a fundamental role in development and homeostasis [99]. Dysregulation of apoptotic signaling pathways is proposed to promote tumourigenesis by preventing the elimination of cells through normal checkpoint controls [100]. Apoptosis is characterised morphologically by chromatin condensation and formation of apoptotic bodies; biochemically, DNA fragments into oligonucleosome-size fractions. Similarities between early events of mitosis and apoptosis, such as nuclear envelope dissolution, have been recognized and moreover, there are evident links between cell cycle checkpoint control and apoptosis [72]. The engagement of cell cycle regulators in the mediation of apoptosis is therefore apposite. The role of CDK11 in apoptotic signaling pathways was one of the earliest established functions of the protein [72]. The initial study demonstrating the influence of CDK11 in apoptosis reported that ectopic expression of the CDK11p58 isoform resulted in the induction of apoptosis in Chinese hamster ovary cells [72]. Subsequent studies and work described in this thesis do not clearly demonstrate induction of apoptosis on ectopic expression of the p58 isoform in human cell lines [25], particularly the MDA-231 and HCT-116 lines used in my work. Lahti et al. (1995) demonstrated that on induction of apoptosis by Fas ligand, transcription of CDK11 mRNA was enhanced [72]. In addition, elevated levels of a novel CDK11 protein of approximately 50kDa were observed, later identified as CDK11p46. CDK11p46 comprises the C-terminal domain of the longer CDK11 isoforms and Lahti et al. (1995) demonstrated that addition of protease inhibitors after application of Fas ligand reversed both the accumulation of CDK11p46 and the apoptotic phenotype [72].

1.6.1 CDK11 and Caspase Cleavage

Beyaert et al. (1997) subsequently determined that CDK11 isoforms underwent cleavage by members of the Caspase family during induction of apoptosis to generate CDK11p46 [26]. In a model of tumour necrosis factor-mediated apoptosis, CDK11p110 was cleaved by both Caspase 1 and Caspase 3 [26]. No cleavage by other members of the Caspase family was identified. Cleavage occurred at Asp393 within the amino acid sequence YVPDS and mutation of this Asp393 base to alanine abrogated cleavage by both Caspase

1 and Caspase 3 [26]. Further Caspase cleavage sites were identified on Fas-mediated apoptosis, with a Caspase 8 cleavage site demonstrated at Asp387 [101]. In addition, ancillary cleavage sequences were identified within the N-terminal domain, resulting in the production of small CDK11 fragments on induction of apoptosis. Serine phosphorylation was determined to influence cleavage at these N-terminal domain sites [101].

1.6.2 CDK11p46 Interacting Proteins

Cleavage of proteins on apoptosis has two primary roles, which are either to ablate the function of proteins whose inactivity is required for apoptosis or to cleave proteins so as to release active fragments that execute the cell death program. It has been reported that the cleavage, kinase activity and localisation of CDK11 influence apoptotic signaling [101-103]. CDK11p46 represents the C-terminal fragment obtained following cleavage of the p110 or p58 isoforms at the Asp387 or Asp393 sites and it is generated by cleavage uniquely found on apoptotic signaling [104]. CDK11p46 contains the kinase domain of the longer CDK11 isoforms, but lacks numerous N-terminal regulatory elements. The p46 isoform has been reported to impart significant influence on anoikis, apoptosis induced by disruption of cell–matrix interaction, which it was found to mediate through interaction with p21-activated kinase 1 (Pak1) [90]. Direct interaction of CDK11p46 and Pak1 was reported to result in reduced Pak1 activity, which correlated inversely with levels of anoikis following expression of the p46 isoform [90].

Other protein interactions with CDK11p46 are reported and a yeast two-hybrid assay identified that the p47 subunit of eukaryotic initiation factor 3 (eIF3f) interacted with the p46 isoform [50]. This occurred through the Mov34 domain within the eIF3f protein and although weak interaction with CDK11p110 was observed, there was strong avidity for CDK11p46. CDK11p46 phosphorylates eIF3f at serine-46 and this phosphorylation is enhanced on induction of apoptosis [105]. On account of this interaction, Shi et al. (2003) interrogated the influence of CDK11p46 on translation and observed impaired synthesis of a reporter gene product on expression of CDK11p46 but not kinase-dead CDK11p46 [50]. This repression of protein

expression was mediated through translation as there was no reduction in transcript levels within the assay. Subsequently, an additional site of CDK11p46-mediated phosphorylation was identified in eIF3f at Threonine-119 within the Mov34 domain [106]. The significance of the dual-site phosphorylation of eIF3f protein by CDK11p46 was interrogated and this demonstrated that abrogation of phosphorylation through mutation of both serine-46 and threonine-119 to alanine reversed the apoptosis induced on CDK11p46 expression [106]. In contrast, phosphomimetic mutations at these residues upregulated apoptosis. Phosphorylation of eIF3f was reported to increase association of the protein with the eIF3 core complex but the mechanisms by which this regulates both protein synthesis and apoptosis remain unclear [106].

Interactions of CDK11p46 with NOT2 and Ran-Binding Protein 9 (RANBP9) were both identified by yeast two-hybrid assays [107, 108]. NOT2 is a subunit of the CCR4-NOT complex that is engaged in regulating mRNA synthesis and degradation, with additional roles mediating repression of RNA Pol II transcription [109, 110]. NOT2 interacts with CDK11p46 via its NOT domain. Shi et al. (2005) found that overexpression of NOT2 enhanced apoptosis but the mechanism for this was not determined [107]. The interaction between CDK11p46 and RANBP9 was identified by Mikolajczyk et al. (2003) and was enabled by the SPRY domain within RANBP9. CK11p46 was found to phosphorylate RANBP9 but the consequence of this interaction was not established [108].

1.6.3 CDK11p46 and Chaperone Proteins

The CDK11p46 isoform remains predominantly nuclear following its generation by caspase cleavage and work has demonstrated that its stability is regulated through interaction with molecular chaperone proteins [104]. CDK11p46 binds to Heat Shock Protein 90 (Hsp90), CDC37, its co-chaperone, and Hsp70, with the kinase activity of CDK11 necessary for its interaction with the Hsp90–CDC37 complex [104]. The treatment of cells with geldanamycin, an Hsp90-specific inhibitor, leads to ubiquitin-mediated

proteasomal degradation of the p46 isoform. This degradation of CDK11p46 was associated with a reduction in apoptosis [104].

While this work demonstrates that chaperone molecules regulate the stability of the CDK11p46, a study by Li et al. (2005) reported that β 1,4-Galactosyltransferase 1 (β 1,4-GT 1) regulates the generation of the p46 isoform [111]. This work demonstrated that ectopic expression of beta 1,4-GT 1 enhanced CDK11-mediated apoptosis induced by cycloheximide [111], whilst in the same model, β 1,4-GT 1 depletion effectively inhibited apoptosis. This β 1,4-GT 1 knockdown inhibited release of Cytochrome C and thereby Caspase cleavage, with the consequent attenuation of CDK11p46 production. The mechanism of this regulation remains elusive but β 1,4-GT 1 is reported to interact with CDK11, despite its localisation at both the trans-Golgi and cell membrane [112]. Indeed, the interaction of CDK11p58 with β 1,4-GT 1 led to the first identification of CDK11 [20]. However, the relevance of this direct interaction to apoptotic signaling is unclear, as β 1,4-GT 1 acts upstream of the CDK11 cleavage required to generate the p46 isoform that mediates apoptosis.

1.6.4 CDK11p60

The majority of published studies interrogating the role of CDK11 at apoptosis have investigated the function of the catalytic CDK11p46 cleavage product. However, it is reported that the N-terminal cleavage product, CDK11p60, may also engage in apoptotic signaling [113]. The p60 isoform comprises the regulatory domain of CDK11p110 and unlike the p46 cleavage product, which remains nuclear in location, the p60 isoform translocates to mitochondria [113]. It is reported that this mitochondrial targeting disrupts mitochondrial membrane potential with the resultant release of Cytochrome C [113]. Furthermore, Feng et al. (2005) demonstrates interaction between CDK11p60 and mitochondrial Hsp70, which acts as a transport protein to provide a mechanism of CDK11p60 entry into the inner mitochondrial membrane [113].

1.6.5 CDK11, Apoptosis and BCL-2 Family Proteins

The influence of CDK11 on Bcl-2 protein family members has been investigated by Chen et al. (2006) [114]. The Bcl-2 protein family comprises proteins with paradoxical influences on apoptotic regulation, whilst members Bcl-2 and Bcl-xl promote survival, others such as BAD and BAX induce cell death. Chen et al. (2006) demonstrated the inhibition of Pak1 kinase activity, secondary to CDK11p46 overexpression, correlated with a reduction in BAD phosphorylation on serine-112 and serine-136 [114]. This diminished phosphorylation caused the translocation of BAD to mitochondria and subsequent release of cytochrome c. A phospho-refractory mutant of Pak1, which was uninhibited by CDK11p46, phosphorylated BAD and resulted in the release of Bcl-2, with the blockage of cytochrome c release. This demonstrated a mechanism of CDK11p46-mediated apoptosis.

Furthermore, it was subsequently observed that CDK11p46 expression caused a reduction in Bcl-2 protein levels following cycloheximide-induced apoptosis, which was found to be dependent on CDK11 kinase activity [115]. Reduced phosphorylation of Bcl-2 residues serine-70 and serine-87 was reported, although this reduction in phosphorylation appeared to correlate with overall reduction in Bcl-2. Yun et al (2007) demonstrated that enforced Bcl-2 expression could rescue the increase in apoptosis observed on treatment with cycloheximide, following CDK11p46 overexpression [115]. However, no direct interaction between Bcl-2 and CDK11 was demonstrated. The authors noted no manifest increase in apoptosis with CDK11p58 overexpression alone [115].

Hao et al. (2011) identified a novel interaction between CDK11p46 and Ribosomal Protein S8 (RPS8) that resulted in the inhibition of both cap-dependent and IRES-mediated translation, with no reduction of mRNA levels on this assay using a bicistronic luciferase reporter [116]. The CDK11–RPS8 interaction synergised Fas ligand-induced apoptosis and provides a novel mechanism for the mediation of translation by CDK11 during apoptotic signaling.

1.7 CDK11 and Disease

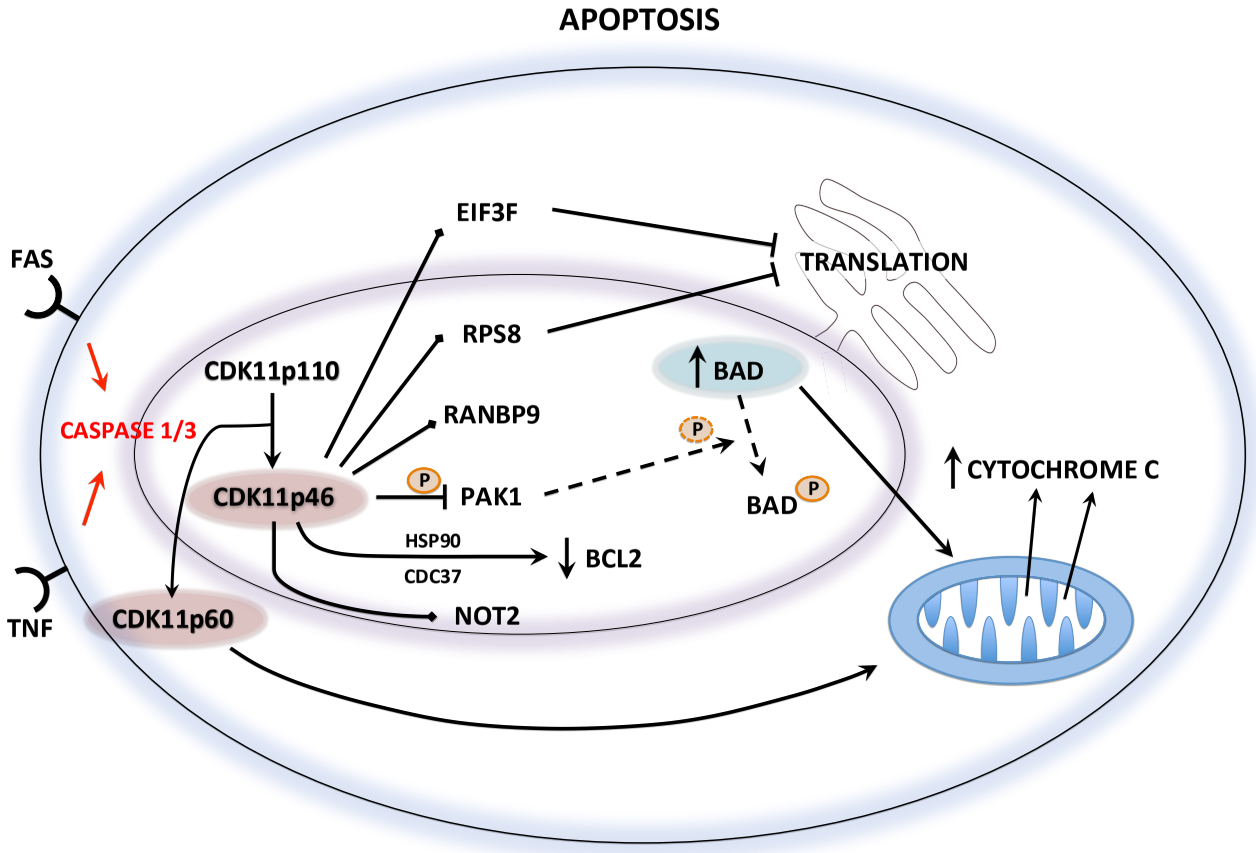

Fig 1.5 CDK11 at Apoptosis. Illustration of the interactions of CDK11 at apoptosis. CDK11p46 phosphorylates PAK1, inhibiting its phosphorylation of BAD; unphosphorylated BAD then translocates to mitochondria resulting in Cytochrome C release. CDK11p60 also translocates to mitochondria resulting in Cytochrome C release. Furthermore, CDK11p46 also interacts with RPS8 and EIF3F to inhibit translation. The influence of interaction with NOT2 and RANBP9 remains uncertain.

The accurate regulation of cellular physiology is requisite for normal development, homeostasis, repair, and ultimately survival of all organisms. Dysregulation of this precise control mediates a plethora of deleterious consequences and this thesis aims to interrogate the consequences of CDK11 dysregulation in both cancer and developmental phenotypes. The roles of CDK11 in regulating diverse cellular processes have been established but its contribution to disease phenotypes remains uncertain.

1.7.1 1p36 Deletion and Cancer

Deletion of the short arm terminus from human Chromosome 1 is an anomaly frequently observed in diverse tumour types. The duplicate *CDK11* genes lie within this region at 1p36.3, a locus frequently deleted in neuroblastomas, malignant melanomas, ductal breast carcinoma, endometrial hyperplasia, non-Hodgkin lymphoma, and early childhood sinus tumours [117-121].

1.7.1.1 1p36 and Neuroblastoma

The deletion at 1p36 on Chromosome 1 is a consistent observation in advanced neuroblastoma and tumour-derived cells, with reports that it correlates with enhanced metastatic potential [119, 121]. The frequency of this deletion is proposed to indicate the presence of a tumour-suppressor gene at this locus. On account of its mediation of mitosis and apoptosis, *CDK11* has been considered a putative candidate tumour suppressor gene. Analysis of neuroblastoma-derived cells demonstrated deletion or translocation of one allele of both *CDK11A* and *CDK11B* in 18 of 20 cell lines examined [119]. Interestingly, not only did the 1p36 deletion correlate with metastatic potential but it was also associated with N-myc gene amplification [122]. The significance of this remains uncertain. Subsequent work has questioned the validity of *CDK11* as a putative tumour suppressor, with an alternate study reporting that the *CDK11* locus was outside of the consensus region of allelic loss, albeit in a small cohort of samples [123].

1.7.1.2 1p36 Deletion and Melanoma

Similar observations have been reported in melanoma [120, 124]; 1p36 deletion is found primarily in nodular melanoma and melanoma metastases

[125]. Initial work analysing the *CDK11* genes in melanoma-derived cells revealed deletion or translocation in 8 of the 14 lines investigated [120]. In addition, mutations of the 5′ promoter region of the *CDK11B* gene were observed in four discrete cell populations. However, this work was subsequently contradicted by analysis of the *CDK11* locus and its promoter in tissue derived from 58 unique malignant melanomas [126]. This found only a single mutation within the promoter region in one melanoma tissue sample. No mutations of the coding sequence itself were observed. In other work, Feng et al. (2002) did not identify common mutations within the *CDK11* coding region but did report different promoter polymorphisms and queried the potential implication of these for transcriptional regulations [124]. Nonetheless, although 1p36 deletion is commonly observed in certain cancers, the contribution of *CDK11* to tumourigenesis in these cases has not been determined.

1.7.1.3 CDK11 and Squamous Cell Skin Tumours

Chandramouli et al. (2007) investigated the influence of *CDK11* haplo-insufficiency on tumourigenesis, adopting a murine model [127]. A single allele of the *CDK11* gene was targeted using gene trap technology to generate haplo-insufficient mice. The $CDK11^{+/-}$ and *CDK11 WT* mice were compared in a model of chemical-mediated skin carcinogenesis. This demonstrated enhanced susceptibility to tumour formation following the loss of a single allele of *CDK11*. No other study has directly interrogated the contribution of *CDK11* dysregulation to tumourigenesis.

1.7.1.4 CDK11 and Wnt/β-catenin in Colonic Adenocarcinoma

CDK11 was identified as a modulator of Wnt/β-catenin-dependent transcription, following an RNAi kinome screen for modulators of Wnt signaling in colorectal cancer cells [128]. Activation of Wnt signaling is observed constitutively in most colon adenocarcinomas [129]. These tumours are often reported to be addicted to Wnt/β-catenin signaling, with the signaling cascade integral to cell survival. CDK11 was one of 11 kinases found to regulate this pathway, with CDK11 knockdown inhibiting Wnt-driven transcription as assessed in a luciferase assay [128]. This work not

only demonstrated a role for CDK11 in regulating the Wnt signaling cascade but also identified CDK11 as a putative target in Wnt-addicted cancers.

1.7.1.5 CDK11 and Multiple Myeloma

Subsequently, CDK11 has been identified as a putative therapeutic target in two RNAi lethality screens of human multiple myeloma [130, 131]. In the first study, the lethality of 639 human kinases or putative kinases was assessed in two myeloma cell lines [131]. CDK11 was one of 15 kinases identified to significantly reduce viability after depletion by RNA interference. The mechanism of this impaired viability is uncertain but other mitotic regulators such as Plk1 and Aurora A were identified, suggesting this may be mediated through mitotic dysregulation [131]. The second paper identified *CDK11* as one of 57 potent myeloma survival genes, from an assay of 6,722 genes selected for putative 'druggability' [130]. This study was again undertaken in myeloma cell lines and once again identified mitotic regulator *Plk1* and *Aurora B* in addition to *CDK11* within the genes inducing lethality on knockdown. Therefore, both studies indicate CDK11 may be critical to myeloma cell survival and thereby a putative target for drug therapy.

1.7.1.6 CDK11 and Sarcoma

Recent work has reported CDK11 expression to be critical for osteosarcoma cell growth and proliferation [132]. This study undertook a viral-based shRNA kinase library assay to identify novel kinases that mediate osteosarcoma survival. CDK11 knockdown caused reduced cell viability with enhanced apoptosis and was associated with a reduction in the expression of pro-survival genes Mcl-1 and Bcl-xL. Further work interrogated this observation *in vivo*, via the subcutaneous injection of osteosarcoma cells into nude mice. Intra-tumoural administration of CDK11 siRNA significantly suppressed tumour growth compared to both vehicle and non-targeting siRNA treatment [132]. The clinical implication of CDK11 expression was assessed through analysis of CDK11 protein levels in tissue microarrays derived from human osteosarcoma. Kaplan–Meier survival analysis demonstrated the outcome for patients with tumours with high CDK11 expression was significantly worse than those with low CDK11

expressing tumours. This work indicates the importance of CDK11 and its expression to tumour biology. The reports of both tumour-suppressing and tumour-promoting functions initially appear paradoxical, with haploinsufficiency of CDK11 reported to enhance tumourigenesis but high CDK11 expression associated with tumour progression [127, 132]. It is proposed to indicate the importance of precise regulation of CDK11 expression; dysregulated CDK11 expression may have deleterious consequences, which dependent on context may promote tumourigenesis or impair tumour cell survival.

1.7.2 CDK11 in Diverse Disease Processes

It is not only in tumour biology that a putative role for CDK11 is proposed. Published studies have indicated potential influence of CDK11 in diverse pathologies, including keloid disease, Alzheimer disease and type II diabetes [133-135]. The scope of these studies was limited and each had significant methodological deficiencies but these papers do advocate the need for further investigation of the role of CDK11 in disease pathogenesis. The speculative contribution of CDK11 dysregulation and mislocalisation to Alzheimer disease is intriguing. CDK11 is reported to mis-localise to the cellular cytoplasm, as opposed to the nucleus, in human Alzheimer disease tissue samples [133]. In addition, expression of both amyloid precursor protein and amyloid-β(25-35) caused enhanced CDK11 expression in neuronal M17 cells [133]. The significance of this is uncertain and is not explored in depth in this study but others have implicated CDK11 in neuronal inflammatory responses [116, 136].

1.7.3 1p36 Deletion Syndrome

Deletion of the distal short arm of Chromosome 1 (1p36), including the *CDK11* locus, is not only an anomaly identified in cancer but congenital deletion of 1p36 causes the developmental disorder termed 1p36 deletion syndrome [137]. This constitutes one of the more common described developmental disorders, with an estimated incidence of 1 in 5,000 live births [138]. The disorder conveys a wide phenotype of dysmorphology, with common features including growth delay, moderate to severe mental retardation, motor hypotonia, and a large anterior fontanelle [138]. The

single gene or multiple genes that contribute to the phenotypic spectrum remain uncertain. It is considered probable that several genes within this locus influence the dysmorphology of the disorder, given the disparate clinical manifestations [138]. In addition, there is little work investigating the consequence of haploinsufficiency of individual genes within this locus. The influence of CDK11 on this developmental pathology therefore remains uncertain. However, no developmental phenotype was observed in haploinsufficient mice, although it is important to note that the murine *Cdk11* locus varies markedly from the human genome [81]. Intriguingly, single nucleotide polymorphisms (SNPs) within both the *CDK11A* and *CDK11B* genes were found to be significantly associated with language abilities in a genome-wide association meta-analysis of two large cohorts, derived from both Australia and the United Kingdom comprising over 6,500 children [139]. Nonetheless, the contribution of CDK11 to more profound intellectual impairment is not determined.

Published literature implicates CDK11 and its dysregulation in the mediation of diverse disease processes. It may play a role in both tumour suppression and tumour promotion, with evidence that it may represent a novel therapeutic target in cancer treatment. Further work is required to better characterize the mechanisms through which CDK11 mediates its influence and to establish its roles in these diverse pathological processes.

1.8 Additional Reported Functions of CDK11

1.8.1 CDK11 and Hedgehog Signaling

In addition to its roles in transcription, splicing, mitosis and apoptosis, CDK11 is reported to engage a variety of alternate processes. Two studies, both using RNA interference screens, identified CDK11 as a regulator of Hedgehog signaling in both drosophila and mouse models [140, 141]. Hedgehog signaling is critical for proper development, with its disruption associated with developmental abnormalities and cancer [142]. The mammalian Hedgehog (Hh) signaling pathway is activated through binding of Hh ligand to the Patched receptor [142]. This enables the translocation of Smoothened and initiation of downstream signaling cascades leading to the

ultimate activation of Glioma-associated (GLI) transcription factors [142]. The protein Suppressor of Fused (SUFU) acts to negatively regulate this pathway; it undertakes this both through prevention of GLI entry into the nucleus and direct inhibition of GLI transcriptional activity. It is reported to mediate this through recruitment of the SIN3-associated polypeptide 18 (SAP18)-mSIN3 histone deacetylase repressor complex [143]. CDK11 was identified to bind SUFU and repress its inhibitory actions on GLI [140]. It is assumed, given the nuclear localisation of CDK11, that it acts to repress SUFU activity within the nucleus. Other studies have since identified SAP18 as a binding partner of CDK11 [60]. This demonstrates an alternative mechanism of transcriptional regulation by CDK11.

1.8.2 CDK11 and Rho Signaling

CDK11 is reported to modulate Rho signaling at cytokinesis in drosophila [144]. Using a drosophila phenotype reported to occur due to ineffective Rho activation at cytokinesis, this study performed a screen examining for genes that modulate the aberrant phenotype when over-expressed [144]. This found that over expression of PITSLRE (drosophila CDK11) suppressed the aberrant phenotype in this model. Notwithstanding the limitations of this model, this implicated CDK11 in the mediation of Rho signaling at cytokinesis [144].

1.8.3 CDK11p58 and Neuronal Inflammation

Numerous papers from the laboratory of Shen and co-workers have interrogated the putative role of CDK11p58 in modulating inflammatory response in neuronal astrocytes, neurons and Schwann cells [136, 145]. These papers report that CDK11p58 mediates astrocytes activation caused by lipopolysaccharide (LPS), with it reported to involve activation of p38 and JNK pathways [146, 147]. In addition, it was reported that CDK11p58 expression enhanced both neuronal apoptosis and Schwann cell apoptosis following LPS administration [145]. The functional significance of these reported observations remains uncertain but the authors propose that this implicates CDK11 in neuronal inflammation and neuronal degeneration [145]. Further work is required to clarify this but the same laboratory has

reported enhanced expression of CDK11p58 following spinal cord injury in a rat model [148].

1.8.4 CDK11 and Autophagy

Work from within this laboratory has recently identified CDK11 as a mediator of cellular autophagy [149]. Autophagy is an intracellular degradation system that delivers cytoplasmic constituents to the lysosome, within double membrane bound vesicles termed autophagosomes [150]. Three distinct types of autophagy are described, which are macro-autophagy, micro-autophagy and chaperon-mediated autophagy [150]. However, the term autophagy is classically used to distinguish macro-autophagy and is the case within this thesis [150]. An RNA interference kinome screen was used to detect autophagy modulators in drosophila S2 cells [149]. This demonstrated that CDK11, or PITLSRE, depletion caused the accumulation of autophagosomes. This thesis describes my initial work to characterize the mechanisms underlying this CDK11-mediated autophagy.

1.9 Statement of Problem

Evidence summarized in this chapter demonstrates the fundamental role CDK11 plays in regulating diverse aspects of cell biology. CDK11 has an essential role in embryonic development, with loss of *Cdk11* causing blastocyst lethality in murine models. Furthermore, CDK11 appears critical not only during development but in later health, with CDK11 dysregulation implicated in various disease states, including cancer. Overexpression of CDK11 correlates with poor prognosis in assorted tumours, with CDK11 identified as a putative therapeutic target. The importance of CDK11 in both health and disease warrants further investigation to better understand its functions in these states.

In this work, I aimed to examine the role of CDK11 in both cancer and developmental phenotypes. CDK11 depletion is reported to influence autophagy and cell migration in cancer cells. Initially, I investigated the influence of CDK11 in these two novel functions. Subsequently, I aimed to characterize the interactomes of discrete CDK11 isoforms to enable greater understanding of the mechanisms through which CDK11 mediates both novel and established functions. Work then aimed to sequence the *CDK11* locus, examining for causative genetic mutations in Cornelia de Lange Syndrome (CdLS).

1.10 Thesis Hypotheses

Published work indicates CDK11 has a critical role in cancer biology and may present a therapeutic target in the treatment of cancer. The principal aim of this thesis was therefore to identify mechanisms through which CDK11 mediates its influence on cancer biology. A greater understanding of CDK11's roles in both cancer and normal biology, including human development, may elucidate pathways that are unique to either, thereby enabling improved targeting of the protein in cancer therapy. Moreover, elucidating co-dependent pathways of specific importance in cancer may also enable synergistic targeting to effect synthetic lethality.

Novel work in this thesis addressed the discovery by others within the laboratory that CDK11 inhibition elicits an autophagy phenotype. Autophagy has been established to influence cancer biology and may provide mechanisms for cancer cells to mitigate cellular stress. It had been hypothesised that CDK11 acts directly on autophagy pathways, with inhibition triggering the autophagy phenotype. I aimed therefore to determine whether CDK11-mediated autophagy could be dissociated from established CDK11 functions. Furthermore, I aimed to investigate CDK11-interacting proteins to determine whether CDK11 associates with autophagy-related proteins. In addition, I aimed to investigate the role of autophagy following CDK11 knockdown.

In this thesis, I also explored the hypothesis that CDK11 directly regulates cancer cell migration. I aimed to confirm the effects of CDK11 depletion on cancer migration (demonstrated in a published siRNA screen) and establish that this does not solely result from impaired cell proliferation. Subsequently, I aimed to elucidate alternate pathways underlying the migratory deficit on CDK11 knockdown. CDK11 contains both SH2 and SH3 binding domains and has established roles in centriole biology. I therefore hypothesised that CDK11 may influence this migratory phenotype either via direct interaction with the cytoskeleton, specifically focal adhesions, or through effects on centriole biology and thereby cellular polarisation. Again, I aimed to characterize the CDK11 interactome through proteomic studies to examine for interaction with pathways involved in cell motility.

Finally, I examined the hypothesis that *CDK11A/B* genes harbour causal mutations for the cohesinopathy developmental disorder Cornelia de Lange Syndrome. This hypothesis was proposed due to the discovery of deletion of the *CDK11* locus in a patient with CdLS; furthermore CDK11 has established functions in cohesin biology at mitosis. I aimed to sequence *CDK11*A/B in a cohort of CdLS patients with no known causative mutation, to determine whether any putative causal variant exists.

CHAPTER 2

Materials and Methods

2.1 Materials

2.1 Materials		
Experiment	**Material**	**Supplier**
Cell culture **Plastic ware**	Falcon tissue culture dishes (60 mm, 90 mm, 120 mm) Cell strainers (40 and 70μm)	*BD Biosciences, Oxford, UK*
	Cell culture flasks (T25, T75, T150) 96-well, 24-well, 12-well plates , 6-well plates, 6cm tissue culture plates.	*Corning, Sigma Aldrich, Gillingham, UK*
	Mr Frosty Cryo 1ºC freezing container	*Thermo Fisher Scienrific, Loughborough, UK.*
	0.22μm filters 0.4μm filters	*Millipore, Hertfordshire. UK.*
Cell culture reagents	Sterile PBS	*ECRC Central Services*
	DMEM Fetal calf serum L-Glutamine 200mM Trypsin solution 2.5% Library efficiency chemically competent cells, DH5α	*Invitrogen Life Sciences Ltd, Paisley, UK*
	Dimethyl sulphoxide (DMSO)	*Sigma Chemical Co, Poole, UK*
	Gel Extraction Kit Miniprep Kit	*Qiagen, Crawley, UK*

	Dimethyl sulphoxide (DMSO) Paraformaldehyde	*Sigma Chemical Co, Poole, UK*
	T4 Ligase enzyme Ligation Buffer	*Roche, Welwyn Garden City, UK.*
Flow-activated cell sorting	Propidium iodide (PI)	*Sigma Chemical Co, Poole, UK*
	HCL EDTA Triton X	*ECRC Central Services*
	BrdU Anti-BrdU antibody RNAse	*Thermo Fisher Scientific, Loughborough, UK.*
	Anti-Rat Alexa 488	*Life technologies, UK*
	Anti-BrdU antibody	*Santa Cruz, UK.*
	FACSScalibur BD Biosciences	*Life, Sciences, UK.*
Immunofluorescence	Superfrost Plus Slides Coverslips	*Thermo Fisher Scienrific, Loughborough, UK.*
	Anti-mouse/rabbit Alexa Fluor® conjugated secondary antibodies DAPI (4',6-diamidino-2-phenylindole)	*Invitrogen, Paisley, UK*
	Formaldehyde	*Sigma Chemical Co, Poole, UK*
	Vectashield mounting medium with DAPI	*Vector Laboratories Ltd,*
Fluorescence In Situ Hybridization (FISH)	Zytolight Fluorescence CEN 7 Probe Zytolight Fluorescence CEN 8 Probe	*Bio SB, Upper Heyford, UK.*
	Trisodium Citrate Potassium Chloride	*ECRC Central Services*

	Methanol Acetic Acid Marvel	
	20XSSC Ultrapure	Life technologies, Paisley UK.
	Fluorochrome-conjugated Avidin (FITC/Texas Red) Biotinylated antiavidin Fluorochrome conjugated antidigoxigenin FITC-conjugated anti-sheep	Vector Laboratories, Peterborough, UK.
Microscopy and Image Analysis	ImageJ software	*National Institute of Health, Bethseda, USA*
	Olympus FV1000 Confocal microscope Olympus ScanR/CellR microscope Olympus BX51 Microscope	*Olympus UK Ltd, Hertfordshire, UK*
	Volocity 3D Image Analysis Software	*Perkin Elmer, USA*
Molecular biology techniques	Tween 20	*Acros Organics, Loughborough, UK*
	2100 Bioanalyzer	*Agilent, Berkshire, UK*
	Agarose gel DNA Hyperladder 1	*Bioline Reagents ltd., London, UK*
	Complete ULTRA Tablets Phosphatase inhibitor cocktail	*Roche Nimblegene, Waldkraiburg, Germany*
	Agarose Ethidium bromide Thymidine	*Sigma Chemical Co, Poole, UK*
	Nanodrop 1000 spectrophotometer	*Thermo Fisher Scienrific, Loughborough, UK.*

	Oligofectamine Reagent Lipofectamine Reagent Opti-MEM Nuclease free water	*Life technologies, Paisley UK.*
	1Kb DNA ladder	*Invitrogen, Paisle.*
	100bp DNA ladder	*Promega, UK.*
	UV Transiluminator Bio Doc-IT system	*UVP, UK.*
	Restriction enzymes and buffers	*NEB or Roche, UK.*
	Scalpel blades	*Swann Morton, Sheffield, UK.*
	Quik Change Site Directed Mutagenesis Kit PfU Ultra DNA polymerase	*Strategene, Agilent, Stockport UK.*
Protein Techniques	BP800 spectrophotometer	*Biohit, Ellsmere Port, Cheshire, UK*
	ECL reagent Semi-Dry and Rapid Blotting Systems	***Life Science**, Biorad Laboratories, Hertfordshire, UK.*
	Atto protein electrophoresis apparatus	*Genetic Research Instrumentation, Dunmow, UK*
	Wet blotting apparatus	*Jencons, Leighton Buzzard, UK*
	Anti-mouse/horseradish peroxidase conjugate Anti-rabbit/horseradish peroxidase conjugate	*New England Biolabs, Hertfordshire, UK*

	Micro BCA protein assay kit Polyvinylidene Difluoride (PVDF) membrane Triton X-100 Tween 20	*Thermo Fisher Scienrific, Loughborough, UK.*
	Bovine Serum Albumin NP-40 Phenylmethanesulfonyl fluoride (PMSF) Protease inhibitor cocktail	*Sigma-Aldrich, Dorset, UK.*
	Nitrocellulose membrane	*Schleicher and Schuell, London, UK*
	3MM filter paper	*Whatman, Maidstone, UK*
	LB Broth	*ECRC Central Services*
	GFP-Trap A Immunoprecipitation of GFP fusion protein	*Chromotek, Planegg, Germany.*
Nucleic Acid Techniques	GenomiPhi V2 Amplification kit	*GE Health, Life Sciences, Buckinghamshire, UK.*
	Reddymix Custom PCR master mix	*Thermo Fisher Scienrific, Loughborough, UK.*
	GC Mix Reagent	*Roche Diagnositics, West Sussex, UK.*
	BigDye® Terminator v3.1 and v1.1 Cycle Sequencing Kits ABI 3730 DNA Analyser	*Applied Biosystems, Life technologies, Paisley UK.*

	Mutation surveyor v3.30	*Soft genetics, Pennsylvania, USA.*
	Ion Xpress Plus gDNA and Amplicon Library Preparation Kit	*Life technologies, Paisley UK.*
	Bioanalyser	*Agilent, stockport, UK.*
	Ion PGM	*Life technologies, Paisley UK.*
	NextGENe Software	*Soft genetics, Pennsylvania, USA*
	Agencourt AMPure XP Kit	*Beckman Coulter, High Wycomb, UK.*
	DynaMag-2 Magnetic Rack	*Life technologies, Paisley UK*
	Eppendorf LoBind Tunes 1.5ml	*Sigma-Aldrich, Dorset, UK.*
	100% Ethanol	*ECRC Central Services*

2.1.2 Stock Solutions and Buffers

All commomly used stock solutions were autoclaved or passed through a 0.22μm filter.

Buffer for DNA PCR product electrophoresis

***TBE – 5X*:**

54g Tris Base

27.5g Boric acid

20ml 0.5M EDTA

to 1000ml water

6xDNA Loading Buffer

30% (v/v) glycerol

0.4% (w/v) Orange

Protein extraction and western blotting

Blocking buffer

0.2% Tween 20 in Tris Base Solution

5% bovine serum albumin

PBS–Tween 20 (PBST)

1X PBS

0.1% (v/v) Tween 20

Radioimmuno-precipitation assay (RIPA) buffer

50mM Tris/HCl, pH 7.4 (25ml of 1M)

150mM NaCl (15ml 5M)

1% sodium deoxycholate (5g)

1% NP40 (5ml)

0.1% sodium dodecyl sulphate (SDS) (0.5g)

to 500ml water

Filter with 0.22µm filter prior to addition of Complete ULTRA Tablets

Phosphatase inhibitor cocktail immediately before use.

NP40 Buffer

5M NaCl 30mls

10% NP40 50mls

1M Tris pH8 50mls

Filter with 0.22µm filter prior to addition of Complete ULTRA Tablets

Phosphatase inhibitor cocktail immediately before use.

Running gel -10%

4.43ml 30% acrylamide

5ml Tris pH 8.8

3.9ml H2O

130ul 10% SDS

125ul 10% APS

6.6ul TEMED

Sample buffer – 2x

800ul 2-mercaptoethanol

1.3ml Tris pH 6.8

2ml glycerol

5ml 10% SDS

1.3ml H2O

Bromophenol to colour

Stacker gel

1.07ml 30% acrylamide

0.83ml Tris pH 6.8

4.67ml H2O

70ul 10% SDS

70ul 10% APS

20ul TEMED

Tank Buffer – 10x

50mM Tris Base (60.4g)

50mM glycine (288g)

0.1% SDS (20g)

to 2000ml water

Transfer Buffer

50mM Tris Base (60.4g)

40mM glycine (230g)

0.04% SDS (4g)

20% methanol (400ml)

to 2000ml water

Preparation of GST Fusion Proteins

Lysis Buffer

For 100ml

500mM NaCl – 10ml 5M

0.5% NP-40 – 5ml 10%

50mM Tris pH 7.6 – 5ml 1M

5mM EDTA – 1ml 0.5M

5mM EGTA – 1ml 0.5M

Nuclear and Cytoplasmic Separation

Buffer 1

10mM Hepes

10mM KCl

0.1mM EDTA

1mM DTT

Prior to use

0.5mM PMSF (Phenylmethanesulfonyl fluoride)

Protease inhibitor cocktail

2.2 Methods

2.2.1 Transfection of cultured mammalian cells

2.2.1.1 Short interfering RNA transfections

Short interfering RNA (siRNA) oligonucleotides (non targeting control siRNA or siRNA targeting *CDK11*) were transfected into monolayer cells using Oligofectamine [Invitrogen]. Cells were seeded in standard culture media (SCM) onto a 12 well plate at $1x10^4/100\mu l/1cm^2$ substrate. Cells were 30-50% confluent at the time of transfection. siRNA was diluted in Opti-MEM (final concentration 5μM) [Invitrogen] and incubated at room temperature for 5 minutes. 2μl Oligofectamine reagent was diluted in 5.5μl of Opti-MEM, gently mixed and incubated at room temperature for 5 minutes. After the 5 minute incubation, the diluted oligonucleotide was combined with the diluted Oligofectamine reagent for 20 minutes before adding to each well of 12 well plate. The cells were incubated in 400 μl of serum free media (SFM) with addition of 100 μl of transfection mix (total volume 500 μ l) for 5 hours (37ºC, 5% CO_2) before replacing with SCM. Assays for target protein expression were performed post-transfection by as appropriate for experiment. The transfection protocol was scaled up or down for different substrate area.

2.2.1.2 Lentiviral Production

293T packaging cells were seeded in 6 cm tissue culture plates at $1.5x10^5$ cells/ml (6ml/plate) in SCM without antibiotic (DMEM 10% FCS). Cells were incubated for 24 hours (37ºC, 5%vCO_2) until the cells were approximately 70% confluent. Transfection plasmids (HIV1, VSV-G/pMD2.G, Vector) were diluted in Opti-MEM to a final volume of 20 μl. Lipofectamine 2000 reagent (10 μl) [Invitrogen] was diluted in Opti-MEM (90 μl). The plasmid mixture was added drop wise to the diluted Lipofectamine 2000 and incubated at room temperature for 20 minutes. This transfection mix was carefully transferred to the packaging cells in SCM (without antibiotic). Subsequent steps were conducted in a Category 2 tissue culture facility. Cells were incubated for 18 hours (37ºC, 5% CO_2). The transfection

mix was removed and replaced with 4mls 30% FCS growth media for viral harvest. The cells were incubated for 24 hours (37ºC, 5% CO_2). The media containing the lentivirus was harvested at approximately 40 hours post transfection. The media was transferred through a syringe filter into polypropylene storage tube. Media was replaced with 6ml 30%FCS growth media for further viral harvest. Lentivirus-containing media was then added to target cells directly or frozen at -40ºC.

2.2.1.3 DNA Transfections

DNA was transfected into monolayer cells using Lipofectamine 2000. Cells were 70% to 90% confluent at time of transfection. For each transfection of cells plated in 12-well plates (~4cm^2/well), two complexes were prepared. The first contained 1.6 μg of DNA in 100 μl of Opti-MEM I Medium and the second contained 4 μl Lipofectamine in 100 μl Opti-MEM. After 5-minute incubation at room temperature the solutions were combined, gently mixed and incubated for 20 minutes at room temperature before adding to the cells. The cells were incubated in 1 ml of SCM (without antibiotics) with the transfection mixture for 18 hours (37ºC, 5% CO_2) after which media was replaced with SCM.

2.2.2 Cell Cycle Blockade and Cell Synchronisation

2.2.2.1 Single Thymidine

Thymidine [Sigma] was was reconstitued in sterile water and added to SCM to a final concentration 2mM. Transfection protocol was followed as above. Transfection media was replaced with SCM containing Thymidine after 5 hours and incubated for 48 to 72 hours as appropriate for assay. The SCM and Thymidine were replaced every 24 hours.

2.2.2.2 Double Thymidine Block, G1/S Cell Synchronisation

Cells were grown in SCM to approximately 40% confluence. Thymidine was added to cells in SCM to a final concentration of 2mM and incubated for 19 hours (37ºC, 5% CO_2). After 3 washes with PBS the media was replaced with SCM without thymidine and incubated for 9 hours (37ºC, 5%CO_2).

Thymidine was added again to a final concentration of 2mM and incubated for a further 16 hours (37ºC, 5% CO_2). Cells were again washed with PBS and media replaced with SCM. At this stage the cells were synchronous in G_1 and were released to progress through the cell cycle over the proceeding 15 hours; cells remain synchronous for 1 to 2 cell divisions.

2.2.2.3 Nocodazole Block

In order to achieve mitotic synchronisation, Thymidine was added to asynchronous cell in SCM to a final concentration of 2mM. Cells were incubated for 16 hours (37ºC, 5% CO_2) then washed in PBS and media replaced with SCM. Cells were cultured for a further 6 hours prior to the addition of Nocodazole [Sigma] at 100ng/ml. Cells were than incubated for 6 hours in Nocodazole prior to careful washing with PBS, so as not to dislodge mitotic cells. Cells were culture for 30 minutes following release from Nocodazole block prior to lysis.

2.2.3 Autophagy Flux

Cells from each condition assayed were either left in SCM or treated with lysosomal inhibitor E64D (10μg/ml) [Sigma] and Pepstatin A (10μg/ml) [Sigma] 2 hours prior to lysis. Cells were lysed with RIPA in standard manner and lysate quantified. LC3 II levels were examined by Western blotting and conditions compared with and without the addition of lysosomal inhbitors.

2.2.4 Agarose gel electrophoresis

Nucleic acid samples were analysed on agarose gels (0.8% - 2% agarose/TBE). Agarose was dissolved in 60 ml of 1x TBE buffer by boiling, prior to the addition of ethidium bromide (final concentration 0.5ug/ml). Each sample was mixed with 6x DNA loading buffer and loaded on to the gel. A DNA ladder of appropriate size (1kB DNA Ladder [Invitrogen] or 100bp DNA ladder [Promega]) was added for accurate size estimation of DNA. 120 volts were applied to resolve the nucleic acid fragments by size. A UV transilluminator was used to visualise the nucleic acids.

2.2.5 Restriction Digest and Purification

Plasmid DNA was digested with the appropriate restriction endonuclease in the buffer supplied by the manufacturer [NEB or Roche]. 1 unit of the enzyme is reported to digest 1μg of DNA over 1 hour but for these digests enzyme was used in excess. The digest was performed with 5μg of DNA (approximately 2μl), 20 U of the appropriate enzyme(s), 5μl of compatible buffer made up to 50μl with Nuclease free water and incubated for 1 hour at 37°C. For double digests the optimal buffer conditions were selected for both enzymes using the manufacturers' guidelines. Where blunting was required, 1μl dNTP (final concentration 10mM) and 1μl blunting enzyme were added and the DNA incubated for a further 60 minutes at 37°C.

DNA fragments produced by restriction digestion were resolved by agarose gel electrophoresis. The DNA fragment of interest was excised and purified using the QiaQuick Gel Extraction kit [Qiagen] as per manufacturers protocol. The DNA was eluted in 30μl elution buffer and used directly or stored at 20℃.

2.2.6 Site Directed Mutagenesis

2.2.6.1 Primers for site directed mutagenesis

Mutagenic primers for use in site directed mutagenesis were designed using the Quikchange Primer Design Program [Agilent]. The following considerations were made in the design algorithm: The primers were between 25 and 55 bases in length, with a melting temperature (Tm) of ≥78℃ (see below) and the desired mutation was located near the middle of the primer with a minimum of 10–15 bases of correct sequence on either side. The Tm of primers was calculated using the following formula:

$$Tm = 81.5 + 0.41\ (\%GC) - 675/N - \%\ \text{mismatch}$$

N is the primer length in bases and the values for percentage GC and percentage mismatch are whole numbers. The algorithm aimed for an optimal GC content of 40%.

2.2.6.2 Site directed mutagenesis (QuikChange Method)

Point mutations were introduced into plasmid vectors using the PCR based QuikChange [Agilent] method. In summary, two complimentary oligonucleotides containing the desired mutation were designed to anneal to the same sequence on opposite strands of the plasmid. The primers were extended by PCR generating a mutated plasmid. The PCR product is treated with DpnI; Dpn I endonuclease is specific for methylated DNA and was used to digest the parental DNA template, selecting for mutation-containing synthesized DNA. Almost all E. coli strains contain DNA that is dam methylated and therefore susceptible to DpnI digestion.

The PCR was composed as follows: 50 ng plasmid, 0.25 mM dNTPs, 0.2 μM mutagenic oligonucleotide primers (forward and reverse), 1 X DNA polymerase buffer with MgCl2 and 1.25U of PfuUltra DNA polymerase. Cycling parameters for site directed mutagenesis were as follows: 95°C for 30 seconds for 1 cycle followed by 95°C for 30 seconds, 55°C for 1 minute, 68°C for 1 minute/kb plasmid length for 18 cycles.

The PCR product was incubated with 1μl of DpnI restriction enzyme (10U/ul) [NEB] at 37℃ for 1 hour to digest parental vector DNA. Following incubation, 1μl of the DpnI treated DNA was used for transformation into DH5*α* E. coli chemically competent cells as described. Resulting colonies were cultured in LB broth, mini-prepped and screened by sequencing.

2.2.7 Ligation of Insert Into Vector

Ligations were performed using T4 DNA ligase [Roche]. Briefly, in 10ul reaction vector and insert DNA were added at a 3:1 insert to vector ratio (corrected for DNA size) such that approximately 2.5ul of vector DNA (100-200 ng), 1.5 ul of insert or control, 0.5 ul of DNA Ligase and 1x Ligation Buffer [Roche] were incubated for 5 hours at room temperature. Following incubation, 2μl ligation mixture was used to transform E. coli.

2.2.8 Transformation of chemically competent cells

Approximately 2µl of T4 DNA ligation reaction was added to 50µl of competent DH5α E Coli cells. Cells and DNA were incubated on ice for 30 min before heat-shock at 42 ℃ for 50 seconds. Following 2 minutes recovery on ice, cells were resuspended in 450µl of SOC media (preheated to 37ºC) and incubated at 37 ℃ for 50 minutes with agitation. 500µl of cells were spread onto LB agar plates containing the appropriate antibiotic(s). The plates were incubated overnight at 37 ℃ to produce discrete colonies. Subsequently, colonies were cultured in LB broth, mini-prepped and screened by sequencing

2.2.9 Fluorescence Activated Flow Cytometry (FAC)

The cells were pulsed with BrdU at a final concentration of 10 µM for 30 minutes (37ºC, 5%CO2). Cells were harvested by trypsinisation and transferred to a 15ml falcon tube. Cells were centrifugation at 1200 rpm for 4 minutes, washed once in PBS and then fixed by resuspending in 1 ml of ice-cold 70% ethanol, added drop wise on vortex. Cells were incubated for at least 1 hour at 4ºC or stored at -20 ºC. Cells were centrifuged at 2500 rpm for 4minutes and resuspended in 2mls of pre-warmed pepsin (37ºC) with incubation for 30 minutes at 37ºC. Cells were then centrifuged at 4000rpm for 4 minutes and resuspended in 1ml 2M HCL for 15 minutes at room temperature. Cells were washed twice in PBS-EDTA at final concentration 1mM prior to blocking with 1ml Antibody Buffer (49.5ml PBS, 1g BSA + 500µl 10% Triton X) for 30 minutes at room temperature. Cells were centrifuged and resuspended in 100 µl anti-BrdU (1:75 with antibody buffer) 30 minutes at room temperature. Cells were then washed with PBS-EDTA (1mM) and resuspended in 100µl anti-rat Alexa 488 (1:200 with antibody buffer) 30 minutes at room temperature. Subsequently cells were washed again with PBS-EDTA (1mM) and resuspended in PBS-EDTA containing 0.1mg/ml RNAse A and 50 µg/ml propidium iodide for 60 min at 4ºC in the dark. Cell sorting was performed on a FACScalibur by Elizabeth Freyer at MRC HGU.

2.2.10 Immunofluorescence Microscopy

Cells were plated on coverslips at $1x10^4$ cells/cm^2. At the time of sampling, media was removed and cells were fixed with 4% Paraformaldehyde (PFA) for 10 minutes at room temperature. Cells were washed with PBS and permeabilised with 0.25% Triton X-100 in PBS 20 minutes at room temperature. Cells were washed three times with PBS and coverslips blocked in 1% BSA in PBS for 10 minutes. Coverslips were incubated with appropriate primary antibody diluted in 1% BSA in PBS for two hours at room temperature in a humidified container. After washing three times for 5 minutes in PBS, coverslips were incubated with an appropriate secondary fluorophore-conjugated antibody (1:200) diluted in 1% BSA in PBS for 1 hour at room temperature in the dark. Secondary antibody was removed and coverslips washes three times for 5 minutes in PBS, prior to nuclear staining with DAPI (1:2500) for 10 minutes. Coverslips were mounted facedown onto Super Frost Plus microscope slides and stored at 4°C. In control staining, the primary antibody was omitted as a control for non-specific binding of the secondary antibody. Imaging was performed using an Olympus fluorescent/brightfield microscope.

2.2.11 Western Blotting

Protein expression and quantification was undertaken using sodium dodecyl sulphate polyacrylamide gel electrophoresis (SDS PAGE) resolution. Cells were lysed with lysis buffer (RIPA/NP40) and lysate protein quantified using the Micro Bicinchoninic Acid (BCA) [Thermo Fisher Scientific] protein assay kit as per manufacturers instructions. Absorbance was measured with a BP800 spectrophotometer at 562nm. 20μg of protein from each sample was made up to an equal volume with RIPA buffer prior to addition of 6 x SDS sample buffer. Alternatively cells were directly lysed with SDS sample buffer. Samples were denatured on the hot block at 95°C for 5 minutes and briefly centrifuged.

Samples were loaded for separation into either a precast Bio-rad (stain free gel) or by 10% SDS PAGE and run at 180V, 230mA and 30W for 60 minutes. The proteins were transferred from the gel to a PVDF membrane (activated

in 80% methanol) or a nitrocellulose membrane in DDB transfer buffer (20% methanol) at 100V 400mA 50W for 70 minutes. Alternatively the Bio-rad semi dry transfer method was used as per manufacturers instructions. 5µl of pre-stained molecular weight ladder was loaded into the first well of each gel to allow the molecular weight of the proteins species to be determined.

Membranes were blocked with 5% Marvel milk in TBST for 60 minutes with gentle agitation. Membranes were then washed 3 times in TBST (10 minutes per wash). Subsequently, membranes were probed with primary antibody in 2% BSA/TBST at appropriate concentrations (see table) at 4°C overnight, with gentle agitation. Antibody was removed and membranes were washed 3 times with TBST (10 minutes per wash). Mouse or rabbit HRP-conjugated secondary antibodies (1:5000) in 2% BSA/TBST were used for detection. Detection was by enhanced chemiluminescence (ECL protocol). 1ml of ECL solution (1:1 mixture solution A : solution B) was pipetted on to the membrane and incubated at room temperature for 1 minute. The membrane was exposed to blue-light sensitive autoradiography film. The film was developed using an AGFA Curix 60 processor. Membranes were then washed with TBST 4 times (5 minutes per wash). After washing membranes were re-probed with loading control primary antibody, alpha-tubulin (1/25000) in 2% BSA TBST as described above.

2.2.12 Silver Staining of protein gels

SDS PAGE gels were further analysed by silver staining using the ProteoSilver™Plus Silver Stain Kit [Sigma] as per the manufacturers instructions.

2.2.13 Wound Healing Assay

MDA-MB-231 cells were subject to CDK11 or NTC siRNA transfection as described in 2.2.1.1. At 28 hours post-transfection, cells were re-plated to obtain a confluent monolayer. At 40 hours post-transfection, the monolayer was wounded using a pipette tip. Wound healing was tracked with sequential image capture every 15 minutes for 12 or 15 hours on an Olympus microscope; images were acquired using scan^R software as per software

developer's instructions. Cell free area (mm^2) at the start and completion of the assay was calculated using Image J software.

2.2.14 Adhesion Dynamics Methods

2.2.14.1 Random Migration Assay

At 28 hours post-transfection, MDA-MB-231 cells were plated at low density. From 40 hours, cell migration was tracked with sequential image capture every 15 minutes for 12 hours on an Olympus microscope; images were acquired using scan^R software as per software developer's instructions. The migration of individual cells was subsequently calibrated using Image J software. Collated migration patterns of 30 MDA-MB-231 cells were mapped using Image J Chemotaxis and Migration Tool.

2.2.14.2 Cell Polarisation Assay

The wound-healing assay was replicated with the use of glass coverslips as substrate. At 40 hours post-transfection, the monolayer was wounded with a pipette tip. At specified time-points, cells were fixed, permeabilised and subject to immunofluorescence (as described above) with GM130 antibody (marking Golgi Apparatus), Phalloidin and DAPI. Polarisation was assessed at each time point. Cells were scored as polarized if the Golgi lay in a 90^o arc anterior to the nucleus, facing the wound edge. A minimum of 50 cells were assessed at each time and condition.

2.2.14.3 Cell Adhesion Assay

At 40 hours post-transfection, cells were trypsinised and placed in suspension for 1 hour at 4^oC with rotation, during which samples were obtained for preparation of protein lysates. At 1 hour, cells were plated on collagen coated cover slips or tissue culture plastic for subsequent immunofluorescence or protein lysate analysis, respectively. At specified time points, cells were washed and cells fixed or lysed accordingly. Protein lysates were analysed by Western Blotting as described previously.

2.2.15 Mutation analysis, sequencing techniques

2.2.15.1 Sanger Sequencing

Genomic DNA was used as a template for whole genome amplification using GenomiPhi V2 DNA Amplification Kit as per manufacturer's protocol. The amplicons encompassing the coding exons and the intronic splice junctions were designed using Primer3 (see below for oligonucleotide sequences). Target sequences were amplified by PCR (total volume 12µl) comprising: 20ng whole-genome amplified DNA (gDNA), 1 X ReddyMix Custom PCR Master Mix, 0.4 mM forward oligonucleotide and 0.4 mM reverse oligonucleotide with the addition of 1 X GC-rich Solution as required. A uniform PCR cycling protocol was performed: 95 °C for 5 minutes followed by 32 cycles of 94 °C for 1 minute, 58 °C for 1 minute, 72 °C for 1 minute and subsequently 72 °C for 10 minutes. PCR products were detected using agarose gel electrophoresis to ensure adequate quantity and size of each exon fragment. Bidirectional direct sequencing using the universal primers was performed using BigDye Terminator v3.1 Cycle Sequencing Kit and resolved on an ABI 3730 DNA Analyzer by the IGMM sequencing service. Sequence files were analysed with Mutation Surveyor v3.30. Cel1 enzymatic mutation detection assay was as described for endonuclease restriction digests.

2.2.16 Ion semiconductor sequencing

2.2.16.1 Preparing equimolar pool of short amplicons

Amplicons (36 amplicons) were pooled in equimolar quantities for Ion Library construction to ensure coverage of target regions. DNA target sequence of interest was amplified by PCR (≤250bp) from 20ng gDNA and the individual amplicons purified. The final amplicon solution was resuspended in Nuclease-free water. 1µl of each amplicon product was analysed with the Bioanalyser instrument and an equimolar pool of amplicon DNA was prepared in nuclease free water. 1µl of this pooled DNA was analysed using the Bioanalyser.

2.2.16.2 End repair and Purification of amplicons

The end-repair reaction (in a LoBind tube) consisted of 72µl of pooled short amplicons (50ng) in nuclease free water combined with 20ul of 5 x End

Repair Buffer and 1µl of End Repair Enzyme made up to a final volume 100µl with nuclease free water. This reaction was incubated for 20 minutes at room temperature.

The end-repaired DNA was purified with the Agencourt AMPure XP Kit. 180µl of Agencourt AMPure SP Reagent (1.8 x sample volume) containing beads was mixed with the DNA sample by pipetting, pulse spun and incubated at room temperature for 5 minutes. The mixture was then pulse spun and the magnetic beads precipitated using a magnetic rack. Supernatant was removed and beads washed in 70% ethanol twice. Beads were air dried at room temperature for 5 minutes. DNA was eluted from beads in 25µl of low TE and supernatant transferred to fresh LoBind Tubes.

2.2.16.3 Ligate Ion Xpress P1, Barcode the adaptors and nick repair

In 200µl PCR tubes, fragmented gDNA, short amplicons, 10X Ligase Buffer, Ion P1 adapter, Ion Xpress Barcode X, dNTP mix, nuclease free water, DNA ligase and nick repair polymerase were combined to a final volume of 100 ul as per manufacturer's protocol. The thermal cycle conditions were as follows: 25ºC for 15 minutes, 72ºC for 5 minutes and hold at 4ºC. The reaction was transferred to 1.5ml LoBind tubes before continuing directly to purification. The end-repaired DNA was purified with the Agencourt AMPure XP Kit, magnetic rack and fresh 70% ethanol as described above.

2.2.16.4 Amplifying and purifying the Amplicon library

Again in 200µl PCR tubes, Platinum PCR Supermix High Fidelity, Library Amplification Primer Mix, size-selected unamplified library and short amplicon unamplified library were combined as per manufacturers protocol to a final volume of 26µl. PCR was performed with 6 cycles of the following thermal cycle conditions: 95ºC for 5 minutes, 95ºC for 15 seconds, 58ºC for 15 seconds, 70ºC for 1 minute and held at 4ºC. The DNA library was purified with the Agencourt AMPure XP beads (1.5 x the sample volume) as above. The Bioanalyser was used to quantify the samples and samples analysed using Ion Torrent semiconductor sequencer by the IGMM sequencing service.

2.2.17 Preparing GST Fusion proteins

Glycerol stock of pGEX vector encoding GST.CDK11p58 in BL21 cells were inoculated into 10ml LB Broth and incubated for 1.5 hours at 37ºC with agitation. After 3 washes bead slurry (20µl) was diluted 2-fold with lysis buffer. IPTG was added (final concentration 1mM) and the mixture shaken for 2.5 hours at 30ºC. Ice was added to the culture before centrifuging at 3000rpm for 10 minutes. The lysate was kept cold to minimise degradation. The pellet was resuspended in 1ml of cold lysis buffer and transferred to 1.5ml tubes. The lysate was sonicated 3 times for 10 seconds and centrifuged in a tabletop microcentrofuge at maximum speed for 15 minutes at 4ºC. The supernatant was transferred into a 1.5ml tube with gluthione-sepharose beads and put on a rotator for 10 minutes at 4ºC. The tubes were spun briefly (3000rpm for 3 seconds) to pellet the beads. The supernatant was removed and discarded. The beads were washed 4 times with 800µl of cold lysate buffer.

2.2.18 Immunoprecipitation of GFP-fusion proteins

For one immunoprecipitation reaction, the cell pellet was resuspended in 200µl ice-cold NP40 lysis buffer by pipetting. The tube was placed on ice for 30 minutes with extensive pipetting every 10 minutes. The cell lysate was centrifuged at 20,000 x g for 10 minutes at 4°C. The supernatant was transferred to a pre-cooled tube and 750µl dilution buffer added. The GFP-Trap_A beads were equilibrated in dilution buffer by resuspending 25µl of bead slurry in 500µl ice cold dilution buffer and centrifuging at 2.500 x g for 2 minutes at 4°C. The supernatant was discarded and the beads washed twice more. The cell lysate was added to the equilibrated GFP-Trap_A beads and incubated on a rotator for 1 hour at 4ºC. The mixture was then centrifuged at 2500 x g for 2 minutes at 4ºC. The supernatant was discarded. The beads were washed twice with 500µl ice-cold dilution buffer and then frozen at –80ºC and sent on dry ice sent to collaborators at University College Dublin.

2.2.19 Nuclear and Cytoplasmic Extracts

Cells were washed twice in ice-cold PBS, lifted and suspended in 500µl ice-cold PBS. Cells were then centrifuged at 13000rpm for 1 minute and the supernatant discarded. Cells were resuspended in 400µl Buffer 1 by pipetting and incubated on ice for 15 minutes. 25µl of 10% NP-40 was added and the mixture vortexed for 10 seconds. Cells were centrifuged again at 13000rpm for 1 minute. The supernatant containing the cytoplasmic fraction was transferred to another tube and retained. 50µl of 0.5% NP40 buffer was added to the pellet and the mixture vortexed to mobilise the pellet. Samples were then incubated at 4ºC for 15 minutes with agitation. Samples were then sonicated in twice for 30 seconds, followed by centrifugation at 13000rpm for 15 minutes. The supernatant containing the nuclear fraction was transferred to a fresh tube and stored at –20ºC.

2.2.20 Fluorescence in situ hybridisation (FISH)

2.2.20.1 Zytolight Fluorescence in situ hybridisation (FISH)

Cells were cultured on glass slides. The Zytolight CEN probe protocol was followed; in brief, 10µl of ZytoLight CEN 7 or 8 probe was added onto each slide, taking care to avoid prolonged exposure to light. Coverslips were placed over each slide with the probe and sealed with a layer of rubber cement. Slides were then denatured at 75ºC for 10 minutes and transferred to a humidity chamber for hybridisation overnight at 37ºC in the dark. Slides were subsequently washed with reducing concentrations of SCC and counterstained with DAPI.

2.2.18.2 2D FISH Method

Cells were suspended in 0.5% Trisodium Citrate/0.25% KCl followed by fixation in Methanol:Acetic Acid (3:1). Cells were droppedSlides were incubated in 100 mg/ml RNase A in 2 x SCC for 1 hour, washed in 2 x SCC and dehydrated through an alcohol series. Slides were denatured in 70% Formamide/2 x SCC for 75 seconds at 70°C. Approximately 100ng of biotin- and digoxigenin-labeled fosmid probes were used per slide, with 10mg of mouse Cot1 DNA and 10mg salmon sperm DNA. Probes were denatured at 70°C for 5 minutes, reannealed with Cot1 DNA for 15 minutes at 37°C and

hybridized to the denatured slides overnight at 37°C. Slides were washed 4 times for 3 minutes in 2X SSC at 45°C, 4 times for 3 minutes in 0.1XSSC at 60°C and transferred to 4X SCC with 0.1% Tween20. Following incubation for 5minutes with blocking buffer (4X SCC with 5% Marvel) biotinylated probes were detected using fluorochrome-conjugated avidin (FITC or Texas Red) then biotinylated anti-avidin followed by fluorochrome-conjugated avidin. Digoxigenin-labeled probes were detected using FITC-conjugated anti-digoxigenin followed by FITC conjugated anti-sheep. Slides were counter-stained in 0.5mg/ml DAPI.

Table 2.1 Primers

CDK11 Sequencing Primers		
Exon	**Primer**	**Sequence**
1	Forward	TTTGGAGTCCTGGACCTGAG
1	Reverse	CAGTCGGAACTCACCCCTAC
1	Forward	TTTATGCGTCATCATCCCG
1	Reverse	CTCGGAAGAAAGACCTCGG
2	Forward	TGCTGTGTCCTGATGTAGGC
2	Reverse	GTTCTAATGGAAAAATGAGGGC
2	Forward	GCACCATAGCTTGCTGTGTC
2	Reverse	ATGGAAAAATGAGGGCAAAG
3	Forward	GGATGTTGCCCAGGTTTG
3	Reverse	ACAGTTGGGTCTTGCACATC
4	Forward	CACTTTCTCAAGCATGACGC
4	Reverse	GGGGAAGGCAGAAGAGTAGG
4	Forward	AATAGCCTGATGCTTTTCCG
4	Reverse	GCTTCTGTACCCCCTTCTGC

4	Forward	ATGACGCAGTGCTGTTGTG
4	Reverse	TTTTCAGTGGTGCTCTGGG
5	Forward	GAAGTGAGGTTTCTTTGCATGAC
5	Reverse	CACGGCCCTTTCATAAAGTC
5	Forward	TCATTAGGGAAGCATGCTAGAG
5	Reverse	GCCAAATTCTTCTTCATTGCTG
5	Forward	GATTACAGGCGTAAGCCACC
5	Reverse	AAGTCCTCAACTGACCCAGC
6	Forward	CTGTTTAGGGGGAATGATGGC
6	Reverse	CTGTGACAGCAAGTGCCCAGC
7	Forward	CTGCTAGTGCCATCTCCCTC
7	Reverse	AAGACTCACACTGTGCTGGC
8	Forward	CACTAGTTTTGGGGTGGTGG
8	Reverse	AGACAGCAGAGCAGAGGGTG
9	Forward	CAGGTTCACCCTCTGCTCTGC
9	Reverse	CACAACACCTCACACAGTCG
10	Forward	CCTCCATATCCATTCTTGGG
10	Reverse	CTCGGAGACAGACAAGGAGG
11	Forward	GATCCTTACTTACTCCTAGCTTCG
11	Reverse	CTCCTGCTTGAGCTCGATGG
11	Forward	AGTTCCAGAGTCACGGTTCG
11	Reverse	CCCTGTGGTAACTCCGACTG
12	Forward	TGTCAGATGGTTTTGCAAGG
12	Reverse	ACTCCATAGGTGCCCTCCTC
12	Forward	CACTGAGACCTCACACAGGC
12	Reverse	GTAGCTGCTCAGGTGAAGCG

13	Forward	AATGCCTCTCAGTGCCGTC
13	Reverse	GAGAGTGTAGGAAGCACCCG
13	Forward	ACCGTGACTTTGAGAATGCC
13	Reverse	GTCGGAAAAGCCTTCCACC
14	Forward	ACCGGAGGTCCTTACTGTCC
14	Reverse	AAGGGCTGTTTCATGGTCTC
14	Forward	CTGCAGGAGATTGTGGTGG
14	Reverse	AGAGGCTTCTCAGGGCTTTC
15	Forward	ACAGGGAAAGCCCTGAGAAG
15	Reverse	CAGCAGGTTGGACGTCTTG
15	Forward	GAAGACCCTGATGATCCAGC
15	Reverse	TTCAGAGGGGATCCGTACTC
16	Forward	ACCTCAAGACGTCCAACCTG
16	Reverse	TACCACTGGGTCACCACGAC
16	Forward	GAGTACGGATCCCCTCTGAAG
16	Reverse	CTAAGACGCCAGGAGAGGTG
17	Forward	TTGGTGCCAAGGTGAGTC
17	Reverse	GATCGATTTCCGAATTCCC
17	Forward	CGTGGACATGTGGTCAGTG
17	Reverse	TCCCGTCAGAGAAGACAAGC
18	Forward	CTTGGTGTGGCTGTTGAAGC
18	Reverse	ACTGGGAAGTCACCGCTATG
19	Forward	ACCACGTTCCAGAACTGCTC
19	Reverse	GAACATGGAGGGGTCGATGG
19	Forward	GCCTCAAGCATGAGTATTTCC
19	Reverse	CTCCTTCAGGTCGTCGTCAC

20	Forward	CATCGACCCCTCCATGTTC
20	Reverse	TGGTTCGTGGTGGTAAGGTG
20	Forward	GTTCTCACGGTAGCCGACTC
20	Reverse	AGTTCCGAGTCTCATCGCAG
20	Forward	CTGAAGGTCAGAGTGGACCC
20	Reverse	AGATGCCCTGGCAAGTCAC

SSU72 Sequencing Primers		
Exon	**Primer**	**Sequence**
1	Forward	GTAGCGCGACGGCCAGTGTGGAGTGCGGGTCTCTG
1	Reverse	CAGGGCGCAGCGATGACACCTGCCTTCCCTGTGATG
1	Forward	GTAGCGCGACGGCCAGTGACACCTTATGACGTCCTGTTG
1	Reverse	CAGGGCGCAGCGATGACGTATGCCGTGATTGTGTTGC
2	Forward	GTAGCGCGACGGCCAGTGCCCGGCCTAGATTAAAAAT
2	Reverse	CAGGGCGCAGCGATGACCAGGCTCCATGTGTATCAG
2	Forward	GTAGCGCGACGGCCAGTGCCCGGCCTAGATTAAAAAT
2	Reverse	CAGGGCGCAGCGATGACCACCAACCTGCAAAGGAAAT
3	Forward	GTCGCGCGACGGCCAGTCATCGCCCACTTTGTTTTCT
3	Reverse	CAGGGCGCAGCGATGACTGCTTCACACTCAGGTCTGC
3	Forward	GTAGCGCGACGGCCAGTGCTGTCCAGGCCTTCGTC
3	Reverse	CAGGGCGCAGCGATGACGAGAAAAGAGGCCCCTTGAA
4	Forward	GTAGCGCGACGGCCAGTTCAGGTTTCCTCGAACCATC
4	Reverse	CAGGGCGCAGCGATGACGTGCCAAAGCTGTGGAGTG
4	Forward	GTAGCGCGACGGCCAGTATTCATTGTGCTCCCCAAAC
4	Reverse	CAGGGCGCAGCGATGACGTGCCAAAGCTGTGGAGTG
5	Forward	GTA GCGCGACGGCCAGTCAGCTTCAGGTCCTGTGAGG

5	Reverse	CAGGGCGCAGCGATGACATTGCTTTCATCTGGCGTTT

Table 2.2 Antibodies

Target	Company	Product No	Source	WB	IHC
LC3	Novus	NB100-2220	Rabbit	1 in 1000	1 in 200
CDK11	Novus	NB100-1816	Rabbit	1 in 2000	1 in 200
CDK11	Abcam	AB19393	Rabbit	1 in 1000	1 in 200
CDK11	Abcam	AB113266	Rabbit	1 in 1000	-
CDK11	CST	D88B3	Rabbit	1 in 1000	1 in 200
CDK11	Bethyl	A300-310A	Rabbit	1 in 1000	1 in 200
CDK11	Bethyl**T**	A300-311A	Rabbit	1 in 1000	1 in 200
p62	Novus	2C11	Mouse	1 in 1000	1 in 200
Alpha tubulin	Invitrogen	DM1A	Mouse	1 in 25000	1 in 1000
BrdU	Abcam	AB6326	Rat		1 in 75 FACS
GFP-TRAP	ChromoTEK	GTA-30			
Pericentrin	Abcam	AB4448	Mouse	1 in 20000	1 in 2000
FAK	Transduction	610088	Mouse	1 in 1000	-
FAK	CST	3285	Rabbit	1 in 1000	1 in 100
CSK	Santa Cruz	SC-285	Rabbit	1 in 500	1 in 100
CSK	Santa Cruz	SC 51580	Mouse	1 in 1000	-
KIF14	Abcam	AB3747	Rabbit	1 in 3000	1 in 500
RAN	CST	4462	Rabbit	1 in 1000	1 in 100

Myc Tag (4A6)	Sigma	16-219	Mouse	0.5ug/ml IP	-
Myc Tag (9E10)	Pierce	88842	Mouse	0.5ug/ml IP	-
Src 36D10	Cell Signalling	2109	Rabbit	1 in1000	1 in 100
P-Src Y419	CST	2101S	Rabbit	1 in 1000	1 in 500
P-Src Y527	CST	2105	Rabbit	1 in 1000	-
Mouse HRP	Upstate	12-349	Goat	1 in 5000	-
Rabbit HRP	Upstate	12-348	Goat	1 in 5000	-
Alexa Fluor Secondary Ab	Invitrogen		Goat	-	1 in 200
p53	Neomarkers	MS-256-P0	Mouse	1 in 1000	-
HSP 90	Transduction	H38220	Mouse	1 in 1000	-
14-3-3e	Transduction	F46820	Mouse	1 in 1000	-
Cyclin L2	Bethyl	A301-667A	Rabbit	1 in 1000	-
Fyn (FYN3)	Santa Cruz	16	Rabbit	1 in 2000	-
c-Yes (F-7)	Santa Cruz	8403	Mouse	1 in 1000	1 in100
Cyclin D3 (C-16)	Santa Cruz	182	Rabbit	1 in 2000	-
Acetylated alpha Tubulin	Abcam	AB24610	Mouse	-	1 in 200
Paxillin	Transduction	610052	Mouse	-	1 in 200
GM130	Abcam	AB 52649	Rabbit	-	1 in 100

CHAPTER 3

CDK11, Autophagy and Mitosis

3.1 Introduction

This chapter describes work I undertook to investigate the effect of CDK11 dysregulation on autophagy flux. Initially, I characterized CDK11-mediated autophagy in human cancer cells; I proceeded to examine the influence of mitotic dysregulation on this autophagy phenotype. Finally, I interrogated the role of autophagy following aberrant mitosis and its putative influence in the maintenance of the aneuploid karyotype.

3.1.1 Autophagy

Autophagy is an evolutionarily conserved catabolic process through which cellular proteins and organelles are sequestered in double-membrane vesicles (autophagosomes) and targeted to lysosomes for degradation [151]. Basal autophagy executes an important homeostatic role in cellular functions but induction of autophagy also affords cells a remodeling mechanism under the influence of numerous stimuli [151, 152]. Recent evidence indicates that these autophagy processes are not generic but comprise a panoply of cellular remodeling conduits targeting specific organelles and proteins, regulated by diverse signaling pathways [152, 153]. This can lead to profound effects many of which may be germane to tumour cells, for example cell survival in response to metabolic stress, regulation of cellular senescence and regulation of cellular signaling [154-157].

Numerous proteins participate in the formation, passage and degradation of autophagosomes. LC3, the human analogue of Atg8, not only localizes to the autophagosome but plays a crucial role in its formation [158, 159]. As the autophagosome matures LC3 is converted to the lipid bound LC3 II; LC3 II has therefore become established as a gauge of autophagy [160]. Although considered a generic marker of autophagy, LC3 II is reported to contribute greatly to the selection of specific cargoes for autophagic degradation [159,

161]. It is thought to undertake this function through its Atg8-family interacting motif (AIM); this conjugates with adaptor molecules such as p62, Nbr1 and Ndp52 to enable the targeting of their specific cargoes to the autophagosome [159, 162, 163]. The interactions of these proteins are therefore critical to selective autophagy [159].

3.1.2 Aneuploidy

Aberrant mitoses are a significant cause of chromosomal instability and potential path to aneuploidy [164]. In health, aneuploidy is poorly tolerated but it is a common finding in cancer. The influence of aneuploidy on tumorigenesis has been controversial; while some argue that it performs a critical role in tumour formation, others suggest it is merely a consequence of deregulated growth [164]. Chromosomal instability may enable the genetic diversity that provides cancer cells with the capacity to overcome xenobiotic stress. Recent study in yeast found aneuploidy conferred certain strains with a greater resistance to a panel of chemotherapeutic and antifungal drugs compared to euploid strains [165].

Mechanisms act to restrain chromosomal instability so that in health, cells successfully maintain an invariable complement of chromosomes. Cell cycle controls and mitotic checkpoints act to prevent potentially aberrant segregation of chromosomes and the development of aneuploidy. Indeed, prolonged mitosis itself has been demonstrated to impede further proliferation despite both the completion of mitosis and the accurate segregation of the genome [166]. This has been shown to be due to a permanent G1 arrest dependent on p38 and p53 [166]. The influence of p53 in curtailing chromosomal instability has been reported in numerous recent studies; these demonstrate that chromosome missegregation causes the accumulation of p53 and retardation of growth [167, 168]. In contrast the absence of p53 permits the propogation of aneuploidy [169].

Aneuploidy itself conveys deleterious effects and is proposed to cause considerable metabolic stress [170]. The induction of aneuploidy in mouse embryonic fibroblasts, through the generation of individual chromosomal trisomies, leads to diminished proliferation and altered metabolism [170]. It

has been hypothesized that stoichiometric imbalance of cellular proteins may be a significant contributor to these effects [170]. Aneuploidy in yeast confers quantitative proteome alterations correlating closely to chromosome copy number [165].

Aneuploid cancer cells must therefore escape cell cycle constraints and cope with the consequential proteotoxic and metabolic stress. This presents a potential frailty in the aneuploid cancer cell that may be exploited therapeutically [171]. It is therefore critical to understand the mechanisms through which cancer cells evade aneuploid-induced stress. A recent publication identified numerous aneuploidy-tolerating mutations and demonstrated the importance of ubiquitin-proteasomal degradation in suppressing aneuploid-related adverse effects [172].

3.1.3 Autophagy and Aneuploidy

The role of autophagy in the aneuploid cell and its relationship to chromosomal instability is unclear. Based on the finding of greater genomic instability in cells deficient in autophagy gene *Beclin1*, it has been reported that autophagy may suppress tumour progression by limiting chromosomal instability [173]. Autophagy has also been proposed to enable transition to cellular senescence following oncogenic stress [174]. However, autophagy may be employed to mitigate proteotoxic stress by the removal and degradation of excess imbalanced proteins in aneuploid cells.

3.2 Characterisation of CDK11-mediated autophagy

This work aimed to characterize the autophagy response to CDK11 knockdown. The capacity of CDK11 to influence autophagy was first identified in this laboratory. MDA-MB-231 breast carcinoma-derived cells were used for initial experiments, as these cells were the first human cells in which the CDK11-mediated autophagy response was described [149]. This followed its identification in a drosophila siRNA kinome screen utilizing S2 cells. In subsequent work, I have demonstrated that the response is not unique to these cells but occurs in a variety of human cancer cells of different origin.

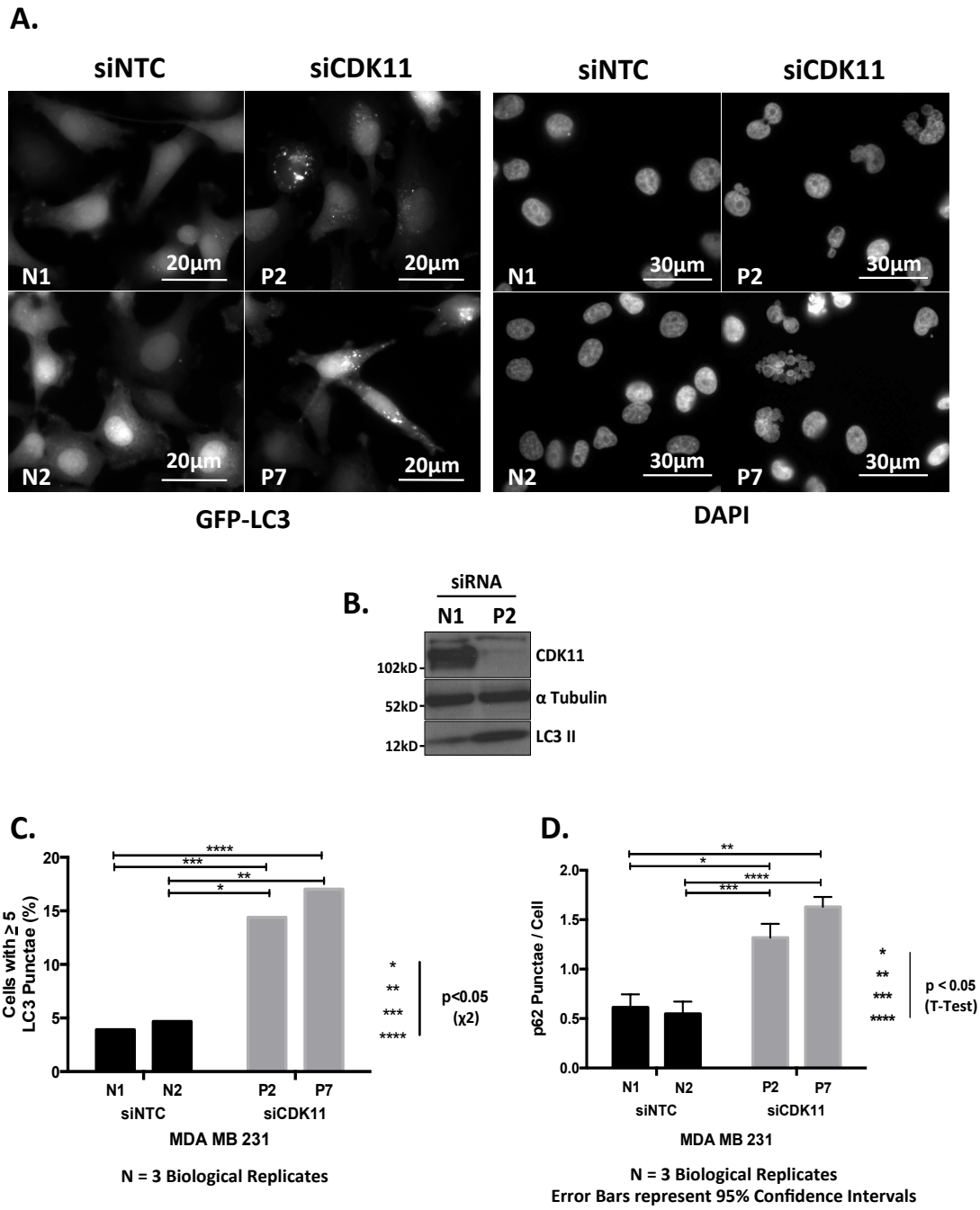

Figure 3.1 CDK11 Knockdown and Autophagy. MDA-MB-231 or MDA-MB-231 GFP-LC3 cells were transfected with CDK11 siRNA (P2 + P7) or non-targeting control (N1 + N2). ***3.1A*** At 72 hours following transfections, MDA-MB-231 GFP-LC3 cells demonstrate accumulation of GFP-LC3 puncta and nuclear dysmorphology following CDK11 siRNA. ***3.1B*** Western Blot of MDA-MB-231 cell lysates at 72 hours demonstrates knockdown of CDK11 with associated accumulation of LC3 II. ***3.1C*** At 72 hours following transfection MDA-MB-231 GFP-LC3 cells demonstrate significant accumulation of LC3 puncta, with and significantly greater proportion of cells demonstrating ≥ 5 LC3 puncta following CDK11 siRNA. ***3.1D*** demonstrates a significantly greater mean number of p62 puncta per cell following CDK11siRNA (Represents replicate experiments N=3)

I performed transfection of MDA-MB-231 cells with distinct CDK11-targeted and non-targeting control siRNA. At 72 hours following transfection, the population of cells subject to CDK11 knockdown demonstrated increased autophagy marker LC3 II on western-blot and increased LC3 puncta on immunofluorescence when compared to the control population [Fig. 3.1]. In addition, a significant increase in p62 puncta was observed following CDK11 knockdown [Fig. 3.1]. p62 is a signaling adaptor protein reported to regulate the aggregation of polyubiquitinated proteins and their subsequent clearance through autophagy pathways [175]. It interacts with LC3 II and cytoplasmic puncta of p62 have been shown to accumulate in autophagy deficient cells [176]. The accumulation of p62 puncta following CDK11 knockdown provides further indication of dysregulated autophagy pathways. Further analysis revealed a marked association between LC3 and p62 puncta [Fig. 3.2]. Due to the different immunofluorescence protocols necessary to optimize detection of LC3 and p62, MDA-MB-231 cells expressing a GFP-tagged LC3 fusion protein were used to assess the relationship. Approximately 75% of cells demonstrating accumulation of LC3 puncta also showed accumulation of p62 puncta. However, confocal microscopy did not demonstrate clear co-localisation of LC3 and p62 cytoplasmic puncta [Fig. 3.2]. While LC3 puncta were considered to represent autophagosomes, the p62 puncta were considered to represent polyubiquitinated aggregates.

Quantification of LC3 II protein levels and cellular LC3 puncta are static parameters of dynamic autophagy pathways. Interpreting these measures alone is insufficient to fully appraise the state of autophagy within the cell [177-180]. Autophagy flux assays are required to determine whether the observed accumulation of autophagy components is a result of increased production or reduced clearance, i.e. whether autophagy is induced or inhibited. I performed a standard autophagy flux assay that demonstrated an inhibition of autophagy at 72 hours following CDK11 knockdown [Fig. 3.2]. This was consistent with the accumulation of p62 puncta observed, which are ordinarily cleared through autophagy pathways. This result correlated with published findings demonstrating an initial induction of autophagy, followed by inhibition at later time points after CDK11 depletion [149].

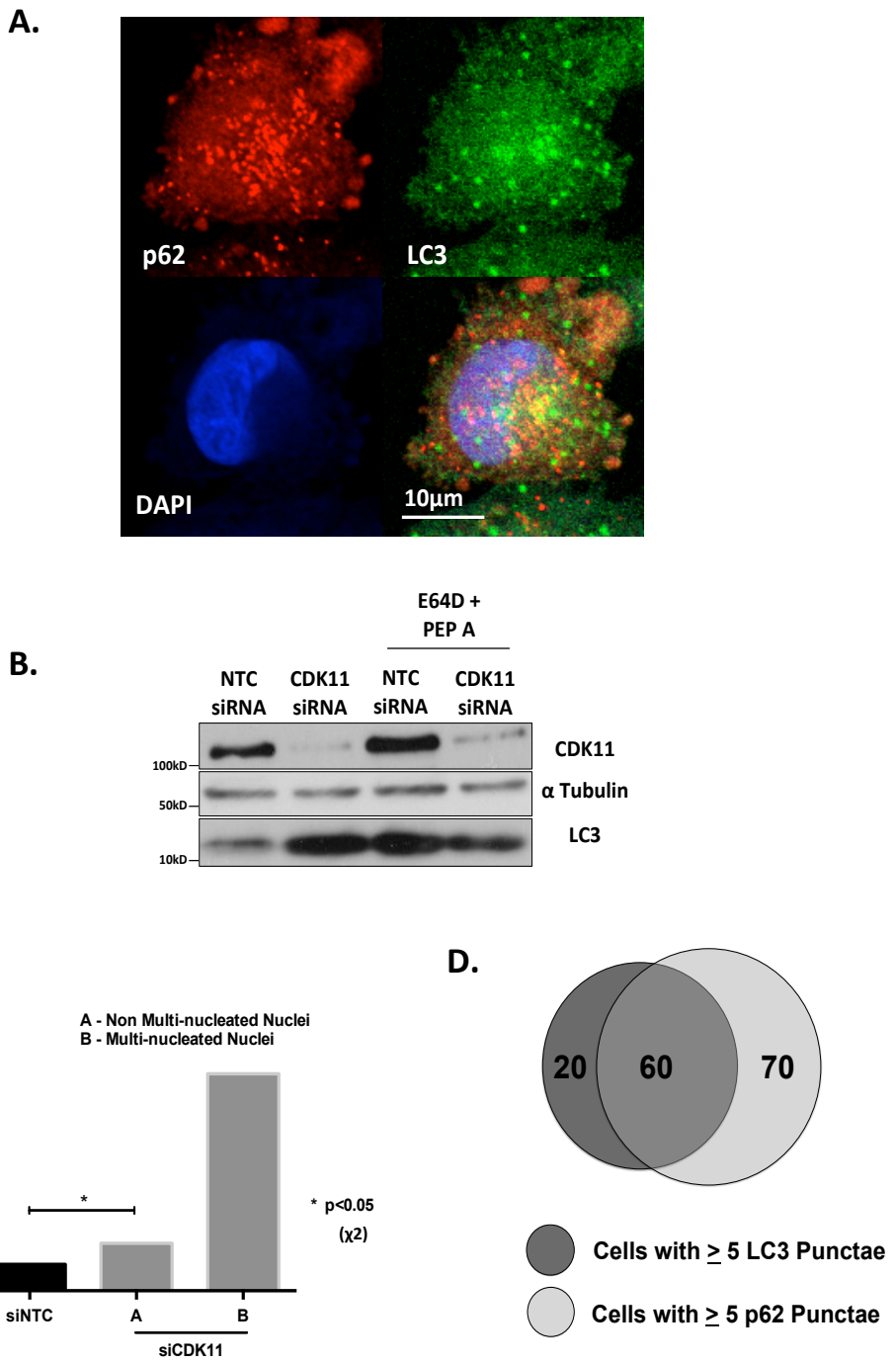

Figure 3.2 MDA-MB-231 cells transfected with CDK11 siRNA (P2 + P7) or NTC siRNA (N1 + N2). ***3.2A*** At 72 hours following CDK11 knockdown, there is a significant accumulation of both LC3 and p62 in cells. ***3.2B*** Autophagy flux assay with lysosomal inhibitors E64D and Pepstatin A demonstrates that at 72hours following transfection with CDK11 siRNA, there is no further accumulation of LC3 II; LC3 II in contrast accumulates significantly in the siNTC control cells. This is considered indicative of reduced autophagy flux following CDK11 siRNA. ***3.2C*** demonstrates a significant association between multinucleation and LC3 punctation, with the multinucleated cells observed to convey the greatest proportion of cells with LC3 accumulation. ***3.2D*** demonstrates significant overlap between LC3 and p62 cellular responses (defined as ≥ 5 puncta per cells) in MDA-MB-231. ***3.2C+D*** represent the cumulative results from 3 biological replicate experiments.

Furthermore, elevated numbers of grossly aberrant nuclei, defined by the presence of multi-nucleation or micronuclei, were observed. This was consistent with the described features of mitotic dysregulation after CDK11 depletion [25]. On analysis, a greater proportion of multinucleated cells displayed elevated LC3 puncta compared to cells with normal nuclei [Fig. 3.2]. This indicated a correlation between anomalous mitosis and altered autophagy. However, this did not determine an association between the two processes, as these two phenotypes may merely co-exist as a manifestation of more profound CDK11 depletion. In addition, as the level of LC3 puncta after CDK11 depletion in cells without disrupted nuclear morphology was also elevated, albeit not to the same extent [Fig 3.2C], these multinucleated cells do not fully explain the elevated LC3 puncta observed after CDK11 knockdown.

CDK11 inhibition resulted in a reduction in cell numbers at 72hrs post-transfection [Fig. 3.3]. On staining with propidium iodide, no increase in the sub-G1 population was observed, indicating this was primarily due to reduced proliferation rather than cell death. The absence of enhanced cell death at this time point, determined by sub-G1 population, did not support alteration in apoptosis secondary to CDK11 knockdown. Furthermore, the inhibition of autophagy flux observed was inconsistent with CDK11-mediated autophagy contributing to an alternate 'autophagic' cell death. A defining characteristic of autophagic cell death is enhanced autophagy flux, although the existence of autophagic cell death is debated [181, 182]. Cell cycle analysis revealed a greater proportion of cells with *4n* DNA content following CDK11 inhibition [Fig. 3.3]. This was due both to an increase in the proportion of cells in mitosis and the failure of cells to undergo cytokinesis, with the acquisition of a tetraploid karyotype. These data correlate with, and extend, previous findings demonstrating the influences of CDK11 on mitosis and autophagy.

3.3 The role of mitosis in CDK11-mediated Autophagy

The roles of CDK11 in the regulation of mitosis, apoptosis, splicing and transcription have been established but demonstrating its effect on

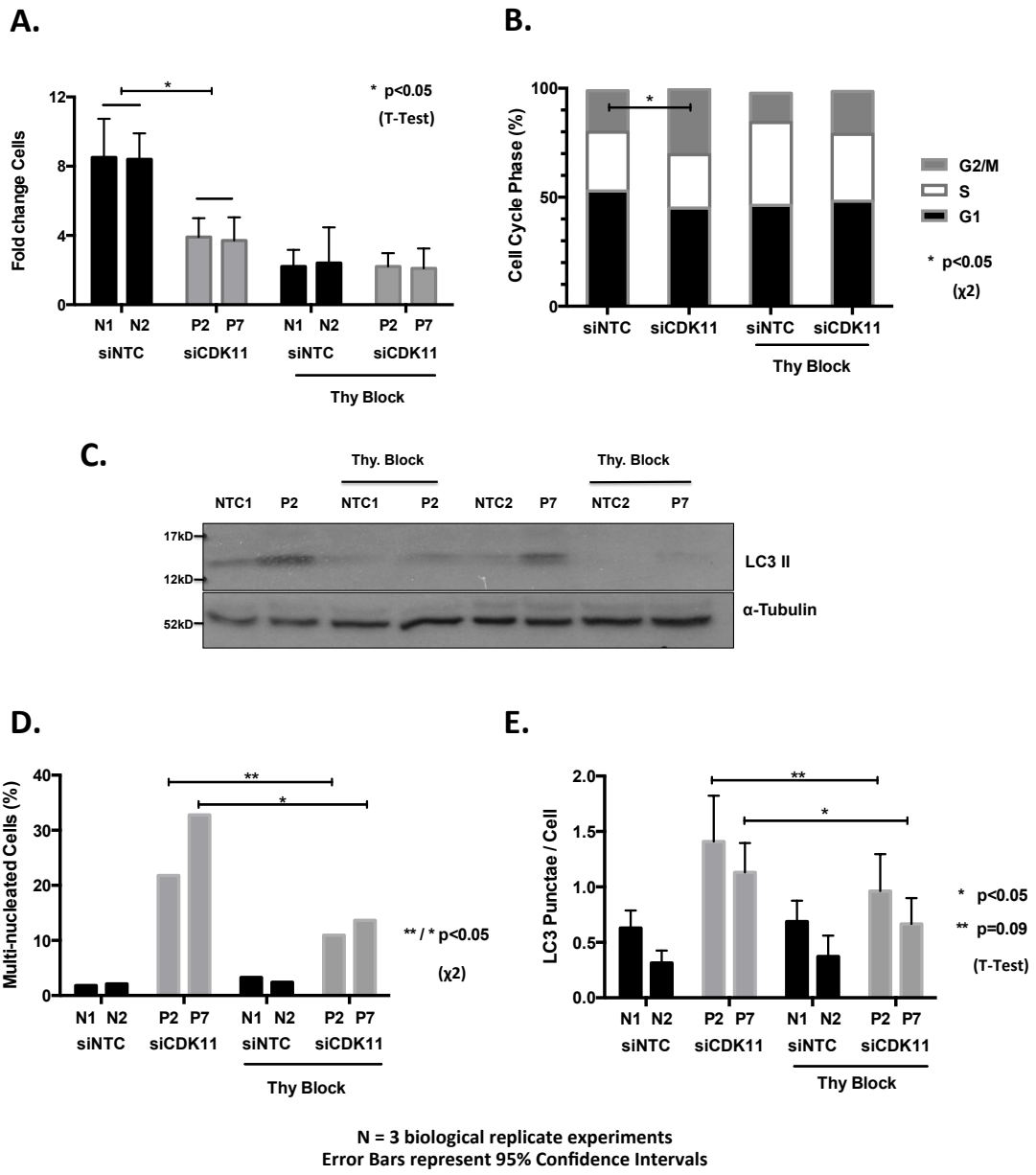

Figure 3.3 CDK11 Knockdown, Autophagy and Cell Cycle Inhibition. MDA-MB-231 cells transfected with CDK11 siRNA (P2 + P7) or NTC siRNA (N1 + N2) then cultures in SCM or SCM + Thymidine 2mM. ***3.3A*** At 72 hours, cell counts were undertaken; this demonstrates a significant reduction in cell number following CDK11 siRNA. This is further reduced with addition of thymidine (Thy. Block) (N=3). ***3.3B*** At 72 hours, cells were methanol fixed, permeabilised and stained with Propidium Iodide. Flow cytometric analysis was undertaken, with live cells selected and gated according to DNA content into 2N representative of G1, 4N considered representative of G2/M and intermediate content representative of S Phase. Graph shows the proportion of cells at each stage in the cell cycle. This demonstrates a greater proportion of cell with 4N karyotype subsequent to CDK11 knockdown. ***3.3C*** demonstrates Western blot accumulation of LC3 II following CDK11 siRNA that is reduced with the addition of thymidine. ***3.3D*** demonstrates a reduction in both multinucleated cells and mean LC3 puncta per cells with the addition of thymidine to prevent cell cycling (N=3).

autophagy was novel. I aimed to elucidate the mechanisms underlying CDK11-mediated autophagy and to determine whether this occurred due to direct mediation of autophagy pathways or indirectly through disruption of recognised CDK11 functions. Therefore, I attempted to determine whether the effects of CDK11 depletion on autophagy could be dissociated from its other roles. As described, a compelling correlation exists between aberrant mitoses and perturbed autophagy and this finding determined the course of subsequent investigations. Several approaches were employed to determine whether mitotic dyregulation could be separated from the autophagy response or whether the two processes were related.

3.3.1 CDK11 Inhibition and Cell Cycle Blockade

To investigate mitotic influences on the autophagy response after CDK11 depletion, MDA-MB-231 cells were transfected with CDK11 and non-targeting siRNA. Cells were then cultured either in the presence or absence of thymidine; thymidine excess blocks DNA synthesis resulting in the accumulation of cells at the G1/S boundary. This was undertaken to assess the effect of cell cycle blockade on the autophagy phenotype following CDK11 knockdown, on the rationale that inhibiting proliferation will limit any influence of mitotic dysregulation on the autophagy.

I found that addition of thymidine diminished the elevation of LC3 II observed after CDK11 knockdown [Fig. 3.3], although did not result in its complete abrogation. Cell counts and propidium iodine staining demonstrated that thymidine block successfully reduced cell proliferation, although without complete cell cycle blockade. A significant reduction in both aberrant nuclei and LC3 puncta was observed [Fig. 3.3].

To further examine the contribution of aberrant mitosis to the autophagy phenotype, MDA-MB-231 cells were synchronized using a double thymidine block following transfection with CDK11-targeted or non-targeting siRNA [Fig. 3.4]. Three days post-transfection, cells were released from thymidine block and sampled at 0, 3, 6, 9 and 12 hours following release. This demonstrated elevated LC3 II protein levels and p62 puncta following CDK11 knockdown, with a marked increase in these parameters as cells

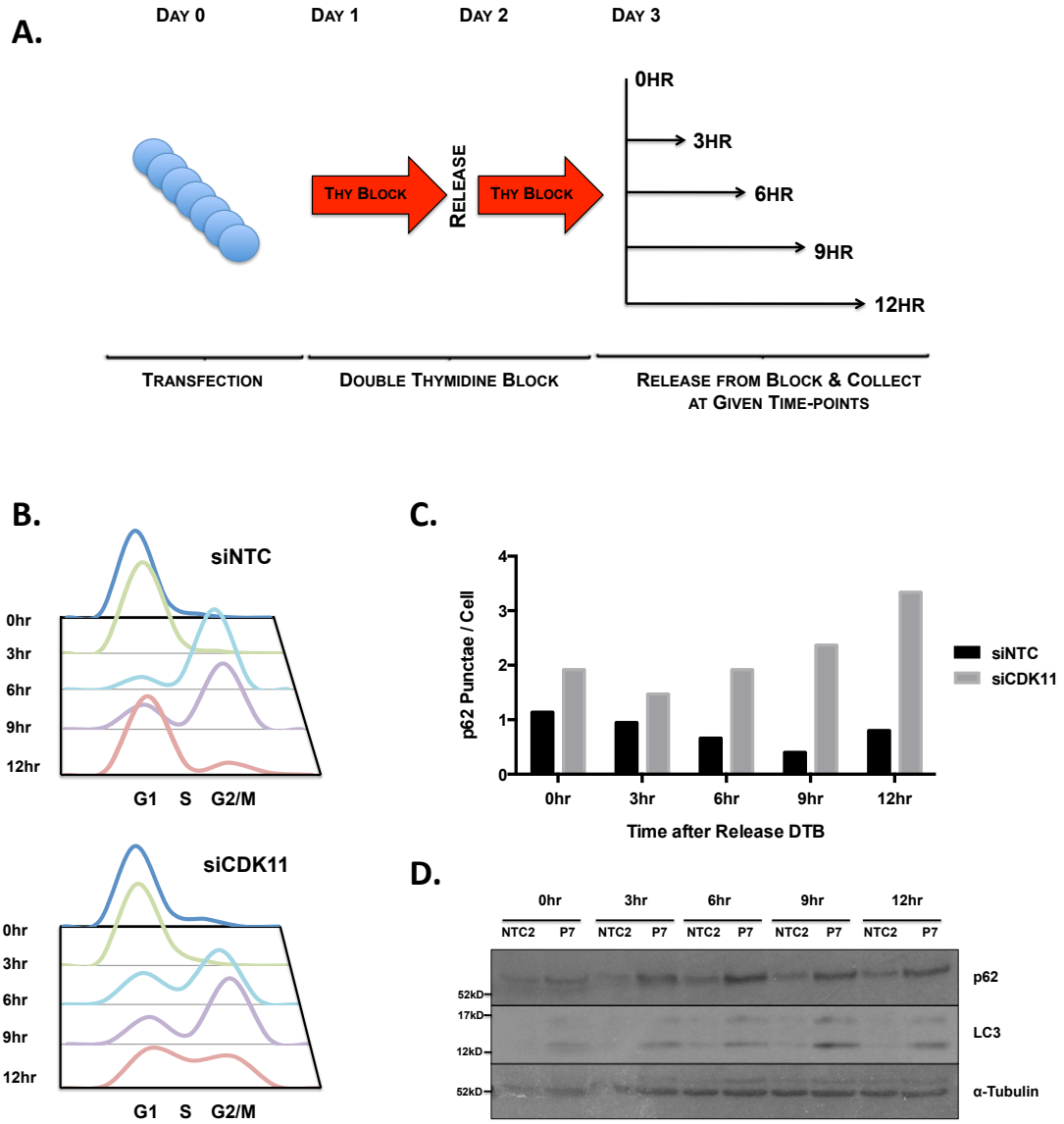

Figure 3.4 CDK11 Cell Cycle Analysis. MDA-MB-231 Cells were transfected with CDK11(P7) or NTC (N2) siRNA, with subsequent cell cycle synchronization employing double thymidine block. On day three, cells were released from block and assayed at specified time points as as protocol ***3.4A***. ***3.4B*** Cells at specified time point and condition, underwent Propidium Iodide staining as described with subsequent flow cytometric analysis. This demonstrates the cellular DNA content and is therefore indicative of cell cycle stage. This demonstrates that at both CDK11 and NTC siRNA transfected cells undergo mitosis at 6 to 9 hours following release. Subsequent to CDK11 siRNA, a greater proportion of cells following retain 4N karyotype. ***3.4C*** graphs the elevation in mean discrete p62 puncta per cell, demonstrated on passage through mitosis following CDK11 knockdown, with a minimum 100 cells counted per condition. ***3.4D*** Western Blot of sample buffer lysates from specified time points and conditions. There is elevated LC3 II punctuation following passage through mitosis, with marked increase at 9 hours and 12 hours. (N=1)

underwent mitosis between 6 and 9 hours [Fig. 3.4]. Furthermore, at 12 hours following release, there remained a greater proportion of cells with a tetraploid chromosome complement following CDK11 knockdown. These findings indicated either failure to exit mitosis or exit of mitosis with failure of cytokinesis.

These results implicated mitotic dysregulation in the autophagy phenotype observed after CDK11 depletion, indicating alterations in autophagy flux occurred secondary to aberrant mitoses. The single thymidine block demonstrated that limiting proliferation limits the autophagy response without an effect on the level of CDK11 depletion. The double thymidine block assay demonstrated a temporal correlation between passage through mitosis and altered autophagy flux [Fig 3.4]. These experiments provide evidence to indicate autophagy dysregulation occurs as a result of mitotic dysregulation after CDK11 depletion.

3.3.2 Plk1 Inhibition

Polo-like Kinase 1 (Plk1) is a serine/threonine kinase known to regulate mitosis [183]. During mitosis, it is integral both to spindle formation at the centrosome and to the regulation of centromeric chromosome cohesion [183-186]. Consequently, both CDK11 and Plk1 regulate similar mitotic processes [83]. Specific inhibitors of Plk1 exist and are being trialed in the treatment of metastatic cancer [187, 188]. To examine whether autophagy dysregulation could be induced with inhibition of another mitotic kinase, MDA-MB-231 cells were treated with Plk1 Inhibitor BI 2536. At 48 hours following treatment with either 10nM or 100nM BI 2536, there was an increase in LC3 puncta, p62 puncta and LC3 II [Fig. 3.5]. Furthermore, aberrant nuclear morphology was prevalent among cells. Indeed, this was more exaggerated following Plk1 inhibition than following CDK11 depletion, with the majority of cells demonstrating multi-nucleation. The induction of a similar disturbance in autophagy after inhibition of another mitotic kinase supports my earlier findings, indicating that alterations in LC3 II expression and LC3 puncta are influenced by mitosis.

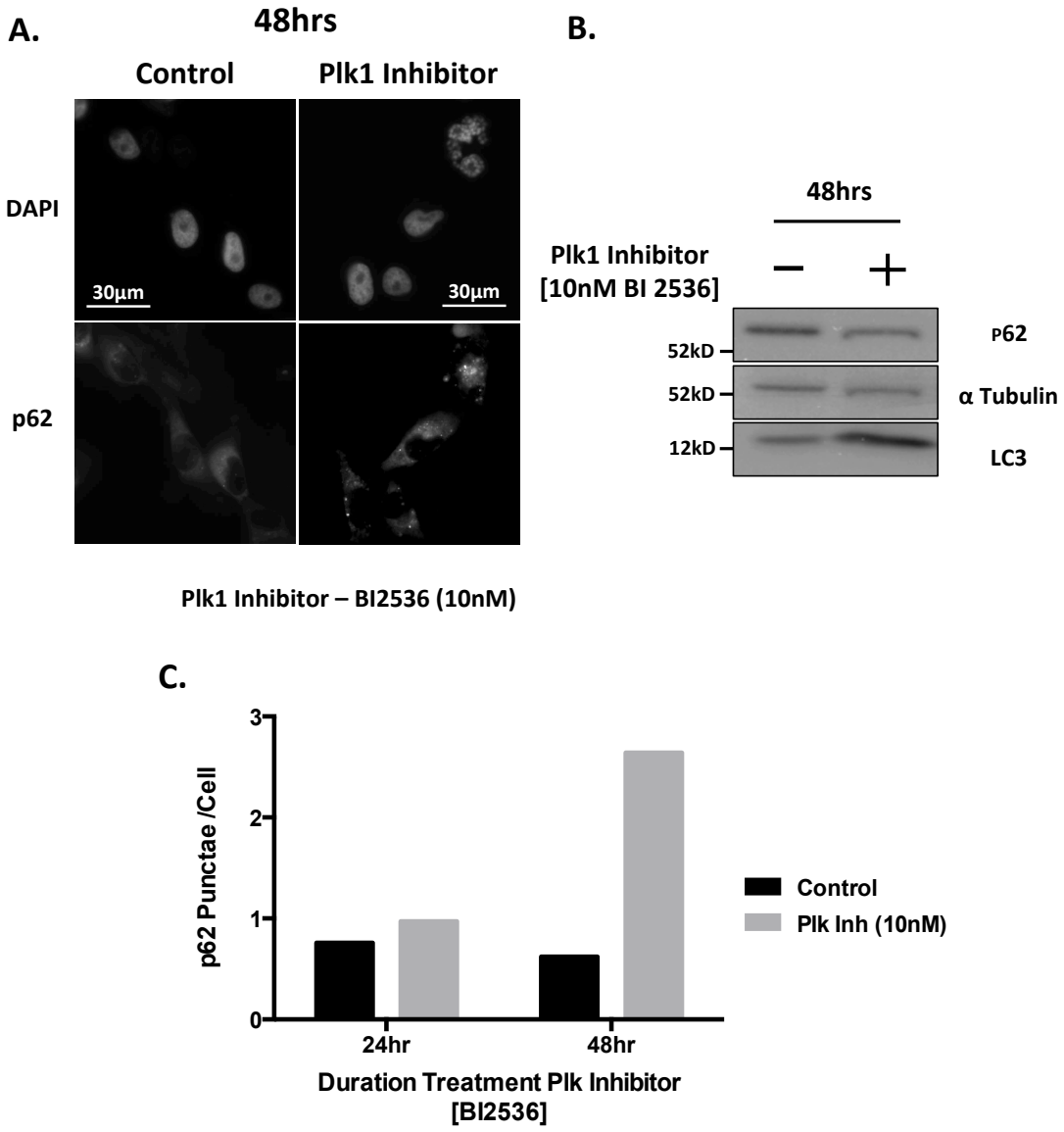

Figure 3.5 Plk1 Inhibitor Assays. MDA-MB-231 cells were cultured in the presence of Plk1 Inhibitor (BI2536) [10nM] for 24 hours or 48 hours. ***3.5A*** constitutes representative images demonstrating the accumulation of p62 puncta and nuclear dysmorphology at 48 hours following addition of BI2536 to media. ***3.5B*** demonstrates the accumulation of LC3 II on Western blot following treatment with BI2536; there is no significant increase in p62 protein despite the accumulation of p62 puncta. ***3.5C*** charts the accumulation of p62 puncta at 48 hours following administration of Plk1 Inhibitor.

3.3.3 CDK11 'Rescue' Constructs

To elucidate the isoform required for autophagy regulation, I aimed to 'rescue' the autophagy phenotype by introducing the different CDK11 isoforms, with RNAi-refractory cDNA sequences. The primary established function of endogenous CDK11p58 is the regulation of mitosis, with reports that its native expression is limited to mitosis [21, 25]. If aberrant mitoses and autophagy dysregulation caused by CDK11 depletion are linked, CDK11p58 should rescue both phenotypes. However, if CDK11p58 rescued the mitotic but not autophagy phenotype, it would indicate that the two functions could be dissociated. Furthermore, this work had the potential to demonstrate the specificity of siRNA CDK11 knockdown, if knockdown phenotypes were rescued with the reintroduction of RNAi-refractory sequences.

Therefore, mutagenesis of cDNA encoding either CDK11p58 or CDK11p110 was undertaken to introduce synonymous mutations that rendered the sequences refractory to siRNA (P2) degradation. In addition, the myc-tag was inserted 5' to CDK11 sequences to allow identification of the fusion proteins. The resulting constructs were inserted into the pBabe vector and the vectors transduced into MDA-MB-231 cells, utilizing retroviral phoenix ecotopic cells. Stable expression of myc.CDK11p58 or myc.CDK11p110 fusion protein was achieved, with transduction of the empty vector acting as a control. Probing for myc-tag on Western blot and immunofluorescence confirmed expression of both proteins, although heterogeneous in each cell population (data not shown).

MDA-MB-231 cells expressing either myc.CDK11p58, myc.CDK11p110 or empty vector were transfected with CDK11 siRNA (P2) to determine whether either protein rescued the observed phenotypes. Following CDK11 knockdown, LC3 II accumulation was observed in cells containing the empty vector alone [Fig 3.6]. In cells expressing either myc.CDK11p58 or myc.CDK11p110, the LC3 II accumulation was abrogated, indicating rescue of the autophagy phenotype [Fig 3.6]. There was also rescue of the aberrant nuclear morphology and the accumulation of p62 puncta with both proteins, although only partially with the myc.CDK11p110 protein [Fig 3.6].

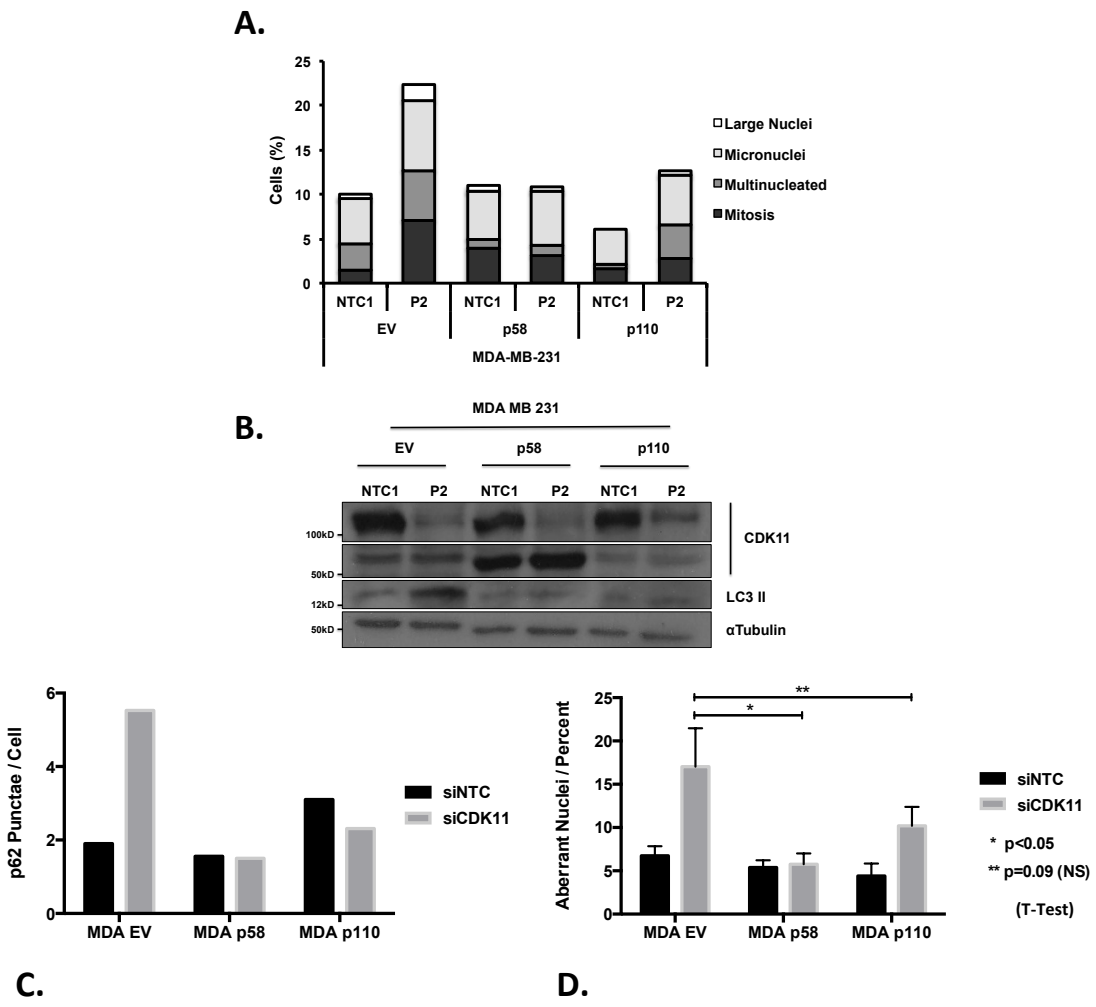

Figure 3.6 CDK11 Rescue Assay. MDA-MB-231 cells were transduced with empty pBabe vector (EV) or vector containing siRNA-refractory CDK11p58 or CDK11p110 constructs. These cell lines were then transfected with CDK11 (P2) or NTC (N1) siRNA. At 72 hours post-transfection cells were fixed and stained with DAPI and p62. Graph ***3.6A*** demonstrates the nuclear phenotype of cell populations; this shows rescue of mitotic phenotypes with both CDK11p58 and CDK11p110 constructs (Minimum 200 cells counted). ***3.6B*** Western Blot demonstrates CDK11 knockdown and rescue with RNAi refractory constructs; there is rescue of LC3 II accumulation. ***3.6C*** demonstrates rescue of p62 puncta accumulation and ***3.6D*** demonstrates rescue of aberrant nuclear morphology by CDK11 constructs (Minimum 200 cells counted / Nuclear morphology experiments N=3). Error bars represent 95% confidence intervals.

This work demonstrated that both the mitotic and autophagy phenotypes could be rescued with CDK11p58. Although this does not prove a relationship between mitotic dysregulation and altered autophagy flux, it again provides evidence of their association. The rescue of autophagy by myc.CDK11p58, following CDK11 knockdown, definitively established that the C-terminus of the protein is required for regulation of both autophagy and mitosis. It did not determine that rescue of these two phenotypes occurred by the same mechanism although this appears likely. Moreover, although it is the p58 isoform that regulates mitosis, my work demonstrated that the myc.CDK11p110 fusion protein was also capable of partial mitotic rescue after native CDK11 depletion. This may have occurred due to a functional IRES region within the myc.CDK11p110 protein, from which the p58 isoform could be translated.

Interestingly, CDK11 knockdown did not lead to a reduction in native CDK11p58 on Western blot in MDA-MB-231 cells transduced with vector alone [Fig 3.6]. The CDK11 siRNA targeted a sequence common to all transcripts and should have depleted both CDK11 isoforms. On account of its size and its migration with myc.CDK11p58 fusion protein on Western blot, this species likely represented CDK11 rather than non-specific signal. Probing with myc antibody did not indicate contamination with the RNAi-refractory p58 construct. An explanation may be that although there was no marked reduction in endogenous CDK11p58; this isoform is primarily expressed during mitosis. I demonstrated an approximate five-fold increase in the cells in mitosis (1.5% v 7.2%) following CDK11 knockdown [Fig 3.6A]. Therefore, although overall a similar quantity of protein was present, the number of mitotic cells expressing CDK11p58 was greater and the expression in individual cells reduced.

Furthermore, I found that the expression of the myc.CDK11p110 fusion protein was lower compared to expression of the myc.CDK11p58 protein. Therefore despite its expression, it was not possible to fully rescue CDK11p110 protein levels following siRNA, or the resultant phenotypes. I was unable to generate cells expressing high levels of myc.CDK11p110 but this was not a unique finding as it has been reported by other laboratories

[23]. Certainly MDA-MB-231 cells did not tolerate strong exogenous CDK11p110 expression.

3.3.4 Live Cell Time Lapse Imaging

The ability to track individual cells over an extended period has the potential to determine whether a direct association exists between anomalous mitoses and alterations in autophagy flux following CDK11 knockdown. It may also identify whether there were subsets of cells that have not undergone aberrant mitoses but show an autophagy phenotype after CDK11 depletion. Live cell time-lapse microscopy with the use of fluorescent-tagged proteins allowed me to address this and was therefore undertaken.

MDA-MB-231 cells were transduced with a retroviral vector that expressed Green Fluorescent Protein (GFP)-tagged Histone H2B with a puromycin resistance cassette to allow selection. Histone H2B.GFP localized to the chromatin structure of DNA and enabled visualization of individual chromosomes during mitosis. Following selection with puromycin, a second retroviral vector expressing Cherry-tagged p62, was transduced to track p62 response; cells expressing Cherry.p62 were selected with blastocidin.

MDA-MB-231 cells stably expressing both Cherry.p62 and H2B.GFP were transfected with CDK11-targeted and non-targeted siRNA. Initially, I confirmed that Cherry.p62 and H2B.GFP behaved in a similar manner to endogenous proteins (data not shown). Immunofluorescence confirmed that these cells display p62 puncta and multinucleation following CDK11 knockdown at a similar frequency to my previous experiments. Likewise, these findings were absent in controls confirming the fusion proteins behaved appropriately.

Unfortunately despite attempts to optimize the system, live-cell tracking using fluorescence microscopy failed to produce reliable results. The duration of microscopy and the frequency of laser exposure to monitor mitosis may have resulted in photo-toxicity [189], which could influence autophagy pathways. This work confirmed that the aberrant nuclear architecture observed after CDK11 depletion occurred due to mitotic

dysregulation. This was expected and consistent with published finding [25]. However using live cell imaging, I was unable to definitively determine that alteration in autophagy flux occurred only after mitotic dysregulation.

Using the Cherry.p62 H2B.GFP MDA-MB-231 cells, I investigated the fate of cells demonstrating both grossly aberrant nuclear morphology and altered autophagy flux after CDK11 knockdown. If these cells fail to proliferate, their contribution to tumour growth and evolution would be limited as they could not propagate their genomic rearrangements caused by mitotic dysregulation. It was therefore important to establish whether these multinucleated cells could re-enter the cell cycle and proceed to cell division.

Following either siRNA CDK11 knockdown or Plk1 inhibition (BI 2536), MDA-MB-231 cells, expressing H2B.GFP and Cherry.p62, were plated at low density. The position of multinucleated cells was recorded and these cells tracked for a period of 3 weeks. Although many of these multinucleated cells remained viable for this period in culture, there was no evidence that they re-entered the cell cycle and formed colonies. Therefore although these multinucleated cells may contribute to the tumour micro-environment, based on this assay they do not appear to replicate.

3.3.5 Conclusion

This work provides evidence that dysregulation of mitosis causes the autophagy phenotype observed after CDK11 depletion. CDK11 has roles in other cellular processes, including transcription and splicing, and there may be other influences on the autophagy response, including direct mediation. However, my work indicated that the predominant contributor to CDK11-mediated autophagy is mitotic dysregulation. It remained unclear whether this is the case for the subset of cells demonstrating altered autophagy but with no nuclear dysmorphology. These cells may be more relevant to tumour biology than the multinucleated cells that do not appear to proliferate. Further work was required to establish whether these cells had also undergone aberrant mitosis or whether other mechanisms underlie their autophagy response. The work described below further interrogated this question.

3.4 Autophagy and Chromosome Mis-segregation

Preceding work in this chapter indicated aberrant mitoses are a cause of CDK11-mediated autophagy. I aimed to investigate what mediated this mitotic dysfunction-induced autophagy. Published studies indicate autophagy may be of importance to the propagation of aneuploid karyotypes [190, 191]. Certainly, published evidence indicates the requirement for protein degradation pathways in the propagation of aneuploid clones and demonstrates the sensitivity of trisomic clones to the autophagy / lysosome inhibitor, chloroquine [192]. However if autophagy is engaged during the acquisition or propagation of aneuploidy, its roles remain unclear. I opted to investigate whether chromosome mis-segregation could induce autophagy and if so the consequence of this autophagy response. Dissociating the influence of discrete mediators is challenging; chromosome mis-segregation requires mitotic dysregulation with the potential for confounding influences. To address this from an alternate perspective, I also aimed to investigate the consequences of autophagy disruption on the acquisition and propagation of aneuploidy.

MDA-MB-231 cell are constitutively aneuploid, limiting their usefulness in the study of chromosome mis-segregation. Therefore, I elected to use the pseudo-diploid colorectal cancer-derived HCT116 cells to examine the influence of chromosome mis-segregation on autophagy. HCT116 cells are pseudo-diploid, which enables monitoring of karyotypic variation. For this reason, HCT116 cells have been used in numerous studies interrogating chromosomal mis-segregation and the acquisition of aneuploidy [167, 193].

3.4.1 Characterisation of CDK11-mediated Autophagy in HCT116

First, I aimed to determine whether depletion of CDK11 in HCT116 cells replicated the mitotic and autophagy phenotype previously observed in MDA-MB-231 cells. Furthermore, this would enable confirmation that CDK11-mediated autophagy was not unique to a single cell type. HCT116 cells were transfected with CDK11-targeted and non-targeted siRNAs. Similar effects were observed on the autophagy marker LC3, with elevated LC3 II evident on Western blots and increased LC3 puncta visible by

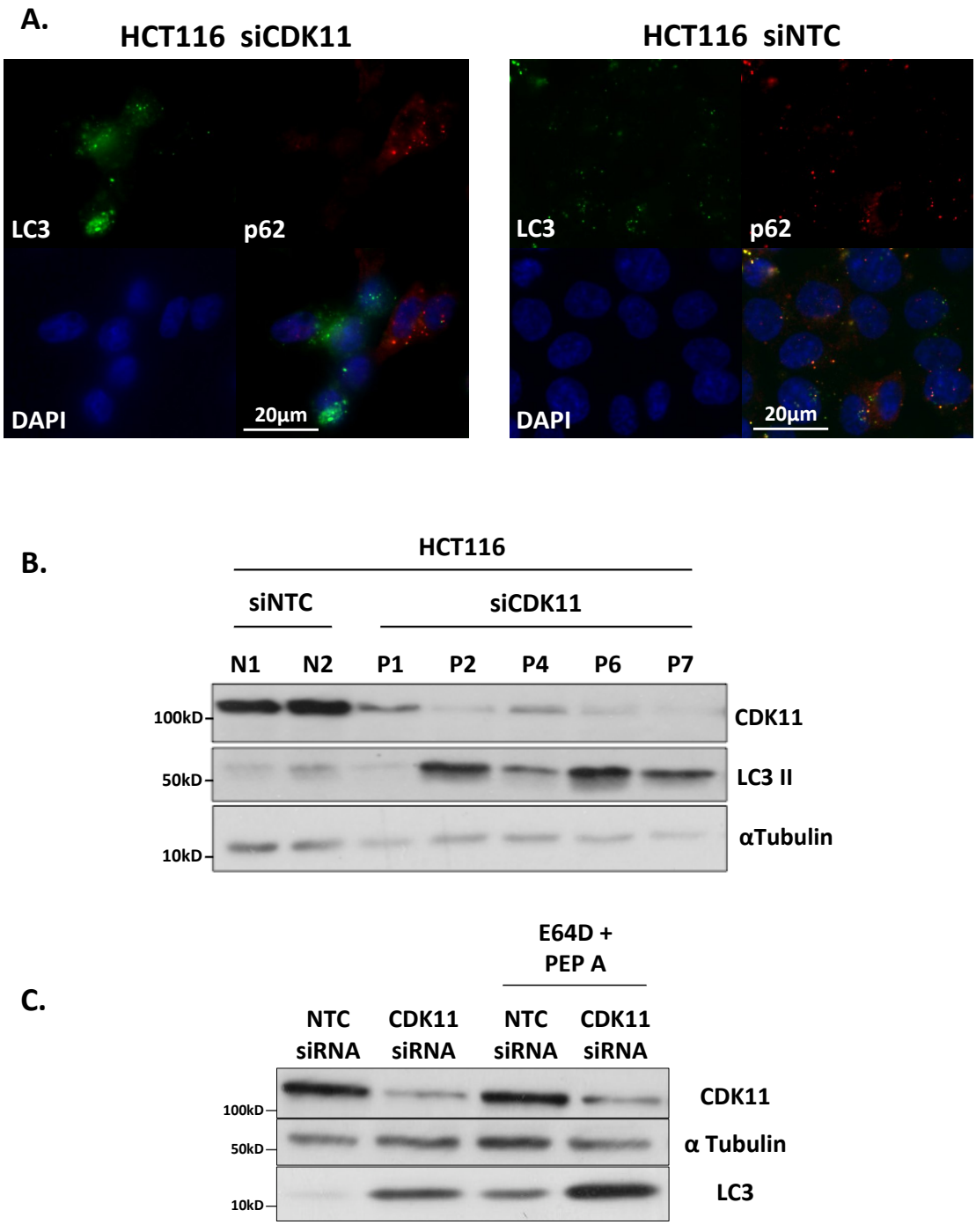

Figure 3.7 HCT116 CDK11 Knockdown Phenotype. HCT116 cells were transfected with CDK11 siRNA (P1, P2, P4, P6, P7) and NTC siRNA (N1 + N2). At 72 hours cell were fixed, permeabilised and stained with DAPI, LC3 and p62 antibody. ***3.7A*** demonstrates the accumulation of LC3 puncta on representative immunofluorescence images following CDK11 knockdown. ***3.7B*** demonstrates elevated levels of LC3 II on Western blot of cell lysates associated with reduced CDK11 protein expression. ***3.7C*** demonstrates that LC3 II continues to accumulate following CDK11 knockdown and with the addition of lysosomal inhibitors; this is indicative of continued autophagy flux and overall enhancement of autophagy.

immunofluorescence [Fig. 3.7]. Interestingly, there was no associated increase in p62 puncta, as observed in MDA-MB-231 cells [Fig 3.8]. I investigated whether other signaling adaptor proteins Ndp52 or Nbr1, also involved in selective autophagy, were engaged in CDK11-mediated autophagy in the HCT116 cell line. There was no evidence of increased Ndp52 or Nbr1 puncta or colocalisation with LC3 (data not shown).

At 72 hours following CDK11 knockdown, autophagy flux assays in HCT116 cells demonstrated that autophagy was not inhibited and LC3 II accumulated at a similar rate to control cells; this was consistent with the absence of p62 puncta [Fig. 3.7]. This differed from the response observed in MDA-MB-231 cells. However as discussed, autophagy flux is induced in the MDA-MB-231 cells at earlier time-points and it is only subsequently that autophagy is suppressed [149]. Wilkinson et al. (2011) proposed that, after initial stimulation of autophagy, suppression occurred due to inundation of autophagy pathways, as the necessary components are consumed and depleted [149]. It may be that this does not occur in the HCT116 cells or that it occurs at later time points.

Furthermore, although there was an increase in aberrant nuclei post-transfection, the proportion of cells demonstrating nuclear dysmorphology was markedly reduced in comparison to the MDA-MB-231 cells [Fig. 3.8]. The reason for this difference was unclear but may have contributed to the difference in autophagy flux described above. HCT116 cells are pseudo-diploid and therefore retain mechanisms to suppress chromosomal instability, including a functional p53 [167, 168]. This may impact on their tolerance of mitotic dysregulation and alter cell fate with induction of cell death rather than mitotic slippage. However, I found no increase in apoptosis to support this in the HCT116 cells at 72 hours following CDK11 knockdown.

Therefore, after CDK11 depletion, HCT116 cells displayed a greater proportion of cells with normal nuclear morphology but altered autophagy. It was important to establish whether dysregulated mitosis occurred in cells with normal nuclear morphology; if not, an alternate mechanism may

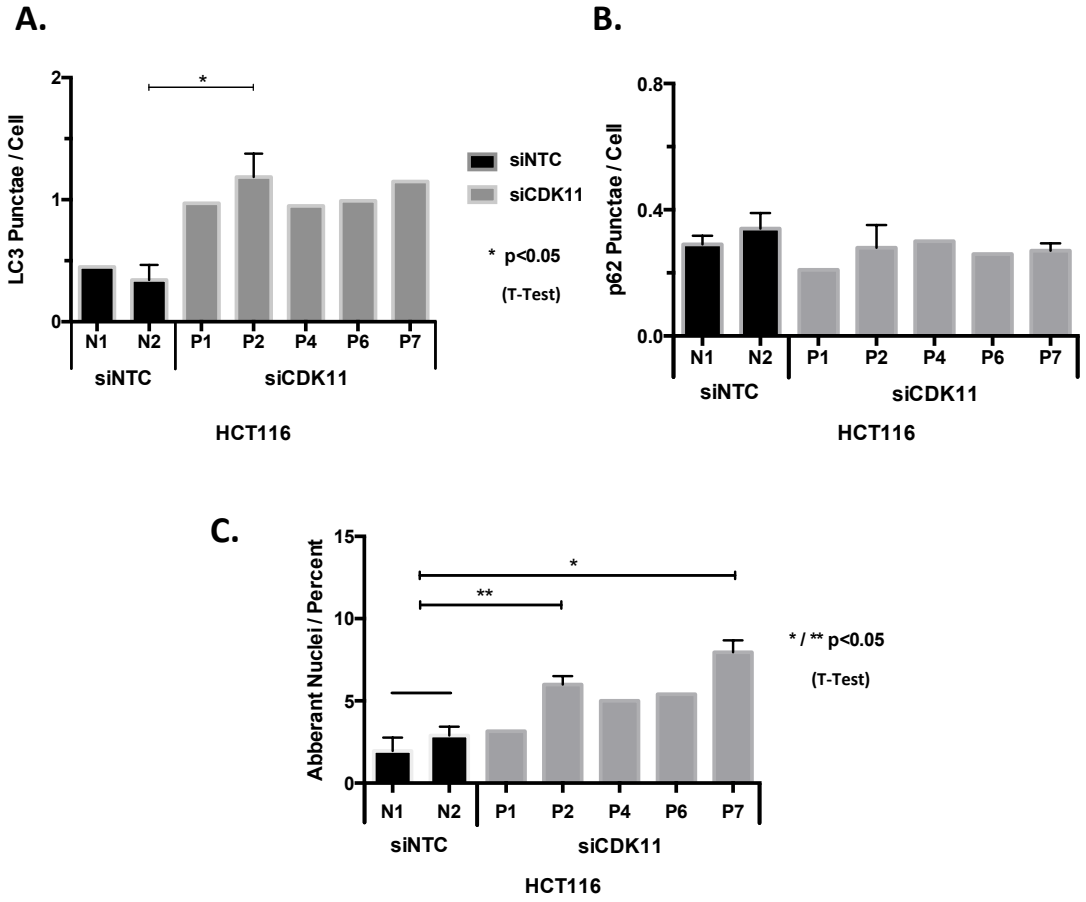

Figure 3.8 HCT116 CDK11 Knockdown Phenotype 2. HCT116 cells were transfected with CDK11 siRNA (P1, P2, P4, P6, P7) and NTC siRNA (N1 + N2). At 72 hours cells were fixed with 10% PFA, permeabilised with methanol and stained with DAPI, LC3 and p62. ***3.8A*** HCT116 cells demonstrate increased LC3 punctation following CDK11 knockdown. ***3.8B*** HCT116 cells do not demonstrate elevate p62 punctation unlike the MDA-MB-231 cell line. ***3.8C*** There remains a greater proportion of cells demonstrating nuclear dysmorphology following CDK11 knockdown, however this less than previously observed with MDA-MB-231. Error bars represent 95% confidence intervals (Experimental repeats N=3)

underlie their autophagy response. This would enable dissociation of the autophagy and mitotic phenotypes in HCT116 cells.

3.4.2 Imaging of mitosis in HCT116 following CDK11 inhibition

HCT116 cells were transduced with H2B.GFP, enabling observation of mitosis. HCT116 cells stably expressing H2B.GFP were selected and subsequently transfected with CDK11-targeted or non-targeting control siRNA. From 48 hours to 72 hours post-transfection, time-lapse microscopy was performed to interrogate the duration and accuracy of mitosis. I found that the average length of mitosis was significantly greater after CDK11 depletion, despite the resultant interphase cells exhibiting few nuclear anomalies [Fig. 3.9]. Furthermore, there was an increase in aberrant mitoses, with lagging chromosomes or more profound chromosome mis-segregation occurring in a significantly greater proportion of cell divisions [Fig. 3.9]. Again, these cells often demonstrated no visible nuclear dysmorphology following dysfunctional mitoses. Although this did not establish that mitotic dysregulation induced altered autophagy, it did demonstrate that mitotic dysregulation occurs despite the reduced nuclear dysmorphology in HCT116 cells. This indicated mitotic dysregulation may also contribute to the autophagy phenotype in cells with normal nuclear architecture.

3.4.3 Assessing chromosome missegregation and autophagy

To address whether chromosome mis-segregation influenced autophagy, I investigated whether there was a correlation between chromosome mis-segregation and autophagy after CDK11 knockdown. To determine chromosome content and evidence of mis-segregation, fluorescence in-situ hybridisation (FISH) chromosome marking was performed. I aimed to use FISH in conjunction with immunofluorescence to examine both chromosome number and LC3 puncta. I aimed to determine whether an association existed between increased LC3 puncta and abnormal chromosome content, after CDK11 depletion. To undertake this work, I attempted to refine immuno-FISH protocols to optimise both LC3 signal and chromosome marking. FISH was performed using chromosome probes or paints (paints comprise composite probe pools designed to hybridise larger regions of the

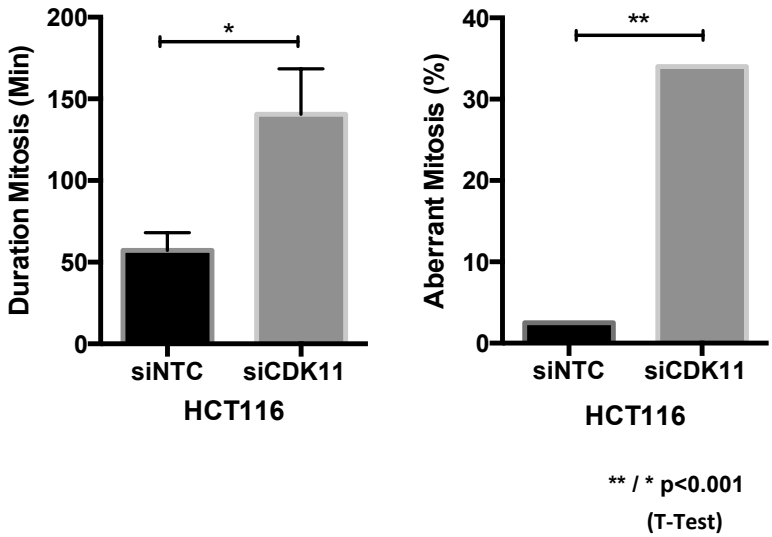

Figure 3.9 HCT116 Time-lapse Mitosis. HCT116 cells were transduced using the retroviral vector pBabe GFP.H2B; cells with successful integration of the construct were selected with puromycin. Subsequent to selection, the HCT116 GFP.H2B cell line was plated in 6-well plates and transfected with CDK11 or NTC siRNA. At 48 hours post transfection, plates were transferred to a humidified incubation chamber on a fluorescent Olympus microscope. Scan^R software was used to acquire sequential images every 5 minutes for 24 hours. The duration of mitosis was determined from the onset of prometaphase to the completion of anaphase. Evidence of lagging chromosomes or other missegregation events were recorded. Cells were noted to endure prolonged mitosis and increased missegregation events following CDK11 knockdown (minimum 60 cell division counted).

chromosome). Unfortunately, staining with chromosome paints proved too diffuse in interphase to allow accurate counting of chromosomes. In contrast, the signal from individual chromosome locus probes was too weak to reliably determine chromosome number. However, chromosome probes targeting alpha satellite regions within the pericentric heterochromatin were effective. Unfortunately, the staining protocols to enable FISH caused disruption of LC3 staining, limiting accurate assessment. Therefore, despite immuno-FISH proving unsuccessful, I was able to optimise of chromosome enumeration using the pericentric probes.

3.4.4 Inducing chromosome missegregation with Monastrol

Due to the technical limitations described above, I was not able to determine a specific association between CDK11-mediated autophagy and chromosome mis-segregation, despite the correlation with mitotic dysregulation being evident. Resolving the influence of chromosome missegregation and aberrant mitoses remained challenging, as a degree of mitotic dysregulation is required to induce chromosome missegregation. To address this question, stringent temporal regulation of mitotic inhibition was required to induce chromosome mis-segregation while limiting mitotic catastrophe or slippage, which may make results difficult to interpret. There were no commercially available inhibitors of CDK11 and no other specific inhibitors described in the literature. CDK11 knockdown with siRNA lacked the temporal control required and therefore alternate approaches were necessary to induce chromosome mis-segregation.

Protocols have been developed to derive stochastic chromosome mis-segregation using mitotic inhibitors [105, 194]. Monastrol is an inhibitor of the motor protein kinesin Eg5, a protein that co-locates with the mitotic spindles, playing a critical role in spindle dynamics and accurate cytokinesis [195, 196]. Pulsed treatment with monastrol causes cells to stall in mitosis, precipitating the formation of merotelic chromosomal attachments with subsequent chromosome mis-segregation on release from inhibition. Transient monastrol treatment has been used to induce chromosome mis-segregation and interrogate the acquisition of aneuploidy [167, 168]. Other

mitotic inhibitors, such as nocodazole, have similar effects but published work has demonstrated that Monastrol is more efficient at eliciting mis-segregation [168].

3.4.5 Monastrol Induced Missegregation and Autophagy

Using pulsed monastrol treatment of HCT116 cells, I aimed to determine whether there was altered autophagy following chromosome mis-segregation. Two approaches were adopted to enrich for mitotic cells and enhance detection of any response. The first strategy was to perform a mitotic shake-off following 9 hours of monastrol (100μM) treatment; control cells were treated with an equal concentration of the monastrol solvent DMSO (10μl/ml) prior to mitotic shake-off. Cells were then plated on glass slides and fixed at specified time-points. This strategy did not demonstrate a significant difference in LC3 II or LC3 puncta between control cells and monastrol-treated cells [Fig. 3.10]. However, both control and monastrol-treated cells demonstrated increased LC3 II and LC3 II puncta. Whilst the cause of this was uncertain, mechanical stress at mitotic shake-off may have engaged autophagy [197].

The second strategy was to synchronise the cells at the G1/S boundary via double thymidine block. Cells were then released from block and after 6 hours treated for a further 8 hours with monastrol or DMSO control. Slides and lysates were collected at specified time intervals after washout. With this approach, the cell cycle distribution of control and monastrol-treated cells was different, due to the monastrol-induced mitotic block. Nonetheless, it was not possible to detect a difference in autophagy markers between control and monastrol-treated cells [Fig. 3.10]. Furthermore, autophagy flux assays were performed at 12 hours following monastrol/DMSO washout. These assays did not demonstrate consistent alteration in autophagy flux after monastrol treatment. Therefore, these experiments failed to detect altered autophagy that could be attributed to monastrol treatment. Control cells in these experiments did demonstrate high background LC3 signal not observed in previous experiments. The reason for this effect is not clear but it may have masked any alteration in autophagy elicited by monastrol

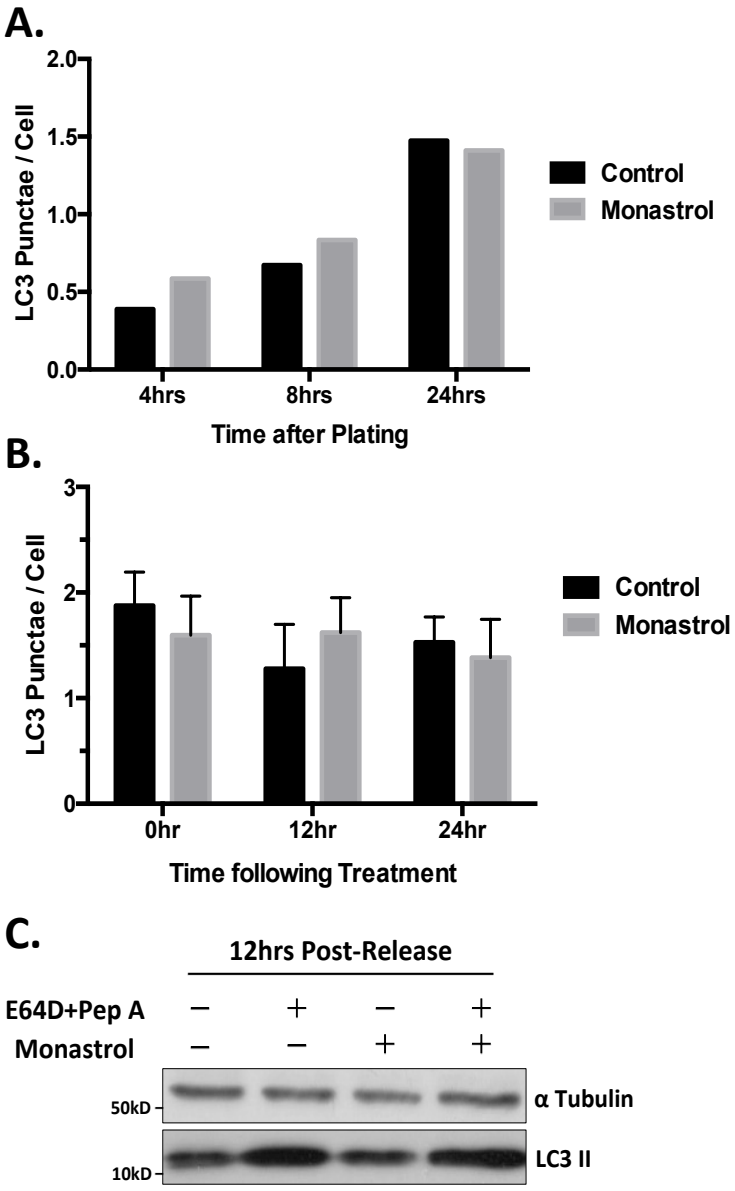

Figure 3.10 Monastrol Treatment and Autophagy. To interrogate an association between chromosome missegregation and autophagy, HCT116 cells were treated with Monastrol to induce mitotic merotelic spindle attachments and precipitate subsequent chromosome missegregation. To enrich for mitotic cells two strategies were employed. In the first, HCT116 cells were treated for 8 hours with Monastrol or DMSO control prior to mitotic shake off; additional control plates were required to compensate for the lower percentage of mitotic cells. Cells were subsequently plated on glass coverslips and slides fixed, permeabilised and stained for LC3 at predetermined time-points. ***3.10A*** No difference between control and Monastrol cells was observed, although LC3 punctation increased in both cohorts at 24 hours following plating. In the second, cells were synchronized at G1/S; at 6 hours following release cells were treated with Monastrol or DMSO for 8 hours. Lysates or coverslips were obtained at given time-points for analysis. ***3.10B*** No significant difference in LC3 punctation was observed between conditions (Technical replicates N=3 / Error bars represent 95% CI). ***3.10C*** No difference in autophagy flux was observed between treatments at the 12-hour time-point.

treatment. Additionally, there are reports of autophagy induction following administration of DMSO, although it is not well understood [198].

I was not able to demonstrate alteration of autophagy as a consequence of chromosome mis-segregation, although there were limitations to the experiments performed, with cells experiencing mitotic delay and potential off-target effects of drug treatment. Therefore, I could not reach definitive conclusions concerning any association between chromosome mis-segregation and autophagy. Whilst in these experiments I did not demonstrate that pulsed monastrol induced chromosome mis-segregation, in subsequent work, I established that repeated monastrol treatment did induce mis-segregation and the development of aneuploidy. It is possible that one treatment with monastrol may not have induced sufficient mis-segregation to stimulate a detectable alteration in autophagy. Studies published since this work was undertaken, have demonstrated induction of autophagy genes following chromosome mis-segregation [191, 199].

3.4.6 Influence of Autophagy on Aneuploidy

I wished to address the effect of autophagy on the acquisition and propagation of aneuploidy, following chromosome mis-segregation. To achieve this, I adopted methods from studies investigating aneuploidy [167, 168]. The principal strategy was based on the work of Thompson et al. (2008) [167, 168]. In this paper, the generation of aneuploid cell populations was described using monastrol-induced mis-segregation [167, 168]. Thompson et al. (2010) used this strategy to demonstrate the importance of p53 loss in the propagation of aneuploid cells [167, 168].

3.4.6.1 Generating HCT116 Knockdown Cell Lines

To investigate the role of autophagy, I aimed to establish cell populations deficient in autophagy to examine its influence on the generation of aneuploid cell populations. In addition, due to the importance of p53 in suppressing aneuploidy, it was necessary to generate cells with p53 depletion. HCT116 have functional p53, which inhibits the generation of aneuploidy [167, 168]. Thompson et al. (2008) used *p53*-/- HCT116 cells generated by Bunz et al. (1998) [200]. For reasons discussed later, I decided to

knockdown both autophagy and p53 using small hairpin RNA (shRNA) that integrate into the genome to produce stable knockdown of targeted genes.

Autophagy inhibition was achieved via shRNAs targeting integral autophagy components; knockdown of ATG5 or ATG7 was attempted but the ATG7 shRNA provided greater inhibition of autophagy and was used for all subsequent work [Fig. 3.11]. HCT116 cells with stable suppression of autophagy were generated through the retroviral transduction of ATG7 shRNA, with non-targeting shRNA transduced into control cells. HCT116 cells with suppression of autophagy were selected and p53 knockdown achieved via lentiviral transduction of p53-targeted shRNA or non-targeted shRNA. This approach generated 4 HCT116 clones: one displaying stable autophagy and p53 knockdown (shATG7.shp53), one displaying autophagy knockdown alone (shATG7.shNTC), one displaying p53 knockdown alone (shNTC.shp53) and one clone in which neither protein was knocked down (shNTC.shNTC).

3.4.6.2 Sequential monastrol treatment, culture and assessment of karyotype

The 4 HCT116 clones were then treated with monastrol (100μM) for 8 hours followed by mitotic shake-off. Cells were plated and allowed to complete cell division for 16 hours. Pulsed treatment with 8 hours of monastrol followed by washout and 16 hours of standard culture was repeated on 4 consecutive days. Following this protocol, all 4 HCT116 clone populations demonstrated significant deviation from the diploid karyotype [Fig 3.12]. The 4 HCT116 clones were then plated at standard or low density and cultured for up to 45 days. The populations plated at standard density were passaged as required and sampled at specified time points. Cells plated at low density were left to form individual clones, which were sampled after 45 days.

At each time-point, FISH was performed to assess karyotype, using pericentric chromosome probes. Two chromosome probes to the alpha satellite regions on Chromosome 8 and Chromosome 7 were used. Both these chromosomes are diploid in HCT116 cells and both had been used to assess karyotype in published studies [167, 193]. In diploid cells, each probe marks two chromosomes but deviation from this number, except at mitosis,

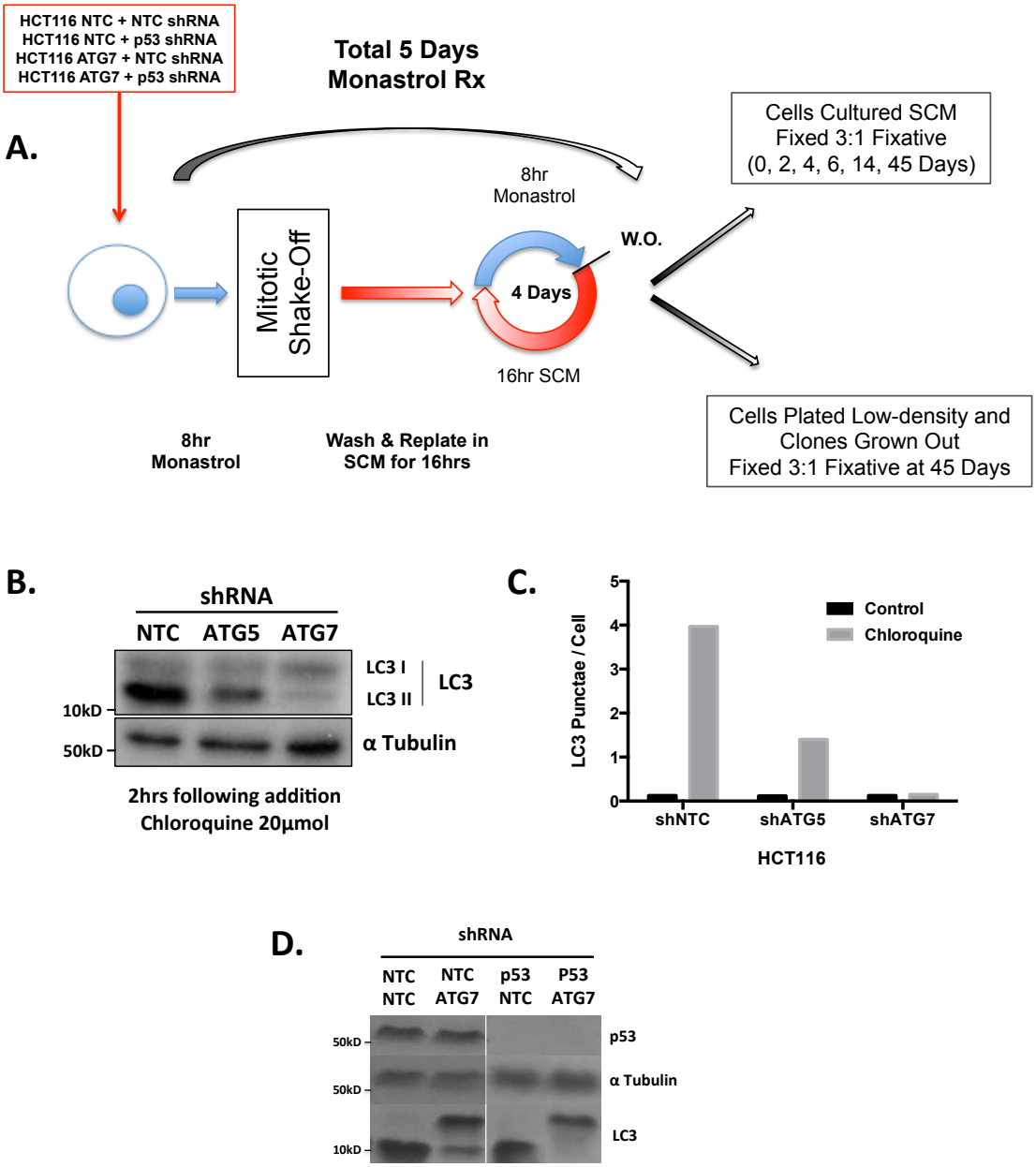

Figure 3.11 Autophagy and Maintenance of the Aneuploid Karyotype. To investigate the effects of autophagy on the generation and maintenance of the aneuploid karyotype, pseudo-diploid HCT116 cells were transduced with combinations of ATG7 shRNA, p53 shRNA and NTC shRNA to generate 4 cell lines. ***3.11A*** delineates the protocol for generating aneuploid cells with sequential Monastrol treatment (WO = Wash Out) followed by collective or solitary cell culture. The aim was to interrogate karyotype with chromosome probes through out the experiment to assess alterations in chromosome number. This protocol is adapted from published work by Thompson and Compton. ***3.11B*** and ***3.11C*** demonstrate effective autophagy knockdown with ATG7 shRNA following chloroquine treatment; this is superior to knockdown achieved with the ATG5 shRNA. ***3.11D*** Western blot of p53 and LC3 in the 4 HCT116 cell lines generated; this demonstrates adequate autophagy and p53 inhibition in the relevant lines on commencing the experiment.

indicates polyploidy or aneuploidy (if an uneven number of chromosomes are present). Obvious only two chromosomes were assessed but published studies demonstrate that this provides a valid representation of overall karyotype [167, 168]. At the final time point (Day 45), mitotic spreads were employed to determine chromosome number, to confirm and validate the results obtained by chromosome probes. Importantly, chromosome probes assess interphase chromosome number unlike metaphase spreads, which examine chromosome number only in dividing cells. Therefore, in cells that undergo aberrant mitoses and experience cell cycle arrest, the karyotype will be assessed by chromosome probes but not metaphase spreads. However, it is apparent that if these cells fail to proliferate, their proportion in the population will fall rapidly over time.

Prior to monastrol treatment, the karyotype of all 4 HCT116 clones was assessed using both chromosome probes and mitotic spreads; no difference between the clones was identified. The karyotype of the HCT116 cells is 45(43-45)X. The chromosome probes demonstrate approximately 5% of cells deviated from diploid karyotype at baseline, which is similar to the rate found by Thompson et al. (2008, 2010) [167, 168].

3.4.6.3 HCT116 shNTC.shp53 and HCT116 shATG7.shp53 Karyotype Variation

All 4 HCT116 clones displayed significant karyotype anomalies after sequential monastrol treatment. However, directly following treatment (Day 0), a significantly smaller proportion of shATG7.shNTC cells deviated from diploid karyotype than the other 3 HCT116 clones [Fig. 3.12]. This may reflect impaired tolerance to chromosome mis-segregation following autophagy knockdown. Over time, comparison of the 4 HCT116 clones revealed that only the shNTC.shp53 cells differed from the others, with a significantly higher proportion of cells with aberrant karyotypes. This accorded with the published findings of Thompson et al. (2010) demonstrating that p53 depletion permits the propagation of aneuploidy [167]. Interestingly, the shATG7.shp53 cells that displayed autophagy knockdown in addition to p53 depletion, did not sustain similar karyotype variation. Again, this implicates autophagy in the survival and/or proliferation of cells with abnormal karyotypes.

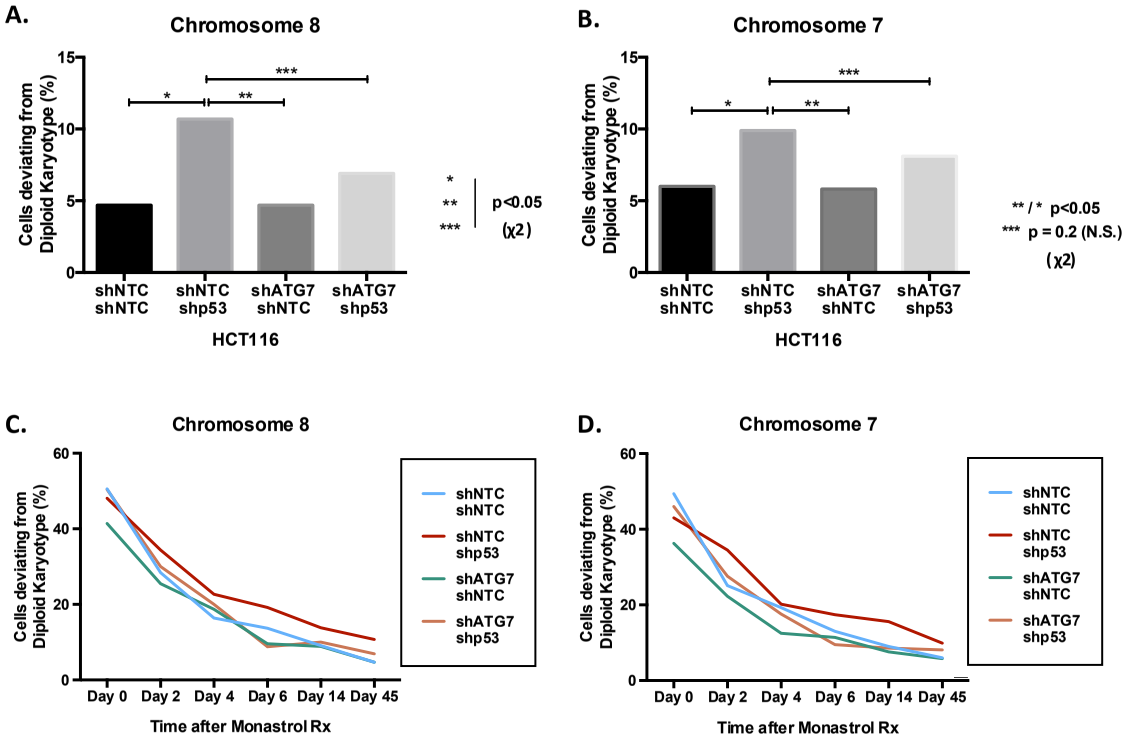

Figure 3.12 Chromosome Enumeration HCT116 Cell Lines. Following sequential treatment with Monastrol as described, each of the cell lines (HCT116 shNTC/shNTC, HCT116 shNTC/shp53, HCT116 shATG7/shNTC and HCT116 shATG7/shp53) was cultured collectively and sampled at predetermined time-points. At each time-point, cells were fixed with 3:1 Methanol:Acetic Acid, placed on glass slides and stained with α-satellite chromosome probes targeting Chromosome 7 and Chromosome 8. The chromosome count per cell for each chromosome was determined using fluorescence microscopy. ***3.12A*** and ***3.12B*** show the number of cells deviating from diploid karyotype of Chr. 8 and Chr. 7 respectively in each of the 4 cell lines at 45 days following final release from Monastrol. This demonstrates a significant divergence between the HCT116 shNTC/shp53 line and HCT116 shNTC/shNTC, with increased deviation in the p53 knockdown cell line. The additional loss of autophagy with shATG7 appears to reduce this karyotypic deviation with significantly fewer cells deviating from diploid karyotype of Chr. 8 and a similar but non-significant trend with Chr. 7. ***3.12C*** and ***3.12D*** show the recorded karyotypic variation across the experiment; there is initial significant deviation in all cell lines. This is lost with time in all lines but to different degrees and at different rates (minimum 300 cells per cell line counted at each time-point).

At the final time point, shATG7.shp53 cells displayed a greater proportion of cells with abnormal karyotype than either shNTC.shNTC or shATG7.shNTC cells. Intriguingly, this was also true of shATG7.shp53 cells not treated with monastrol but cultured for 45 days in standard media as a control [Fig. 3.15]. However, these differences were not statistically significant but the trend would agree with data demonstrating loss of autophagy predisposes to chromosome instability [155, 201]. The apparent paradox that autophagy may both inhibit and support chromosomal instability [202] is discussed below. I found that control shNTC.shp53 cells, not treated with monastrol, did not display abnormal karyotypes above baseline at Day 45. Once more, this was in agreement with the published observation that p53 loss alone is insufficient to generate aneuploidy [203].

At Day 45, chromosome counts on metaphase spreads were consistent with findings from the two individual chromosome probes, confirming the chromosome probes were a valid readout of karyotype [Fig. 3.13]. These metaphase spreads demonstrated that shNTC.shp53 HCT116 cells differed from normal karyotype to a greater degree than other cohorts, in agreement with the results from the chromosome probes.

3.4.6.4 Individual cell clone chromosome counts

Experiments to assess the growth of individual cell clones following monastrol treatment were not informative. No significant difference in the number of aneuploid clones was found between the 4 HCT116 cell types [Fig. 3.14]. This differed from the findings of Thompson et al. (2010), who reported a significantly greater proportion of aneuploid clones in p53 deficient cells [167]. The reason for this difference is unclear but may be a sampling error as I counted only a limited number of clones.

Interestingly, the individual cell clones that demonstrated aneuploidy displayed a background tetraploid population. There were few diploid cells in any of the individual colonies with marked aneuploid populations. Each individual colony was derived from a single progenitor cell and it was improbable that if this cell was aneuploid it would have derived a significant tetraploid progeny. If the founder cell had been diploid, there was likely to

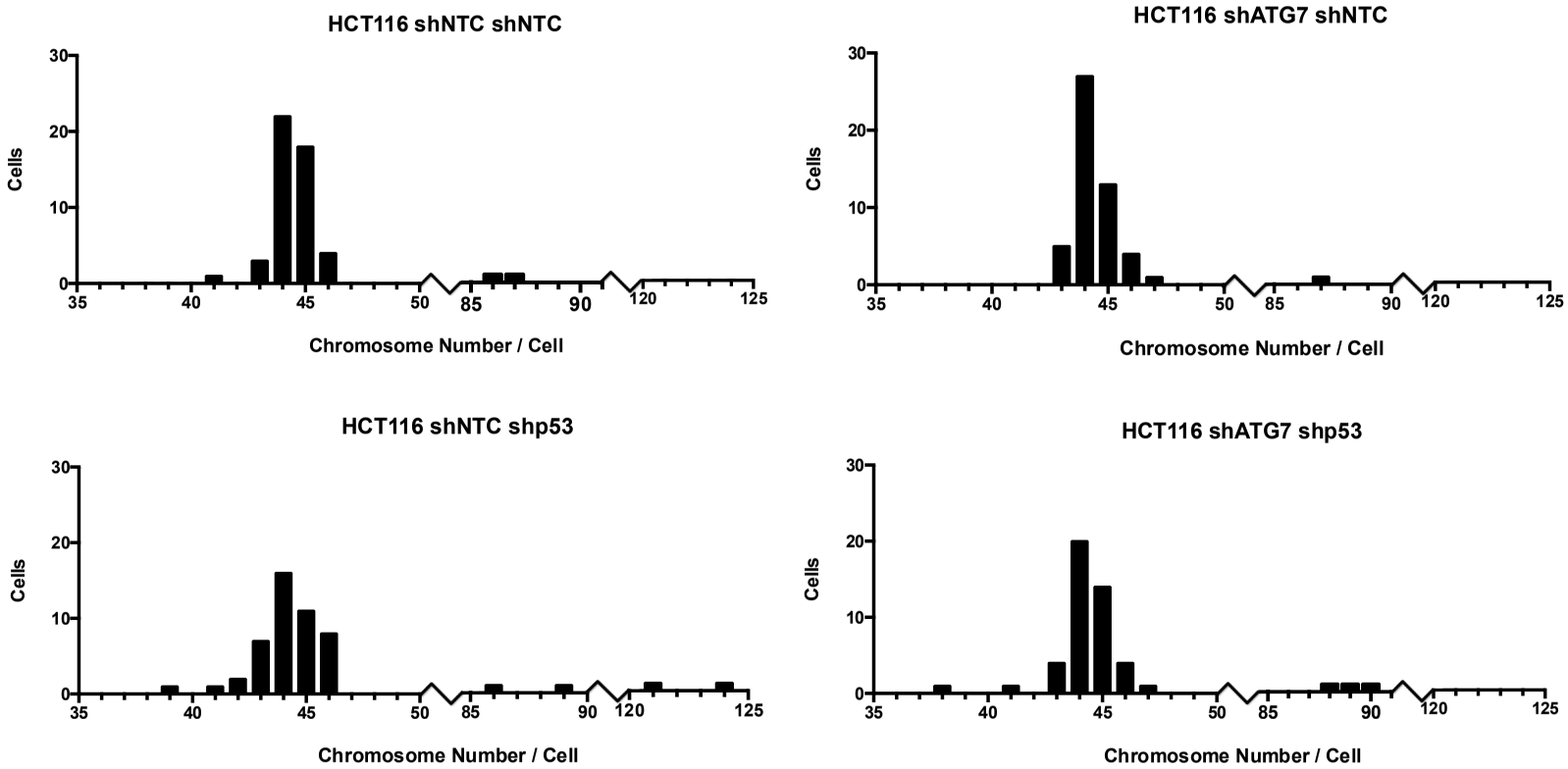

Figure 3.13 Chromosome Counts HCT116 Cell Lines Day 45. At day 45 following final release from Monastrol treatment, aliquots of the four collectively cultured HCT116 cell lines were treated for 1 hour with Colcemid 1ug/ml. Cells were subsequently trypsinised, washed and placed in hypotonic KCl (0.54%) for 6 minutes. Cells were centrifuged, supernatant aspirated and 3:1 Methanol:Acetic Acid added drop-wise while agitating the pellet. The sample was again centrifuged and the pellet re-suspended in fixative. The suspension was then dropped onto clean glass slides to generate metaphase spreads. Slides were allowed to dry prior to the addition of DAPI. Chromosome number was then determined using fluorescence microscopy (50 cells counted per cell line). ***3.13*** plots the chromosome number of each of the 50 cells for all four cell lines. This is consistent with the chromosome enumeration probes; the HCT116 shNTC/shp53 shows greatest deviation from normal karyotype (43-45). It is noted that this method enumerates the chromosome count in dividing cells only.

have been a residual diploid population. Therefore, the high proportion of tetraploid cells, in the absence of diploid cells, indicated that aneuploidy in these populations was likely to have occurred via multipolar mitoses of tetraploid cells. Tetraploidy is recognized to be a metastable state and others have described the derivation of aneuploid clones from tetraploid progenitors [193, 204]. Therefore, my findings were consistent with work demonstrating tetraploidy as a mediator of chromosomal instability in tumourigenesis [193].

3.4.6.5 Discussion of experiment methods

I used shRNA to knockdown both p53 and autophagy. The advantage of this approach was that all cells in the experiment were derived from the same HCT116 cell population, providing confidence that the 4 HCT116 cell types were syngenic. The *p53*-/- HCT116 cells were generated clonally by Bunz et al (1998) over 15 years ago and therefore may differ from the wild-type HCT116 cells used in my work. Furthermore, HCT116 cells with dual *p53* and *ATG7* knockout did not exist and it was considerably easier to generate these cells utilizing shRNA knockdown.

The disadvantage of shRNA over constitutive knockout includes the risk of off-target effects. I used a single shRNA for each target, *ATG7* and *p53*, which may have increased this risk. Moreover, the effect of shRNA may be suppressed over time if there is a strong negative selection pressure due to its deleterious effects. In my experiment, autophagy knockdown was well maintained but there was a reduction in p53 knockdown over the experimental period [Fig. 3.15]. In addition, it is recognized that gene knockdown is not necessarily equivalent to gene knockout, although my results correlated well with the findings by Thompson et al. (2010), using cells with constitutive *p53* knockout [167].

3.4.6.6 Autophagy and Chromosomal Instability

In this experiment, I found that autophagy knockdown impaired the capacity of cancer cell to tolerate abnormal karyotypes. This was demonstrated both by the lower proportion of shATG7.shNTC cells with aberrant karyotype directly after monastrol treatment and the lower proportion of

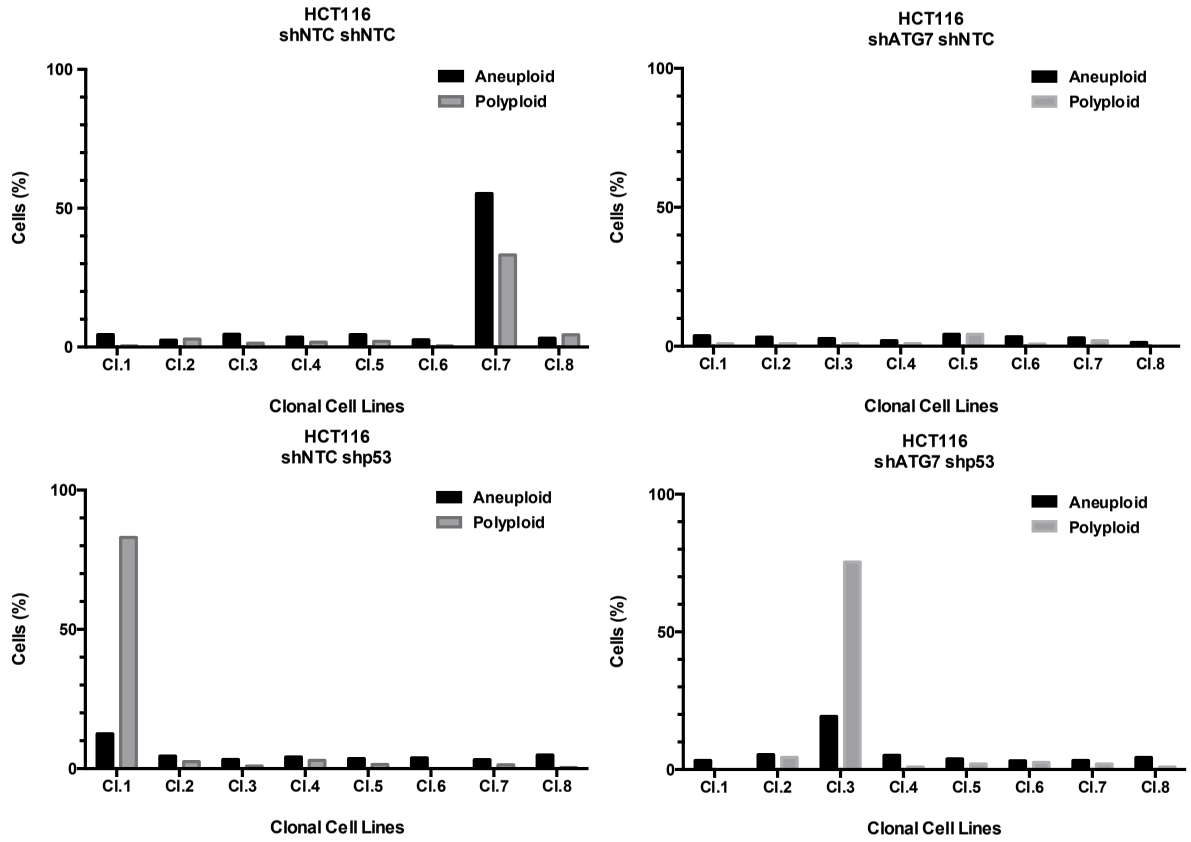

Figure 3.14 Karyotype of Clonal Cell Populations at Day 45. Following final release from Monastrol treatment, a proportion of each cell line was plated at low density to allow the formation of clonal colonies. For each cell line, 8 colonies were randomly selected at Day 45. Each colony was fixed with 3:1 Methanol:Acetic Acid and subject to staining with Chromosome 7 and Chromosome 8 CEN probes. The chromosome count was undertaken for each colony using fluorescence microscopy (minimum 200 cells counted). 3.14 shows the percentage of cells demonstrating either aneuploid or polyploid chromosome counts of Chromosome 8 within each colony (similar appearance with Chromosome 7 probe not shown). With the exception of HCT116 shATG7/shNTC, each cell line grew one colony in which virtually all cells were polyploid or aneuploid.

shATG7.shp53 cells with aberrant karyotype compared to shNTC.shp53 cells at Day 45 following treatment. My findings appeared contrary to previous studies on autophagy and chromosomal instability [155, 201], which indicate inhibition of autophagy leads to genetic instability. In one study, heterozygous loss of *Beclin1* combined with expression of BCL2 predisposed cells to develop chromosomal instability [155]. Furthermore, a recent paper found loss of autophagy was associated with genetic instability under conditions of metabolic stress, such as starvation [201]. This appears to create a paradox where autophagy inhibition may both inhibit chromosomal instability and induce it. However, these different findings are not irreconcilable and indeed the influence of autophagy depletion on tumourigenesis is similarly contradictory. This is discussed prominently in the literature, with autophagy loss found to both limit tumour survival and promote tumour progression [202, 205]. Autophagy enables the sequestration and degradation of cellular products and if accumulation of these products is deleterious then loss of autophagy may impair survival. However, if these products are genotoxic then loss of autophagy may impair their degradation and potentially enhance genetic instability in cell that survive. Chromosomal instability can induce protein imbalances leading to proteotoxic stress that autophagy may mitigate. Since my work was performed, other papers have demonstrated that chromosomal mis-segregation induces autophagy genes [191]. More recently, Santaguida et al. (2015) have demonstrated that aneuploidy and specifically chromosome mis-segregation induces autophagy phenotypes, with elevated LC3 II [206]. In addition, they demonstrated that autophagy targets such as protein aggregates accumulate in lysosomes and induce a lysosomal-stress response in aneuploid cells [206]. Furthermore, Lui et al. (2016) have found that increased autophagy flux rescues oxidative stress and apoptosis due to chromosomal instability [207]. These recent papers are consistent with my result.

3.4.6.7 p53 and Autophagy

It is established that p53 itself can regulate autophagy, with reports that it both stimulates selective autophagy pathways and inhibits basal autophagy [208-210]. Therefore, p53 inhibition in this setting may itself alter autophagy

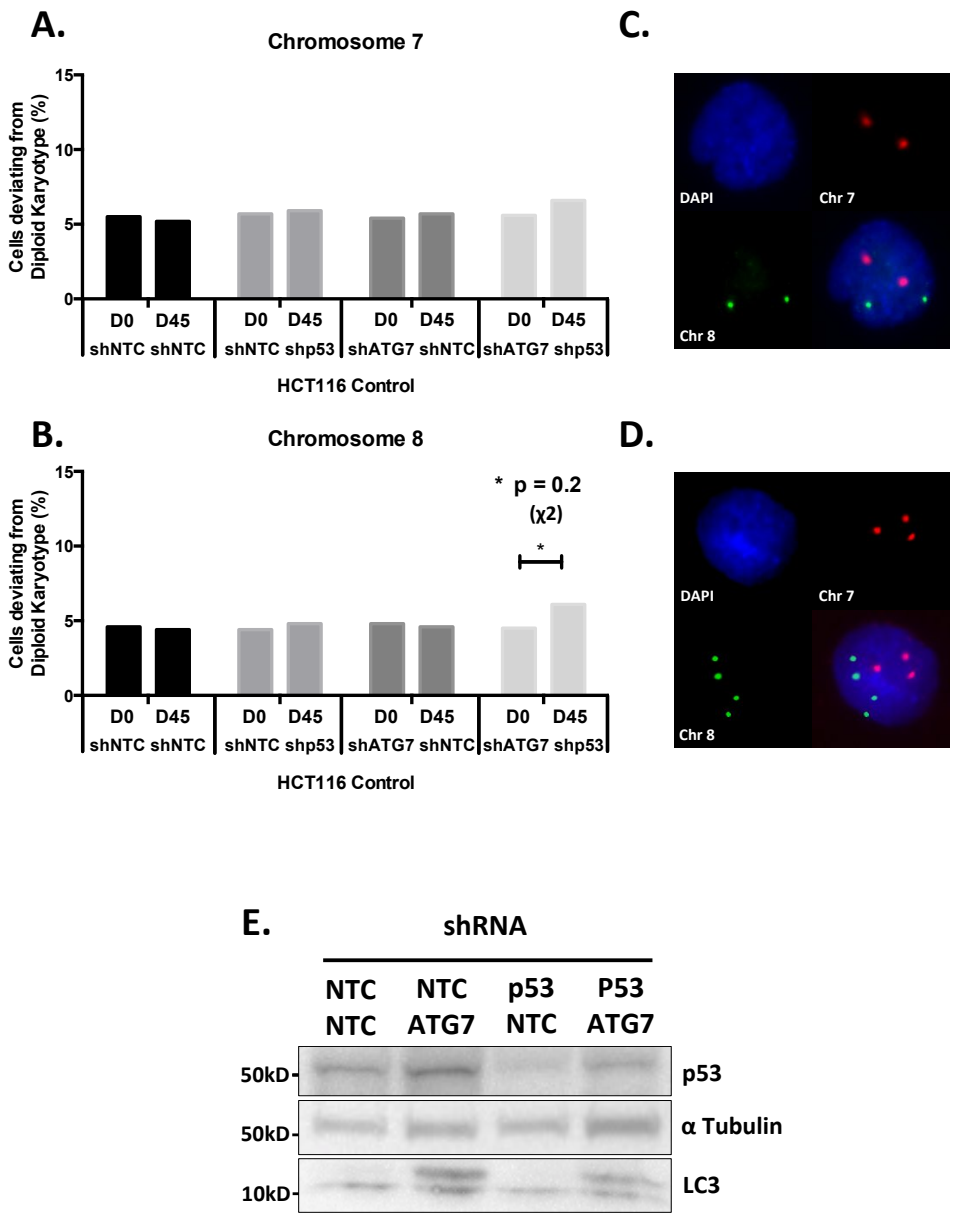

Figure 3.15 Aneuploidy Experiment – Ancillary Images. The four HCT116 cell lines were assayed at the outset of the experiment. Cells were fixed with 3:1 Methanol:Acetic Acid and stained with Chromosome 7 and Chromosome 8 α-satellite probes. This was to enable determination of baseline chromosome count. Each cell line was then cultured in SCM for 45 Days without prior Monastrol treatment; at the end of this period each cell line was again subject to chromosome enumeration. This was undertaken as an experimental control to confirm there was no deviation from karyotype subsequent to shRNA knockdown alone. ***3.15A*** and ***3.15B*** shows the chromosome count for each of the cell lines at Day 0 and Day 45. As is demonstrated, there is no significant deviation from baseline karyotype without prior Monastrol treatment. ***3.15C*** and ***3.15D*** provide representative images obtained utilizing the chromosome enumeration probes; *3.15C* show a cell diploid for both Chr. 7 and Chr. 8, while *3.15D* demonstrates a cell aneuploidy for Chr. 7 and tetraploid for Chr. 8. ***3.15E*** shows a Western blot of lysates obtained at Day 45 from each cell lines subject to Monastrol treatment and cultured collectively. This shows autophagy inhibition is maintained, however p53 knockdown is less well maintained particularly in the ATG7 knockdown cell line.

responses. Furthermore, ATG7 is reported to modulate p53 function under conditions of metabolic stress, mediating cell survival [211]. In HCT116 cells, I found loss of p53 did not abrogate the increased LC3 II observed after CDK11 knockdown (data not shown). This indicated p53 is not an integral component in the CDK11-mediated autophagy response, which results from aberrant mitosis.

The status of p53 appears to significantly influence the role of autophagy in tumorigenesis, emphasising the importance of examining influences of both p53 and autophagy individually and together. This is of particular relevance given the prevalence of p53 pathway disruption in cancer and the potential for any future use of autophagy inhibitors as chemotherapeutic agents. A recent study undertaken by Rosenfeldt et al. (2013) demonstrates the influence of autophagy inhibition on tumourigenesis is dependent on *p53* status [212]. In a murine model of pancreatic adenocarcinoma driven by aberrant KRAS, autophagy inhibition was found to restrict tumour progression in the presence of a functional p53. Conversely, in the absence of p53, autophagy inhibition enhanced tumorigenicity. This paper indicates that abrogation of autophagy, by either genetic loss or chemical inhibition, enhanced tumour progression following loss of p53 [212]. Rosenfeldt et al. (2013) did not examine chromosomal stability or karyotype.

3.5 Conclusion

This chapter characterised the autophagy response observed on CDK11 knockdown. My work demonstrated that the predominant influence on this phenotype is mitotic dysregulation. Aberrant mitoses appear to engage autophagy pathways. However, this work was unable to determine the influence of chromosomal mis-segregation itself on autophagy pathways. Subsequent papers have demonstrated up-regulated mRNA expression of autophagy genes following chromosome missegregation [190, 191]. More recently, upregulation of autophagy itself has also been found on chromosome mis-segregation and others have shown autophagy enhances tumour cell survival after chromosome mis-segregation [206].

Aneuploidy is common in cancer and its role in tumour progression is debated. Interestingly, my work indicates aneuploid clones in these experiments were generated through tetraploid intermediates. Published work demonstrates the survival advantages of the capacity to rapidly alter genetic content through loss of faithful genomic replication [213]. However this comes at a potential cost and there is increasing evidence that aneuploidy causes proteotoxic stress due to stoichiometric protein imbalance with corollary elevation in reactive oxygen species (ROS) [53]. This protein imbalance is proportional to the chromosomal regions duplicated [53] and ROS themselves are observed to stimulated autophagy responses [87, 88]. In addition, ROS are reported to induce further chromosomal instability [89], while autophagy may potentially mitigate this stress.

This work indicates that autophagy has a role in the maintenance of the aneuploidy, with loss of autophagy impairing the survival of cells with aberrant karyotypes. Hopefully, further work will continue to assess the link between autophagy and aneuploidy, to identify either the beneficial or deleterious effects of autophagy in distinct settings.

CHAPTER 4

CDK11 and Cell Motility

4.1 Introduction

4.1.1 Cell Migration

The ability of cells to migrate is essential to all multicellular organisms [93]. It proves integral not only to their development but also subsequently to processes such as immune surveillance and wound healing. The strict control of cell migration is therefore essential to health and its dysregulation plays a significant role in human disease, particularly cancer. Dysregulated migration is fundamental to the capacity of the cancer cell to metastasize and it is this metastasis of the tumour from its site of origin that is responsible for the greatest burden of mortality. Indeed the ability of a tumour cell to both migrate and invade forms the basis of differentiating tumours into those categorized as benign or malignant.

Cell migration requires the coordinated and dynamic regulation of numerous cellular processes and pathways. In essence, these pathways serve to integrate three fundamental elements, permitting and regulating cell migration; these are adhesion (and de-adhesion) to the extracellular matrix (ECM), cytoskeletal reorganization and cellular polarization [93]. Whilst multiple patterns of migratory behavior are recognized, these elements are integral to all patterns of migration.

4.1.2 Migratory Morphologies

Modes of cell migration are linked to cellular morphology [214]. Epithelial cells are characterized by planar polarity and strong inter-cellular adhesion with resultant limitations on motility [214]. The motility displayed is often that of collective migration of cell sheets. Mesenchymal cells, in contrast, display weak cellular contacts and enhanced motility [214]. Invasion and migration during both health and disease is frequently associated with

epithelial cells adopting a mesenchymal phenotype, termed epithelial-to-mesenchymal transition [214]. Numerous mechanisms have been described to regulate this transition [90].

Amongst mesenchymal cells, differing morphologies of migration are recognized, including protrusive and amoeboid phenotypes [215]. The best characterized is that of the protrusive phenotype, most prevalent in 2D systems, as described in this chapter. This involves protrusion of structures, termed lamellipodia, at the front of the cell with de-adhesion at the rear [215]. Actin assembly and regulation of adhesion are reported to be fundamental components to this mode of migration. In contrast, cells migrating with an ameoboid phenotype demonstrate a rounded morphology; this mode of migration is found to be less dependent on actin assembly and more so on actomyosin contractility [96]. Amoeboid cell migration is best described in 3D systems [215]. These two modes of migration are not considered mutually exclusive and the capacity of cells to transition from protrusive to amoeboid morphologies has been demonstrated [215]. These phenotypes have been defined *in vitro* and their relevance *in vivo* during health and disease remains uncertain.

4.1.3 Integrins and Focal Adhesions

Adhesion to the extra-cellular matrix, its regulation and the capacity to respond to external stimuli are integral to cellular migration. Integrins constitute the predominant receptor type that mediates adhesion to the extracellular matrix [103]. These trans-membrane integrin molecules are expressed at the cell surface as obligate heterodimers comprising non-covalently associated α and β subunits [216]. Mammalian cells express a cohort of distinct α and β subunits (18 α and 8 β subunits) that derive a complement of unique heterodimers; these recognize numerous discrete ligands to enhance cellular sensitivity and specificity to environmental cues [216].

Attachment to the extracellular matrix induces integrin receptor clustering [217]. This cluster of intracellular domains within the cytoplasm acts as a trigger for the recruitment of cytoskeletal and signaling complexes to initiate

the formation of structures termed focal adhesions [218]. The engagement of proteins including Talin, Vinculin and α -actinin enable linkage of these nascent adhesions to the actin cytoskeleton. Recruitment of ARP 2/3 further strengthens this connection with the capacity to nucleate novel actin filaments in the vicinity of integrin clusters [219]. These structures are subsequently able to augment integrin avidity through further clustering of integrin and actin components. These focal adhesions enable structural connectivity of the cytoskeleton to the cellular surroundings, with the establishment of tractile forces essential to cell motility [218].

Focal adhesions not only provide a physical link to the extracellular matrix but also act as signaling complexes to assimilate and interpret environmental stimuli and regulate cellular responses [218]. A plethora of signaling molecules locate to focal adhesions; prominent among these is the influential Focal Adhesion Kinase (FAK). FAK is a non-receptor tyrosine kinase that is engaged early in the formation of nascent adhesions and is a principal mediator of adhesion dynamics and signaling [220]. The mechanisms regulating FAK activation are well described [220]. Auto-phosphorylation of the tyrosine residue (Y397) on FAK, in response to various stimuli, causes conformational rearrangement of the protein to reveal a high-affinity binding site for the Src Homology 2 (SH2) domain [220]. This enables association of Src and FAK and Src activation. Src activation leads to phosphorylation of FAK at multiple tyrosine residues, in addition to phosphorylation of numerous other substrates. FAK phosphorylation both enables full enzymatic activation of FAK and creates further binding domains for other signaling molecules [220]. The influential FAK-Src complex acts to regulate adhesion dynamics and intracellular signaling, with evidence demonstrating its capacity to modulate adhesion, cellular polarity and the cytoskeleton [220-222]. Indeed, FAK-Src signaling controls many facets of malignancy-associated phenotypes [223].

4.1.4 Cell Polarity and the Cytoskeleton

Cell polarity is defined by the acquisition of spatial asymmetry; this comprises the asymmetrical organization of cellular structures including cell

membrane, intracellular organelles and cytoskeleton [224]. Cell polarity is integral to sustained directional migration as it allows discrete, divergent molecular processes to occur at front and rear of the cell such as assembly of nascent adhesions at the leading edge with disassembly of adhesions at the rear [224]. The establishment of cell polarity obligates stringent temporal and spatial regulation of discrete cellular pathways. CDC42, a Rho GTPase, has been determined to be the master regulator of planar epithelial polarity [224, 225]. It is found to act through effectors such as the PAR6/PAR3/aPKC complex [225]. These regulate polarization of the nucleus, golgi apparatus and centrosome. In slow migrating mesenchymal cells, such as described in this work, the nucleus moves rearward on polarization to lie posterior to both the golgi and centrosome [226]. The centrosome is the major microtubule organizing centre (MTOC) within the cell; through its regulation of microtubule dynamics it plays an integral role in the maintenance of cell polarity and migration [227]. The golgi apparatus co-locates with the centrosome in migrating cells and this interaction is found to be influential in the maintenance of polarity [228].

The cytoskeleton is another element essential to operative cell migration [225]. Actin filaments contribute to the establishment of polarity, with actomyosin contractility fundamental to the generation of tractile forces required for cell motility. Microtubules play important roles in mediating polarization and the transportation of components necessary to enable the migration. Although many molecules are implicated in cell migration, the Rho GTPases including Rac, Rho and CDC42 are fundamental regulators of cytoskeletal dynamics [229]. Their activity is conformationally regulated by binding to GTP and GDP; they are activated on GTP binding and inactive when GDP-bound [229].

4.1.5 CDK11 and Cell Migration

As described in previous chapters, CDK11 has defined roles in transcription, splicing and mitosis. Prior to commencing the work described in this chapter, there was little in the literature describing the role of CDK11 in cell migration. However, a large genetic screen utilizing siRNA mediated

knockdown of human phosphatases and kinases identified *CDC2L1* (*CDK11B*) as one of 66 putative regulators of cellular migration [230]. This paper undertook the high throughput screen using MCF10A cells, transformed, non-cancerous breast cells with epithelial morphology. The primary outcome measure was area of wound closure at 12 hours following wounding of a confluent monolayer, utilizing the 2-D 'wound-healing' or 'scratch' assay [230]. Secondary outcomes included examination of cellular morphology and migratory behavior.

Inhibition of CDK11 protein expression was linked to reduced cell migration; however, no gross alteration in cell morphology or migratory behaviour was observed following CDK11 knockdown [230]. The study did report aberrant nuclear rotation following knockdown of CDK11, indicating abnormal cell polarization [230]. However, no detailed examination was performed. Based on this evidence, I was interested to examine the role of CDK11 in cell migration because of its potential implication to cancer phenotypes.

CDK11 is required for accurate centrosome duplication at mitosis [83]. Aberrations in centrosome biology during mitosis have implications for its function in interphase [231]. As described, the centrosome exercises a fundamental role in microtubule behavior and the maintenance of cellular asymmetry during migration. CDK11 may therefore influence migratory behavior through effects on centrosome function. Moreover, unpublished work has identified interaction between CDK11 and various cytoskeletal proteins including tubulin [106]. CDK11 is implicated in the regulation of microtubule dynamics at mitosis and may be engaged in similar processes through interphase [84, 89]. Finally the role of CDK11 in cellular adhesion has not been previously examined but CDK11 contains a Src Homology 2 (SH2) binding domain [47]. No interaction with Src family kinases is reported but this domain may provide a mechanism through which CDK11 may influence cellular adhesion and migration. However, numerous proteins with diverse roles contain SH2 domains and the functionality of this domain within CDK11 remains untested.

4.2 CDK11 and Cell Migration

I aimed to determine whether published findings on the role of CDK11 in cell migration could be recapitulated in other cell lines, with the aim of subsequently elucidating the underlying mechanisms. It was decided to undertake initial experiments utilizing the simple wound healing or scratch assay. Although this assay has limitations, its use is prevalent in published literature and it has informed understanding of cell migratory behaviour. In addition, the assay was employed in the study by Simpson et al. (2008) that predicated this chapter [230]. Therefore, it was considered a valid initial strategy, as any findings could be subsequently interrogated in a more detailed manner.

4.2.1 Results of the Wound Healing Assay

I aimed to determine the optimal conditions to perform the migration assays. Over time, the predominant phenotype observed following CDK11 knock-down is one of mitotic dysregulation, demonstrated by nuclear dysmorphology. Determining the time, following siRNA transfection, at which to undertake the assay was critical. Simpson et al. (2008) performed the assay at 56 hours following transfection, during which period the mitotic phenotype caused by CDK11 knockdown becomes prominent in MDA-MB-231 cells [230]. I aimed to determine the shortest time following transfection at which consistent knockdown of protein levels, of 75% or greater, could be achieved. This was undertaken to reduce the influence of the marked mitotic phenotype, demonstrable at 72 hours following transfection, as this was likely to impair cell migration. Time course experiments, utilizing the MDA-MB-231 cells, identified that at 40 hours consistent knockdown of the required magnitude (≥75%) could be achieved using pooled siRNAs. Pooled siRNAs were used to reduce the influence of off-target effects of a single siRNA. Increasing siRNA concentration did not lead to a more rapid reduction in CDK11 protein levels. Therefore I opted to undertake the assay at 40 hours following siRNA transfection. This represented a compromise between attaining optimal reduction in protein level whilst limiting time-dependent confounding effects attributable to the role of CDK11 in mitosis.

It was decided to undertake this work using two cell lines: MCF-7 cells and the MDA-MB-231 cells. The MCF-7 cells represent oestrogen receptor positive breast cancer-derived cells and display an epithelial morphology, with the capacity to form monolayers in 2D culture. MDA-MB-231 cells are derived from a hormone receptor negative breast cancer and have a mesenchymal phenotype. Work confirmed that similar knockdown of CDK11 could be achieved with both cell lines at 40 hours following transfection. These cells were used to interrogate migratory effects in cells displaying either mesenchymal or epithelial morphology, given their known different modes of migration. Simpson et al. (2008) examined migration only in an epithelial cell line [230]. Therefore my experiments had the potential to broaden the generality of any findings.

In order to reduce the impact of differences in cell density caused by CDK11 inhibition, cells were plated at equal density 12 hours prior to wounding. No alteration was visible in the adhesion of CDK11-depleted or control cells that may have challenged the validity of the assay. The absence of altered adhesion was consistent with findings described later in this chapter. Plastic plates without collagen coating were used to reduce the potential for error created by the variable loss of the collagen coating during wounding, a recognized limitation of 2-D wound healing assays [232, 233].

Initial work was undertaken using time-lapse microscopy, visualizing the wound edge for up to 15 hours following wounding. This allowed not only quantification of the area recovered following wounding but also study of the general migratory behaviour of the cells during this process. Both the MCF-7 and MDA-MB-231 cells transfected with CDK11 siRNA showed significant retardation of migration into the wound, compared to cells transfected with non-targeted siRNA [Fig 4.1]. Time-lapse images demonstrated that this deficit was temporal, i.e. cells took longer to migrate into the wound, but there was no gross morphological change in the migratory patterns between either cell type on knockdown of CDK11. These findings were in keeping with the published results [230].

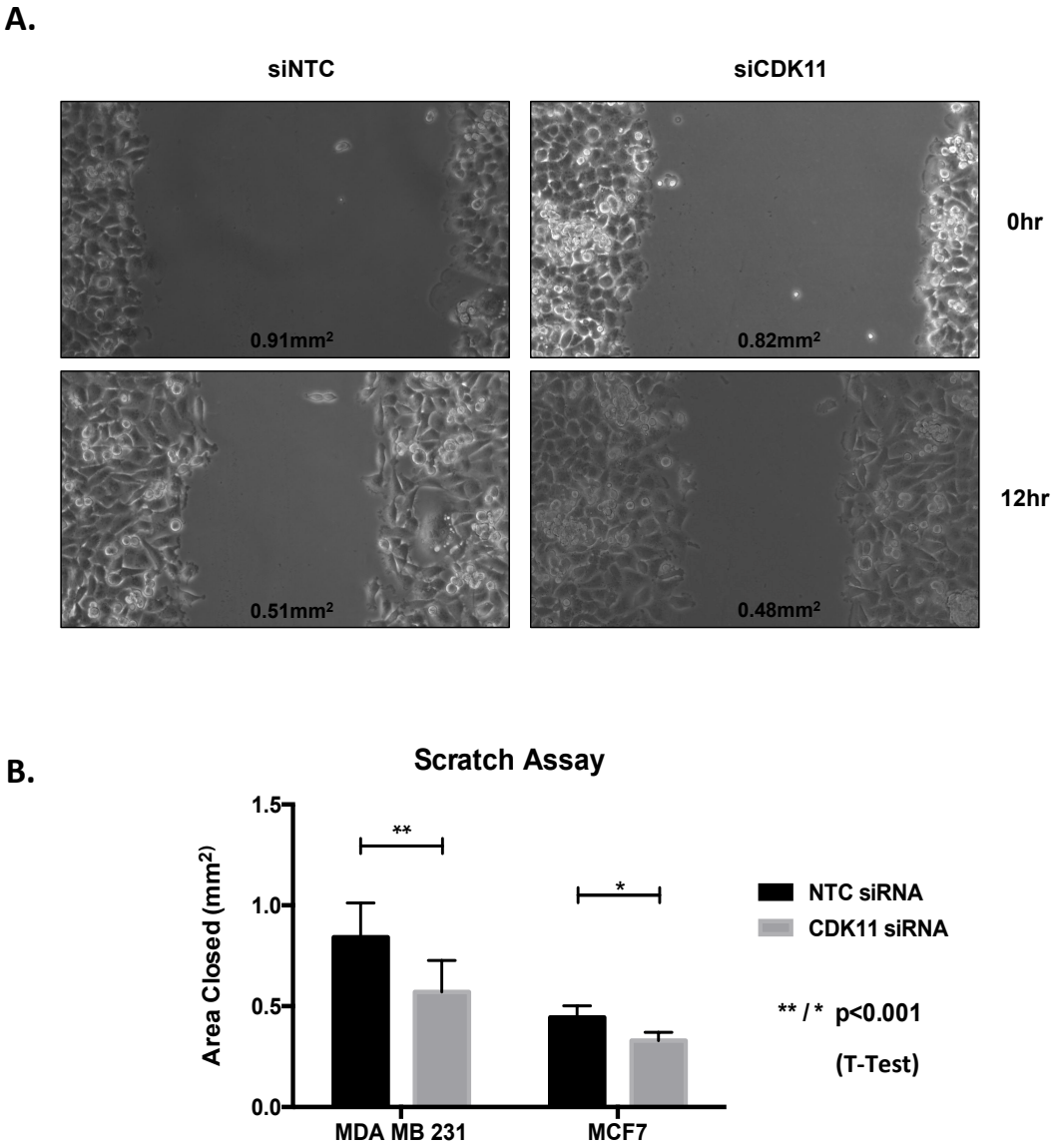

Figure 4.1. Wound Healing Assay. MDA-MB-231 and MCF7 cells were transfected with pooled CDK11 or NTC siRNA. At 28 hours post-transfection cells were re-plated to obtain a confluent monolayer. At 40hrs post-transfection the monolayer was wounded using a pipette tip. Wound healing was tracked with sequential image capture every 15 minutes for 12 or 15 hours on an Olympus microscope; images were acquired using scan^R software. Cell free area (mm^2) at the start and completion of the assay was calculated using Image J software. ***4.1A*** shows representative images of the assay in the MDA-MB-231 cells taken at 0hour and 12-hour time points; cell free area (mm^2) is appended to the image. Graph ***4.1B*** shows the area closed by cells over the course of the 15-hour assay in both the MDA-MB-231 cells and the MCF7 cells. This represents 4 replicate experiments; error bars show 95% confidence intervals. This demonstrates a significant reduction in the migration of both MDA-MB-231 cells and MCF7 cells following CDK11 knockdown.

4.2.2 Dissociating the effects of CDK11 on proliferation and migration

Having established that CDK11 depletion impaired cell migration, I aimed to identify the underlying mechanism. Cell proliferation can influence migration assays and I have demonstrated a significant reduction in proliferation on CDK11 knockdown, primarily observed between 48 hours and 72 hours (Chapter 3). It was important to determine whether the impaired migration observed on CDK11 knockdown resulted from its effect on proliferation. Furthermore, CDK11 inhibition caused an accumulation of cells with aberrant nuclear morphology that may migrate differently. Although I aimed to reduce these proliferative/mitotic effects by undertaking the assay at 40 hours following siRNA transfection, this did not exclude their influence. This work therefore aimed to assess the influence of aberrant mitosis and reduced proliferation on the impaired migration demonstrated in the 2-D scratch assays. Several approaches were used for these further investigations. The first approach was to attempt to rescue migration with the different CDK11 isoforms, attempting to dissociate proliferation and migration. The CDK11p58 isoform is integral to mitosis and this isoform rescues mitosis following CDK11 knockdown, as described in Chapter 3. If the CDK11p58 isoform could not rescue migration as it did mitosis, it would indicate that the impaired migration was unrelated to mitotic dysregulation.

4.2.2.1 Migratory Rescue with CDK11 Isoforms

I performed this work using the MDA-MB-231 cells expressing CDK11p58, CDK11p110 or empty vector that had been created and validated in my earlier work (Chapter 3). In this experiment a single CDK11 siRNA (P2), was used as the CDK11 constructs were mutated to be refractory to this oligonucleotide. Both CDK11p58 and CDK11p110 were found to rescue the migratory deficit caused by CDK11 knockdown in the empty vector MDA-MB-231 cells [Fig 4.2]. As both CDK11p58 and IRES-competent CDK11p110 rescued migration, I was unable to dissociate the impaired migration and mitotic dysregulation. However in this assay, I established that the C-Terminus of CDK11 was required for normal migration.

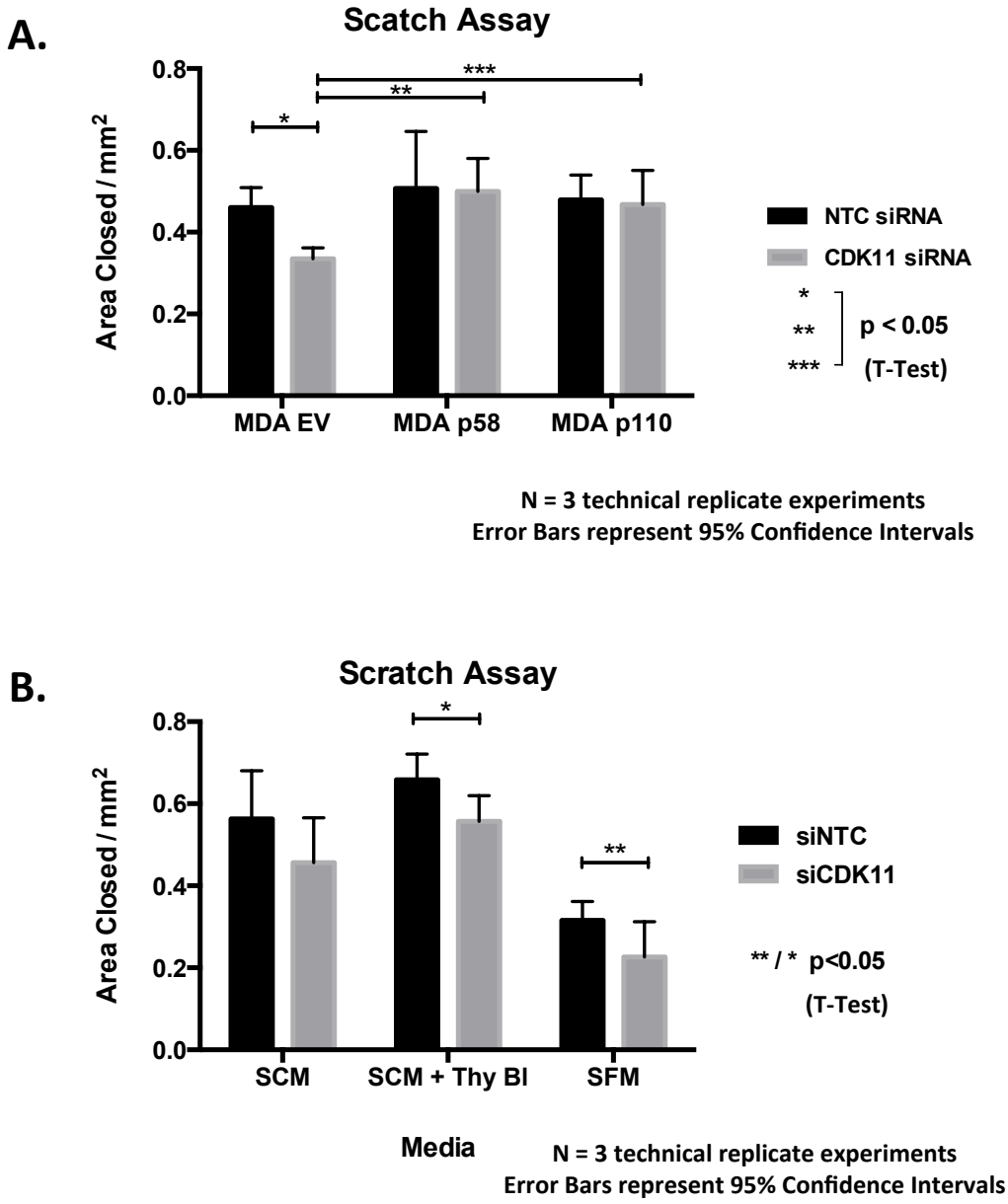

Figure 4.2. Wound Healing Assay. ***4.2A.*** MDA-MB-231 cells transduced with vector constructs CDK11 p58 (MDA p58), CDK11 p110 (MDA p110) or empty vector (MDA EV) were subject to transfection with CDK11 (P2 oligo) or NTC (N1 oligo) siRNA and the wound healing assay performed as previously described. Graph *4.2A* shows area closed at 12hour time point in each condition; expression of CDK11 p58 or p110 construct rescues the migratory deficit, subsequent to CDK11 inhibition, seen in MDA EV control cells. ***4.2B.*** MDA-MB-231 cells subject to siRNA transfection as described were plated at 28hours. Subsequent culture was undertaken in standard serum containing media (SCM), standard serum containing media + thymidine (2mM) (SCM + Thy Bl) or serum free media (SFM) and wound healing assay performed as previously described. Graph *4.2B* shows the area closed at 12hours. Culture in serum free media significantly retards migration but no condition abrogates the significant migratory deficit on CDK11 knockdown.

Expression of the recombinant CDK11p58 or CDK11p110 proteins did not affect migration compared to the empty vector [Fig 4.2], indicating that overexpression of CDK11 did not appear to promote or inhibit migration in the MDA-MB-231 line. This was consistent with a recently published study that found CDK11p58 expression inhibited migration through oestrogen receptor (ER) dependent mechanisms [234]. The authors found no effect on migration in MDA-MB-231 (ER negative) cells with CDK11p58 expression but reported impaired migration with its expression in ZR-75-30 (ER positive) breast cancer-derived cells [234]. However, I have demonstrated CDK11 knockdown inhibits migration in both MCF-7 (ER positive) cells and MDA-MB-231 (ER negative) cells.

4.2.2.2 Impact of inhibiting proliferation on the CDK11 mediated migration

The second approach I adopted to investigate the influence of proliferation on CDK11-mediated mitosis was to repeat the migration assay following CDK11 knockdown, whilst inhibiting proliferation. Inhibiting proliferation would reduce the effect of proliferation or mitosis on migration in the scratch assay. I used two strategies to inhibit cell proliferation; in the first, cells were treated with thymidine and in the second, cells were cultured in serum free media. In both cases, these treatments were applied after plating, 12 hours prior to the scratch assay. Both treatments may have consequences other than blockade of cell proliferation but both methods have been used to discern proteins that regulate migration through proliferation [99, 235]. I demonstrated that both thymidine-treated cells and serum deprived cells deviate in their migration from cells cultured in standard media, with thymidine enhancing migration and serum deprivation inhibiting migration [Fig. 4.2]. However, there remained a significant inhibition of migration following CDK11 knockdown in each condition. Interestingly, thymidine block enhanced migration in this assay contrary to its negative influence on proliferation, an effect that has only been previously described in endothelial cells [236].

Suppressing proliferation failed to abrogate the impaired migration following CDK11 knockdown. This indicated that the impaired migration

observed on CDK11 knockdown did not result from its effects on mitosis or proliferation. Thymidine and serum-free media were only applied to cells 12 hours prior to the assay, in order to obtain sufficient cells for seeding of a confluent monolayer. Therefore, a proportion of cells may have undergone aberrant mitosis prior to these culture conditions but this was unlikely to significantly influence the result given the established timeframe and kinetics of CDK11 knockdown.

4.2.2.3 Results of random cell migration following CDK11 knockdown

I utilized random migration assays as the final approach to exclude the influence of cell proliferation on CDK11-mediated migration. I interrogated migration of individual MDA-MB-231 cells, tracked by single cell imaging, following transfection with CDK11 siRNA or non-targeting siRNA. Although similar pathways regulate both directional and random migration, random migration represents a mode of migration that lacks the directional impulse of external cues and instead relies on intrinsic motility [237]. Migration of isolated cells in this assay is not driven by proliferation.

Following CDK11 knockdown, cells were plated at low density both to enable tracking of individual cells and reduce the influence of cellular contacts on migration. Cells were then imaged using time-lapse microscopy and cell motility quantified using Image J software. This conclusively demonstrated impaired random migration following CDK11 knockdown compared to control [Fig 4.3]. Again, this indicated that proliferation did not cause the migratory deficit on CDK11 knockdown. Furthermore, it showed that CDK11 is required for optimal random migration of cells.

4.3 CDK11 and Cell Polarity

Having established impaired migration after CDK11 depletion was not a consequence of aberrant mitosis or impaired proliferation, I aimed to identify other factors that may explain the altered migration observed. Simpson et al. (2008) proposed that aberrant cell polarisation caused the impaired directional migration detected following CDK11 knockdown in the 2D wound-healing assay [230]. Therefore, I elected to assess cell polarization

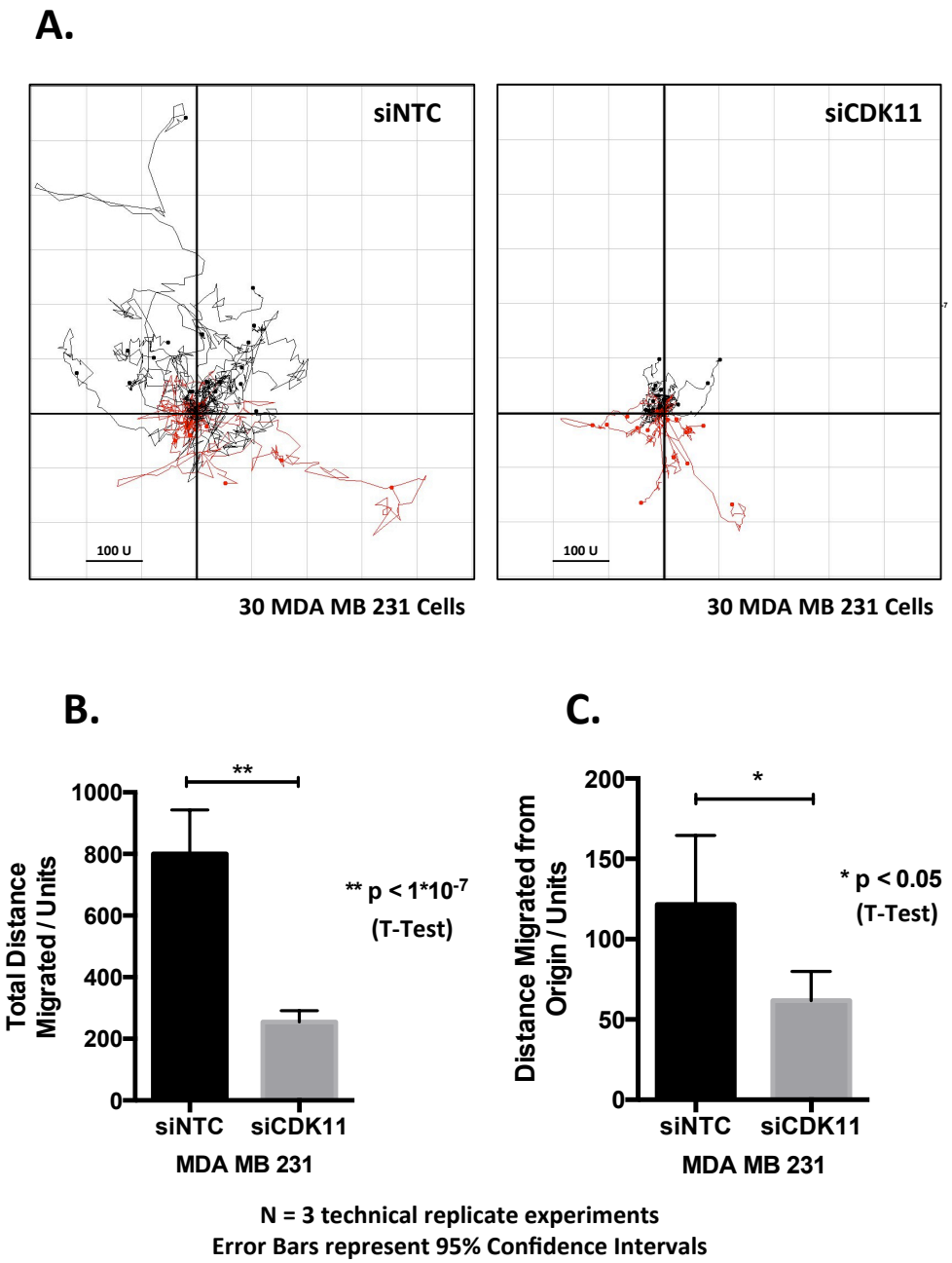

Figure 4.3. Random Migration Assay. MDA-MB-231 Cells were subject to CDK11 or NTC siRNA transfection as described. At 28 hours post-transfection, cells were plated at low density. From 40 hours cell migration was tracked with sequential image capture every 15 minutes for 12 hours on an Olympus microscope; images were acquired using scan^R software. Individual cell migration was subsequently calibrated using Image J software. ***4.3A*** shows collated migration patterns of 30 MDA-MB-231 cells over the assay at each condition, mapped using Image J Chemotaxis and Migration Tool. This demonstrates impaired migration following CDK11 knockdown. Graph ***4.3B*** shows mean distance migrated by the 30 cells in each cohort over the assay; error bars show 95% confidence intervals. Graph ***4.3C*** shows mean distance from each cells original position at final time-point; again error bars show 95% confidence intervals. Both demonstrate significant deficit on CDK11 knockdown.

following CDK11 knockdown. The wound-healing assay was replicated at 40 hours post-transfection with CDK11 or non-targeting siRNA using MDA-MB-231 cells plated onto glass coverslips. This confirmed that the impaired migration on CDK11 knockdown also occurred when cultured on glass. In subsequent assays, cells were fixed immediately following wounding and at 30 minutes, 90 minutes, 180 minutes and 360 minutes after wounding. Cells were permeabilised and stained to localize the golgi apparatus, the centrosome, the nucleus and the actin cytoskeleton. Polarity was assessed on fluorescence microscopy as previously described [238]. Cells were considered polarized if the golgi was positioned anterior to the nucleus, relative to the 'wound' edge. The percentage of polarized cells at each time point was assessed. Approximately 20% of cells display 'polarization' at wounding, consistent with the 25% expected to show 'polarization' by random positioning of the golgi. At subsequent time points, the proportion of polarized cells at the wound edge increased [Fig 4.4]. The percentage of cells demonstrating cell polarization was lower than that previously described in similar assays but the time course for polarization was comparable [239, 240]. There was no significant decrease in polarized cells observed following CDK11 knockdown at any time point [Fig 4.4]. Centrosome staining revealed no visible dissociation of this structure from the golgi apparatus following CDK11 knockdown, with it displaying similar polarity. This demonstrated that under these conditions and contrary to the mechanism of CDK11-mediated migration proposed by Simpson et al. (2008) [230], CDK11 knockdown did not impair cell polarization. Furthermore, no marked morphological effect on cytoskeletal components was detected during this polarization assay, with no significant alteration in the localization of actin, tubulin or acetylated tubulin, a marker of stable microtubules. However, more subtle effects on cytoskeletal networks cannot be excluded.

4.4 CDK11 and Focal Adhesions

Adhesion to the extracellular matrix is also important for cell migration. Therefore I aimed to identify whether CDK11 knockdown affected cellular adhesion, focal adhesion formation or the signaling events at nascent

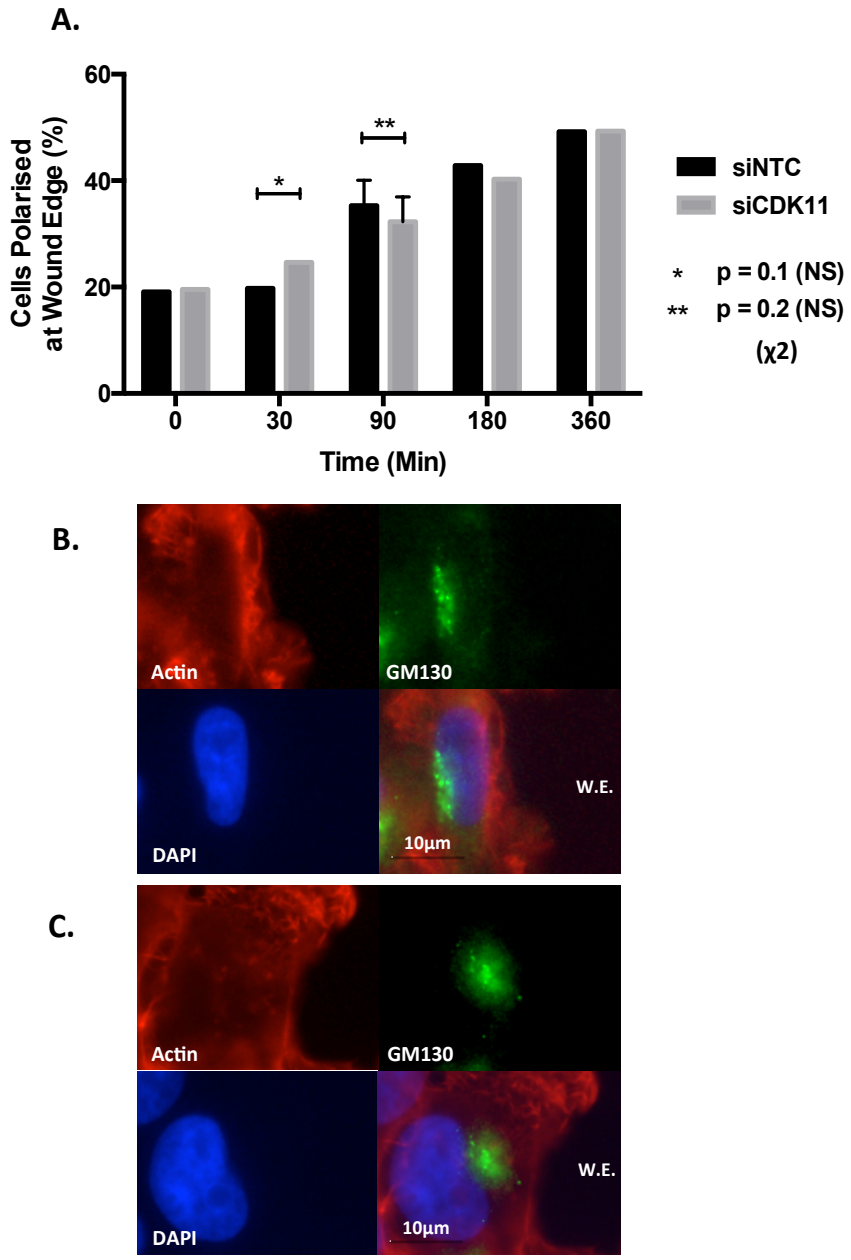

Figure 4.4. Cell Polarity Assay. Following transfection with pooled CDK11 or NTC siRNA, the migration assay was undertaken as described; with the exception cells were plated onto glass coverslips. At specified time-points, cells were fixed, permeabilised and subject to immunofluorescence with GM130 antibody (marking Golgi Apparatus), Phaelloidin and DAPI. Polarity was assessed at each time point: cells were scored as polarized if the golgi lay in a 90^{o} arc anterior to the nucleus, facing the wound edge (WE). A minimum of 50 cells was assessed at each time and condition. Graph ***4.4A*** demonstrates percentage of cells polarized at the wound edge at each time point; there is no significant divergence between control or CDK11 knockdown cells. Error Bars at 90minutes indicate 95% confidence intervals; this represents 3 replicate experiments. Image ***4.4B*** shows a representative non-polarised cell. Image ***4.4C*** shows a representative polarized cell. Wound edge marked W.E. in both images.

adhesions [Fig. 4.5, Fig 4.6, Fig 4.7]. At 40 hours following transfection with non-targeting or CDK11 siRNA, MDA-MB-231 cells were treated with trypsin and placed in suspension on a rotor at 4°C for one hour, to enable disassembly of focal adhesions. After one hour, cells were plated on collagen-coated substrates for immunofluorescence or cell lysis. Adhesion was assayed at predetermined time points after the plating. Representative images demonstrated no morphological difference between cells after CDK11 knockdown [Fig. 4.5]. Images from the adhesion experiment, clearly demonstrated initial spreading of cells from their rounded morphology in suspension. Cells then adopted a mesenchymal phenotype, irrespective of whether CDK11 was depleted or not, with numerous protrusions extending from the cell body. This morphological change suggests functional adhesions were formed and appropriately linked to the actin cytoskeleton.

This adhesion assays demonstrated that not only was morphological change absent after CDK11 knockdown but there appeared to be no alteration in the number of adherent cells. To confirm the latter observation, equal number of control or CDK11 knockdown cells were plated onto collagen coated plates. Plates were subsequently washed to remove non-adherent cells and nuclei stained with fluorescent marker DRAQ5. The fluorescent signal was quantified utilising a LiCor plate reader. There was no significant difference in fluorescent signal after CDK11 knockdown, confirming no demonstrable difference in the number of adherent cells. In addition, this study demonstrated that the majority of cells adhere rapidly (within 15 minutes) to the matrix, with no significant increase in adherent cells over time [Fig. 4.7B].

Signaling events at nascent adhesions were examined. Cell lysates collected prior to and after plating were quantified and resolved by SDS-PAGE prior to Western blot analysis. FAK and Src are influential in regulating adhesion and adhesion-dependent signaling pathways and I examined for alteration in their protein levels or activation.

Activation was determined by probing for phosphorylation of FAK at Tyrosine 397 (Y397) and phosphorylation of Src at Tyrosine 419 (Y419). No alteration in total FAK or phosphorylated FAK (Y397) was identified after

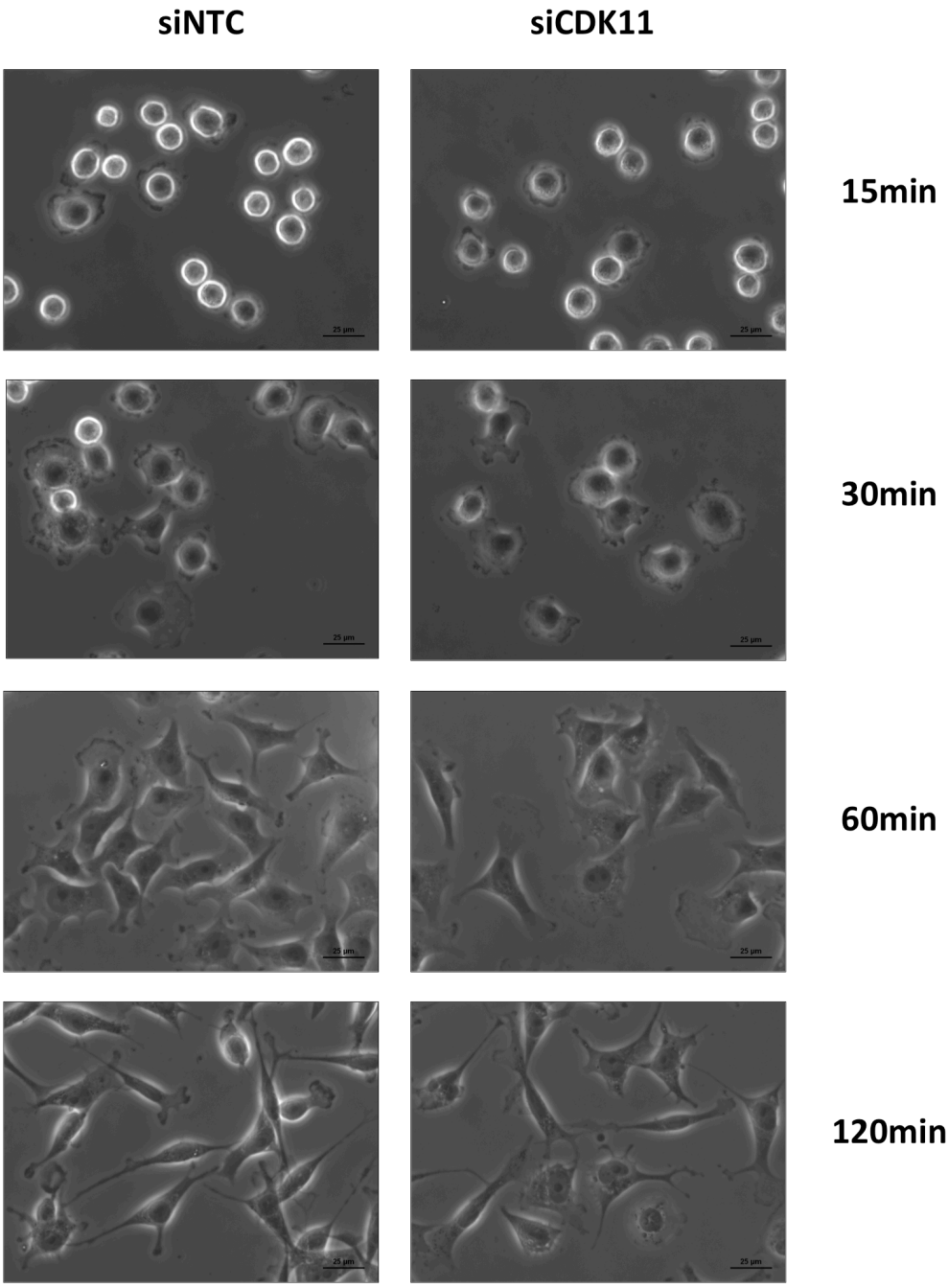

Figure 4.5. Cell Adhesion Assay. MDA-MB-231 cells were subject to pooled CDK11 or NTC siRNA transfection as described. At 40 hours cells were trypsinised and placed in suspension for 1 hour at 4^{o}C on a rotor, during which samples were retrieved for preparation of protein lysates. At 1 hour, cells were plated on collagen coated coverslips or tissue culture plastic for subsequent immunofluorescent or protein lysate analysis respectively. At specified timepoints, slides were washed and cells fixed or lysed accordingly. Images in this figure show representative images of cells, at given times points, following plating in both control and CDK11 knockdown cohorts. This demonstrates there is no significant morphological divergence between cohorts. Cells of both cohorts demonstrate the adoption of a mesenchymal phenotype with development of filopodia. This is indicative of operative adhesion formation and cytoskeletal dynamics.

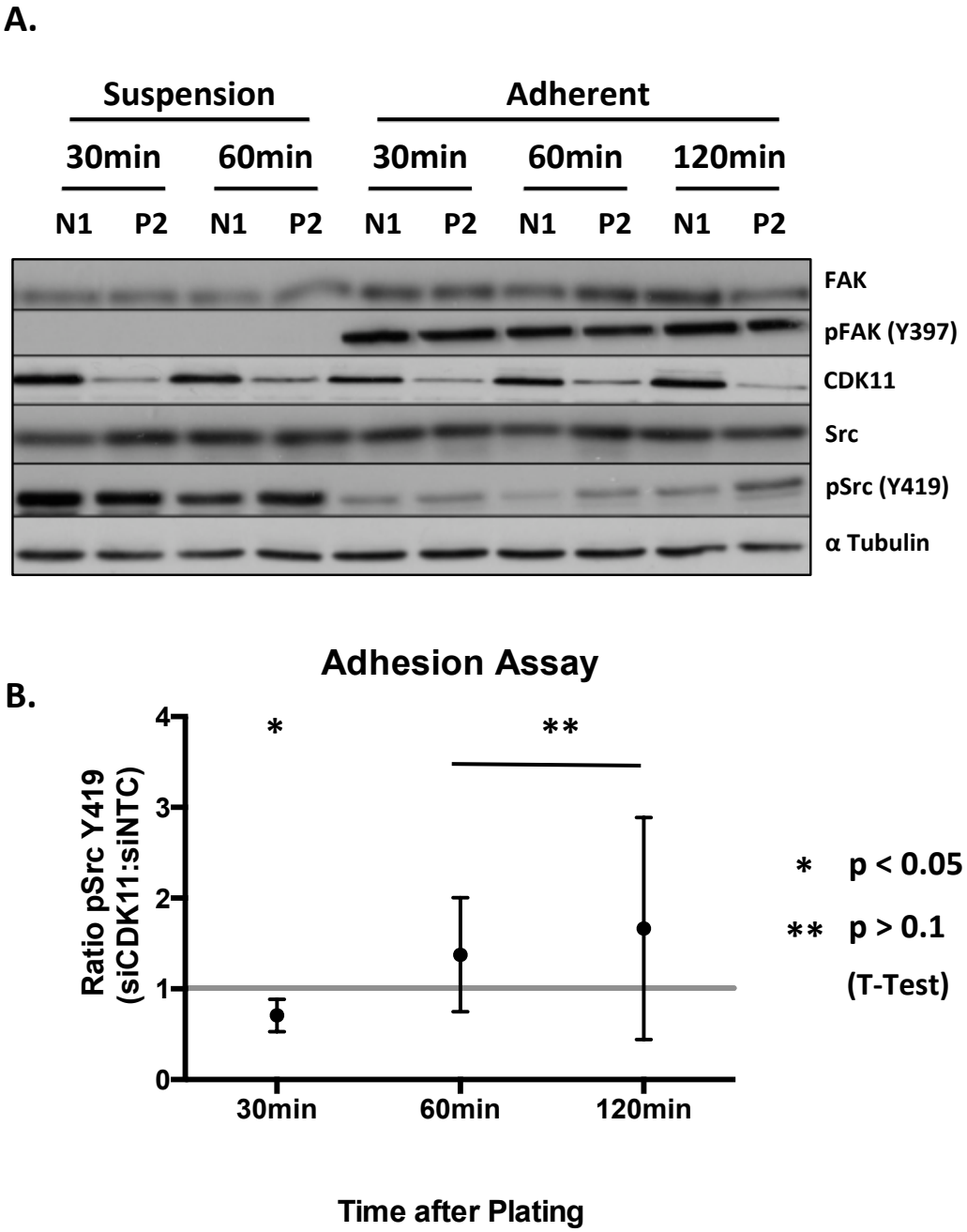

Figure 4.6. Cell Adhesion Assay. MDA-MB-231 cells were subjected to RNAi transfection and cell adhesion assay as described previously. Cells were lysed on ice using RIPA buffer; lysates were quantified prior to separation on SDS-Page gel. ***4.6A*** demonstrates representative Western Blot images of lysates collected at specified time-points during suspension or following plating (Adherent). These do not demonstrated significant alterations in levels of FAK, phosphorylated FAK (Y397) or Src. There is a significant decrease in levels of phosphorylated Src (Y419) following plating in both cohorts. Plot ***4.6B*** shows mean ratio of phosphorylated Src (Y419) between CDK11 knockdown and control cell lysates; this represents 4 replicate experiments with error bars representing 95% confidence intervals. Levels were generally inconsistent, however there was a small but significant decrease in levels at early time-points following CDK11 knockdown.

CDK11 knockdown, either in suspension or following plating [Fig. 4.6]. A marked increase in phosphorylated FAK (Y397) was demonstrated after plating but this occurs, irrespective of CDK11 depletion. Again, no alteration in total Src was observed but there was a marked reduction in phosphorylated Src (Y419) following plating, occurring largely both with and without CDK11 knockdown. After plating, a small but significant reduction in phosphylated Src (Y419) was observed at 30 minutes in the CDK11 knockdown cells [Fig. 4.6B]. Given the small reduction, the biological relevance remains uncertain. At later time points, alterations in phosphorylated Src (Y419) after CDK11 knockdown were inconsistent and no significant difference was observed.

For immunofluorescence, cells were fixed and permeabilised after plating. Immunofluorescence was performed to examine for altered localization of Src [Fig. 4.7A], phosphorylated Src (Y419), FAK, Actin or Paxillin following CDK11 knockdown. No altered localization of these proteins was observed at all time points examined.

4.5 CDK11 and Src

Published work has demonstrated that CDK11 contains an SH2 binding domain [47], which was identified using the Blk SH2 domain to affinity purify CDK11p110. The SH2 domain within Blk has significant homology to the Src SH2 domain. Therefore, I decided to investigate whether the Src SH2 domain could bind to CDK11.

Glutathione S-transferase (GST) recombinant proteins comprising GST fused to the Src SH2 domain, the Src SH3 domain or both the SH2 and SH3 domains combined were synthesised in bacterial cells, purified and conjugated to glutathione-coated agarose beads. These GST fusion protein were added individually to asynchronous MDA-MB-231 cell lysate and affinity purification undertaken. GST-conjugated agarose beads were used as the control. All three GST fusion proteins comprising the SH2 domain, the SH3 domain and the SH2/SH3 domains were able to precipitate different isoforms of the CDK11 from the lysate, whilst GST alone did not. The SH2

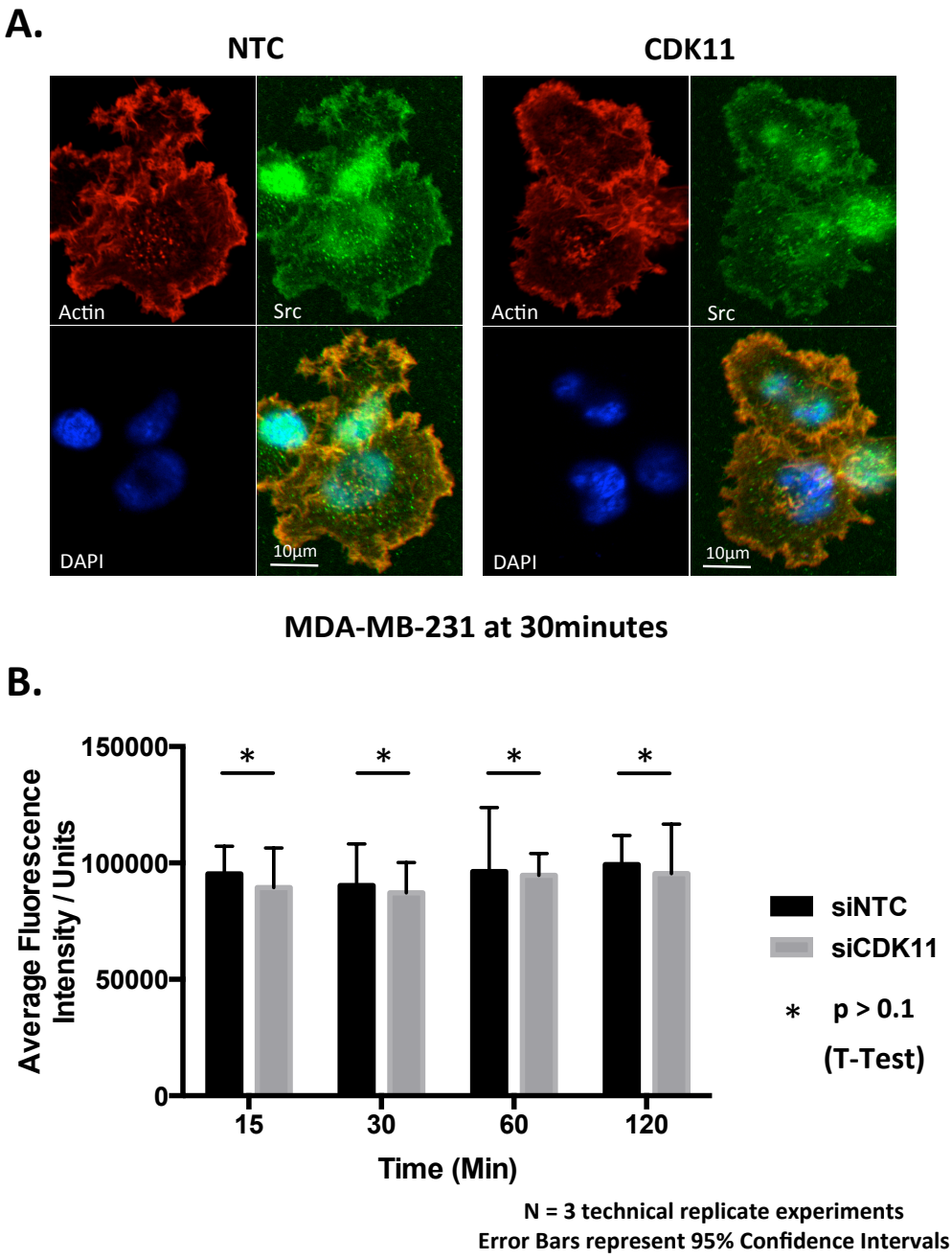

Figure 4.7 Cell Adhesion Assay. MDA-MB-231 cells were subject to the Cell Adhesion Assay as previously described. Following suspension, cells were plated onto glass coverslips or 12-well plates. For immunofluorescence, coverslips were fixed at specified time-points with 10% PFA and permeabilised with Triton-X. Coverslips were then stained with given antibody. 12-well plates were washed at specified time-points and stained with DRAQ5; fluorescence was measured with Licor plate reader. ***4.7A*** shows cells transfected with siCDK11 or siNTC at 30 minutes following plating. Coverslips were stained for Actin, DAPI and Src. No altered localisation is demonstrated between cell populations. ***4.7B*** shows the fluorescence signal obtained by DRAQ-5 nuclear staining of adherent cells at specified time-points, this provides a representation of relative number of adherent cells. No difference is demonstrated between populations.

domain primarily precipitated CDK11p110, while the SH3 domain precipitated CDK11p58. Additionally in the SH3 pull-down, a slower migrating species was demonstrated. As CDK11p110 is the longest isoform that can be generated from known transcripts, the slower migration of this species was presumed to be a consequence of post-translational modification. The size differential was not consistent with phosphorylation and may represent another modification such as sumoylation; CDK11 is found to be sumoylated in screens of sumoylated proteins. However, further work is required to characterize this larger species.

Having confirmed that isolated domains of Src could interact with CDK11, I attempt to determine whether Src and CDK11 interacted *in vivo*. No peripheral co-localisation was observed on immunoflorescence staining with Src and CDK11 targeted antibodies. Moreover, no co-immunoprecipitation of either CDK11 with Src, or Src with CDK11, could be demonstrated when precipitating endogenous proteins. Precipitation of myc-tagged CDK11 fusion protein also failed to co-precipitate Src. Therefore no interaction could be identified between endogenous Src and CDK11 in cells. As discussed previously, SH2 domains are distributed widely across the proteome and the role of the SH2-binding domain within CDK11 remains unclear. Although no interaction with Src was identified under these experimental conditions, this does not exclude interaction with other Src family members or indeed Src under specific conditions not tested, such as cellular stress or mitosis.

4.6 CDK11 and the Cytoskeleton

A further element important in cell motility is the actin cytoskeleton. As described, no morphological alterations in migratory pattern were observed after CDK11 knockdown. In addition, there was no morphological change in individual cells either upon adhesion or during migration. Furthermore, MDA-MB-231 cells expressing the exogenous CDK11 proteins at supra-physiological levels, were morphologically indistinguishable from cells transduced with empty vector.

No difference in the actin cytoskeleton was observed either during adhesion

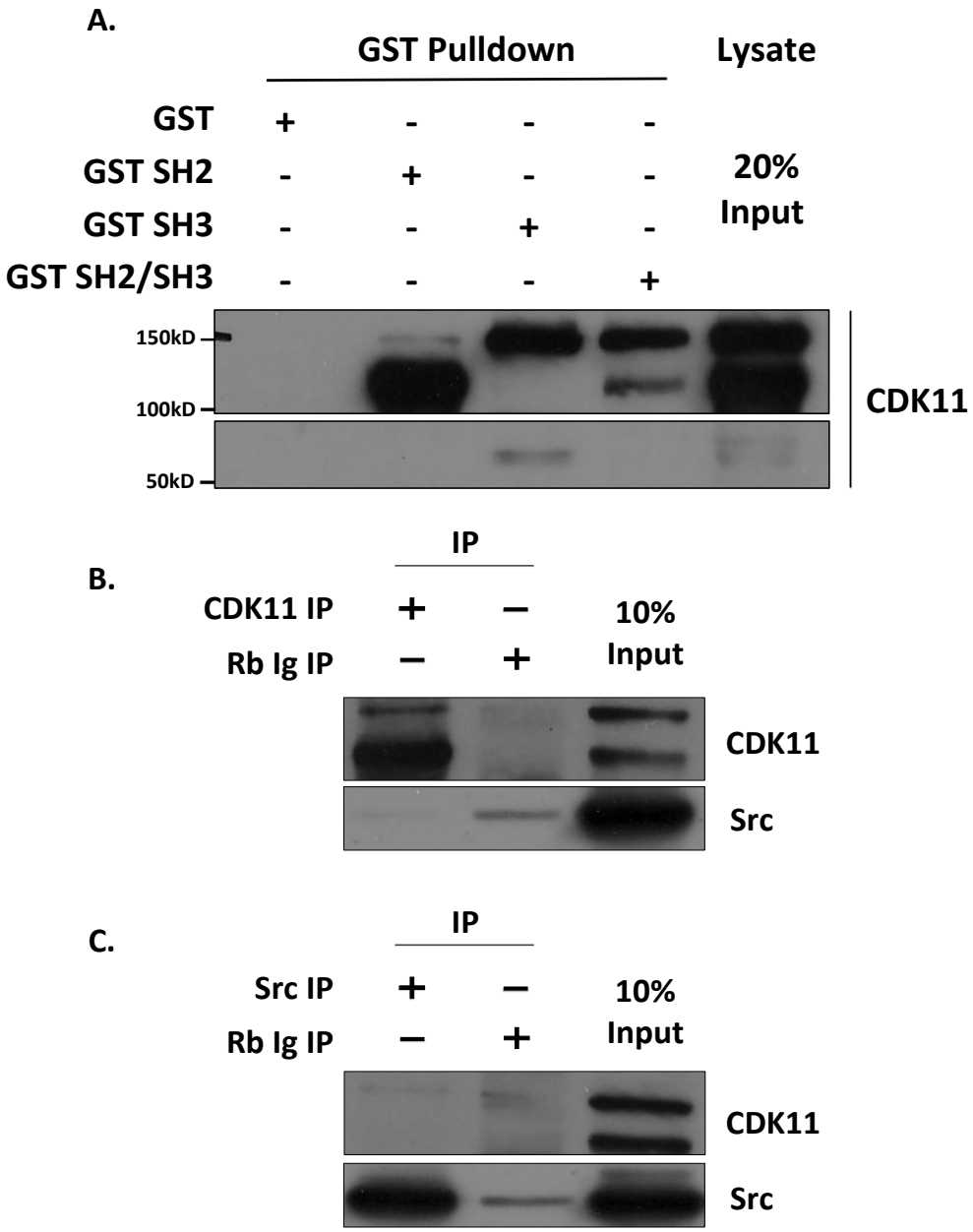

Figure 4.8 GST Affinity Purification. pGEX Vectors conveying GST alone and GST fused to Src SH2, Src SH3 or Src SH2-SH3 were transformed into BL21 cells. Cells were grown at 37°C prior to induction of protein synthesis with IPTG. Cells were lysed and protein retrieved on GSH conjugated agarose beads. MDA-MB-231 cell lysates were incubated with the protein conjugated agarose beads for 1 hour prior to washing with PBS. Protein was retrieved from the beads by addition of Sample Buffer and placement on hot block at 95°C for 5minutes. Sample were resolved on SDS PAGE gel and transferred to nitrocellulose. ***4.8A.*** Blots were stained for CDK11. This demonstrates that Src SH2 can affinity purify CDK11p110; in contrast Src SH3 can precipitate CDK11p58 and a longer isoform, assumed secondary to post-translation modification. ***4.8B.*** MDA-MB-231 cells lysates were subject to immunoprecipitation with CDK11 or Src antibody and anti-rabbit agarose beads, with Rabbit IgG antibody control. This failed to demonstrate Src-CDK11 interaction in vivo with endogenous protein.

or migration assays, on staining with phalloidin. This was also true of the interphase microtubule network, with localisation of both tubulin and acetylated tubulin similar between control and CDK11 knockdown cells stained with tubulin or acetylated tubulin antibodies. Cell polarity requires both a functional microtubule network and actin cytoskeleton and the absence of altered polarity in my work was indicative of an operative cytoskeleton. These adhesion and polarity assays therefore provide insight into cytoskeletal dynamics and did not demonstrate any alteration in the cytoskeleton or adhesion after CDK11 inhibition.

4.7 Conclusion

Work presented in this chapter has confirmed there is a migratory deficit mediated by CDK11 knockdown. This is true of both epithelial and mesenchymal cancer cells and in the context of both directional and random migration. I did not find any effect of CDK11 on mesenchymal cell polarisation, cytoskeleton dynamics or cell spreading following CDK11 depletion. Despite containing SH2 and SH3 binding domains, I was unable to demonstrate any interaction between CDK11 and Src that may regulate CDK11-mediated migration. Furthermore, I have demonstrated this migratory deficit on CDK11 depletion is not related to the function of CDK11 in mitosis / proliferation.

The diverse functions of CDK11 could impinge on cell motility indirectly, irrespective of whether CDK11 also directly mediates migratory pathways. CDK11's role in transcription and splicing may have a role in indirectly regulating migratory pathways. Rescue of the phenotype by the p58 isoform demonstrates that the C-terminus of CDK11 is sufficient to mediate motility. However, a role for endogenous CDK11p58 in transcription and splicing has not been established and the endogenous protein is primarily expressed in mitosis. Work described in Chapter 5 indicates that CDK11p58 may indeed have a role in splicing. Furthermore, although there is evidence that CDK11p58 participates in nuclear receptor signaling pathways, it is reported that p58 and p110 isoforms have opposing roles in these signaling pathways [65]. This finding is not consistent with my data indicating both isoforms

similarly rescue migration. A recent paper by Tamura et al. (2016) has reported CDK11p58 to mediate migration in prostate cancer cells through interaction with GADD45 α and γ [241]. This complex enhances migration via degradation of the epithelium-specific Ets transcription factor SPDEF, which suppresses migration and invasion [241]. During subsequent interrogation of the CDK11 interactome (Chapter 5), I was unable to precipitate GADD45 α or γ with CDK11p58 but did detect potential interaction with GADD45 γ binding protein (GADD45GIP). On account of the work by Tamura et al. (2016), this finding requires further investigation.

CDK11 knockdown therefore inhibits migration but I did not determine the precise mechanism. Further characterization of the CDK11 interactome may be beneficial in order to identify interacting partners that may directly mediate migration. Preliminary work has been undertaken to investigate CDK11 interacting partners, which is described in Chapter 5.

CHAPTER 5

Characterization of the CDK11 Interactome

5.1 Introduction

This chapter describes work I undertook to interrogate the CDK11 interactome. CDK11 regulates transcription, splicing, apoptosis and mitosis [22, 23, 24]. In addition, I have previously demonstrated the roles of CDK11 in mediating autophagy and cell migration. The following work aimed to provide a greater understanding of how CDK11 regulates these processes by further characterizing the proteins and pathways with which it interacts.

5.1.1 CDK11 Protein-Protein Interactions

The capacity of a protein to form various distinct protein-protein interactions enables it to undertake multiple roles within diverse cellular processes and pathways [242]. These interactions may be dynamic, modulatory, stable or transient; in addition, they may be both spatially and temporally defined [242]. Characterization of these interactions is fundamental to understanding the biology of a protein.

The disparate roles performed by CDK11 are enabled not only by its varied protein interactions but also by the regulated expression of discrete CDK11 isoforms. Published studies have identified numerous CDK11 interactors, reviewed in Chapter 1 [Table S1 (Appendix)]. However, there remains uncertainty regarding the role of individual isoforms, their distinct interactomes and the precise mechanisms of their action.

NCBI records 55 proteins that interact with CDK11A and 42 proteins that interact with CDK11B; 13 of these proteins are common to both *CDK11* gene products [243, 244]. A further 30 proteins not listed by NCBI, are reported to interact with human CDK11 or its eukaryote homologues [23, 41, 60, 62, 107]. Therefore in total 114 interacting proteins are reported. Although certain protein interactors have been assigned to either the CDK11A or CDK11B

protein, this differentiation often appears arbitrary, as the gene products cannot be differentiated when performing immunoprecipitation or affinity purification of endogenous protein. Furthermore, several studies have not stated which gene (*CDK11A* or *CDK11B*) was used in determining the interaction when employing other methods [63, 91, 112]. Moreover, only the human genome contains two *CDK11* genes therefore protein interactions identified in other species cannot be accurately assigned to either of these specific human proteins. Certainly no study has demonstrated, or indeed examined, whether any interaction is specific to CDK11A or CDK11B and at present it is assumed the two proteins are functionally equivalent.

5.1.1.1 Methods Used in Characterizing the CDK11 Interactome

Various methods have been described to characterize the CDK11 interactome; I aimed to adopt different strategies to identify novel interactions and elucidate CDK11 biology. The majority of early studies interrogating CDK11 interactions used the yeast two-hybrid system; this method was integral in the initial identification of CDK11's interaction with splicing components and responsible for characterizing a significant proportion of the established CDK11 interactome [41]. All published CDK11 interactions identified using the yeast two-hybrid system have been confirmed using immunoprecipitation or GST affinity purification, which although limiting false positives, may also have resulted in the rejection of a number of true interactions.

Co-purification with column-based fast protein liquid chromatography has been used to identify proteins that associate with CDK11, which fractionates with large macromolecular complexes [23]. Subsequent analysis of these complexes led to the identification of FACT and CK2 as interactors, with these interactions confirmed by immunoprecipitation [23].

Co-immunoprecipitation with subsequent analysis by mass spectrometry or Western blotting has been used to determine numerous CDK11 interactors [22, 60]. This has been undertaken using both immunoprecipitation of endogenous protein and tagged recombinant CDK11 [245, 246]. The

interaction between Chk2 and CDK11 was identified through TAP tag purification of Chk2 [60].

5.1.1.2 Methods to Characterise Protein-Protein Interactions

Numerous approaches exist to characterise protein-protein interactions. These approaches may be classified as *in vitro*, *in vivo* or *in silico* [247] and may identify physical protein-protein interactions (direct or indirect) or functional protein-protein interactions. *In vitro* methods include affinity purification and co-immunoprecipitation. *In vivo* techniques comprise the yeast two-hybrid system, synthetic lethality assays and siRNA screens. Synthetic lethality assays and siRNA screens may be used to demonstrate functional interactions, which may or may not require physical interaction [248, 249]. Large-scale siRNA screens have demonstrated the functional interplay of CDK11 with Hedgehog signaling pathways [141, 144] and were integral in the first identification of CDK11-mediated autophagy. *In silico* techniques include gene expression profiling, protein structural approaches and phylogenetic analysis. These approaches are used to support functional interactions, with the concept that interacting partners will share aspects of expression pattern, protein evolution or related structural elements [247]. As I aimed to identify direct or indirect physical interaction with CDK11 to elucidate specific pathways in which it functions, I planned primarily to use *in vitro* assays to investigate these interactions.

5.1.1.2.1 The Yeast Two-Hybrid System

The yeast two-hybrid system has been critical in characterizing the known CDK11 interactome. It enables the identification of protein-protein interactions in a transcriptome-wide screen. Furthermore, prior knowledge of potential interactors or involved pathways is not required and it therefore facilitates identification of novel aspects of protein biology. It allows weak or transient interactions to be identified more easily as the reporter gene strategy results in significant signal amplification [250]. The system detects direct protein-protein interactions but as a result of the binary nature of these interactions, it provides less information regarding the wider associated protein network. Other disadvantages of the system include the potential for

false positive results arising from the non-physiological distribution of interacting proteins. Proteins are generated in yeast and interactions that require post-translational modification may not be identified. Furthermore, yeast two-hybrid interactions occur in the nucleus and therefore cytoplasmic proteins that undergo nuclear-export may not be identified. Moreover, the whole protein sequence may not be utilized to generate bait or prey altering the interaction profile. Since completion of genome sequencing by the human genome project and the greater accessibility of mass spectrometry, the importance of the yeast two-hybrid system has diminished.

5.1.1.2.2 Affinity Purification and GST-Pulldown

Affinity purification or affinity chromatography relies on specific covalent binding interactions. A ligand is coupled to an insoluble matrix and molecules with specific binding affinity to the ligand are separated from the solution. Examples include purification of polyhistidine (His) through binding to metal ions, such as cobalt or nickel, Glutathione S-Transferase (GST) pull-down through its interaction with glutathione and avidin purification via biotin. The fusion of these protein tags (His/GST/Avidin) to the protein of interest enables its affinity purification.

Adaptions of this technique allow the GST-tagged fusion protein to be first captured to a glutathione support via the glutathione-GST affinity interaction and immobilized. The immobilized GST-tagged fusion protein can then be used to affinity purify binding partners. Affinity purification using the GST-tag is an established technique in protein interaction studies [251]. Primarily, it is used to interrogate specific protein-protein interactions and is commonly employed to determine the domains required for interaction. Classically, the GST-tagged recombinant protein is synthesized in bacterial cells, purified and applied to the assay of putative targets. Affinity purification is achieved via the glutathione coupled affinity matrix.

The use of GST affinity purification as a proteome-binding assay coupled with mass spectrometry has been reported, with proponents describing it as a protein based yeast two-hybrid equivalent [23, 252]. It involves addition of the GST-tagged protein of interest to cell lysates with subsequent purification

and mass spectrometry. Again, this strategy has both strengths and weaknesses. Major attributes include its simplicity and the lack of any requirement for exogenous protein expression within cultured cells. Dependent on the wash strategy applied to the matrix, weaker interaction may be identified as interactions need only to be maintained briefly in high stringency lysis buffer [247]. Inversely, weaknesses include the promiscuity of the GST-tag and the synthesis of GST recombinant protein in bacterial cells; proteins may therefore not have the correct conformation or necessary post-translational modifications to capture binding partners. Furthermore, in similarity to the yeast two-hybrid system, false positive interactions may occur due to the lack of target compartmentalization.

5.1.1.2.3 Co-immunoprecipitation

Co-immunoprecipitation is integral to the study of protein-protein interactions [247]. In principle, antibody targeted to the protein of interest forms immune complexes with the protein, which are then precipitated using an affinity matrix that adheres to the primary antibody. The resultant matrix with the captured protein of interest is washed and binding partners can be assessed, most frequently using Western blot or mass spectrometry. Co-immunoprecipitation may be performed on endogenous protein or with tagged fusion protein, following its expression in cells.

Immunoprecipitation of endogenous protein allows the protein of interest to be captured at physiological levels in its native state, potentially making interactions identified more biologically relevant [253]. It avoids the difficulties that may arise with expression of recombinant fusion protein, discussed below. However, caveats exist to immunoprecipitation of native protein.

The first concern relates to the protein of interest, which must be expressed at sufficient levels to enable precipitation of the target above background non-specific binding that can occur with any antibody or affinity matrix. The target protein must be within the soluble fraction and contain epitopes amenable to antibody derivation and binding. Consequently,

immunoprecipitation of endogenous protein may be less suited to discerning rare or weak interactions [247].

The second concern relates to the antibody, which must recognize the protein in a physiological conformation at an epitope accessible under assay conditions. It must be of sufficient sensitivity to extract adequate quantity of target, while demonstrating specificity to minimize the direct precipitation of non-target proteins.

The third concern relates to experimental controls. There should ideally be a control to determine non-specific binding of both the antibody and affinity matrix [254]. Cells with constitutive knockout of the protein of interest provide the optimal control to determine non-specific binding patterns but may not exist.

Immunoprecipitation of recombinant tagged protein is commonly used. However recombinant protein is not equivalent to endogenous protein and localization, expression and binding may all differ from its native form. Therefore it is necessary to validate the recombinant protein prior to use. However, tagged fusion proteins do offer advantages; they enable protein over-expression that may permit the identification of weak or rare protein interactions. Reliable, validated antibodies targeting the tag are available and facilitate not only precipitation but also confirmation of protein co-localization to confirm putative interactors. In addition, cells expressing the protein tag alone may act as the immunoprecipitation control. Synthesis of recombinant tagged protein remains the only mechanism available to undertake discrete precipitation of the CDK11p58 isoform. However, overexpression of fusion protein may also inhibit certain interactions as it distorts the reaction equilibrium in a 'prozone' effect [255].

5.1.1.2.4 Other *in vitro* Methods in Protein Interaction Detection

Tandem affinity purification involves double tagging of the protein of interest and is often combined with mass spectrometry [256]. Purification of both tags is achieved sequentially either by affinity purification or immunoprecipitation, with cleavage of the primary tag prior to secondary purification. This strategy enhances specificity of the assay [247]. It is

however a more complex precipitation strategy, which can adversely affect both yield and sensitivity [257].

Other *in vitro* assays exist including Phage Display, which uses a transcriptome library to express proteins on the surface of bacterial phages; these phages are then exposed to the protein of interest immobilized on a solid support [247]. The support matrix is washed and phages expressing protein that binds to the target remain. This cycle can be repeated to enrich for binding phages, termed panning. Protein microarrays can be used for interactions studies with thousands of full-length proteins spotted on slides in precise locations [247]. The protein of interest is purified and added to the assay with binding at individual spots detected by immunofluorescence. Protein complementation assays employ a reporter protein that is split, with half the reporter protein covalently linked to the protein of interest [247]. The other half of the reporter protein is linked to individual proteins from a transcriptome library. Interaction between the prey and bait proteins leads to formation of full-length reporter protein and a detectable signal output. All these techniques provide distinct mechanisms to identify protein interactions but can be expensive and are complex to initiate without prior experience, with no evidence of these producing more reliable results than affinity purification or immunoprecipitation strategies.

5.1.1.3 Interpreting the Results of Protein Interaction Assays

Correlation between protein-protein detection methods varies and can be low. Estimates of false positives for the yeast two-hybrid system lie between 30 to 60%, with high through put assays estimating it may be higher still [257-259]. However, the poor correlation may not only arise from false positive and false negative results but can occur due to the different interactions (direct or indirect) that different assays identify [258]. The yeast two-hybrid system detects binary direct interactions where as affinity purification and co-immunoprecipitation identifies both direct and indirect interactions, as whole protein complexes may be precipitated. These precipitation methods therefore provide a wider analysis of the interacting networks but as a consequence do not necessarily demonstrate direct contact.

No method alone can provide definitive evidence of true interactions, which should be confirmed by different techniques. Interpretation of the results must take account of several potential pitfalls. False positives interactions may occur due to non-specific binding or loss of protein localization, allowing proteins without endogenous co-location to bind. Co-immunoprecipitation, although often considered the most valid gauge of interaction, is not necessarily specific, as all precipitation strategies and affinity matrices can generate non-target binding [260, 261]. Again, co-immunoprecipitation cannot prove direct interaction, as precipitation may occur through binding intermediaries.

Protein interactions are not optimized to occur in buffer even if corrected for osmolality and pH. All protein –protein interactions within the cell occur in a concentrated milieu of macromolecules with protein concentrations in the cytosol reaching that of protein crystals [257]. This macromolecular crowding is likely to effect differences in binding affinities *in vivo* and *in vitro*.

5.1.2 Proteomics

Improvements in mass spectrometric detection and analysis have enabled significant advances in the study of the proteome. Current techniques enable not only identification of protein interactors but their accurate quantification [262].

Prior to recent advances, accurate protein quantification by mass spectrometry was dependent on metabolic labeling such as Stable Isotope Labeling with Amino acids in Cell culture (SILAC) [262]. However, SILAC quantification is not only expensive but requires intricate culture conditions, which can limit experimental methods [263]. Label-free mass spectrometry enables quantification without protein labeling, relying instead on either calculation of mean ion intensity or spectral counting. The technical advances in both mass spectrometers and software tools permit the reliable analysis of the complex datasets and have led to significant improvements in the accuracy of label-free methods [263]. Several recent studies have reported the reliable and accurate quantification of dynamic protein interactions by label-free methods [264, 265].

5.1.2.1 Label-free On-bead Mass Spectrometry

Improvements in label free quantification had enabled the adoption of label-free on-bead mass spectrometric analysis [265]. Traditional mass spectrometric analysis of protein from affinity purification or immunoprecipitation assays involved resolution of precipitates with SDS-PAGE. Gels were subsequently silver stained and unique bands present in target protein precipitate but not control were excised and analysed with mass spectrometry. Obviously this allowed high specificity as unique bands were selected but sensitivity with the technique was poor as only proteins sufficiently enriched to demonstrate a differential band on silver stain could be assessed. In the on-bead method, accurate quantification enables multiple proteins in target and control precipitate to be assessed and quantified; proteins significantly enriched in the target precipitate, representing putative interactors, can be determined. This on-bead protocol reduces the steps necessary prior to mass spectrometry, therefore not only simplifying experiments but reducing the potential for contamination or protein loss [265]. This has the potential to significantly enhance sensitivity, although there is the potential for a loss of specificity and a high rate of false positive results if specific precipitation cannot be achieved. However, this label-free on-bead protocol is proven to achieve accurate analysis, although replication is critical in ensuring reliable results, with two technical replicates for each of three biological replicates analysed at each condition [265]. Our laboratory has successfully used label-free on-bead mass spectrometry, demonstrating good correlation of results to labeled mass spectrometry but at a significant reduction in cost. The on-bead digestion and mass spectrometry was undertaken at our collaborating institution.

5.1.3 Experimental Plan

There are no published studies that interrogate and compare the discrete interactomes of the two major CDK11 isoforms, CDK11p110 and CDK110p58. Better characterization of these individual interactomes may elucidate novel CDK11-associated pathways. Furthermore, no study has investigated the CDK11 interactome during mitosis. CDK11p58 regulates

mitosis but few interacting proteins have been identified that are specific to mitosis. Moreover, although CDK11p110 is established to regulate splicing in interphase, the function of this protein in mitosis is uncertain.

I elected to use three distinct strategies to precipitate CDK11 and its binding partners, with the intention of undertaking label-free on-bead mass spectrometry on the precipitates. I aimed to undertake these precipitation assays in both asynchronous cells and mitotic cells. The first approach was to immunoprecipitate endogenous protein using CDK11-targeted antibody. The second approach was to undertake affinity purification with GST.CDK11 recombinant protein. The third approach was to co-immunoprecipitate binding partners via tagged CDK11 fusion proteins.

The precipitation of the two CDK11 isoforms offers particular challenges. The principal difficulty arises in differentiating the binding partners of the alternate native isoforms. Antibodies targeting the N-Terminus of CDK11p110 exist and therefore discrete precipitation of CDK11p110 may be possible. However the protein sequence of the CDK11p58 is identical to the C-Terminus of the CDK11p110 isoform and it is not possible to generate an antibody that will specifically differentiate the p58 isoform. Discrete immunoprecipitation of CDK11p58 must therefore be performed with tagged CDK11 fusion protein.

5.2 Immunoprecipitation of Endogenous CDK11

The first method I used investigated the CDK11-interactome via immuno-precipitation of endogenous CDK11 from MDA-MB-231 cell lysates. Employing this strategy, there is no disturbance of cellular physiology or protein conformation prior to lysis. Furthermore, there is no requirement to introduce recombinant protein expression vectors.

5.2.1 Immunoprecipitation with Commercial CDK11 Antibodies

Proprietary antibodies reported to immunoprecipitate CDK11 were identified and 5 distinct antibodies purchased. I undertook immunoprecitiation using asynchronous MDA-MB-231 cell lysate. Antibodies were used at the concentration indicated in the material data

sheet. Experimental conditions were optimized with a trial of alternate conditions varying lysis buffer, wash buffer and wash frequency to enhance CDK11 immunoprecitation. No marked variation in precipitation of CDK11p110 or Cyclin L2 was observed between conditions and I elected to use NP40 0.5% as both lysis and wash buffer (data not shown). This provided a compromise between the high stringency RIPA buffer and less stringent detergents. The choice of lysis buffer may impact significantly on co-immunoprecipitate and represents a balance between higher stringency buffers that enhance specificity but reduce sensitivity, and lower stringency buffers with the opposite effect.

I was unable to demonstrate immunoprecipitation of CDK11p58. Several factors contributed to this. First, levels of the p58 isoform in the lysate were low. Second, only one mouse antibody to CDK11 was commercially available and I found staining with this unreliable; the rabbit Abcam antibody used to probe Western blots could not be used due to the position of CDK11p58 relative to the heavy chain of rabbit antibody used in immunoprecipitation. To overcome this, I used CDK11-targeted biotin-conjugated rabbit antibody with a streptavidin-HRP conjugate for the secondary step in detection. Again, this identified CDK11p110 but not CDK11p58, although staining was not optimal (data not shown).

Using NP40 0.5%, asynchronous MDA-MB-231 cells were lysed and the lysate quantified. Immunoprecipitation was undertaken using the panel of CDK11 antibodies. This demonstrated precipitation of CDK11p110 and its major cyclin partner Cyclin L2 with 3 of the 5 antibodies: Abcam, Bethyl N-Terminus and Bethyl C-Terminus [Fig 5.1]. Under the experimental conditions, the Bethyl C-Terminus antibody was the most efficient at precipitating CDK11 and Cyclin L2 and this antibody was chosen for further experiments.

Next, I examined whether other established CDK11 interactors could be detected following immunoprecipitation. Antibodies to CDK11 interactors HSP90 and 14-3-3ε were obtained and the precipitate probed on Western blot following SDS-PAGE resolution. This demonstrated co-precipitation of both HSP90 and 14-3-3ε with CDK11 over control [Fig 5.1].

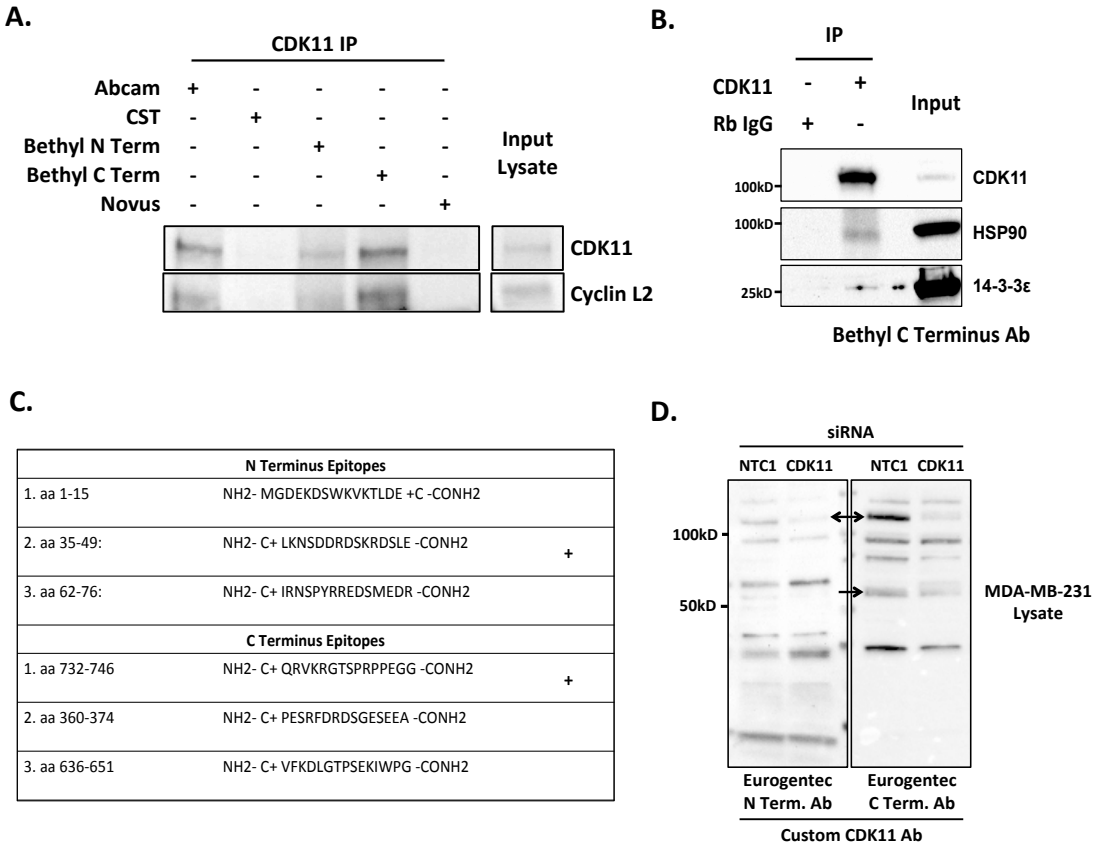

Figure 5.1 Immunoprecipitation of endogenous CDK11. MDA-MB-231 cells were lysed with NP40 buffer; the lysate was quantified and subject to immunoprecipitation with a panel of commercial CDK11 antibodies followed by Protein A conjugated agarose beads. The precipitate was washed and resolved utilizing SDS-PAGE gel. Western blot ***5.1A*** was probed with CDK11 and Cyclin L2 antibodies; CDK11p58 was not visualised due to proximity to the precipitant heavy chain antibody. This demonstrates precipitation of CDK11 with Abcam, Bethyl C Term and Bethyl N Term antibodies. Cyclin L2 is demonstrated to co-precipitate. Western blot ***5.1B*** demonstrates co-precipitation of established CDK11 interactors HSP90 and 14-3-3E with CDK11 using Bethyl C Term antibody; there is no precipitation using control Rabbit IgG antibody. Table ***5.1C*** shows putative epitopes within the N Terminus and C Terminus of CDK11 derived by Eurogentec. These were curated for homologous sequences and a single peptide (marked with +) within both the N Terminus and C Terminus used for custom antibody preparation. Custom antibody was used to interrogated lysates obtained from MDA-MB-231 cells subject to siNTC or siCDK11 RNAi. Western blot ***5.1D*** demonstrates the identification of CDK11 (marked with arrow) using both antibodies but there are a significant number of non-specific species on the blot. This precludes their use in the planned IP assay.

Therefore I had demonstrated immunoprecipitation of endogenous CDK11 with co-precipitation of its major cyclin partner and selected established interactors. However, to undertake mass spectrometry, it was critical to demonstrate both the efficiency and specificity of CDK11 co-immunoprecipitation over control. I repeated co-immunoprecititation and resolved the precipitate using SDS-PAGE. The polyacrylamide gel was then subject to silver staining. This demonstrated two obstacles to further analysis by mass spectrometry. The first was the inability to discern a discrete band representative of CDK11p110 above background on silver stain. The second was the high background in the control precipitate.

Despite optimization of conditions, the efficiency of immunoprecipitation of CDK11 remained relatively low. To illustrate this the input on the western blots in Fig 5.1A represents approximately 2% of the lysate used in each precipitation assay. This may be due to poor accessibility of the epitope under these experimental conditions.

The inability to distinguish CDK11 on silver stain indicated that the result of mass spectrometric analysis of the immunoprecipitate would likely have been invalid. However, although I was unable to demonstrate the specificity necessary to enable label-free on-bead mass spectrometry, I was able to optimize endogenous CDK11 immunoprecipitation strategies.

5.2.2 Novel CDK11 Antibodies

Having demonstrated the efficiency of CDK11 immunoprecipitation using proprietary antibodies was not sufficient to allow analysis by mass spectrometry, I decided to generate novel CDK11 antibodies in an attempt to overcome this obstacle. Due to time constraints and experience, this work was undertaken in partnership with biotechnology firm, Eurogentec, an approach used successfully within our laboratory. I chose to derive two antibodies, one targeting an epitope within the N-Terminus of CDK11p110 and a second targeting a C-Terminal epitope. The aim was to allow discrete precipitation of CDK11p110 via the N-Terminus derived antibody.

The design requirements and protein sequence of CDK11 were communicated to Eurogentec. A list of suitable peptide epitopes was

determined using proprietary models. To lessen off-target binding, I curated peptides from this list to exclude those containing non-related homologous sequences, using NCBI peptide blast. An N-Terminus sequence and a C-Terminus sequence were identified that shared the least homology to alternate peptides and these were chosen for antibody derivation [Fig. 5.1]. Following peptide synthesis, antibodies were derived in rabbit using a rapid 28-day four-stage inoculation protocol. Serum was obtained and the polyclonal antibody purified prior to delivery.

The performance of these two antibodies was assessed using MDA-MB-231 lysates, with or without siRNA CDK11 knockdown. This demonstrated that both antibodies had the capacity to detect CDK11 on Western Blot but with significant non-specific staining despite the use of various blocking strategies [Fig 5.1]. This precluded the reliable use of the antibody in immunoprecipitation experiments. The sites of the antibody epitopes was similar to that described for other antibodies derived against CDK11, with the short epitope sequence potentially contributing to poor specificity.

In this work, I was unable to achieve adequate specificity or efficiency of endogenous CDK11 immunoprecipitation to allow mass spectrometry. On account of the on-bead method, specificity is critical as the precipitate is not resolved on SDS-PAGE prior to analysis. Immunoprecipitation of native CDK11 was always going to prove challenging given the inability to adequately differentiate distinct CDK11 isoforms, the low level of endogenous CDK11p58 expression and the absence of a knockout control. Nonetheless, the advantages of endogenous immunoprecipitation made the technique worth pursuing. However, my work did enable optimization of endogenous immunoprecipitation.

5.3 Affinity Purification of GST and GST-CDK11

CDK11p58 cDNA was inserted into the pGEX 4T3 vector, with the GST-tag 5' of the insertion site. Following sequencing to confirm correct insertion, the vector was transformed into the *E Coli* BL21 cell line. The production of GST.CDK11p58 was optimized through adjustments to induction conditions. CDK11p110 cDNA was also successfully inserted into the pGEX 4T3 vector

but its expression could not be induced despite alterations to induction temperature and IPTG concentration. Potentially the recombinant protein was too large for synthesis using this system, based on the recommended maximum construct length, and full-length GST.CDK11p110 fusion protein could not be generated. Work proceeded with the GST.CDK11p58 protein alone [Fig. 5.2]. GST and GST.CDK11p58 were conjugated to the agarose bead matrix through glutathione.

Asynchronous MDA-MB-231 cells and MDA-MB-231 cells synchronised in mitosis by nocodazole block were lysed and the lysate quantified. Prior to incubation with lysates, the agarose-bound GST proteins were quantified to confirm a similar level of both GST and GST.CDK11p58 protein was added to the lysate. Lysates were incubated with unconjugated agarose beads prior to the assay as a pre-clearing strategy to reduce subsequent non-specific binding. The agarose beads conjugated to the GST proteins were incubated with lysates then washed and frozen at -80ºC. The experiment was repeated in triplicate to improve accuracy of mass spectrometric analysis. The resultant affinity matrix agarose beads were sent for on-bead digestion and mass spectrometry at University College Dublin, the institution that devised the label-free on-bead protocol adopted.

Proteins identified within each condition were quantified using label-free methods and the average of these quantifications used to generate a list of proteins enriched in the GST.CDK11p58 affinity purifications over GST alone for both asynchronous and mitotic lysate. Significant enrichment was determined on the ratio of averages and significance testing, with proteins found to be both enriched 2-fold (or greater) and above the threshold of significance (t-test $p<0.05$) considered significant. This method to determine significant enrichment has been reported by the collaborating institution [265].

5.3.1 Mass Spectrometry Results

In total 41 proteins were significantly enriched in GST.CDK11p58 affinity purifications, with 35 from the mitotic lysate and 22 from the asynchronous lysate [Fig. 5.2]. There was significant overlap in proteins identified, with 16

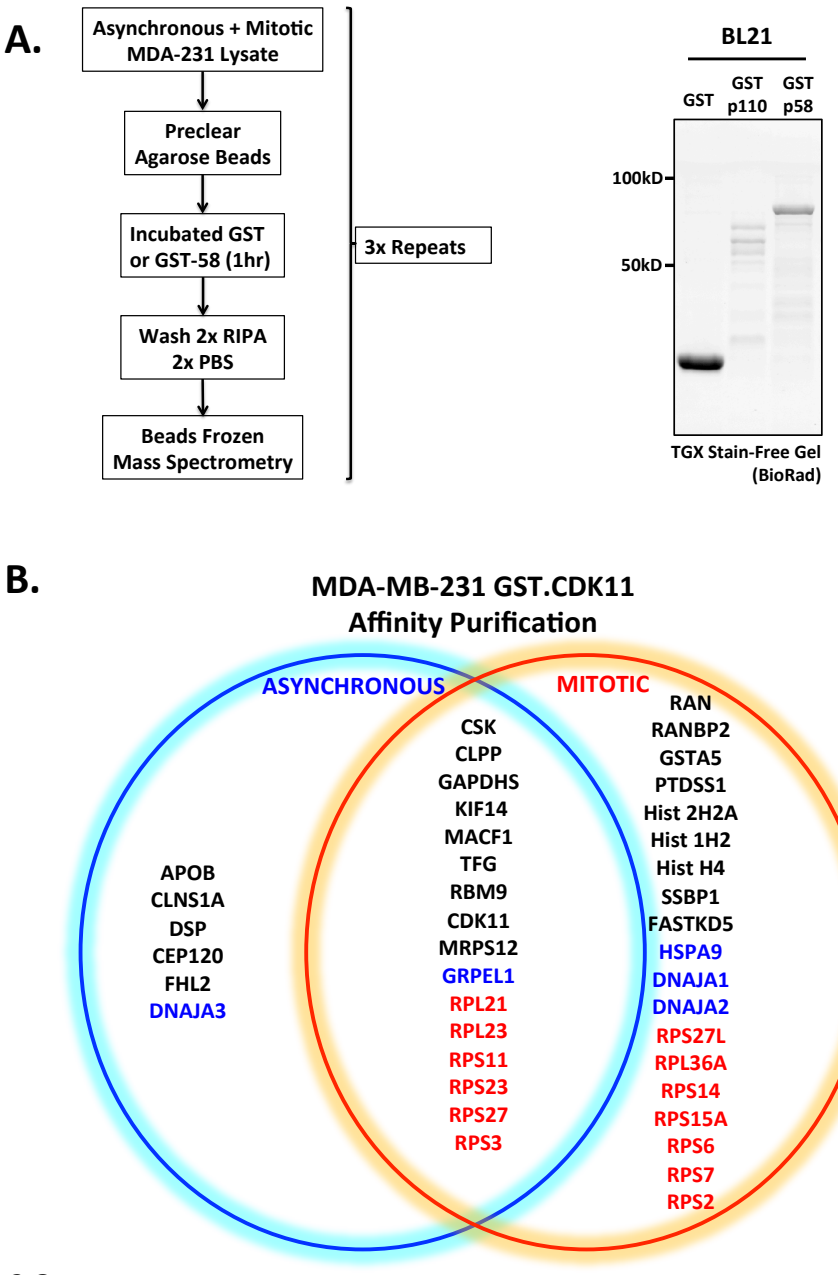

Figure 5.2 GST Affinity Purification. CDK11p58 and CDK11p110 cDNA were cloned into the GST vector pGEX4T3. The vectors were sequenced to confirm fidelity and transformed into BL21 bacterial cells. Production of the GST.CDK11p58 and GST.CDK11p110 fusion proteins was induced with the addition of IPTG. Bacterial cells were lysed and protein purified with conjugation to GSH-Agarose beads. ***5.2A*** shows a TGX Stain-free Gel of purified GST proteins; CDK11p110 could not be synthesised correctly. In addition *5.2A* delineates the protocol for affinity purification of GST.CDK11 from MDA-MB-231 lysates; samples were subsequently sent for on-bead digestion and mass spectrometry. Subsequent to label-free quantification, proteins found to be significantly enriched on GST.CDK11p58 beads over GST beads in either condition (mitotic or asynchronous MDA-MB-231 lysates) were identified. ***5.2B*** shows proteins significantly enriched (Fold >2 and $p<0.05$) and therefore putative CDK11 interactors in mitotic and asynchronous cells; there is significant overlap of proteins identified. Two principal classes of proteins were enriched; highlighted in blue are chaperone proteins and in red are ribosomal proteins.

reciprocal proteins. Importantly, the mass spectrometric analysis revealed that CDK11 represented the most enriched protein present in both the mitotic and asynchronous GST.CDK11p58 affinity purifications.

The enriched proteins identified by this technique were considered to be putative CDK11 interactors. Analysis of these proteins revealed two predominant classes within the interactors; these were ribosomal proteins and chaperone proteins. Ribosomal proteins comprised 13 (33%) of the proteins identified. Apoptosis-related CDK11p46 interacts with ribosomal protein RPS8 but no ribosomal interaction has been identified with the longer isoforms [246]. However, ribosomal proteins are frequently reported to contaminate purification assays [261, 266].

The second class identified was cellular chaperone proteins, with 5 (13%) proteins enriched. HSP70, HSP90 and CDC37 proteins are established binding partners of CDK11 but of these only a different member of the HSP70 family was identified in this assay. Furthermore, although CDK11 binds chaperone proteins, these proteins commonly bind mis-folded proteins. The production of the GST.CDK11p58 in bacteria for this assay may result in aberrant conformation and may explain the frequency of this class of proteins in the results [266].

The list of 40 putative interacting proteins was compared to the 114 established CDK11 interactors. No established CDK11 binding partner was identified in this assay. Obviously this raised concerns as to the validity of the affinity purification strategy. However, there are caveats that may explain the absence of established interactors. First, few studies have exclusively examined CDK11p58 binding partners and those that have primarily used the yeast two-hybrid system [63, 91]. Correlation between the results of different protein-protein interaction assays is often poor and this may be particularly relevant with use of the yeast two-hybrid system [258, 267]. No study has interrogated CDK11p58 interactors exclusively in mitotic cells as undertaken here with mitotic synchronization.

5.3.2 Validating Putative CDK11 Interactors

To validate this list of putative interactors, interactors were curated and proteins of interest identified. Although interaction with either ribosomal or chaperone proteins may be genuine, due to the caveats discussed above, I considered it appropriate to correlate these results with those of the co-immunoprecipitation before pursuing these putative interactors. Initially, three other proteins were chosen for validation due to aspects of their biology that align with established CDK11 functions; these were RAN, KIF14 and CSK.

5.3.2.1 Identifying Interactors for Validation

CDK11 is a RAN-GTP dependent microtubule stabilizer in mitosis but no direct interaction between CDK11 and RAN has been demonstrated [84]. RAN is integral in this role to microtubule dynamics at mitosis [84]. CDK11 interacts with the RAN Binding Protein 9 but it was the apoptotic p46 isoform, not the larger isoforms, for which this was established [108]. Therefore, the identification of RAN in this screen was of interest.

KIF14 is a member of the Kinesin-like family. The kinesin superfamily of microtubule-associated motors plays important roles in intracellular transport and cell division [268]. KIF14 functions during mitosis, localizing to the spindle body at anaphase and is believed to mediate abscission and cytokinesis [269, 270]. CDK11 also plays a critical role in these processes [144, 271].

C-terminal Src Kinase (CSK) regulates members of the Src family kinases through phosphorylation of their C-terminal domain [272]. It phosphorylates Src at Tyrosine 527, resulting in suppression of Src activity [272]. CSK contains both an SH2 and SH3 domain and as identified in Chapter 4 Src SH3 was able to precipitate CDK11p58. Src regulates cell adhesion and motility but is also reported to mediate mitotic pathways [273-275].

5.3.2.2 Repeating Affinity Purification to Identify CSK, RAN, KIF14

To confirm the validity of the mass spectrometry results, affinity purification with GST and GST.CDK11p58 was repeated and the precipitate probed on Western blot following SDS-PAGE resolution. I was able to demonstrate

affinity purification of CSK with GST-CDK11p58 [Fig. 5.3]. However, RAN and KIF14 could not be detected following affinity purification with GST.CDK11p58. The reasons for this remain unclear as both proteins were significantly enriched in the GST-CDK11p58 precipitate on mass spectrometry, representing enrichment in three biological replicate experiments. Following receipt of the mass spectrometry results, the GST.CDK11p58 fusion protein was resynthesized in *E. Coli* BL21 cells using the same conditions as previously but it is possible the conformation of the protein was altered, which may explain the failure to bind.

Despite the inability to replicate the mass spectrometry results for KIF14 and RAN, I decided to investigate all three putative interactors further prior to classifying any as false positives. I investigated for evidence of interaction using co-immunoprecipitation, protein localization with immunofluorescence and protein expression following CDK11 knockdown.

5.3.2.3 Immunoprecipitation of CSK, RAN, KIF14 and CDK11

Asynchronous MDA-MB-231 or synchronized mitotic MDA-MB-231 cells were lysed and lysate quantified. Immunoprecipitation from both asynchronous and mitotic lysate was performed using antibodies targeted to KIF14, CSK and RAN. No co-immunoprecipitation of endogenous CDK11p58 or CDK11p110 was detected with either KIF14 or CSK precipitate in either asynchronous or mitotic conditions [Fig. 5.3]. I was unable to obtain satisfactory immunoprecipitation of RAN to probe interactors. Furthermore, I was unable to detect KIF14, RAN or CSK following the reverse immunoprecipitation of endogenous CDK11 or tagged CDK11 fusion protein. These putative CDK11 interactors were identified using CDK11p58 and the endogenous levels of this isoform were low even in the synchronized mitotic cells. However, immunoprecipitation of CDK11p58 fusion protein, expressed at supra-physiological levels, did not identify any interaction with these proteins. Therefore on co-immunoprecipitation, I could not demonstrate that these interactions were genuine. This did not exclude any interaction between the proteins as any interaction may occur at low frequency or in a highly-regulated spatiotemporal manner, which was not detected under these experimental conditions.

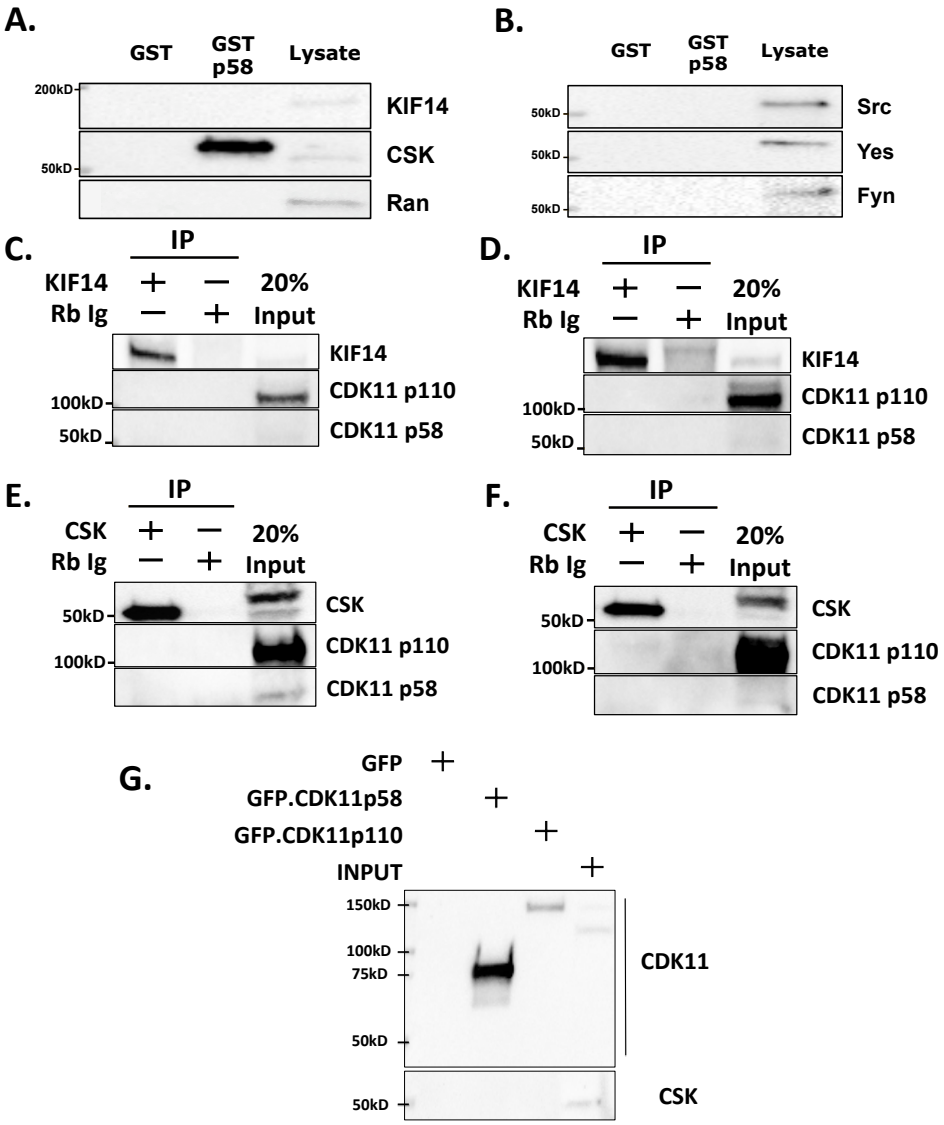

Figure 5.3 GST.CDK11p58 Affinity Purification. Agarose beads conjugated to GST or GST.CDK11p58 were incubated with MDA-MB-231 lysates for 1 hour. Beads were subsequently washed twice with both RIPA and PBS sequentially, as per the affinity purification protocol in *Fig 5.2A*. Sample buffer was added to the beads and the precipitate resolved with SDS-PAGE and Western blot. Western blot ***5.3A*** confirms purification of CSK with GST.CDK11p58 from asynchronous MDA-MB-231 lysate but fails to demonstrate pull-down of KIF14 or RAN. Western blot ***5.3B*** demonstrates that GST.CDK11p58 does not pull-down other Src SH3 domain containing proteins, including Src, Yes and Fyn. Immunoprecipitation of KIF14 from mitotic (***5.3C***) or asynchronous (***5.3D***) MDA-MB-231 lysate fails to demonstrate co-precipitation of either CDK11p58 or CDK11p110. Similarly, immunoprecipitation of CSK from mitotic (***5.3E***) or asynchronous (***5.3F***) MDA-MB-231 lysate also fails to show co-precipitation of CDK11 isoforms. Blots were probed with CSK murine antibody and CDK11 antibody conjugated to biotin with secondary streptavidin HRP to minimize interference from precipitant antibody heavy chain proteins. ***5.3G*** shows immunoprecipitation of GFP.CDK11p58 and GFP.CDK11p110; there is no co-precipitation of CSK.

5.3.2.4 Interrogating CSK Affinity Purification

Interesting, on the Western blot following GST.CDK11p58 pull-down, the CSK species in the lysate appeared to migrate differently to the species precipitated. The slower migration on SDS-PAGE of the precipitated species was replicated in further pull-down assays. The reason for this was unclear but may have represented precipitation of the protein following post-translational modification. I probed for CSK-Homology Kinase (CHK) to confirm this species did not represent CHK, as cross-reaction of CSK antibody to CHK is reported, but no CHK was detected in the precipitate (data not shown). Western blot following immunoprecipitation of CSK demonstrated two CSK species in the lysate, the smaller species of which was precipitated. This finding may explain why immunoprecipitation of CSK did not precipitate CDK11, as GST.CDK11p58 may have affinity purified the larger species. However, neither species was identified following immunoprecipitation of the CDK11 fusion protein.

In addition, CDK11p58 is reported to contain an SH3 binding domain and my work in Chapter 4 confirmed precipitation of CDK11p58 with the Src SH3 domain. CSK contains a similar SH3 domain. Given the ability of GST.CDK11p58 to affinity purify CSK, I examined whether this was specific to CSK or whether CDK11p58 could also precipitation SH3 domain-containing Src family members. The ubiquitously expressed members of the Src family kinases, Src, Yes and Fyn, contain SH3 domains but none of these proteins were affinity purified with GST.CDK11p58 [Fig. 5.3].

5.3.2.5 Localisation of CSK, KIF14 and RAN

MDA-MB-231 cells, plated on glass coverslips, were transfected with CDK11 targeted or non-targeted siRNA. At 48hrs, cells were fixed and permeabilised. Immunoflourescence demonstrated CSK and KIF14 predominantly localized to the cytoplasm at interphase, which has been previously described [270, 276]. Staining with RAN antibody was poor, with little signal above background. At mitosis, CSK and KIF14 localised to the nucleoplasm with no localization to the mitotic spindle or other structures. However, at anaphase KIF14 clearly localized to the midbody consistent with

its role in cytokinesis and abscission. No similar localization of CSK was observed.

Although myc.CDK11p58 fusion protein localised to both the cytoplasm and nucleus during interphase, native CDK11 was localised solely in the nucleus throughout interphase, as demonstrated by immunofluorescence and cell fractionation. At mitosis, CDK11 was distributed throughout the nucleoplasm. I was unable to identify localization of CDK11 to the centrosome, mitotic spindle or midbody. There was no evidence that it may co-localise to the mid-body with KIF14.

No marked alteration in CSK localization was observed after CDK11 depletion, indicating that any interaction did not regulate protein localization [Fig 5.4]. Following CDK11 knockdown, KIF14 continued to localize to the midbody; in certain cells, the signal appeared more diffuse but this finding was inconsistent [Fig 5.4]. Furthermore, interpretation was complicated by the markedly abnormal morphology of the midbody/spindle complex following CDK11 depletion.

5.3.2.6 Expression of CSK, KIF14 and RAN after CDK11 Depletion

Next, I examined for alteration in KIF14, CSK and RAN expression, after CDK11 knockdown. In addition, I assessed Src expression and Src activation, using phosphorylated Src (Y419) and phosphorylated Src (Y527) antibodies. The rationale for performing this was due to the role of CSK in regulating Src activation. The effects of CDK11 depletion may differ through the cell cycle and therefore MDA-MB-231 cells were synchronized at G1/S via double thymidine block. At 48 hours post transfection with CDK11 targeted or non-target siRNA, MDA-MB-231 cells were released from thymidine block. Cells were lysed at specified time points following release. This enabled interrogation of protein levels through the cell cycle. No significant alteration in level of RAN or KIF14 was observed after CDK11 depletion; an elevation in CSK was identified at 6 hours following release but was not consistent in repeat experiments [Fig 5.5]. Interestingly, although no alteration in Src was found, there was a marked increase in phosphorylated Src (Y419) during S-Phase after CDK11 depletion; this was replicated in a further experiment. No

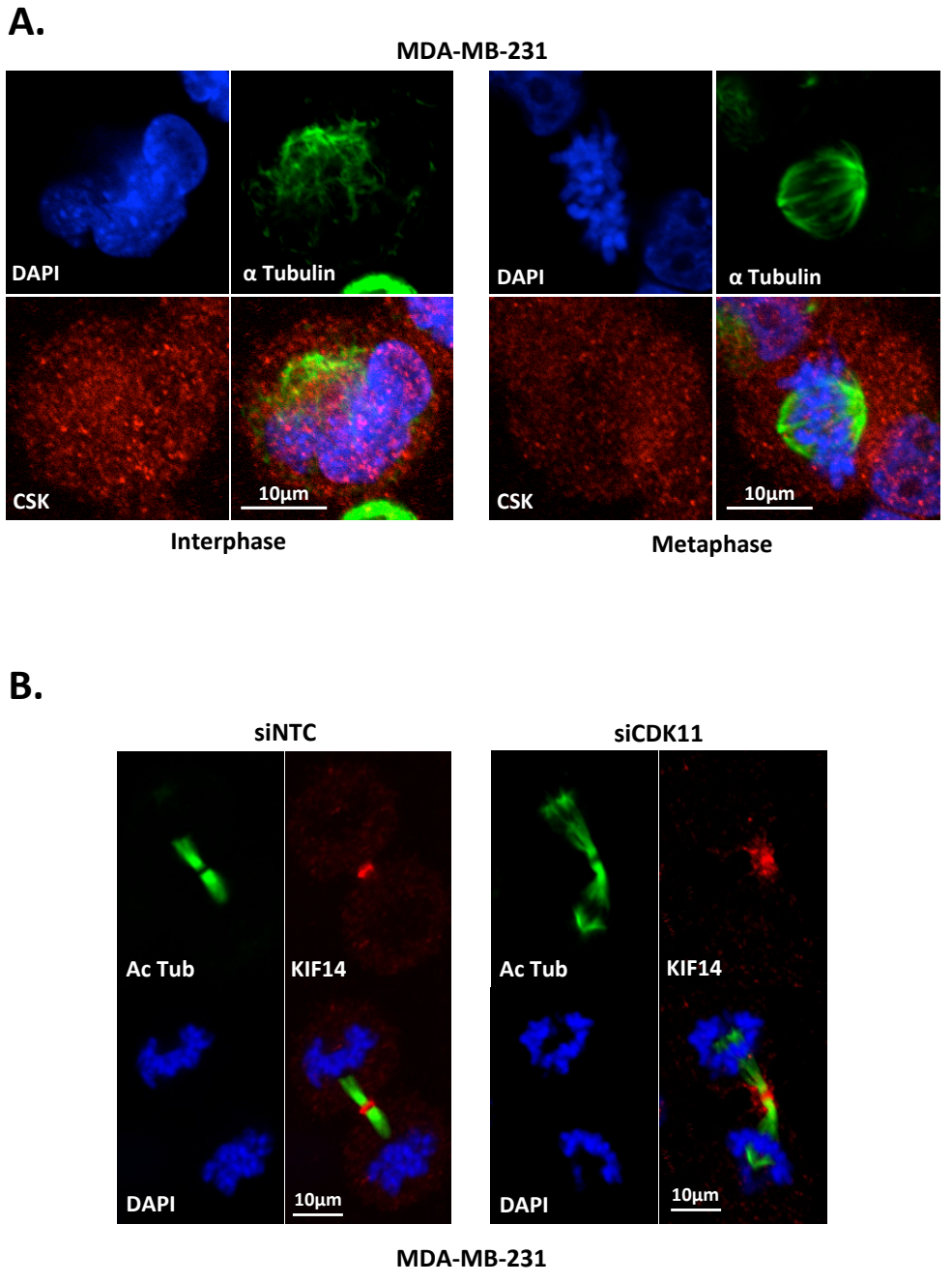

Figure 5.4 CSK and KIF14 Localisation. MDA-MB-231 cells, cultured on glass coverslips, were fixed with 10% PFA and permeabilised with Triton-X. Cells were subsequently stained with a combination of antibodies targeted to CSK, α Tubulin and KIF14 with DAPI nuclear stain. ***5.4A*** shows representative images of CSK localization in cells at interphase and metaphase. CSK localizes to both the cytoplasm and nucleus at interphase and throughout the nucleoplasm at mitosis. ***5.4B*** shows localization of KIF14 to the midbody at cytokinesis. Throughout earlier stages of mitosis it localizes throughout the nucleoplasm (not shown); no localization to the centrosome is seen. *5.4B* demonstrates that KIF14 continues to localize to the midbody following CDK11 knockdown. Aberrant cytokinesis is recognized following CDK11 dysregulation. It is however noted that fewer cells show normal midbody formation following CDK11 knockdown; this may therefore represent cells with lesser CDK11 knockdown.

change in phosphorylated Src (Y527) was observed, which is the site of CSK phosphorylation. However, our laboratory has found inconsistencies in commercial antibody staining of this phosphorylated residue and no positive control was present to confirm the validity. These alterations in phosphorylated Src (Y419) were not a consequence of altered cell cycle phase as demonstrated by propidium iodide and BrdU staining performed in parallel [Fig 5.5]. BrdU demonstrated no alteration in the duration of S-phase. Obviously further experiments are required to confirm the results, assess its relevance and investigate the mechanism of regulation.

5.3.2.7 Src Activation in S-Phase following CDK11 Depletion

Although CSK may regulate this Src activation, no consistent alteration in CSK or phosphorylated Src (Y527) was observed after CDK11 knockdown. Furthermore, no interaction between CDK11 and CSK has been demonstrated *in vivo* and therefore Src activation may occur via other mechanisms. Src activation is reported to regulate G1/S progression via phosphorylation of p27KIP [277]. Phosphorylation of p27KIP causes the loss of repression of the CDK2, with subsequent CDK2/Cyclin E mediated degradation of p27KIP [277]. In addition, Src may regulate aspects of mitosis, including promotion of satisfactory spindle orientation and abscission [275, 278]. The significance of increased Src activation after CDK11 depletion was not clear; this occurred at 6 hours and 9 hours following release when cells were progressing through S-phase and entering mitosis. My work demonstrated that Src activation following CDK11 knockdown did not effect cell cycle progression. Further work is therefore required to investigate this observation.

5.3.3 Conclusion GST Affinity Purification Experiment

In summary, the validity of the results of GST affinity purification is questionable given the inability both to demonstrate established interactors and to confirm putative interactions *in vivo*. Moreover, only one of the three proteins was validated on repeat affinity purification. The alteration in Src activation after CDK11 depletion was interesting and further work is required to investigate this observation.

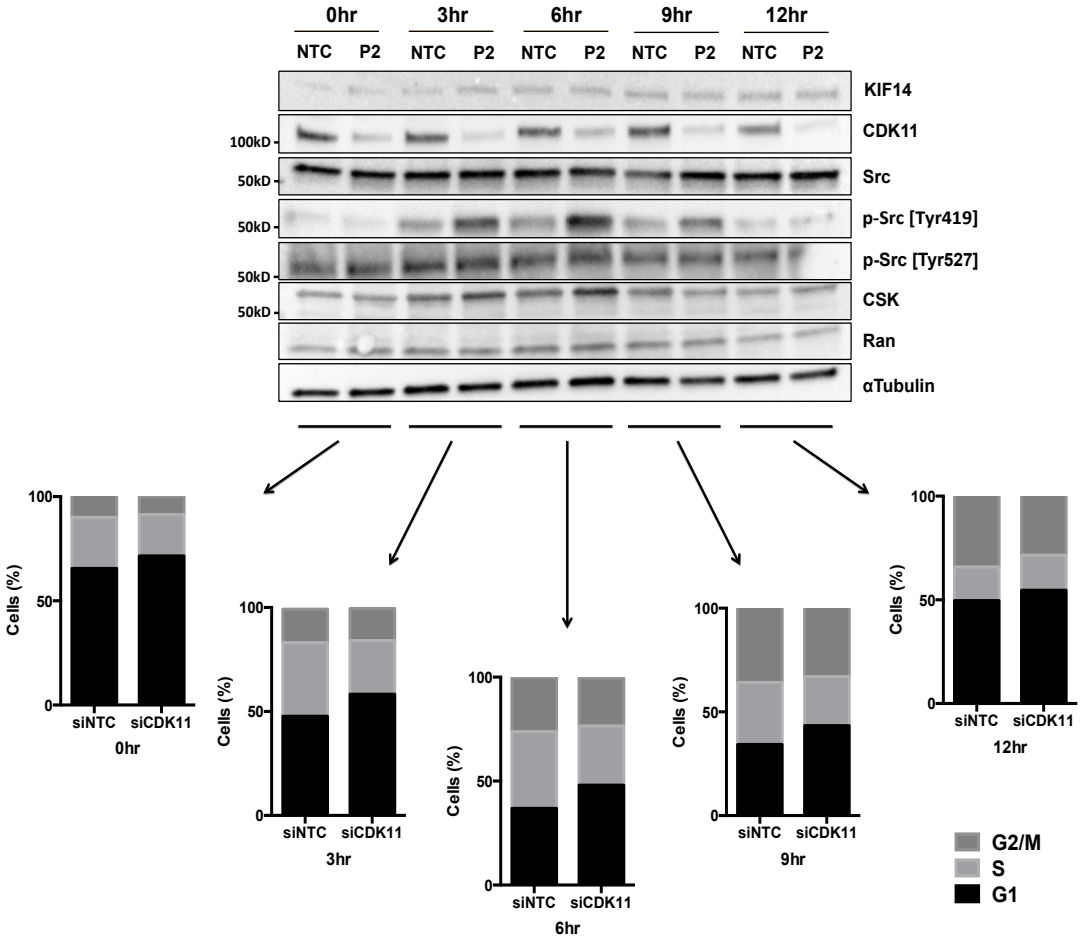

Figure 5.5 Cell cycle, CDK11 Knockdown and Putative Interactors. MDA-MB-231 cells were subject to transfection with siCDK11 or siNTC RNAi prior to synchronisation at G1/S with double thymidine block. On release from block, cells were assayed at predetermined time points; cells were pulsed with BrdU at 3 hours following release to enable tracking of cells through S-Phase. At each time point, cells were either fixed with methanol for FACS cell cycle analysis or lysed for protein quantification. This was undertaken to interrogate for levels of putative interactors or alteration to Src / Src activation, a target of CSK. This does not demonstrate alteration in levels of RAN or KIF14. A small increase in CSK levels was observed at 6 hours following CDK11 knockdown. No alteration in total Src was observed but a pronounced increase in Src [Try419] phosphorylation was demonstrated following CDK11 knockdown. This appeared maximal during S-Phase. There was no reciprocal alteration in Src [Try 527] phosphorylation. Cell cycle analysis determined this was not attributable to altered cell cycle phase; no gross alteration in the duration of S-Phase was observed (data not shown). This blot is representative of two replicate experiments; further work is required to confirm findings.

5.4 Immunoprecipitation of recombinant tagged CDK11

Next, I aimed to use tagged CDK11 fusion proteins to co-immunoprecipitate CDK11 interacting proteins. As the construction of such tagged recombinant proteins may compromise both the functionality and binding of the protein, it was important to confirm that any fusion protein localized and functioned in a similar manner to endogenous protein.

5.4.1 Immunoprecipitation of myc.CDK11

The myc.CDK11 fusion proteins had been synthesized and validated in earlier work (Chapter 3), with the ability to rescue CDK11 knockdown. These recombinant proteins were therefore used in initial experiments. I undertook immunoprecipitation in the stable expressing MDA-MB-231. The use of the stable expressing cells has both advantages and disadvantages compared to transient construct expression. The stable cell lines express CDK11 at a level tolerable to cells. Cells enduring transient transfection potentially suffer not only significant stress as a result of the transfection but the high level of protein expression may alter protein interactions and have other deleterious effects. Paradoxically, the potential disadvantage of stable expressing cells is that high levels of protein expression may not to be achieved, reducing the likelihood of identifying novel low-level interactors.

MDA-MB-231 cells expressing myc.CDK11p58, myc.CDK11p110 or empty vector were lysed with NP40 buffer and the lysate quantified. To optimize precipitation, immunoprecipitation of the myc.CDK11 fusion proteins was performed with two distinct myc-targeted antibodies, conjugated to agarose or magnetic beads. I demonstrated successful immunoprecipitation of the CDK11 fusion proteins using this strategy [Fig. 5.6]. However, despite the successfully precipitation of the myc.CDK11 fusion proteins, significant background signal was apparent. This once again prevented the identification of bands enriched in the CDK11 precipitates on silver stain [Fig. 5.6]. Others both within the laboratory and externally have reported similar difficulties with the myc-tag [279], often attributed to precipitation of endogenous myc. In addition, no control cell line expressing myc-tag alone

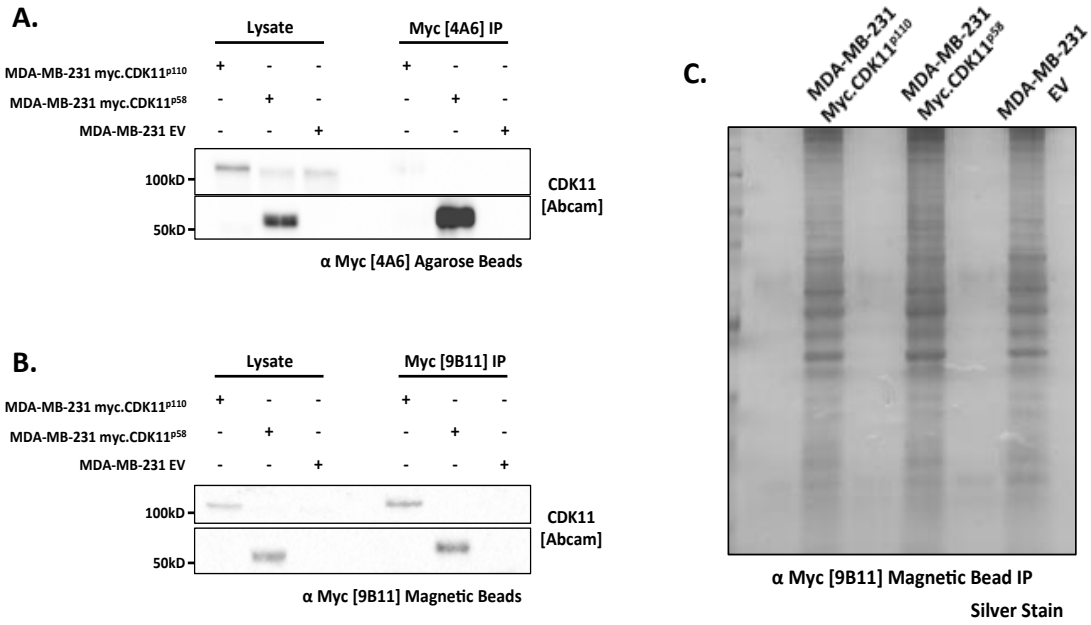

Figure 5.6 Myc Tag Immunoprecipitation of CDK11. MDA-MB-231 cells, stably expressing myc tagged CDK11p110 or CDK11p58, were lysed with NP40 buffer. Lysates were quantified and between 1mg and 5mg protein aliquoted dependent on assay. Anti-myc tag antibodies conjugated to agarose or magnetic beads were used to precipitate the myc.CDK11 chimeric proteins. Beads were washed with NP40 buffer, prior to the addition of sample buffer and resolution with SDS-PAGE and Western blot. Western blot ***5.6A*** shows the successful precipitation of CDK11 with agarose conjugated anti-myc antibody 4A6; CDK11p58 appears most efficiently precipitated. Western blot ***5.6B*** demonstrates immunoprecipitation of both CDK11 isoforms with anti-myc antibody 9B11 conjugated to magnetic beads. ***5.6C*** demonstrates silver stain of SDS-PAGE gel following myc precipitation from MDA-MB-231 lysates of cells stably expressing CDK11 constructs or containing Empty Vector (EV) alone. Significant background is visible in the control EV lysate and distinct species representing the CDK11 constructs are not visible. This may be due a combination of inefficient precipitation, low-level protein expression and high background.

had been created. I decided due to both the high background signal and the lack of control cell line to generate a novel CDK11 fusion protein.

5.4.2 Generating Stable Cell Lines Expressing GFP.CDK11

Numerous tags are available with differing strengths and weaknesses. Small tags may be less likely to influence protein function but others within the unit had successfully utilized the GFP Trap system. The GFP-tag has limited interactions with mammalian proteins and therefore less non-specific or tag specific immunoprecipitation [260]. In addition, the GFP-tag enables proteomic work to be correlated more easily with co-localisation using immunofluorescence.

CDK11 isoforms, again containing RNAi refractory sequences, were inserted in-frame into the EGFP-N vector. The EGFP-CDK11 cassettes were then excised and inserted into the pBabe retroviral vector to allow transduction. The constructs were sequenced to confirm their fidelity and transduced into both the HCT116 and MDA-MB-231 cell lines.

5.4.2.1 Confirming Localisation and Function of GFP.CDK11

Following successful transduction of the GFP.CDK11 constructs, I aimed to validate these fusion proteins, confirming similar behavior and function of the proteins to endogenous CDK11. Localisation of both GFP.CDK11p110 and GFP.CDK11p58 was similar to that of both endogenous CDK11 and the validated myc.CDK11 fusion proteins. GFP.CDK11p110 was demonstrated to be primarily nuclear throughout the cell cycle. GFP.CDK11p58 was both cytoplasmic and nuclear at interphase, while localized to the nucleoplasm through mitosis. This was the case in both HCT116 and MDA-MB-231 cells. Although putative nuclear localizing sequences are described in the p58 isoform, the localization of these in the vicinity of the kinase domain may render them functionally irrelevant. In addition, endogenous CDK11p58 is primarily mitotic at which time no nuclear envelope exists [23].

In my experiments, CDK11 was not demonstrated to localize to either the mitotic centrosome or the mitotic spindle; this was the case for the myc-tag proteins, the GFP-tag proteins and endogenous CDK11, localised with antibody [Fig. 5.7]. Although localization of CDK11 to the mitotic spindle has

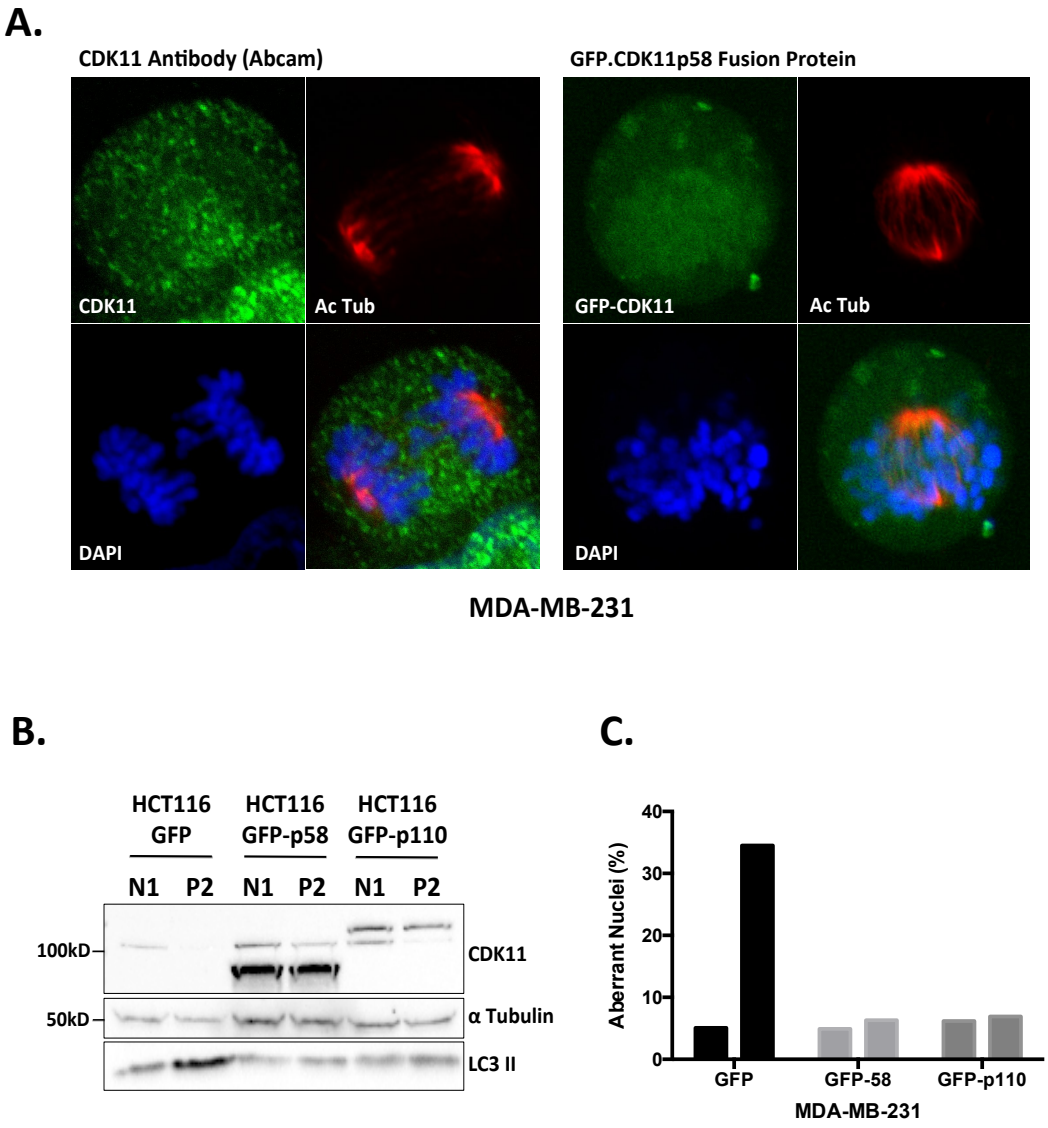

Figure 5.7 Validating GFP.CDK11 Constructs. CDK11p58 and CDK11p110 were cloned into the pEGFP-N1 vector in frame, with the removal of the myc-tag. The GPF.CDK11 cassette was then excised and cloned into the pBabe retroviral vector. Following sequence verification, the constructs were transduced into MDA-MB-231 and HCT116 cell lines. Localisation of the fluorescent fusion proteins was examined with microscopy. The distribution of GFP.CDK11p110 and GFP.CDK11p58 was found to mirror that of the myc-tagged constructs. GFP.CDK11p110 was primarily nuclear during interphase similar to endogenous protein; GFP.CDK11p58 was both nuclear and cytoplasmic at interphase (data not shown). ***5.7A*** demonstrates similar localization of GFP.CDK11p58 and endogenous CDK11 during mitosis to the nucleoplasm. Unlike other reports, no localization to the centrosome or spindle was identified with antibody or fusion protein. Western blot ***5.7B*** shows rescue of LC3 II accumulation 72 hours following siCDK11 or siNTC transfection in HCT116 cell lines expressing both GFP.CDK11 constructs but not the control cell line expressing GFP alone. ***5.7C*** shows rescue of aberrant nuclear morphology at 72 hours following CDK11 knockdown with siRNA; again this occurs with both MDA-MB-231 cell lines expressing GFP.CDK11 constructs but not GFP alone. This indicates the constructs are functional.

been reported, these reports are inconsistent as to its precise location [83]. One paper observed localization to the centrosome [23], while the other demonstrated robust localization to the spindle itself [83]. The inability to show localization of CDK11 to the spindle was not unique, as others groups have also failed to observe spindle localization [217].

This work therefore established that the GFP.CDK11 localized in a similar manner to endogenous CDK11. However as discussed, although similar localization is important, it is also necessary to determine functionality of the chimeric proteins. Therefore, I aimed to confirm the ability of both GFP.CDK11 proteins to rescue the phenotypes mediated by CDK11 depletion. In the MDA-MB-231 cells, both GFP.CDK11p58 and GFP.CDK11p110 rescued the marked mitotic phenotype and in HCT116 cells the fusion proteins rescued the autophagy phenotype [Fig. 5.7]. This demonstrated that both GFP.CDK11 proteins were functional and would provide a valid tool for co-immunoprecipitation.

5.4.3 GFP-Trap Immunoprecipitation

Having demonstrated functionality of the GFP proteins, I confirmed the successful immunoprecipitation of both GFP.CDK11p58 and GFP.CDK11p110 using the GFP-Trap system. In addition, I confirmed the co-precipitation of regulatory partner Cyclin L1. The decision was made to undertake co-immunoprecipitation and mass spectrometry using the HCT116 cells. Not only had these cells been used in the mitotic experiments but also higher expression of GFP.CDK11p110 was achieved in these cells.

Both asynchronous and mitotic synchronized HCT116 cells were used for the co-immunoprecipitation. Additionally, I decided to undertake precipitation on nuclear extracts in the asynchronous HCT116 cells. Published studies have used this strategy to enrich for the CDK11p110 [176] and recombinant GFP.CDK11p110 was also primarily nuclear, as demonstrated on immunofluorescence and on cell fractionation [Fig 5.8]. Furthermore, cell fractionation reduced the potential for non-physiological interactions caused by GFP.CDK11p58 within the cytoplasm during interphase. During mitosis, no nuclear envelope exists and whole cell lysates were obtained.

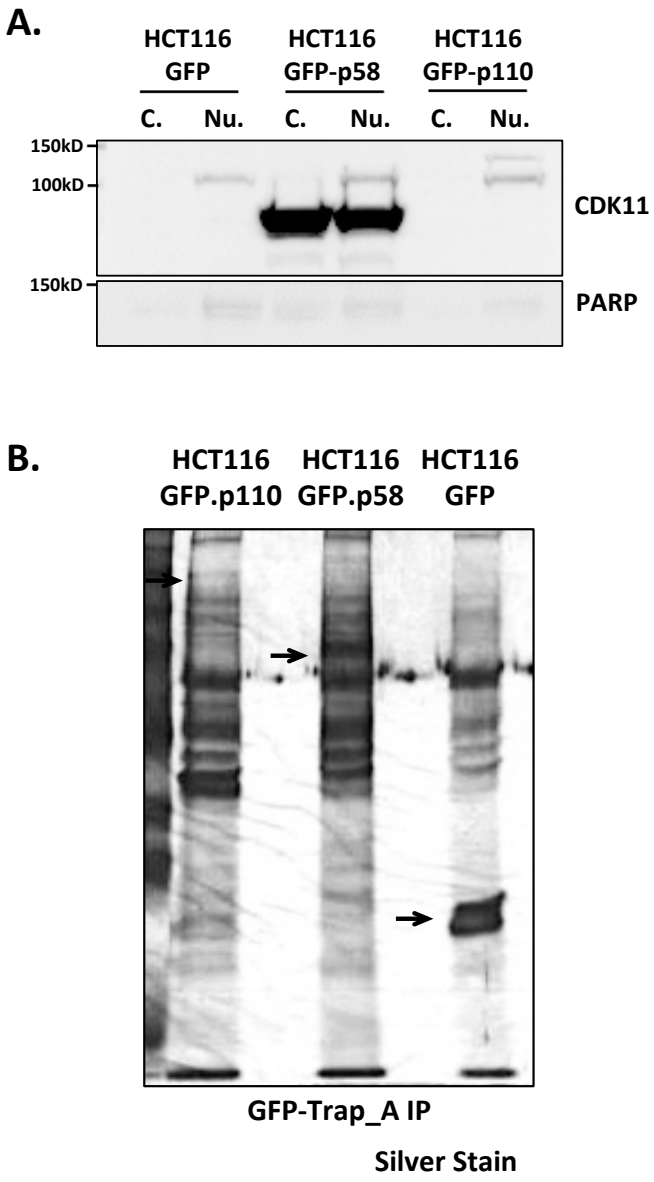

Figure 5.8 GFP.CDK11 Immunoprecipitation. HCT116 cell lines, with stable expression of GFP.CDK11p110, GFP.CDK11p58 or GFP, were cultured without synchronization or synchronized in mitosis. Mitotic synchronization was achieved with the addition of thymidine to culture media for 16 hours followed by release; 6 hours following release nocodazole was added to culture media for 6 hours. Cells were released from nocodazole block for 30 minutes prior to sampling. Mitotic cells were lysed with NP40 buffer; asynchronous cells underwent nuclear extraction prior to addition of NP40 buffer to the nuclear fraction. Immunoprecipitation of GFP or GFP fusion protein was undertaken with the GFP-TRAP agarose beads. Western blot ***5.8A*** shows localization of endogenous CDK11p110 and GFP.CDK11p110 to the nuclear extract; GFP.CDK11p58, as determined with immunofluorescence, localizes to both the nuclear and cytoplasmic fractions. ***5.8B*** shows the silver stain of an SDS-PAGE gel comprising GFP precipitate of asynchronous nuclear lysates of the three HCT116 cell lines. Bands representing GFP, GFP.CDK11p58 and CDK11p110 are marked with arrows. Prior to mass spectrometry experiments, further work was undertaken to reduce the putative contaminant species seen in this gel.

Prior to mass spectrometry, I confirmed that GFP proteins could be detected above background on silver stain and that background signal was acceptable [Fig. 5.8]. The GFP Trap antibody was used to precipitate either GFP or GFP.CDK11 proteins from asynchronous HCT116 nuclear extract lysate or mitotic HCT116 whole cell lysate. These lysates were incubated for 1 hour with GFP-Trap agarose beads prior to precipitation and washing. Supernatant was removed and the agarose beads sent frozen at -80°C for on-bead digestion and mass spectrometric analysis at the collaborating institution. Experiments were repeated in triplicate for mass spectrometry. Proteins identified within each precipitate were quantified and significant enrichment determined. Once again, significant enrichment was determined by average enrichment of two fold or greater and significance of $p<0.05$.

Approximately 200 proteins were enriched over GFP in each of the 4 conditions: GFP.CDK11p110 asynchronous, GFP.CDK11p58 asynchronous, GFP.CDK11p110 mitotic and GFP.CDK11p58 mitotic [Tables S2 – S5 (Appendix)]. Graphs demonstrate the distribution of identified proteins plotted with ratio enrichment against significance [Fig 5.9]. This showed a skew to the right consistent with greater enrichment in the GFP.CDK11 precipitates.

5.4.4 Mass Spectrometry Results

First, in order to confirm the quality and reproducibility of the experimental results, I undertook statistical correlation of the mass spectrometry results of each biological and technical replicates. This demonstrates excellent correlation between technical replicates [Fig 5.10] and good correlation between biological replicates, similar to that reported by other studies [265].

To further assess the validity of the experimental results, I compared the putative interactors identified with established CDK11 interactors. I identified 554 unique proteins significantly enriched following co-immunoprecipitation with mitotic or asynchronous CDK11 isoforms. As discussed, in published literature, there are 114 proteins reported to interact with human CDK11 or its eukaryote homologues. Of these established interactors, 33 (29%) were identified in my immunoprecipitation assays.

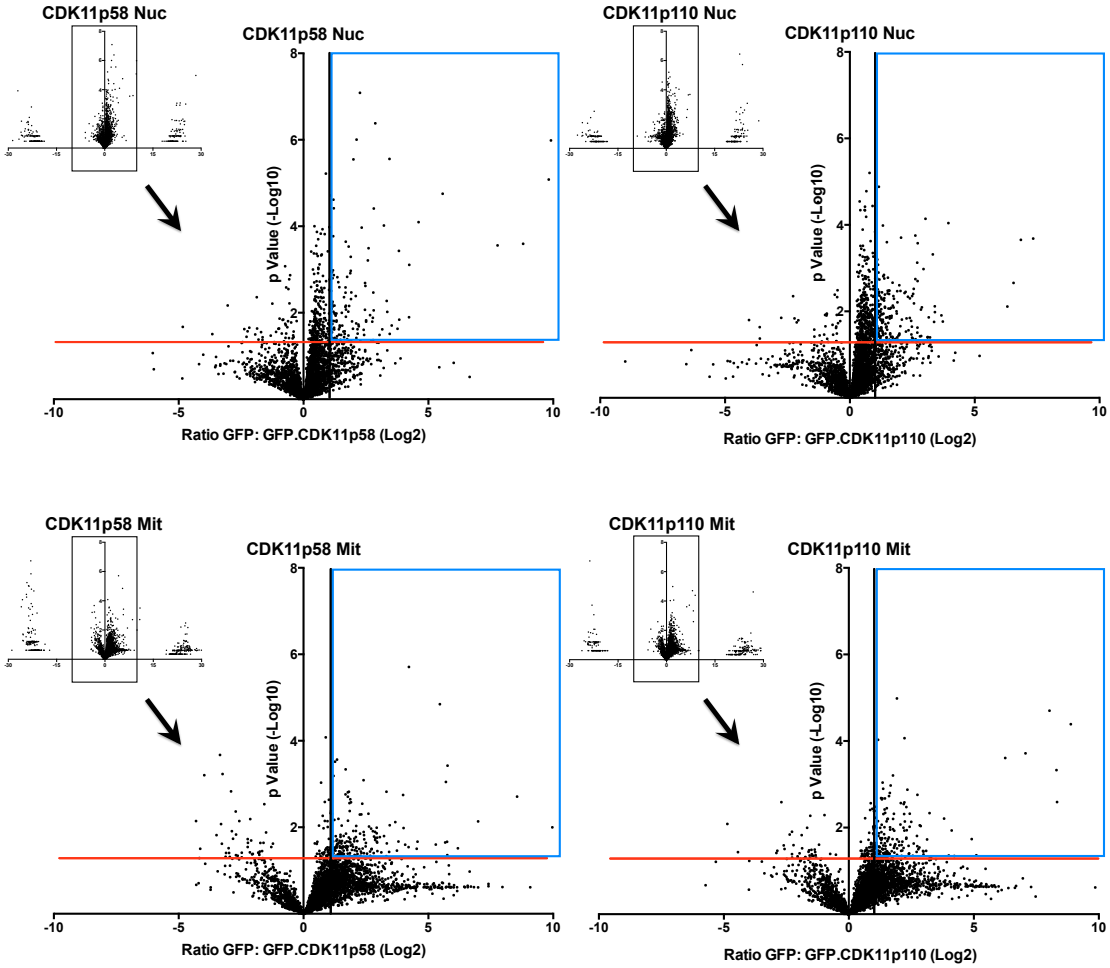

Figure 5.9 Mass Spectrometry Results. Asynchronous or mitotically synchronous HCT116 cells, with stable expression of GFP.CDK11p110, GFP.CDK11p58 or GFP, were lysed as described. 5mg of protein was subjected to immunoprecipitation using GFP-TRAP agarose beads. Beads were subsequently washed and placed at -80^{o}C; samples were then transferred on dry ice to the collaborating institute for on-bead digestion and mass spectrometric analysis. Three biological replicates were obtained for each culture condition (asynchronous or mitotic) for each of the three HCT116 cell lines (GFP, GFP.CDK11p110 and GFP.CDK11p58). ***5.9*** plots the ratio (Log2) of each protein detected in GFP.CDK11 to GFP co-immunoprecipitate; this is based on the mean protein quantification in each condition across biological and technical replicates. The ratio of enrichment is plotted against its statistical significance (-Log10) [T-Test]. The smaller graph for each condition shows all proteins detected, while the larger graph shows only proteins with smaller ratios of enrichment, to enable better visualization. The blue square marks the proteins on the graph that are considered to be significantly enriched (Fold increase >2 + $p<0.05$) in GFP.CDK11 precipitates. CDK11p58 Nuc and CDK11p110 Nuc represent the asynchronous conditions, while CDK11p58 Mit and CDK11p110 Mit represent the conditions synchronized in mitosis.

Importantly, both CDK11 and Cyclin L were significantly enriched in all CDK11 precipitates. In addition, other established interactors achieved the level of significance but not enrichment to be identified as interactors on this assay. Furthermore, numerous proteins identified as interactors on this assay were of a similar class to CDK11-interacting proteins or were subunits of complexes containing CDK11-interacting proteins. Moreover, although 114 interactors are reported, many of these interactions were identified with other cell lines, other species or other CDK11 isoforms, i.e. CDK11p46 and CDK11p60. Therefore, this experiment identified a substantial number of known CDK11 interactors. The high correlation of replicates and the high number of established CDK11 interactors identified provide confidence in the validity of the results.

The enriched proteins (putative CDK11 interactors) were analysed using DAVID, STRING and KEGG pathway databases. I used these tools to determine enrichment of Gene Ontology (GO) terms or KEGG pathways among the putative CDK11 interactors from each precipitate. The KEGG pathways enriched for each CDK11 precipitate are reported in Table 5.1.

5.4.4.1 Mitotic GFP.CDK11p58 Interacting Proteins

In the mitotic GFP.CDK11p58 precipitate, 210 proteins were significantly enriched. Of these putative CDK11 interacting proteins, 122 were unique to mitotic CDK11p58 and 88 interactors were identified in other GFP.CDK11 precipitates. 72 interacting proteins were detected in both the mitotic GFP.CDK11p58 and the mitotic GFP.CDK11p110 precipitates. On KEGG pathways enrichment analysis, spliceosome-associated proteins were the most enriched protein group found to interact with mitotic CDK11p58, with 26 spliceosome-associated proteins. Comparison with asynchronous GFP.CDK11p58 precipitate revealed that spliceosome-associated proteins were also significantly enriched among asynchronous CDK11p58 interactors, although not to an equal extent with only 7 spliceosome-associated proteins identified. The role of CDK11 in splicing is established but this primarily relates to CDK11p110. No published study has reported the interaction of CDK11p58 with the spliceosome *in vivo*, although CDK11p58 is reported to inhibit splicing on *in vitro* splicing assays [55]. The CDK11p58 isoform lacks

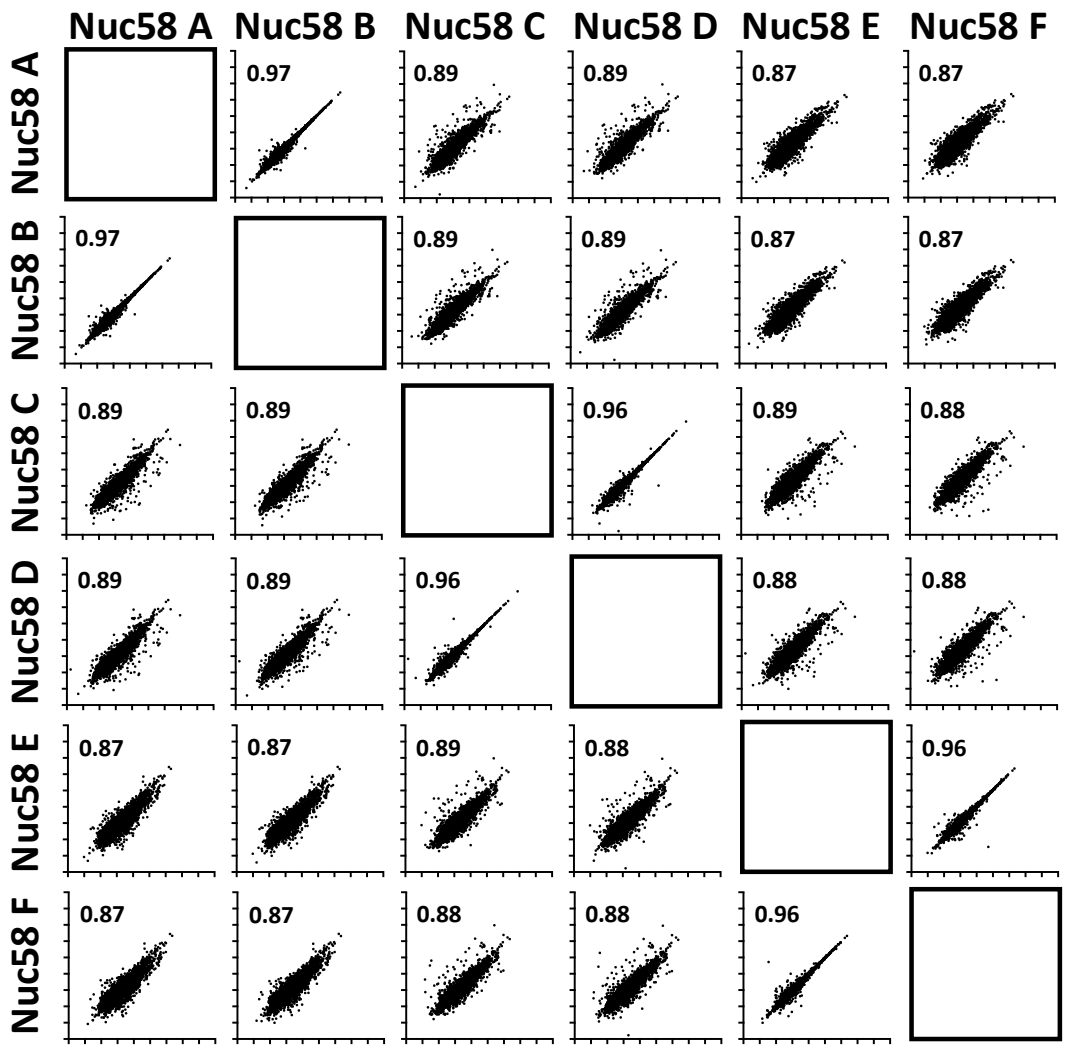

Figure 5.10 Mass Spectrometry Replicates. Asynchronous or mitotically synchronous HCT116 cells, with stable expression of GFP.CDK11p110, GFP.CDK11p58 or GFP, were lysed as described. 5mg of protein was subjected to immunoprecipitation using GFP-TRAP agarose beads. Beads were subsequently washed and placed at -80^{o}C; samples were then transferred on dry ice to the collaborating institute for on-bead digestion and mass spectrometric analysis. Three biological replicates were obtained for each culture condition (asynchronous or mitotic) for each of the three HCT116 cell lines (GFP, GFP.CDK11p110 and GFP.CDK11p58). ***5.10*** shows plots of biological and technical replicates from a single experimental condition, asynchronous HCT116 GFP.CDK11p58 (p58 Nuc); similar results were obtain for the other experimental conditions. These plot the mean intensity measurement for each protein identified, based on integrals of composite peptide ion intensities, on logarithmic axes for each of the corresponding replicates. The figure in the top left of each plot is the calculated Spearman Correlation Coefficient. These plots demonstrate excellent correlation of technical replicates (A+B, C+D, E+F) with adequate correlation between biological replicates.

KEGG Pathway	No. Observed Genes	False Discovery Rate (Corrected p value)
CDK11p58 Asynchronous		
Spliceosome	7	0.00593
Protein Processing in ER	8	0.00593
CDK11p58 Mitotic		
Spliceosome	26	1.70E-24
Proteasome	9	6.11E-08
mRNA Surveillance Pathway	11	1.17E-07
Antigen Processing and Presentation	9	1.64E-06
RNA Transport	12	2.92E-06
Herpes Simplex Infection	12	1.16E-05
Epstein-Barr virus infection	11	0.000167
Protein Processing in ER	9	0.00161
Ribosome Biogenesis in Eukaryotes	6	0.00325
Phagosome	7	0.0187
Gap Junction	5	0.0421
Pathogenic Escherichia Coli Infection	4	0.0467
CDK11p110 Asynchronous		
Nil		
CDK11p110 Mitotic		
Spliceosome	29	9.13E-31
Ribosome	21	1.16E-18
Herpes Simplex Infection	14	5.48E-08
RNA Transport	12	8.34E-07
mRNA Surveillance Pathway	6	0.00704
Ribosome Biogenesis in Eukaryotes	5	0.0238

Table 5.1 KEGG Pathway Terms. ***5.1*** shows KEGG Pathway terms that are significantly enriched among putative GFP.CDK11 interactors identified in each co-immunoprecipitate. There are no enriched terms among the interactors identified within the GFP.CDK11p110 Asynchronous co-immunoprecipitates.

the N-Terminal regulatory domain of CDK11p110, which contains the RE domain important for spliceosome interaction. However, CDK11p58 did interact with both Cyclin L1 and Cyclin L2, which contain RNA-binding RS domains that enable binding to splicing proteins. Therefore, the interaction of CDK11p58 with splicing proteins may occur through its cyclin partners, Cyclin L1 or L2. Alternately, CDK11p58 may form a heterodimer with the CDK11p110 isoform and interact indirectly with the spliceosome via the longer isoform. However, although homodimerisation of both the CDK11p58 and CDK11p110 isoforms are described [61] [56], there is no published evidence for dimerization between the distinct isoforms. Certainly in my work immunoprecipitation of CDK11p58 or CDK11p110 did not precipitate the alternate isoform [Fig 5.3].

GO term and KEGG pathway enrichment analysis revealed the significant enrichment of proteins related to mRNA surveillance, RNA transport and viral infection within the mitotic CDK11p58 interacting proteins. Furthermore, the second most enriched protein group identified among mitotic CDK11p58 interactors was the proteasome-related proteins, with 9 proteins identified. No enrichment of proteasomal proteins was identified in other CDK11 precipitates, particularly among asynchronous GFP.CDK11p58 interactors. Precipitation of GFP.CDK11p58 in asynchronous cells was performed on nuclear extracts rather than whole cell lysate but proteasomes are recognized to locate to both the nucleus and cytoplasm in interphase. No interaction has previously been determined between CDK11 and proteasomes, although CDK11p58 is recognized to target certain nuclear receptors for proteasomal degradation [2, 65]. The GFP.CDK11p58 fusion protein was expressed at supra-physiological levels and the protein excess may have been targeted to the proteasome for degradation, explaining these interactions. However, proteasome protein enrichment was not demonstrated with asynchronous GFP.CDK11p58, which was similarly over-expressed. Nonetheless, proteasomal degradation plays an integral role in mitotic control and the putative interaction between mitotic CDK11p58 and proteasomes requires further investigation. In addition, I did not identify Cyclin D3 or PAK1 as interacting proteins with mitotic GFP.CDK11p58. I

confirmed this finding with further immunoprecipitation and Western blot analysis (data not shown). Cyclin D3 and PAK1 are reported to be essential for the mitotic function of CDK11p58 [89] but this does not appear to be the case in HCT116 cells. This finding indicates other mechanisms/proteins may also regulate the mitotic functions of CDK11.

5.4.4.2 Asynchronous GFP.CDK11p58 Interacting Proteins

In the asynchronous nuclear GFP.CDK11p58 precipitate, 155 interacting proteins were identified, with 95 proteins occurring in other CDK11 precipitates and 60 unique to asynchronous CDK11p58. The predominant protein networks enriched relate to RNA processing, with spliceosome-associated proteins again the most significantly represented. The significance of CDK11p58 interactions out with mitosis is uncertain, as expression of native protein through interphase is low or absent.

5.4.4.3 Mitotic GFP.CDK11p110 Interacting Proteins

In the mitotic GFP.CDK11p110 precipitate, 183 putative interacting proteins were found, with 99 proteins unique to mitotic CDK11p110. The protein group demonstrating greatest enrichment was the spliceosome-associated proteins, with 29 proteins identified. Although the role of CDK11p110 in mRNA splicing is well characterised, the interaction of CDK11p110 with splicing components in mitosis had not been established. As discussed, enrichment of spliceosomal proteins was also evident in the mitotic GFP.CDK11p58 precipitate. CDK11p110 is reported to enhance splicing activity on *in vitro* splicing assays whilst CDK11p58 inhibits splicing on similar assays [55]. However, the effect of either protein on splicing may differ both *in vivo* and during mitosis. Furthermore, splicing is suppressed during open mitosis in eukaryotes following nuclear envelope dissolution, with the disassembly of many spliceosomal complexes [280]. Therefore, the interaction of both CDK11 proteins with splicing components during mitosis would benefit from further characterization.

Numerous spliceosome components are found to engage in mitotic regulation, with inhibition resulting in aberrant mitosis [280]. The mechanism of this regulation remains unclear. Whilst there is evidence to

indicate that it occurs due to splicing dysregulation during interphase that results in the incorrect splicing of mitotic proteins [280], others argue that it occurs as a consequence to splicing independent functions during mitosis [281].

The second most enriched protein group detected among mitotic CDK11p110 interacting proteins was the ribosomal proteins, with 21 ribosome-associated proteins identified by KEGG pathway enrichment analysis. Ribosomal proteins represented a significant proportion (33%) of the enriched proteins identified on GST.CDK11p58 affinity purification but in this immunoprecipitation assay there was no significant enrichment of ribosomal proteins with the CDK11p58. The affinity purification was undertaken with the p58 isoform not the p110 isoform. However, the GST.CDK11p58 protein was not expressed in human cell but synthesised in bacteria and applied *in vitro*, therefore interactions detected with this p58 protein bait may be relevant to both the p110 and p58 isoforms given the shared peptide sequence. Nonetheless, only 3 of the ribosomal proteins identified by either assay were present in both assays. As discussed, no published interaction has been identified between the CDK11p58 or CDK11p110 and any ribosomal proteins. Ribosomal proteins are recognized to contaminate precipitation assays but there was no enrichment with mitotic GFP.CDK11p58 to indicate this was non-specific contamination, particularly given the greater precipitation of GFP.CDK11p58 due to its higher expression. The significance of this interaction with ribosomal proteins that is unique to the mitotic CDK11p110 also requires further investigation.

Interestingly, in both mitotic CDK11p58 and mitotic CDK11p110 interactors, there was significant enrichment of proteins involved in ribosome biogenesis. CDK11 has been identified previously as a component of Parvulin 14 complexes, which are involved in ribosome biogenesis [282]. Furthermore, this work and unpublished work of others has identified the interaction of CDK11 with DDX15 [106], a helicase with roles in both spliceosome disassembly and ribosome biogenesis.

5.4.4.4 Asynchronous GFP.CDK11p110 Interacting Proteins

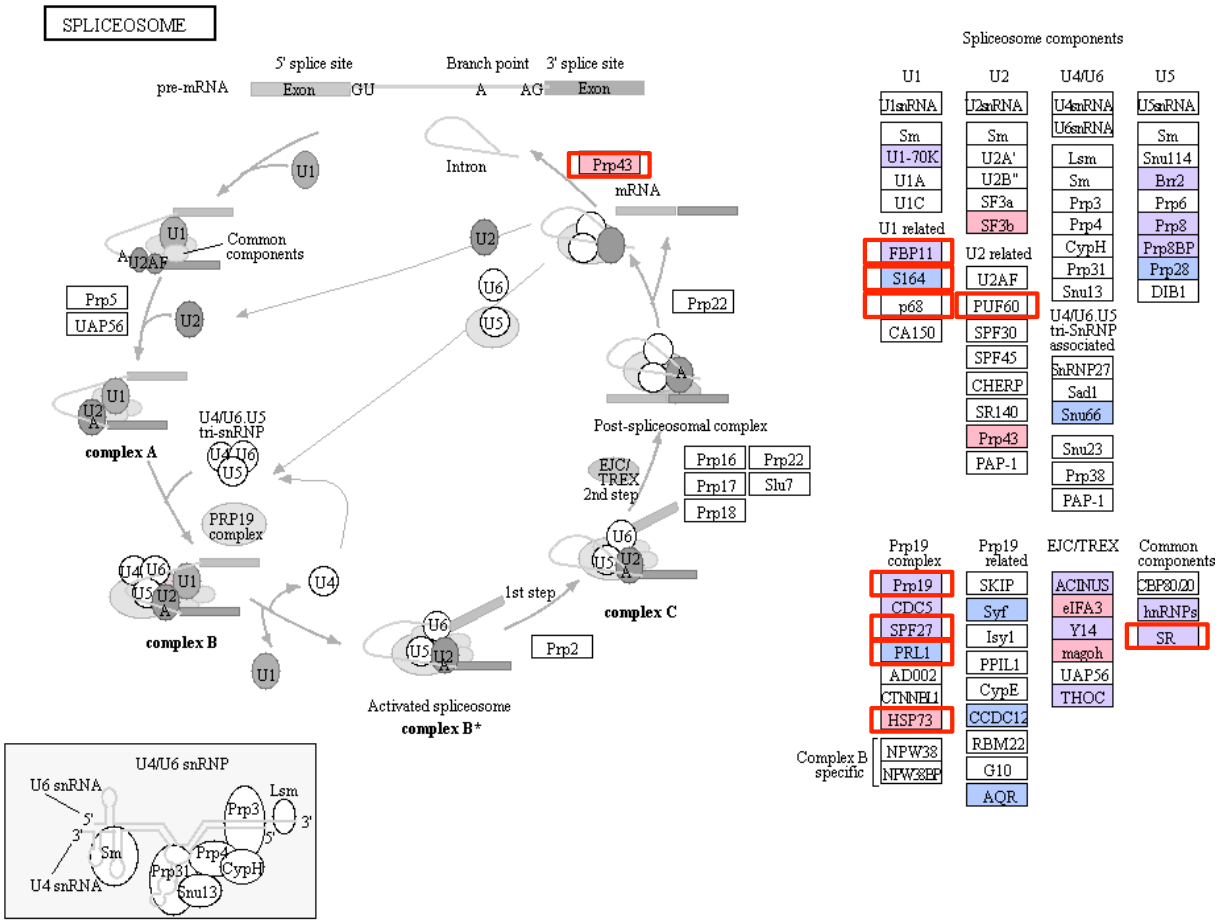

Fig 5.11 Putative mitotic CDK11 Interacting Proteins and the Spliceosome. Proteins significantly enriched in mitotic GFP.CDK11 co-immunoprecipitates over mitotic GFP co-immunoprecipitates were analysed using KEGG pathway terms. 29 mitotic CDK11p110 interactors were associated with the spliceosome, while 26 mitotic CDK11p58 interactors were spliceosome-associated. In addition, 11 established CDK11 interactors were associated with the spliceosome. ***5.11*** illustrates these proteins on the KEGG spliceosome pathway. Analysis performed at KEGG website (http://www.genome.jp/kegg/kegg2.html), with image downloaded following analysis. Red highlighted proteins represent mitotic CDK11p58 interactors, blue highlighted proteins represent mitotic CDK11p110 interactors and purple highlighted proteins are found to interact with both mitotic CDK11p110 and CDK11p58. Red boxes mark established CDK11 interacting proteins. SR proteins and hnRNPs comprise a number of proteins including CDK11 interactors SRSF1, SRSF2 and SRSF7 (SR proteins).

In the asynchronous nuclear CDK11p110 precipitate, 208 putative interacting proteins were identified, with 90 shared CDK11 interactors and 118 proteins unique to asynchronous CDK11p110. Although 13 established interactors were identified in these 208 proteins, there was no significant pathway enrichment as determined by KEGG pathway enrichment analysis. GO terms enrichment analysis revealed there was enrichment in proteins that function in tRNA processing and modification but there was no enrichment of proteins associated with established CDK11p110 functions. This is surprising as it is during interphase when this CDK11p110 is considered to exercise its primary influence on transcription and splicing. In contrast, all other CDK11 precipitates were found to contain significant enrichment of spliceosomal components. Whilst this was the one condition that would be expect to enrich these proteins, this may be related to the poor expression of GFP.CDK11p110 in the HCT116 cells, resulting in significantly less CDK11 precipitation with GFP.CDK11p110, especially in the asynchronous cells. Therefore, this may have limited the identification of enriched pathways, although overall, there were no less putative interactors (208 proteins) identified with asynchronous CDK11p110.

Interestingly, established CDK11p110 interactors were identified including CK2 and components of the Mediator complex. Mediator complex interaction with CDK11 had not been demonstrated previously in metazoan species but these findings indicate that the interaction may occur in humans.

5.4.4.5 Autophagy, Cell Motility and the CDK11 Interactome

I have demonstrated a role for CDK11 in mediating autophagy and migration. CDK11-mediated autophagy is predominantly a response to dysregulated mitosis, as I established in Chapter 3. Therefore, CDK11 may have no direct interaction with autophagy proteins. To investigate this, I examined all the putative CDK11 interactors found on co-immunoprecipitation to discern autophagy-related proteins. The only core autophagy-related proteins identified were ATG4 and MTOR; these proteins were both co-immunoprecipitated with GFP.CDK11p110 in asynchronous cells. The significance of this is unclear as ATG4 and MTOR do not interact. Furthermore, neither protein was enriched in GFP.CDK11p58 precipitates,

with CDK11p58 established to rescue CDK11-mediated autophagy. Moreover, there was no enrichment of autophagy-related proteins as determined by GO term and KEGG pathway enrichment analysis.

The mechanism of CDK11-mediated migration has not been fully characterized. A recent study reported that CDK11 enhanced migration through interaction with GADD45α and GADD45γ, resulting in the degradation of Ets transcription factor SPDEF [241]. I identified GADD45γ binding protein in both CDK11p58 and CDK11p110 mitotic but not asynchronous precipitate. However, I was unable to identify interaction with GADD45α and GADD45γ. There was no enrichment for proteins assigned to the cell motility KEGG pathway or GO terms related to cell polarization, the actin cytoskeleton or cell adhesion.

5.4.4.6 Significant Enrichment and Correction for Multiple Testing

The method I employed to determine significant enrichment and therefore putative interactors was adopted from published protocols. This used both enrichment level and significance testing to determine significant enrichment. These protocols used a significance level of $p < 0.05$ on Students T-test. Although this method included fold enrichment, there was no correction for multiple testing. In my immunoprecipitation assays, approximately 3000-4000 proteins were detected in each sample, therefore the risk of false positives using an uncorrected significance level is high.

However, I utilized these co-immunoprecipitation assays with mass spectrometric analysis as a screen to identify novel CDK11 interactions and protein networks, with subsequent enrichment analysis. Enrichment analysis provides greater confidence in interactors identified if other associated proteins are also precipitated. In addition, any putative interactor would require confirmation prior to more in depth study. Given that it is accepted that putative interactions require verification, it was reasonable to tolerate a greater proportion of false positive interactions rather than false negative interactions.

If the Bonferroni correction for multiple testing were applied to my results only 7 proteins in total remain significantly enriched: CDK11, Cyclin L1,

HSP90, DERP6, DERL2, ZNF8 and PAM16. If instead the Benjamini-Hochberg correction were applied to control False Discovery Rate the number of detected CDK11 interacting proteins increased to 64 but only 8 established CDK11 interactors would be detected. Therefore, the False Discovery Rate correction resulted in the loss of 75% known interactors from the assay, with the loss of true interactors that have not been previously established likely to be similar. Therefore, although it is reported that FDR calculations may provide the best balance between false positive and false negative results [283], this did not appear to be the case for my results.

The reverse analysis demonstrated between 40 and 80 proteins significantly enriched with GFP precipitates over each of the asynchronous or mitotic CDK11 precipitates. These may have represented either true protein binding to GFP or the result of multiple statistical testing. However, KEGG pathway enrichment analysis of these enriched GFP 'interacting' proteins revealed no KEGG pathway enrichment, thus demonstrating the validity of my methods.

5.4.4.7 Discussion of Experimental Methods

In these co-immunoprecipitation assays, the direct comparability of the different assays was compromised. The control GFP precipitates were valid and therefore interactors in each precipitation assays could be accurately established relative to control. However, the relative interaction with a specific protein between one CDK11 isoform and the other isoform could not be accurately determined, i.e. I was unable to determine that CDK11p58 interacted with a certain protein twice as much as CDK11p110. This occurred for two principal reasons. First, the level of CDK11 precipitated varied markedly between the conditions and ideally this should have been uniform. The major cause of this discrepancy was the poor expression of the CDK11p110 compared to the p58 isoform. This was noted with both the myc-tagged and GFP-tagged proteins and as discussed has been observed by other laboratories [176].

In addition the strategies for preparation of the samples varied. Although the final cellular or nuclear lysis buffer in all conditions was NP40, the sample preparation techniques were different with either nuclear extraction in

asynchronous cells or whole cell lysis in mitotic cells. This again had the potential to compromise the validity of any direct comparison of the relative levels of interactors between mitotic and nuclear CDK11 precipitates. Purification of CDK11 from nuclear extracts has been used commonly in published studies and the benefits of both CDK11 enrichment and limiting cytoplasmic interaction of the CDK11p58 fusion protein have been discussed.

The use of the stable cells lines may also have influenced the different levels of GFP.CDK11p110, GFP.CDK11p58 and GFP tag expression. Potentially, the transient transfection of fusion protein constructs may have enabled not only more equitable protein expression but also higher expression of the proteins. In retrospect, this would have certainly been an easier methodology and may have even allowed use of the myc.CDK11 constructs. The higher exogenous protein expression may have provided greater confidence in the reliability of the CDK11p110 asynchronous interactors. However, the cancer cells I used did not tolerate high levels of CDK11p110 and it is therefore possible that transient transfection may have had deleterious effects that would influence the interactome identified.

The nocodazole synchronization method is the predominant method of mitotic synchronization described in published literature and is validated to synchronise cells at prometaphase [284]. In addition, published work using HCT116 cells has demonstrated that following release from nocodazole block the majority of cells progress though telophase within 1 hour [285], thus I lysed cells 30 minutes following release. However, any synchronization method (particularly drug-induced) may have undesired effects on cellular physiology; in my work, this had the potential to lead to the identification of abnormal or mitotic arrest-related interactions. Certainly, there was no clear evidence of this on GO term or KEGG pathway enrichment, with CDK11 interacting in described pathways and with established interactors. The duration in nocodazole block represents a balance between mitotic enrichment and the potential for mitotic disruption, with longer block increasing mitotic cells but impairing recovery from mitotic arrest [285]. I elected to release from nocodazole block at 6 hours consistent with the published methods [285]. Not all cells undergoing mitotic synchronization

were in mitosis but there was marked enrichment of mitotic cells following nocodazole synchronization. Although I did not formally undertake FACS to confirm mitotic synchronization, this was evident on account of the rounded mitotic appearance of cells and elevated phospho-Histone H3 staining (data not shown). Furthermore, this approach, using nocodazole synchronization, has been used in published work examining the mitotic interactome of proteins by mass spectrometry [286].

Although, the on-bead digestion lacks the specificity of conventional techniques that digest and analyse unique bands on silver stain, it is substantially more sensitive, with 3000 to 4000 proteins identified in each of my assays. Obviously this caused it's own difficulties such that within the putative interacting proteins identified, there are likely to be numerous false positives. In addition, this co-immunoprecipitation did not prove direct interaction and indeed many 'interactors' may have been detected due to precipitation of protein complexes. Nonetheless, irrespective of whether interactions are direct or indirect, this work has enabled further characterization of the CDK11 interactome.

5.4.4.8 Comparison with GST Affinity Purification

Results were compared to the findings of the GST affinity purification to assess for correlation. This demonstrated that only 6 interacting proteins were identified in both screens (15% GST assay pulldowns); these were FASTKD5, DNAJA1, DNAJA2, RPS6, RPS7, RPS27L. Putative interactors identified on GST pulldown, CSK, KIF14 and RAN, were not identified with the co-immunoprecipitation assays. Overall, the correlation was poor and this was consistent with the inability to identify any established CDK11 interactors in the affinity purification assay.

As discussed the interaction with ribosomal proteins in both assays is interesting although there was relatively limited correlation in the ribosomal protein identified and therefore the validity remains uncertain. However, it would be useful to exclude ribosome interaction in mitosis. The inhibition of cap-dependent translation is critical in accurate mitotic progression and in published studies, CDK11 is reported to be a downstream regulator of

mitosis secondary to suppression of cap-dependent translation and subsequent IRES translation of CDK11p58 [79, 287]. It would be useful to exclude any upstream effects on ribosome translation that would itself explain the mitotic rescue, by CDK11, of cells that fail to suppress of cap-dependent translation, particularly given the requirement for 14-3-3σ in the suppression of cap-dependent translation and the established mitotic binding of CDK11p110 to 14-3-3 [287].

5.5 Conclusions

This chapter presented work intended to identify novel binding partners of CDK11 and elucidate interacting networks. The work could not achieve adequate immunoprecipitation of endogenous protein to enable mass spectrometric analysis. Furthermore, the GST affinity purification was also of limited success, with only one of three putative interactors assessed being confirmed on repetition of the assay. Interaction with CSK could not be subsequently confirmed *in vivo*, although further work is required to investigate both this and the other finding of differential Src activation on CDK11 depletion.

The immunoprecipitation of GFP-tagged CDK11 was successful, based on the reproducibility of biological replicates and the number of established interactors identified. These assays have yielded a number of results of significant interest. However, it is difficult to reliably interpret the significance of these results without further validation. Unfortunately, the results of co-immunoprecipitation returned at the completion of my project and I was unable to take forward any validation work. Future projects will hopefully explore the findings identified and assess their validity.

CHAPTER 6

Screening for CDK11 Mutations in a Cornelia de Lange Syndrome Cohort

6.1 Cornelia de Lange Syndrome

Cornelia de Lange syndrome (CdLS) is a rare development disorder comprising anomalies of multiple organ systems [288]. It is characterised by a classical facial dysmorphology, pre and post-natal growth retardation, intellectual disability, limb malformations and assorted visceral anomalies [288]. The distinctive facial features of CdLS include low set ears, a flattened mid-face with short nose and long philtrum, arched eyebrows and synophrys [288]. Although the precise incidence of CdLS remains uncertain, estimates lie between 1 in 10000 and 1 in 50000 live births [289]. Traditionally the diagnosis of CdLS was clinical, based solely on the identification of a number of the disorder's characteristic features. Over the last decade, as disease-associated genes have been identified, suspected cases are routinely screened for known causative genetic mutations [289].

6.1.1 CdLS Genetics

Causative genetic mutations have been identified in approximately 65% of patients with CdLS [290]. The vast majority of these mutations occur *de novo* and familial cases of CdLS are rarely reported, with most inherited cases found to be a consequence of genetic mosaicism [291, 292]. The majority of cases are caused by mutations of the *NIPBL* gene, which are ubiquitously dominant, haploinsufficient mutations [292]. Mutation of *NIPBL* gives rise to the classical phenotype of CdLS, described above [292].

Four other disease-associated genes have been identified; these are *SMC1A*, *SMC3*, *Rad21* and *HDAC8*. Mutations within these four genes combined cause approximately 5% of CdLS cases [290]. The phenotypes associated with mutation of these genes differ from the classical phenotype but possess a number of the principal features by which the disorder is characterized.

Despite the identification of these disease-associated genes, the causative genetic mutation remains undiscovered in approximately 40% of patients. It has recently been reported that *NIPBL* mutations may cause a far greater proportion of CdLS cases [293]; this study found that *NIPBL* mosaicism explained the genetic aetiology in a further 25% of cases. However, this report was based on only a small case series of 44 patients and the generality of its findings require clarification [293]. Depending on the contribution of mosacism, there still remains no identified mutation in between 15% and 40% of cases.

In mutation negative cases, the identification of novel causative variants can provide a genetic diagnosis to patients and families, not only elucidating disease causation but also basic cellular physiology. In addition, it allows clinicians to determine, through parental sequencing, whether the mutation is indeed *de novo* or whether it represents a recessive inherited variant. This clarification of heritability provides parental certainty over the risk of the disorder occurring in their future offspring.

6.1.2 Cohesin and Cohesinopathies

Cohesin is an evolutionally conserved multi-subunit protein complex, comprising a heterodimer of two structural maintenance of chromosomes (SMC) proteins, SMC1A and SMC3, and two non-SMC proteins, RAD21 and STAG [86]. Numerous proteins are established to mediate cohesin biology, such as its loading and removal from chromatin; these proteins include NIPBL, WAPL, PDS5 and Sororin [86].

All established CdLS-associated genes are either components of the cohesin complex or regulators of cohesin biology [86]. *NIPBL* is not only the gene most commonly mutated but also was the first CdLS-associated gene to be identified [291]. *NIPBL* is the human homologue of drosophila *Nipped-B* and yeast *Sister Chromatid Cohesion 2* (*Scc2*). It mediates the loading of the cohesin complex onto chromatin [86]. *SMC3*, *Rad21* and *SMC1A* are all components of the cohesin complex itself, which topologically embraces the DNA molecule to mediate cohesion. *HDAC8* is the most recently identified gene found to harbor causative mutations [294]. It was identified as the human

orthologue of yeast *HOS1*, which encodes a protein established to deacetylate SMC3 at anaphase and considered to enable the proper function of SMC3 throughout the subsequent cell cycle [294]. This finding led to the identification of mutations within the gene in the CdLS cohort [295]. Although HDAC8 acts during mitosis to regulate cohesin, it is yet to be fully characterised how or if it influences cohesin biology outside of mitosis. No mutations in other cohesin-associated genes, such as *WAPL* and *PDS5*, have been identified to explain the latent genetic causation of CdLS [296].

The role of the cohesin complex is best characterised in mitosis, where it plays an integral role in the maintenance of sister chromosome cohesion [296]. This enables the accurate segregation of the genome at mitosis. Dysregulation of cohesion predisposes to chromosomal missegregation and mutations in cohesin complex subunits are frequently reported in cancer [296]. However, studies indicate that the maintenance of cohesion in mitosis is not integral to the developmental disorder. Although variable defects in sister chromatid cohesion are observed in CdLS cohorts [297], the majority of studies report no precocious sister chromatid separation [298]. Certainly, there is no reported increase in the incidence of malignancy in CdLS patients [289]. The mechanisms through which these mutations cause CdLS remain uncertain but it is widely held that it is through disruption of cohesin's role at transcription [299, 300]. As discussed in Chapter 1, cohesin is involved at different stages of transcription; these included mediating chromatin looping to facilitate enhancer and promoter apposition and regulating proximal pausing during transcription [36].

CdLS is classified as a cohesinopathy based on the fundamental role cohesin is considered to play in the pathogenesis of the disorder [301]. CdLS is not the only cohesinopathy and Robert's syndrome is also termed a cohesinopathy. Robert's syndrome has a distinct phenotype and is predominantly caused by mutations in the *ECSO2* gene [301]. ESCO2 mediates the acetylation of cohesin, enabling the establishment of cohesion in early S-phase [302].

Despite this, debate continues as to the precise contribution of the cohesin complex to the syndrome, with some suggesting classical CdLS caused by *NIPBL* mutation results from other NIPBL functions unrelated to cohesion [303, 304]. However, most dismiss this proposition, given both the phenotypic similarities of CdLS cases caused by the mutation of different cohesin-associated genes and the finding that NIPBL and cohesin mediate the expression of a similar cohort of genes [299, 301].

6.1.3 Screening approaches in CdLS Cohort

To confidently identify novel disease-causing mutations, a rigorous screening protocol is required. The Fitzpatrick laboratory within the Human Genetics Unit, Edinburgh is an internationally recognized group with expertise in this disorder. The work presented was undertaken in this laboratory, which has developed the following screening strategy for CdLS patients. First the validity of the clinical diagnosis is confirmed, with verification of phenotypic features consistent with CdLS. It is then necessary to those identify cases with mutation of established causative genes and therefore sequencing of *SMC1A*, *SMC3*, *HDAC8*, *NIPBL* and *Rad21* is performed. Cases without mutation of known causative genes are further investigated with array Comparative Genomic Hybridisation (aCGH) to identify regions of chromosomal loss or gain. It was the identification of a common regional deletion on Chromosome 5 in CdLS cases that led to the original discovery of *NIPBL* mutations [291].

At the time this work was undertaken, the Fitzpatrick CdLS cohort with no established causative mutation comprised 84 patients. Prior to the outset of this project, several cases within the cohort were identified to have deletion of chromosomal regions on aCGH. In one case, this regional deletion was found to involve the *HDAC8* gene and concurrent work in other laboratories identified mutations of *HDAC8* as pathogenic [294]. This led to the sequencing of *HDAC8* in others within the cohort and the identification of two additional cases with *HDAC8* mutations. The final stage in the screening protocol is to undertake whole exome sequencing (WES), which has

significant cost implications. When undertaken, WES is performed as a trio, with the DNA of both biological parents.

One proband (Dutch13) within the CdLS cohort was established to have a 1.1Mb deletion of the 1p36.3 locus, with loss of both *CDK11* alleles in addition to 44 other genes [Fig. 6.1]. This predicated the work, described in this chapter, to screen the CdLS cohort for putative causative genes contained within this region.

6.1.4 1p36 Deletion

The identification of a 1.1Mb deletion, involving the short arm of chromosome 1 at 1p36, required further characterization of the case's phenotype. As described in Chapter 1, deletion of this locus has been shown to cause the disorder termed 1p36 Deletion Syndrome. Although there are features common to both disorders, there is significant divergence in the characteristic dysmorphology. Prior to further investigation, it was important to discern whether this case had 1p36 Deletion Syndrome or CdLS. The phenotypic features and clinical history were reviewed by three geneticists with international expertise in dysmorphology including Professor Fitzpatrick; they concluded that the features were indicative of CdLS not 1p36 Deletion Syndrome. They used recognized CdLS diagnostic classifications, with the phenotypic features fulfilling the criteria for the diagnosis of CdLS. On account of the limited understanding of the mechanisms underlying these disorders, but particularly 1p36 Deletion Syndrome, it is possible that common aetiologies underlie both syndromes.

Regarding the validity of clinical diagnostic criteria for CdLS, *HDAC8* mutations were identified in cases diagnosed with CdLS. The phenotypes of these cases differ from the classical CdLS phenotype but still meet the criteria for the diagnosis of the disorder [295]. This demonstrates the capacity to identify cases with cohesin-associated gene mutations based on their phenotype using diagnostic criteria for CdLS. This validates the diagnostic criteria for CdLS and adds support to the proposal that this case with 1p36 deletion case may have a cohesin-associated gene mutation.

6.1.4.1 1p36.3 Genome Mapping

The locus 1p36.33 within the human genome had been identified as an area of sequence ambiguity. This arose due to duplication within the region and the resulting sequence homology; *CDK11A/B* and *MMP22/23* are tandemly duplicated in the human genome. At the time this work was undertaken, the human genome reference sequence lacked Exon 4 and Exon 5 in the *CDK11B* gene due to this ambiguity. However, Exon 4 and 5 were present in transcripts ascribed to both *CDK11A* and *CDK11B*. This led UCSC to overlay the first exons of both *CDK11A* and *CDK11B* in their mapping, with the implication that exons 1 to 6 were shared between the genes. In contrast, NCBI aligned the genes separately and did not include Exon 4 and Exon 5 in *CDK11B*. Whilst the absence of Exons 4 and 5 in *CDK11B* was generally held to be a consequence of error in the reference sequence, this required clarification. Furthermore, this ambiguity compromises the accuracy of whole genome/exome strategies to identify mutations within this region, due to the erroneous alignment of sequences to the duplicate gene.

6.1.4.2 Screening candidate genes

The 1.1Mb deletion at 1p36.3 results in the loss of 46 genes. These genes were interrogated to identify genes that may engage cohesin or mediate its function. The function and interactions of each gene was interrogated using NCBI to determine genes with a reported role in cohesin biology or interactions with members of the cohesin complex or its accessory proteins. Genes with unforeseen roles in cohesin biology may have been excluded but this is a common approach used to identify candidate genes to reduce the experimental cost and complexity of subsequent sequencing.

This assessment of the deleted genes identified three with described roles in cohesin biology; these were *CDK11A, CDK11B* and *SSU72*. Both *CDK11* and *SSU72* have been implicated in aspects of cohesin biology and therefore are plausible candidate genes. In addition, both genes may present difficulties to analysis by WES/WGS protocols, providing a further rationale for screening these two genes in the CdLS cohort. The problem with analysis by WES/WGS occurs due to both the duplication of *CDK11* genes and the

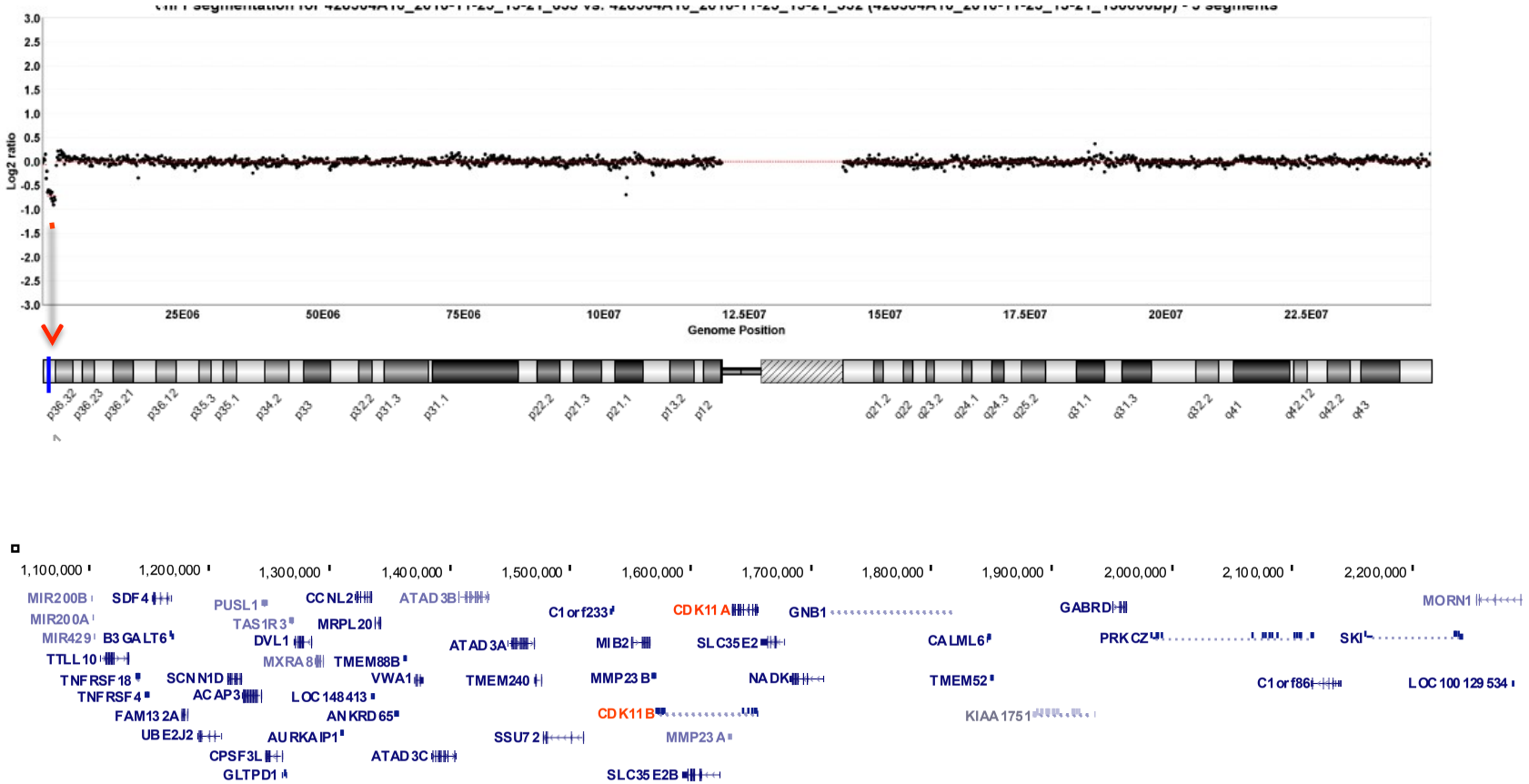

Figure 6.1 1p36.3 Deletion in CdLS Proband Dutch13. Display of the array CGH results from CdLS proband Dutch13. This demonstrates regional loss of chromosomal DNA in the patient sample at 1p36.33, indicative of a micro-deletion (marked by the red arrow). The image below shows the 46 genes that lie within the area of deletion. These genes were curated for genes that may be involved in cohesin biology. CDK11 and SSU72 have putative roles in cohesin biology and transcriptional control; in addition they would not be amenable to detection by whole genome/exome screening methodologies due to sequence duplication.

presence of 8 *SSU72* pseudogenes; these *SSU72* pseudogenes with homologous sequences lack introns. The homologous sequences related to both *CDK11A/B* and *SSU72* may reduce the identification of any causative mutation in WES/WGS due to incorrect alignment of sequences, as discussed below.

If no plausible causative mutations were identified on my sequencing of candidate genes, this cohort would be subject to WES, enabling assessment of other genes within the region. I decided to undertake sequencing of the exons of both candidate genes. Although mutations within introns and promoter regions may contribute to genetic disorders, it is more often difficult to determine causality.

6.2 Screening for *CDK11* mutation in a CdLS Cohort

There are no reports of direct interaction between CDK11 and the cohesin complex but CDK11 mediates the maintenance of sister chromatid cohesion at mitosis. Although the mechanism of this regulation remains uncertain, it indicates CDK11 is directly or indirectly engaged in the mitotic cohesin cycle. As demonstrated with *HDAC8*, disruption of the mitotic cohesin cycle may lead to deleterious consequences [294]. In addition, CDK11 is engaged in the regulation of similar transcriptional events to the cohesin complex, with involvement in transcription initiation and elongation. It is possible that CDK11 may mediate these pathways through similar mechanisms to cohesin. Initially, this work therefore aimed to investigate for the presence of *CDK11A* or *CDK11B* mutations in the CdLS cohort.

6.2.1 Next Generation Sequencing v Sanger

In deciding on experimental design, I had to consider the most appropriate sequencing method. Sanger sequencing is highly accurate and the method most commonly used to identify mutations within a single gene. It remains the 'gold standard' sequencing method employed to confirm mutations identified through next generation sequencing techniques [305]. However, the major disadvantage of Sanger sequencing in this experiment was the homology of *CDK11A* and *CDK11B*. Due to this homology, I was unable to

uniquely prime sequences discrete to each gene. A mutation within an allele of either gene will consequently be diluted within sequence from four alleles of the two genes, impairing its detection using conventional Sanger sequencing techniques. The heterozygous variant/mutation of a gene with two alleles should be detected in approximately 50% of sequences. In practice, this does not occur due to the different priming efficiencies of alternate alleles, often as a consequence of distinct single nuclear polymorphisms (SNPs). *CDK11A* and *CDK11B*, due to the homology of the duplicate genes, comprise in effect four alleles and therefore the frequency of a mutation within retrieved sequence could fall to considerable less than the expected 25%. This renders detection problematic above background sequencing signal.

Next generation sequencing (NGS) with the ability to sequence regions of the genome in depth has the potential to overcome these difficulties. However, NGS techniques also have disadvantages. The combined influence of sequence depth and inherent inaccuracies that occur with all NGS platforms, may lead to the identification of false positive variants [306]. To overcome these difficulties, software exists to minimize false positives through increased stringency of variant calling in areas of sequence known to cause NGS errors, such as homopolymers. This enhanced curation of sequencing data improves accuracy, but any increased stringency may impair sensitivity over specificity. However, recent studies have recommended the adoption of NGS strategies for the sequencing of individual genes or loci, stating the accuracy achieved may equate to traditional Sanger sequencing [307].

The Human Genetics Unit (HGU), Edinburgh uses the Ion Torrent system for these applications. This system is one of the numerous available NGS technologies. During sequencing, the incorporation of a nucleotide into the advancing DNA molecule by the polymerase causes release of a hydrogen ion [308]. This positively charged proton causes a local distortion in pH that is detected by the sequencer. Each microwell on the chip contains clonally amplified copies of a single DNA sequence. The Ion Torrent chip is sequentially flooded with each individual nucleotide. The addition of a

nucleotide complementary to the sequenced DNA causes electrochemical fluctuations within the microwell that are detected and recorded. If two identical consecutive bases are present within the sequence, two nucleotides will be incorporated and the voltage output doubled accordingly. This sequencing method enables the rapid sequencing of DNA molecules, with the 314 Chip successfully used to sequence nucleotide amplicons of up to 250 base pairs (bp) in length.

6.2.2 Primer Design

The next important method to consider was the design of sequencing primers. As discussed, due to sequence homology, it was not possible to design primers for the majority of CDK11 exons that would exclusively prime one gene. Therefore the decision was made to design primers that would prime both *CDK11A* and *CDK11B*. Primer design was undertaken using Primer 3 software. All primers were designed with similar length, GC content and thermodynamic properties to enable the concurrent PCR of all amplicons. On account of the limitation in length of readable sequence obtained using the Ion Torrent system, the maximum amplicon size was set at 250 bp. If any exon could not be covered by a single amplicon, additional amplicons were designed across the exon. Importantly all primers were checked to exclude those with possible off-target priming, using the NCBI nucleotide blast software. It was not always possible to design primers with exact homology to both sequences. To minimize the potential for preferential priming of one gene over the other, primers were designed so as not to contain more than two mismatched nucleotides or single nucleotide polymorphisms (SNPs) and none within the 3' end of the primer. This strategy resulted in the design of 36 primer pairs, to obtain 36 amplicons, covering the 20 exons of both *CDK11A* and *CDK11B*.

6.2.3 CDK11 Dominant v Recessive Model

To filter variants identified on sequencing *CDK11*, it was important to consider the genetic dominance of any putative pathogenic variant. Almost all causative genetic mutations identified in CdLS are autosomal dominant, with mutation of a single allele resulting in the disease phenotype [289].

However, although causative mutations in CdLS are autosomal dominance, this is not the case for all cohesinopathies [309]. An example being Robert's syndrome which is an autosomal recessive disorder caused by homozygous mutations within *ESCO2* [309]. Furthermore, autosomal recessive monogenetic disease may also be caused be compound heterozygous mutations such as in Miller Syndrome, where different rare recessive mutations of *DHODH* occur in each alleles of the gene [310]. Therefore the analysis of any variants must consider both the possibility of an autosomal dominant and an autosomal recessive model.

The phenotype of Dutch13, the CdLS proband with the 1p36.3 deletion, may arise through either a dominant or recessive model. In the dominant model, loss of a single allele within this region (i.e. the regional deletion observed) would cause the disorder, reflecting haploinsufficiency. In the recessive model, deletion of this region may potentiate a deleterious recessive variant within the remaining allele. The phenotype of this Dutch13 differs from the typical 1p36 Deletion Syndrome and more closely resembles CdLS, therefore a recessive model may better explain the difference in phenotype between this case and patients with 1p36 Deletion Syndrome. However, obviously this would require the co-existence of two rare genetic events.

In the dominant model, a causative single heterozygous mutation will cause the disorder and therefore will not be present in databases of known human SNPs in carriers without developmental phenotypes. Therefore any variant present either in unaffected parents or in Exome Variant Server can be excluded from analysis in this model. Exome Variant Server collates SNPs identified through NGS exome sequencing; it comprises data from over 6000 patients without reported developmental disorders.

In the recessive model, either homozygous or compound heterozygous rare SNPs may contribute to the disorder and therefore these cannot be excluded from analysis. To interrogate this, any variant identified was screened against databases of known SNPs. Given the incidence of the disorder, only a combination of rare variants could contribute. On account of the published incidence of CdLS at between 1 in 10000 and 1 in 50000 live births,

particularly as in at least 60% of cases the causative mutation is established, it is implausible that SNP variants with a frequency of greater than 1 in 200 would contribute to the disorder. To minimize the possibility of erroneously excluding variants, in this analysis only variants with a frequency of greater than 1 in 100 were excluded.

6.2.4 Disease Causation

On account of the autosomal dominance of established pathogenic mutations in CdLS, it is more plausible that any mutation would occur *de novo*. However, no deleterious developmental phenotype is reported with heterozygous loss of *CDK11* in murine models [127]. As discussed, the murine locus differs substantially from the human locus, with the major difference being the presence of a single *CDK11* gene. Nonetheless, if this observation of normal development with haplo-insufficiency remains valid in humans, it would indicate that a causative *CDK11* mutation must be dominant negative or recessive, rather than haplo-insufficient.

The second important element to consider is how to determine causation of any putative mutant variant identified. This is obviously more difficult on account of the duplication, as the significance of the two *CDK11* genes remains uncertain. It is not known whether one gene is able to amply compensate for the loss of the other or whether they are both requisite. Certainly the promoter regions and promoter binding motifs differ, with the expression of the two genes reported to vary in certain tissues [112, 142]. This would suggest both genes are indeed necessary but this remains untested. In addition, it cannot be excluded that a dominant negative mutation of a single *CDK11* gene may affect the function of the alternate *CDK11* gene product.

To determine causation, any novel variant, or combination of variants in the recessive model, would require not only be unique to the case over both unaffected parents but also for mutation of the gene to be observed in more than one solitary case. This remains a critical tenet in the determination of genetic causation, with the significance of novel variants in single individuals difficult to definitively establish. Corroboration in multiple cases reduces the possibility of identifying novel SNPs, with no functional

consequence, as causative mutations. The putative causative variant identified should result in a non-synonymous amino acid alteration. Again, synonymous changes may contribute to disease phenotypes but determining both causation and mechanism are challenging. Programs such as PolyPhen-2 are of use in determining the likely deleterious consequences of observed variants. In part, these programs undertake comparisons of amino acid variation in the protein through speciation to determine the likelihood it is pathogenic. Obviously subsequent interrogation of protein function, with the generation of mutant protein, would be required to validate the findings.

6.2.5 CDK11 Sequencing Protocol

The Fitzpatrick CdLS cohort comprised cases from around the world, with DNA samples collected internationally. Genomic DNA of each CdLS case was extracted from blood or buccal swabs within the Human Genetic Unit, Edinburgh. Due to the limited quantity of genomic DNA available, sequencing was undertaken on whole genome amplified (WGA) DNA. Whole genome amplification of patient samples was performed using the Illustra GenomiPhi V2 Amplification Kit (GE Healthcare Life Sciences).

The designed primers were tested to confirm adequate reaction efficiency, with similar quantities of product synthesized following PCR. This also enabled determination that there was no visible anomalous product derived from putative off target reactions. All primers appeared to produce adequate quantity of product without addition products observed [Fig 6.2].

The Ion Torrent system was used for the sequencing. This required preparation of amplicon libraries for sequencing [Fig 6.3]. The amplicons were obtained through PCR of genomified patient DNA, using the designed primers. The amplicons for each patient were pooled and end repair undertaken in preparation for ligation of adapter sequences, necessary for sequencing on the Ion Torrent. These samples were than purified and the adapter ligated to each end of the amplicon using nick repair polymerase. In order to sequence greater than one case on each chip, barcode adapters were used. A distinct barcode sequence was ligated to all the amplicons from a single patient so that their sequences would be identifiable subsequently.

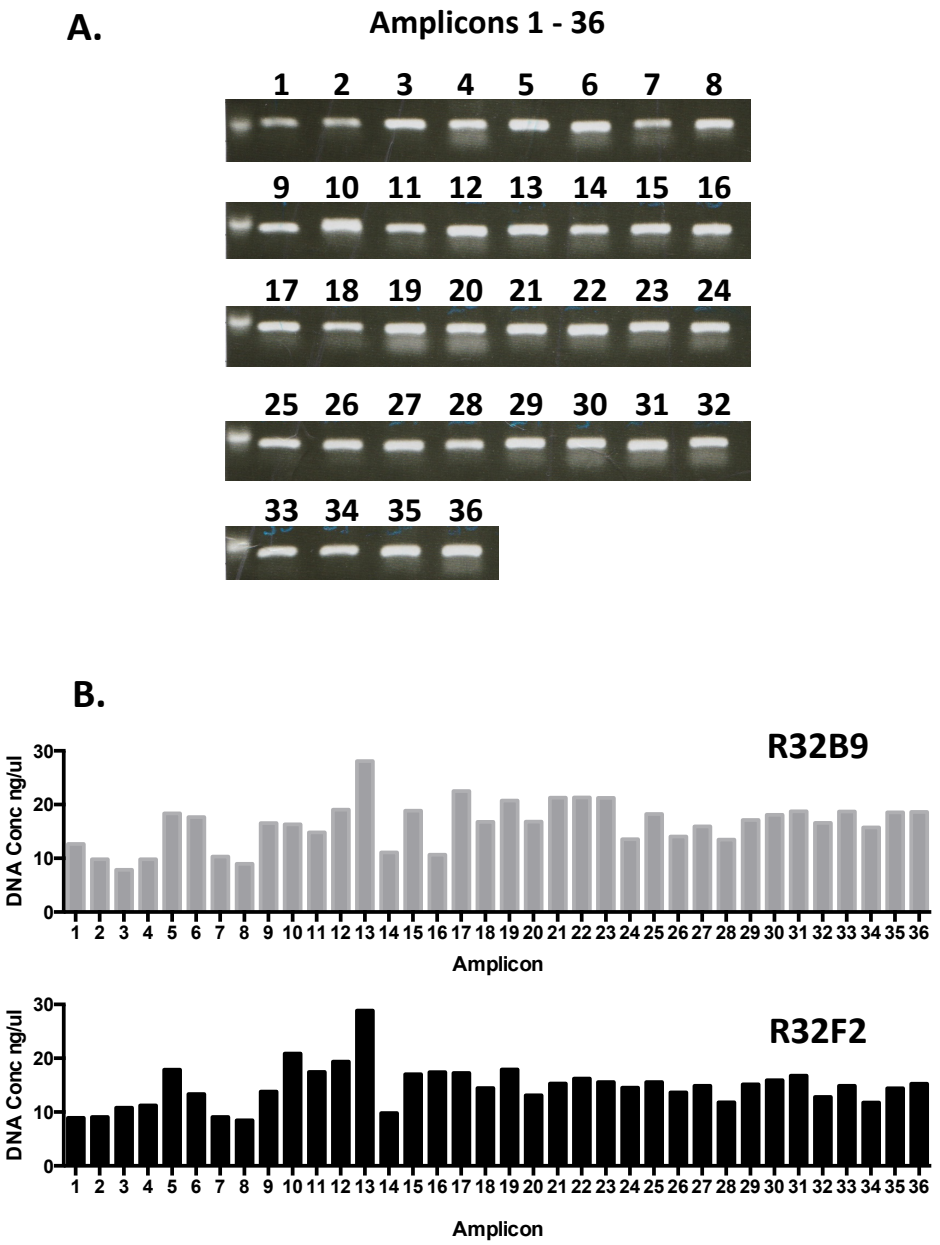

Figure 6.2 CDK11 Amplicons for IonTorrent Sequencing. Primers were designed using Primer3 to sequence the CDK11 exome. Due to homology between CDK11A and CDK11B, primers were designed to prime both sequences simultaneously. On account of limitations imposed by Ion Torrent, all amplicons were designed with a maximum length of 250bp; larger exons were subdivided for sequencing. In total 36 primer pairs were designed to sequence the 20 exons of both CDK11A and CDK11B. ***6.2A*** shows the product of each primer pair following PCR of control human DNA resolved by agarose gel electrophoresis. Each product is of the correct size and there is no evidence of addition bands to indicate off-target priming or primer-dimer formation. ***6.2B*** shows the quantification of PCR products for two representative patient samples R32B9 and R32F2 using SYBR Green quantification. This demonstrates adequate concentration of each amplicon to proceed with library preparation.

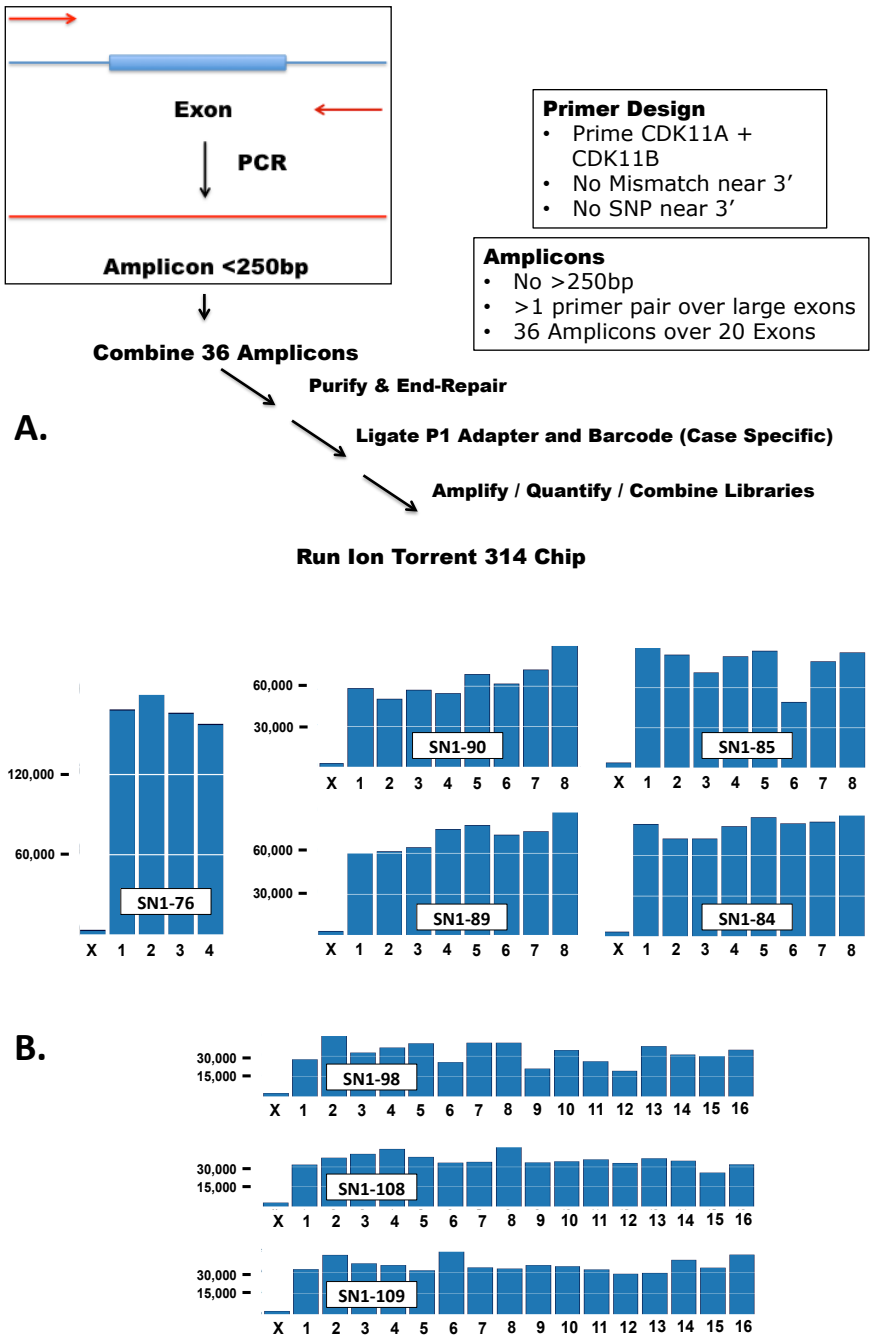

Figure 6.3 Ion Torrent Sequencing. ***6.3A*** shows the library preparation protocol for Ion Torrent sequencing. Amplicons generated by PCR were purified and end-repaired to enable ligation of adapter and barcode sequences. The barcode allowed multiple cases to be interrogated on the single chip. The rules used to design primers and their respective amplicons are reported. ***6.3B*** shows the valid library reads (Y Axis) recorded for each case (X Axis – Barcode label) across all 8 chips (prefixed SN1@). Initially 4 cases were combined and sequenced on a single chip; it was apparent due to sequence quality and read depth that additional cases could be sequenced. Subsequently 8 cases then 16 cases were combined for sequencing on a single chip.

Samples were again purified prior to amplification of the library to increase the read depth. Each library, with its unique barcode ligated, was then quantified utilizing the Agilent Bioanalyser. Equal quantities of each patient library were then collated and delivered to the core sequencing department for cloning onto Ion Spheres and placement on the 314 Ion Torrent Chip.

6.2.6 Ion Torrent Sequencing Results

The chip contains internal control sequences to confirm accuracy of the sequencing run. In addition, sequencing outputs are aligned with the given reference sequence as a further control of sequencing. Initially, as similar sequencing had not previously been undertaken in the unit, 4 cases were combined on each chip. Subsequently, it was apparent on account of the read depth that additional samples could be sequenced on each chip. Consequentially, 8 cases then 16 cases were successfully sequenced per chip. The total valid library reads for each patient sample is shown [Fig 6.3B]. The parameters of chip sequencing are also shown [Fig 6.4 and Table 6.1]. This demonstrated good sequence quality and read depth. The percentage of valid library reads is considered a quality indicator, with 70% valid library reads considered an excellent output. A figure of approximately 70% was achieved with all but one chip. The proportion of Q20 reads was also higher than that reported in the literature. This indicated that the sequencing runs were of acceptable quality.

Any areas where read depth fell below 10 reads were in addition sequenced with Sanger sequencing. The amplicon sequencing Exon 9 in 6 cases and the last 20 bases of Exon 13 in 5 cases were the only two regions where read depth fell below this requirement. Indeed in over 95% of regions, read depth exceeded 100.

The sequencing data generated was analysed using NextGene software. Reference sequences for *CDK11A* and *CDK11B* were obtained from NCBI and input into the analysis software for alignment. The NextGene software enables the analysis to be customized to the preferences of the user. This allows the sensitivity of the assay to be enhanced for the detection of low frequency variants. The resultant limitation is the loss of specificity, with an

A.

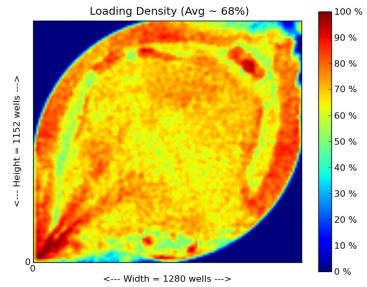

B.

		314 Chips							
		SN1 76	SN1 84	SN1 85	SN1 89	SN1 90	SN1 98	SN1 108	SN1 109
Microwells containing	Library Reads	906898 (96%*)	892997 (96%*)	859255 (95%*)	774790 (91%*)	847729 (94%*)	805358 (96%*)	762891 (94%*)	869007 (95%*)
	Polyclonal	234628 (26%)	202195 (23%)	236401 (28%)	234408 (30%)	239882 (28%)	213520 (27%)	159770 (21%)	210143 (24%)
	Primer dimer	5 (<1%)	21 (<1%)	35 (<1%)	3 (<1%)	6 (<1%)	3 (<1%)	3 (<1%)	5 (<1%)
	Low quality	44996 (5%)	56123 (6%)	75608 (9%)	31776 (4%)	219952 (26%)	63964 (8%)	42320 (6%)	47418 (5%)
	Valid Library Reads	627269 (69%)	634658 (71%)	547211 (64%)	508603 (66%)	387889 (46%)	527871 (66%)	560798 (74%)	611441 (70%)

Figure 6.4 Ion Torrent 314 Chip Outputs. ***6.4A*** shows a representative image of microwell loading across an Ion Torrent 314 chip (SN1-98) with amplicon conjugated Ion Spheres (ISPs). This demonstrates adequate loading density and distribution of ISPs over the chip. ***6.4B*** is a table of outputs from each 314 chip; this records the number of microwells containing ISPs with the defined attributes. Library reads indicate ISPs conjugated to any sequence (*percentage shown is that of microwells containing any ISP, including those without sequence). Polyclonal indicates ISPs conjugated to more than one clonal sequence and therefore uninterpretable. Primer dimer indicates ISPs conjugated to primer dimers. Percentages are those of total library reads (Row 1). Indicators of quality include low quality reads <10% and primer dimer <1%. In addition, a value of approximately 70% Valid Library Reads, the number of ISPs containing readable sequence, is considered excellent. Only one chip (SN1-90) fell significantly below this level. Read depth and sequence quality for this chip however remained adequate for CDK11 sequencing.

	314 Chips							
	SN1 76	SN1 84	SN1 85	SN1 89	SN1 90	SN1 98	SN1 108	SN1 109
Total Number Bases (Mbp)	115.06	119.6	101.98	94.03	68.05	96.11	97.70	110.53
Number Q20 Bases (Mbp)	82.14	95.42	79.24	72.05	49.49	70.81	69.95	82.43
Valid Library Reads	627269	634658	547211	508603	387889	527871	560798	611441
Mean Read Length (bp)	183	189	186	185	175	182	174	181
Mean AQ20 Read Length (bp)	129	138	136	134	129	126	120	130
Mean Coverage Depth	2384	1245	1057	977	705	499	507	574
Longest Alignment (bp)	276	285	285	289	264	268	252	252
Longest Read (bp)	386	391	396	394	397	398	392	389

Table 6.1 Ion Torrent 314 Chip Outputs 2. Table 6.1 shows the output characteristics of each chip following sequencing on the Ion Torrent. It records the total number of bases sequenced on each chip, in addition to a high estimated quality (Q20). This compares favourably with published applications of Ion Torrent sequencing. It demonstrates good average sequence read length for each chip; in addition the mean AQ20 (the greatest sequence length at which error rate is less than 1% subsequent to alignment) is consistently over 100. This performance is also superior to published specification and expected outputs from the 314 Chip. It shows excellent mean coverage depth; this is confirmed on subsequent sequence alignment and analysis, with minimal requirement for additional sequencing.

increased false positive rate. The mutation detection rate was established at 10% of reads, i.e. a variant present in 10% or more of sequences was identified. As explained above, any single allele variant that could not correctly be aligned to either *CDK11A* or *CDK11B* should make up 25% of total sample reads. To compensate for any differential allele priming, a lower thresh-hold was set for the mutation detection rate (10%). In effect, this constituted a compromise between sensitivity and specificity. Mosaic mutations may pass undetected but this was accepted given the potential difficulties of determining the significance of mosaicism in either *CDK11* gene, especially due to the inherent complexities of this region.

Across the 84 patient samples, 3592 variants were detected, at an average of 42.8 variants per patient (Range 36-64). It was noted that the vast majority of variants identified were common to most if not all samples. This occurred for two principal reasons. The first was that the variants identified were common SNPs within either *CDK11A* or *CDK11B*. The second reason was the identification of variants that arose as a result of sequencing errors. All NGS sequencing platforms have particular susceptibility to certain errors. Bidirectional sequencing reads were obtained, allowing a reduction in the error rate compared to unidirectional strategies. Erroneous sequencing was identified by both its the occurrence in the majority of cases, including the two control cases, and its the distribution in a non-allele specific manner. Control cases were those within the cohort, in which a mutation in a established causative gene had been identified. As discussed many next generation sequencing strategies are expressly vulnerable to errors at sites of homopolymers. This occurs due to the method of sequencing, with sequences of multiple consecutive identical nucleotides leading to difficulty in ascertain the precise number of nucleotides incorporated. These homopolymer errors are recorded as insertions or deletions. Virtually all variants were excluded as either common SNPs, with a reported frequency of greater that 1 in 100, or as erroneous sequencing.

6.2.7 Novel Variants in CDK11 Identified

Following exclusion of the variants as described, there remained two variants within *CDK11A* or *CDK11B* in the cohort that did not constitute either common reported SNPs or sequencing error. Neither of these SNP variants had been previously described in Exome Variant Server, dbSNP or COSMIC databases; in addition both variants were non-synonymous.

6.2.7.1 Variant in Case R32F11

The first comprised a variant within coding Exon 4 of case R32F11, with this mutation of guanine to cytosine causing a change of amino acid residue from Glycine (118) to Arginine. This variant appeared to occur within *CDK11A*, although as discussed the *CDK11B* reference sequence does not contain Exon 4 for comparison. This mutation was present in 196 of 1196 reads (16%), with all reads at this exon aligned to *CDK11A*. This amino acid sits within the 14-3-3 binding domain and putatively may alter its function. This residue is conserved through all vertebrates and PolyPhen-2 predicted this mutation to be damaging. The PolyPhen-2 score was 1, the maximum obtainable score to indicate damaging potential. To interrogate this further, the parental samples were obtained, as neither had been previously collected. Following this, both parents were sequenced using Sanger sequencing for the presence of the mutation. This demonstrated the mother of R32F11 had the same variant [Fig 6.5]. There was no rare SNP in the alternate allele to indicate a recessive disorder and the mother did not suffer with CdLS. Therefore, this variant was determined to be a novel SNP variant, as it had not been previously identified in SNP databases, but the variant was not causative.

6.2.7.2 Variant in Case R34A6

The second variant comprised a base substitution within coding Exon 7 in case R34A6. This mutation of guanine to adenine encoded Lycine in place of Glutamate. This residue is adjacent to the SH2 binding domain and may putatively alter SH2 binding. PolyPhen-2 also predicted this mutation to be damaging, with a score of 0.934. Sanger sequencing to confirm the presence of the mutation demonstrated that this variant would not have been detected using conventional Sanger sequencing due to low signal [Fig 6.6]. This

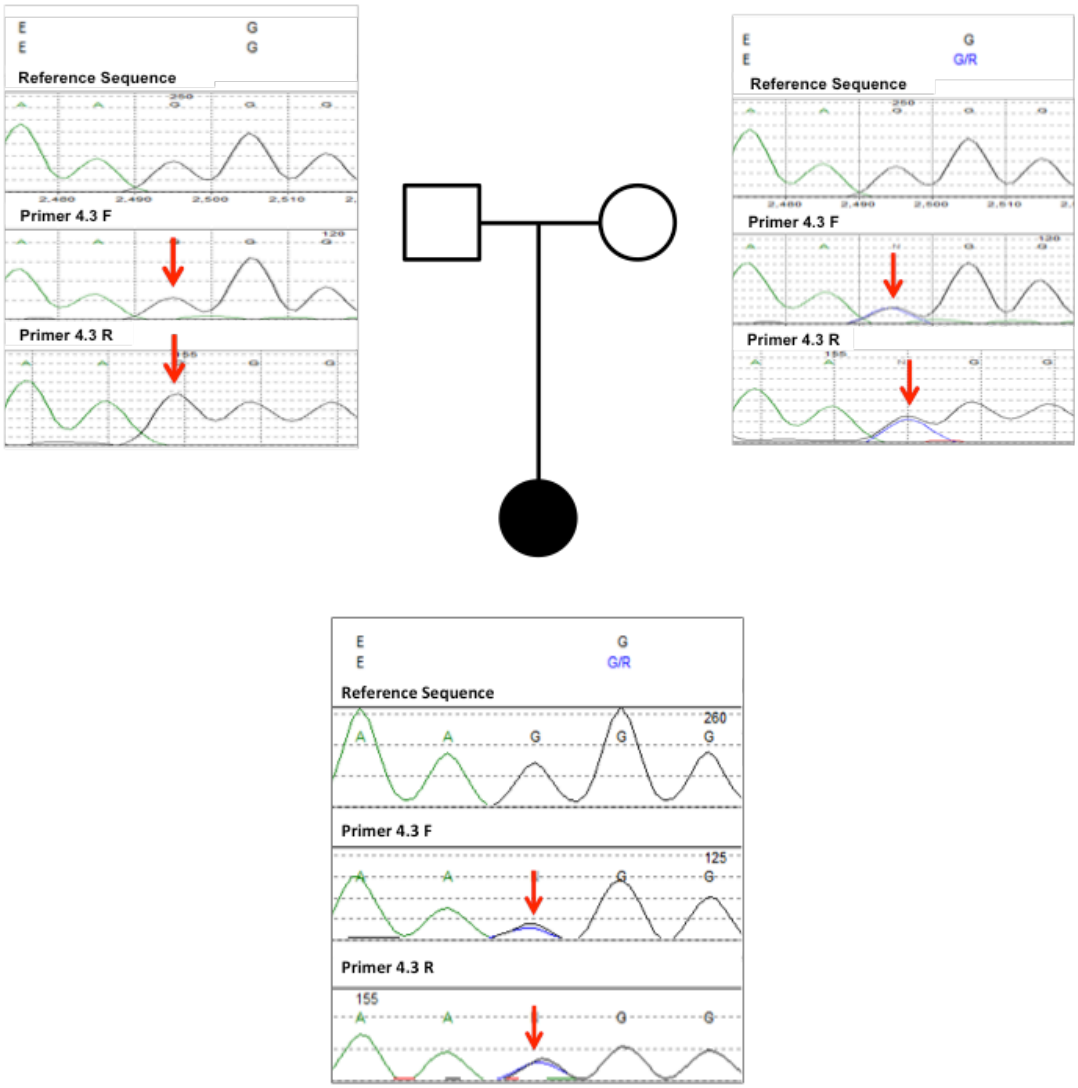

Figure 6.5 Sequencing Proband R32F11. Ion Torrent sequencing identified a novel variant in proband R32F11. This occurred at Exon 4 within *CDK11A*; there is no reference sequence for *CDK11B* Exon 4 so the variant may sit within either gene. This mutation of guanine to cytosine was non-synonymous with the Glycine 118 converted to Arginine. This is a highly conserved amino acid among vertebrates, lying within the 14-3-3 binding site; it was predicted damaging using PolyPhen2 software. Sanger sequencing confirmed the variant in the proband but, subsequent to obtaining parental samples, the variant was also present in the unaffected mother. This was therefore considered to be a novel non-causative variant within *CDK11*.

variant was present in 56 of 237 reads aligned to *CDK11A* and 60 of 472 aligned to *CDK11B*, with the variant sequence aligned to both genes due to sequence homology and therefore software was unable to differentiate between the two genes. This variant therefore was present in 116 of 709 reads in total (16%). As this variant could not be robustly differentiated on Sanger sequencing, it was decided to undertake CEL1 restriction. This variant was the only nucleotide mismatch within this amplicon between both alleles, enabling CEL1 restriction. CEL1 restricts DNA at sites of heterozygosity. Amplicons of this locus were generated and annealed. Addition of CEL1 to the WGA DNA of R34A6 generated a fragment corresponding to the size expected by restriction at the variant. Surprisingly, no variant was observed in the parental samples or the stock DNA sample of R34A6 [Fig 6.6B]. The presence of the variant in the whole genome amplified DNA but not the stock DNA inferred that either the variant was introduced during amplification or the amplified DNA had been incorrectly assigned during processing and constituted an alternate patient DNA. To interrogate this, CEL1 restriction was undertaken on all 15 stock DNA cases amplified in parallel with R34A6 but the variant was not present in this stock DNA. It was therefore concluded that this variant must have resulted from an error introduced in whole genome amplification.

Finally, examination of sequencing from case Dutch13 with the deletion of 1p36 did not reveal any low frequency SNP or other variants to indicate loss of heterozygosity in either *CDK11A* or *CDK11B* gene. Interesting, analysis of the *CDK11* sequence for proband Dutch13 with known monosomy at this locus, demonstrated the presence of two alleles of both Exon 4 and Exon 5. This was the region of ambiguity lacking Exon 4 and Exon 5 in the reference sequence. This sequencing demonstrated that there were indeed two Exon 4 and two Exon 5 sequences within this region and confirms that contrary to the UCSC alignment, the genes did not share Exons. This was expected and entirely consistent with the accepted paradigm. Both UCSC and NCBI alignments have been altered to reflect this in the most recent genome build.

6.3 Screening the CdLS Cohort for SSU72 Mutation

SSU72 is an established cohesin binding protein that not only mediates sister chromatid cohesion during mitosis but is also involved in transcription as a RNA Polymerase II CTD phosphatase [311, 312]. Both its role in cohesin biology and its role in transcription made it an interesting candidate in the search for novel causative mutations in CdLS.

6.3.1 SSU72 sequencing

CDK11 sequencing was planned using the Ion Torrent NGS sequencing platform. This had not been undertaken in the unit previously and its suitability for this strategy was unclear, with particular uncertainty over the quality and length of sequencing that would be obtained. Therefore, it was decided to undertake only the *CDK11* screen using the Ion Torrent. The second gene identified as a putative candidate, *SSU72*, was sequenced using traditional Sanger sequencing. The *SSU72* genomic sequence holds different challenges compared to sequencing of *CDK11*, with regions of the genomic sequence containing high GC content. However, there was no intronic homology to prevent the synthesis of specific exon amplicons.

Primers pairs were designed using Primer 3, with similar length, GC content and thermodynamic properties to those described above. There was no limitation on amplicon length and all exons could be primed with a single amplicon. Once again primer product was assessed prior to sequencing, confirming both adequate reaction efficiency and the absence of off-target priming. During primer design, it was apparent that the *SSU72* sequence contained areas of high GC content, which can impair sequencing reactions. This was evident during primer testing and the reaction required the addition of GC-rich mix to enhance sequencing. With the use of this, it was possible to achieve adequate amplicon production.

To exclude variants, bidirectional sequencing was required. Sequencing using the GC-rich mix was generally adequate to achieve this. For the few cases where this remained inadequate, a second primer set was used, in addition to further replication of amplification with the original primer pairs.

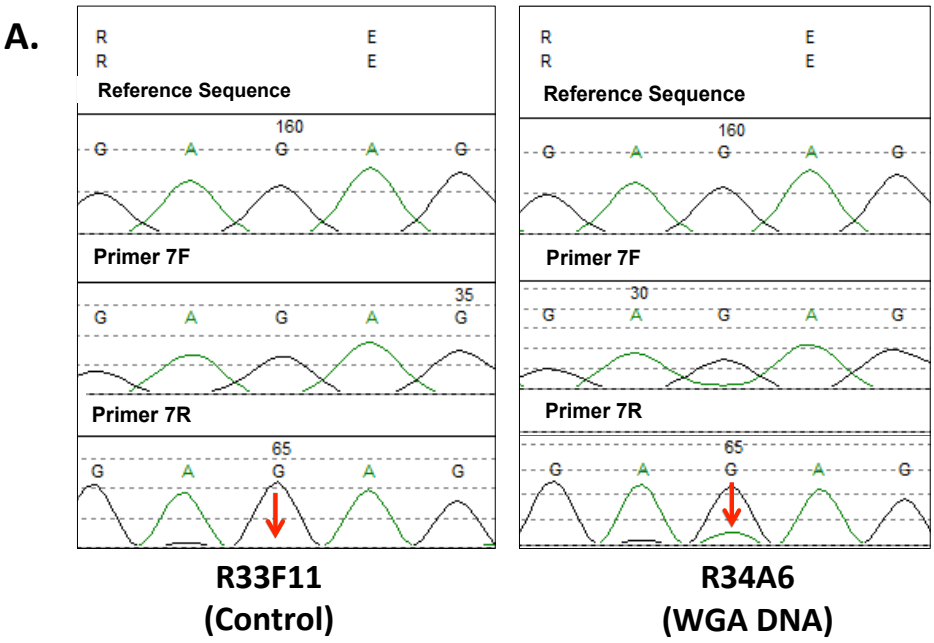

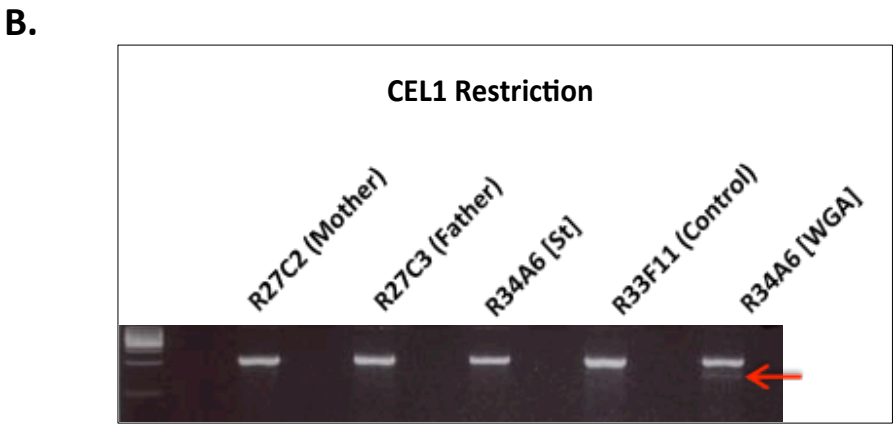

Figure 6.6 Sequencing Case R34A6. Ion Torrent sequencing identified a novel variant in case R32A6. This comprised a base substitution at Exon 7 with mutation of guanine to adenine; this was non-synonymous with conversion of Glutamate 218 to Lysine. This was again a highly conserved residue with preservation throughout vertebrate species. This was predicted damaging with PolyPhen software. It is adjacent to the SH2 binding domain within the N Terminus of CDK11p110. Subsequent Sanger sequencing confirmed the presence of the variant in whole genome amplified (WGA) DNA compared to DNA of case R33F11 with no identified mutation of this region. This demonstrates the difficulty of Sanger sequencing *CDK11* (***6.6A***). The variant aligned to both *CDK11A* and *CDK11B* on account of the absence of sequence variation between the two genes at this site; sequence could therefore be aligned to either gene with equal accuracy. This sequence duplication resulted in the variant being difficult to discern by Sanger sequencing (Red Arrow). The presence of a variant was confirmed by CEL1 restriction, as this variant was the only variant in this amplicon. CEL1 nuclease cuts at sites of mismatches. This demonstrates the generation of a fragment of the correct size on CEL1 restriction in the WGA DNA (***6.6B***). This is not present in either parents or stock DNA. Following further investigation this was considered to be a mutation inserted during WGA.

The core HGU sequencing service undertook sequencing. Sequencing data obtained was aligned to the reference genomic sequence of *SSU72* using Mutation Surveyor software. Few variants from the reference sequence were observed in the CdLS cohort and no rare variants of a frequency below 1 in 100 were identified in any of the cases. Therefore, I did not identify a causative mutation in the *SSU72* gene.

In retrospect, due to the success of Ion Torrent sequencing, the *SSU72* Sanger sequencing could have been performed on the Ion Torrent platform concurrently with *CDK11* sequencing. This would have reduced the requirement for additional sequencing and therefore cost. However, it is uncertain whether the high GC content would have impaired *SSU72* sequencing with this strategy.

6.4 Conclusion

This chapter described work to screen for causative genetic mutations within a cohort of CdLS cases. This work was predicated by the identification of a 1p36 deletion in a patient diagnosed with CdLS. Sequencing failed to identify a novel causative mutation within any of three candidate genes (*CDK11A, CDK11B* and *SSU72*) at this locus. Two novel variants were identified in these cases but one was inherited from an asymptomatic parent, while the other resulted from error introduced during genome amplification. Given the putative involvement of these gene products in cohesin biology, in addition to the difficulty in sequencing these genes using WES, individual sequencing of both genes remained a valid approach.

The question remains of whether this case truly represents the cohesinopathy CdLS or whether it may represent an atypical presentation of 1p36 Deletion Syndrome. 1p36 Deletion Syndrome is recognized to cause a wide spectrum of phenotypes due to the different loci and genes involved in the deletion. Papers have described regions of minimum deletion in 1p36 Deletion Syndrome but these do not always overlap and the disorder may result from the disruption of a differing combination of genes [313, 314]. An overlap with CdLS cannot be excluded until mechanisms underlying both syndromes are

better understood. Nonetheless, Gervasini et al. recently reported genomic imbalances in 8% of mutation negative CdLS probands, which may provide an alternate explanation for their developmental phenotype [315].

This work therefore did not identify any mutation to explain the latent genetic aetiology of CdLS. It did however demonstrate that the human reference sequence of the 1p36.33 locus was erroneous. The identification of two Exon 4 and two Exon 5 alleles within *CDK11* at this area of monosomy confirmed the presence of discrete Exons 4 and Exons 5 in *CDK11A* and *CDK11B*. This is consistent with accepted knowledge of the *CDK11* gene locus. Further exploration of the exomes of this CdLS cohort will be undertaken using WES in an attempt to elucidate novel causative genetic mutations.

CHAPTER 7

Conclusion

7.1 CDK11 and Disease Phenotypes

The work in this thesis explores novel roles of CDK11 in cancer and developmental phenotypes. CDK11 has an essential role in embryonic development, with loss of *Cdk11* causing blastocyst lethality in murine models [81]. Furthermore, CDK11 appears critical not only during development but in later health, with CDK11 dysregulation implicated in the pathogenesis of various disease states, including cancer. Overexpression of the protein has been associated with poor prognosis in malignancies, such as breast cancer, ovarian cancer and osteosarcoma [316-318]. Moreover, numerous studies have identified CDK11 as a potential therapeutic target in cancer [130, 316, 318].

The importance of CDK11 in both health and disease warrants further investigation to better understand its functions in these states. Characterising these CDK11 functions may not only provide a greater understanding of cell biology but also enable better targeting of CDK11 and synergistic pathways in diseases, such as cancer. CDK11 engages in transcription, splicing, mitosis and apoptosis. This thesis has interrogated novel functions of CDK11 in cancer cells, including its mediation of autophagy and cell migration. Additionally, I have investigated the CDK11 interactome in order to elucidate the mechanisms that underlie both novel and established CDK11 functions. Finally, I have investigated *CDK11A*/*CDK11B* as candidate disease-associated genes in the developmental disorder CdLS.

7.2 CDK11 and Autophagy

Autophagy is recognised to influence both tumorigenesis and subsequent tumour proliferation; it may perform functions beneficial or deleterious to tumour biology, depending on the cellular components targeted for degradation by selective autophagy. The initial work in this thesis explored

the altered autophagy flux observed following CDK11 depletion. The aim was to provide a greater understanding of CDK11-mediated autophagy and its influence in cancer cells. I studied this CDK11-mediated autophagy in KRAS mutant cancer cells (MDA-MB-231 and HCT116). Although KRAS mutant cancers are reported to demonstrate increased dependence on autophagy pathways [319], this autophagy phenotype is not unique to KRAS mutant cells and is observed in other non-cancer cells, including drosophila S2 cells [149].

I demonstrated that the autophagy phenotype could be abrogated by inhibition of the cell cycle and replicated by chemical inhibition of mitotic regulator PLK1. Furthermore, there appeared to be a temporal relationship between passage through mitosis and the subsequent autophagy phenotype. This indicated that the autophagy phenotype occurred secondary to mitotic dysregulation rather than due to direct effects on autophagy pathways.

Matsui et al. (2013) reported that inhibition of autophagy in states of nutrient starvation led to mitotic delay and aberrant mitoses, with associated genomic instability [201]. This demonstrates the capacity of dysregulated autophagy to influence the cell cycle and faithful chromosome segregation during mitosis. However, my work does not indicate that CDK11's regulation of mitosis occurs through disruption of autophagy. My work was undertaken in nutrient replete states, where the autophagy phenotype occurred secondary to mitotic dysregulation rather than the opposite.

The autophagy phenotype I investigated was the significant accumulation of LC3 II protein and LC3 puncta following CDK11 depletion; it was this phenotype that was associated with mitotic dysregulation. I did not exclude that more minor alterations in autophagy flux could be directly mediated by CDK11, separate to its mitotic function. Other splicing proteins components are recognized to influence tumour biology and specifically autophagy through modulation of stress pathways and regulation of MTOR [320]. However, CDK11-mediated autophagy is primarily a consequence of mitotic dysregulation.

7.3 Autophagy, Mitosis and Chromosome Missegregation

Mitotic catastrophe results from aberrant mitosis with failure of chromosome segregation; it describes a process of cell death or senescence that occurs through apoptosis, necrosis or nuclear fragmentation [321]. Autophagy induction is recognized to occur following mitotic catastrophe [321]. In this thesis, I have demonstrated inhibition rather than induction of autophagy at 72 hours following CDK11 knock-down in MDA-MB-231 cells. However, this was not replicated in HCT116 cells, with continued autophagy flux despite LC3 accumulation. These findings are consistent with those of others in the laboratory that demonstrate autophagy induction at early time-points, with subsequent autophagy inhibition [149]. This is proposed to occur secondary to inundation of autophagy pathways, with resultant depletion of autophagy proteins [149]. Mitotic catastrophe is therefore likely to explain the CDK11-mediated autophagy phenotype; in my work, multinucleated cells that display the autophagy phenotype appear to undergo cell senescence, remaining viable for extended periods in culture but failing to undergo further cell division.

Aneuploidy is a consequence of chromosome missegregation and is a common occurrence in cancer. Debate persists as to its contribution to tumorigenesis but aneuploidy does result in stoichiometric imbalances within the proteome [165]. Published studies indicate the resulting proteomic stress may drive ROS production, with deleterious consequences for aneuploid cells [322, 323]. These deleterious effects present a potential vulnerability within aneuploid cancer cells; pathways that mitigate the associated proteomic stress may therefore provide therapeutic targets [324].

I aimed to assess whether autophagy may function to mitigate the cellular stress caused by chromosome missegregation/aneuploidy. Although effects on autophagy following aberrant mitosis are evident, I was unable to demonstrate altered autophagy following chromosome missegregation itself. However, others laboratories have subsequently demonstrated this, with induction of autophagy following chromosome missegregation [191, 206].

I have presented evidence in this thesis that autophagy is important for the survival of aneuploid cells. I demonstrated that loss of autophagy (through ATG5 knock-down) impaired the maintenance of aneuploid cell populations, in the absence of p53. Further work is required to confirm these findings, which were again observed in KRAS mutant tumour cells. Moreover, ATG5 has recently been reported to mediate mitotic catastrophe through mechanisms other that autophagy [325]. Further work is required to assess how this may have influenced my results but it appears unlikely that loss (rather than gain) of ATG5-mediated mitotic catastrophe would have impaired the maintenance of aneuploid populations.

7.4 CDK11 and Cell Migration

The evidence presented in this thesis demonstrates that CDK11 depletion impairs breast cancer cell motility. This occurred with both mesenchymal hormone-receptor negative and epithelial oestrogen-receptor positive breast tumour cells. I demonstrated that this was not simply a consequence of CDK11's effect on cell proliferation, with motility impaired in both directional and random migration assays. The mechanism of this impaired migration could not be ascribed to a specific deficiency in cell adhesion or cell polarization.

CDK11 is not unique among CDKs in mediating cell migration, with CDK5 established to regulate cell motility [326]. However, the localization and structure of CDK5 is markedly different to CDK11; CDK11 does not clearly locate to the cell periphery and remains predominantly nuclear. In the RNAi screen undertaken by Simpson et al. (2008), CDK4 and CDK9 also impaired cell migration, although CDK9 had confounding effects on cell viability/proliferation [230]. CDK2, CDK6, CDK7 and interesting CDK5 had no effect on cell motility in this assay.

Interactome studies in Chapter 5 did not identify enrichment of proteins associated with cellular motility among CDK11 interactors (as determined by GO annotation). Furthermore, I did not identify significant alteration in

localization or phosphorylation of focal adhesions proteins FAK and Src during adhesion assays or interphase following CDK11 depletion; I have not examined whether CDK11 directly modulates other signaling proteins involved in cell migration. CDK11 may influence cell motility through its effects on splicing, with other mediators of splicing established to influence cell migration [327]. Furthermore, cancer cells are reported to vary from non-cancerous cells in their use of alternate splice sites and this has been postulated to contribute to tumour biology and phenotypes such as cell migration [328]. This may therefore contribute to the effect of CDK11 on migration, as CDK11 is established to influence alternate splicing decisions [55].

Further work to interrogate the influence of CDK11 on migration may involve examining associated signaling pathways, such as with reverse protein arrays. Once again, it will be difficult to accurately interpret the results due to the wide-ranging effects of siRNA-mediated CDK11 depletion on transcription, splicing and mitosis. Unfortunately there are no specific inhibitors of CDK11 currently available to enable precise temporal regulation of the protein activity to characterize its influences more accurately. However, specific CDK11 inhibitors are under production for trial in the treatment of cancer; these inhibitors may facilitate this work.

7.5 CDK11 Proteomics

My work examining the CDK11 interactome has identified numerous novel putative interactors. However, affinity purification of GST-tagged CDK11 protein did not generate reproducible results, with only one of three interactors, chosen for validation, subsequently confirmed on repetition of the assay. Moreover, although GST.CDK11p58 consistently precipitated endogenous CSK, I was not able to demonstrate the interaction *in vivo*. These difficulties were likely a reflection of inherent weaknesses in the affinity purification protocol. However, work predicated on this finding did reveal alterations in Src phosphorylation during S phase on CDK11 knock-down; this requires further validation prior to investigation of its significance.

Immunoprecipitation of GFP-tagged CDK11 identified a significant number of established interactors, providing confidence in the validity of the assay. The good correlation between results of biological replicate experiments is also reassuring, when considering the reliability of the results.

Examination of the CDK11 interactome revealed significant enrichment of spliceosomal proteins among putative CDK11 interactors in three of the four GFP.CDK11 co-immunoprecipitates. Interestingly, this was identified in both GFP.CDK11p58 co-immunoprecipitates and particularly at mitosis. It is uncertain whether this interaction with spliceosomal proteins contributes to CDK11's mitotic regulation. CDK11p58 has not been implicated in splicing previously, although it too interacts with Cyclin L proteins containing RS domains. This result may indicate a role for CDK11p58 in splicing at mitosis, although splicing is generally considered to be suppressed during M phase. However, numerous spliceosomal proteins are reported to influence mitotic regulation. It remains unclear whether this occurs due to dysregulation of splicing in preceding interphase, dysregulated mitotic splicing or alternate non-splicing functions.

I did not have the opportunity to confirm any novel CDK11 interactors but these findings may provide a foundation for further investigation by others. Several potentially interesting interactions were noted, including the interaction of CDK11p110 with members of the human Mediator complex. This is consistent with findings in yeast but it has not been demonstrated previously in metazoan species. In addition, I identified a putative role for CDK11 in ribosome biogenesis; this finding supports published work identifying CDK11 as a constituent of complexes engaged in ribosome biogenesis. Unpublished work has also identified the interaction of CDK11 with DDX15, homologue of yeast PRP43, which has role in both splicing and ribosome biogenesis. My work confirms DDX15 as a putative CDK11 interactor, although the implications of this interaction require further interrogation.

7.6 Review of Thesis Hypotheses

The overarching hypothesis predicating this thesis was that CDK11 may provide a therapeutic target in cancer. The aim of this thesis was to investigate CDK11's role in both cancer and developmental phenotypes, through which to understand better the influence of CDK11 in cancer biology and its related pathways. This may allow the development of targeted synergistic therapies.

In the Chapter 3, I explored the hypothesis that CDK11 directly mediates autophagy to effect the autophagy phenotype observed on CDK11 depletion. I aimed to determine whether the effects of CDK11 on autophagy were dissociable from its established roles at mitosis and transcription. It was apparent that the autophagy phenotype was closely associated with mitotic dysregulation. On CDK11 knockdown, there was a clear association between nuclear dysmorphology and accumulation of LC3 / p62 puncta. I established a temporal relationship between passage through mitosis and the autophagy phenotype, while cell cycle blockade abrogated both nuclear dysmorphology and the autophagy phenotype. Furthermore, the autophagy phenotype could be replicated through inhibition of an alternate mitotic regulator (PLK1). My findings therefore indicate that the autophagy phenotype observed on CDK11 depletion is primarily a response to mitotic catastrophe rather than direct mediation of autophagy.

Whilst alone this does not exclude a direct influence on autophagy by CDK11, it does exclude a direct influence as the mechanism for the autophagy phenotype observed on CDK11 depletion. Furthermore, work undertaken in Chapter 5 did not demonstrate enrichment of autophagy-related proteins in the any of the CDK11 co-immunoprecipitates. Moreover, although a small number of autophagy proteins were among the putative interactors, none were reciprocal between CDK11 isoforms, with both isoforms established to rescue the autophagy phenotype.

In addition, in investigating the role of autophagy following aberrant mitoses, I examined the effect of autophagy depletion on the survival of aneuploid cell populations following induced chromosome mis-segregation.

I hypothesized that autophagy may mitigate the cellular stress engendered following aberrant chromosome segregation; therefore I aimed to establish whether autophagy depletion impaired the survival of aneuploid cell populations. I demonstrate evidence to support this hypothesis; furthermore studies published subsequent to my work also endorse this proposition.

In Chapter 4, I examined the hypothesis that CDK11 directly regulates cancer cell migration. I confirmed that CDK11 depletion impaired cancer cell migration in breast cancer cells. I then aimed to determine whether this effect was distinct to its influence on mitosis and proliferation. I demonstrated that neither culture in serum free media or cell cycle blockade with thymidine abrogate the effect of CDK11 depletion, despite inhibiting cell mitosis and proliferation. I also demonstrate the impairment of migration following CDK11 knockdown with the use of single cell random migration assays, excluding the influence of impaired cell proliferation.

CDK11 contains both SH2 and SH3 binding domains and has established roles in centriole biology; I therefore examined the hypothesis that CDK11 may influence cell migration either via direct interaction with the cytoskeleton, specifically focal adhesions, or through effects on centriole biology and thereby cellular polarisation. I was unable to demonstrate direct interaction between CDK11 and focal adhesions or their prime constituents. Furthermore, following CDK11 depletion, I was unable to demonstrate consistent effects on focal adhesion signaling (via assays of Src and FAK phosphorylation) or influence on cellular adhesion to a substrate following culture in suspension. In addition, I did not demonstrate any significant effect on cellular polarisation using directional wound healing assays.

Finally in Chapter 6, I explored the hypothesis that mutations within *CDK11A/B* may cause the cohesinopathy CdLS. This hypothesis was proposed due to the discovery of deletion of the *CDK11* locus in a patient with CdLS and the established functions of CDK11 in cohesin biology at mitosis. I found no potentially causative variants within *CDK11A* or *CDK11B* in a cohort of CdLS probands, with no known causative mutation.

7.7 CDK11: a therapeutic target in cancer

CDK11 inhibitors are currently under development, based on work in myeloma and osteosarcoma indicating CDK11 may present a therapeutic target. Understanding the biology of CDK11 both in cancer and in health may improve targeting or the development of synergistic therapies. Several inhibitors of alternate mitotic regulators are currently under investigation in the treatment of cancer, including PLK1 inhibitors. It is improbable that any of these therapies alone will constitute Ehrlich's 'zauberkugel' or 'magic bullet'.

The majority of traditional chemotherapy agents target dividing cells, relying primarily on the rapid division of cancer cells to provide their limited specificity. Identifying pathways or proteins that are up-regulated in cancer cells may enable more specific therapies, limiting the side-effect of such agents. Moreover, these pathways or proteins may gain in influence in cancer cells such that these elements become critical for tumour survival. However, difficulties in targeting these pathways or proteins remain due to their functions in the biology of healthy, non-cancerous cells; this is true of CDK11.

Nonetheless, identifying interdependent pathways specific to cancer cells may allow the development of combination chemotherapies that induce synthetic lethality. Autophagy appears to play a role following mitotic dysregulation; my work and that of others indicate that it is important for the survival of aneuploid cell populations. Targeting mitotic regulators such as CDK11 in addition to autophagy may therefore synergise therapy. Further work is required to investigate this hypothesis.

7.8 Conclusion

In conclusion, this thesis describes work I undertook to interrogate the role of CDK11 in cancer and developmental phenotypes. I have demonstrated the impact of mitotic dysregulation on autophagy and the role of autophagy in the maintenance of aneuploid populations in KRAS mutant cancer cells. I have identified both novel putative CDK11 interactors and novel

mechanisms through which CDK11 may mediate its functions. Further work is required to confirm these findings and to assess their significance.

References

1. Johnson, L.N., *The regulation of protein phosphorylation.* Biochemical Society transactions, 2009. **37**(Pt 4): p. 627-41.
2. Manning, G., et al., *The protein kinase complement of the human genome.* Science, 2002. **298**(5600): p. 1912-34.
3. Hanks, S.K., *Genomic analysis of the eukaryotic protein kinase superfamily: a perspective.* Genome biology, 2003. **4**(5): p. 111.
4. Malumbres, M. and M. Barbacid, *Mammalian cyclin-dependent kinases.* Trends in biochemical sciences, 2005. **30**(11): p. 630-41.
5. Lim, S. and P. Kaldis, *Cdks, cyclins and CKIs: roles beyond cell cycle regulation.* Development, 2013. **140**(15): p. 3079-93.
6. Russell, P. and P. Nurse, *Schizosaccharomyces pombe and Saccharomyces cerevisiae: a look at yeasts divided.* Cell, 1986. **45**(6): p. 781-2.
7. Guo, Z. and J.W. Stiller, *Comparative genomics of cyclin-dependent kinases suggest co-evolution of the RNAP II C-terminal domain and CTD-directed CDKs.* BMC genomics, 2004. **5**: p. 69.
8. Sherr, C.J. and J.M. Roberts, *CDK inhibitors: positive and negative regulators of G1-phase progression.* Genes & development, 1999. **13**(12): p. 1501-12.
9. Gururajan, R., et al., *Duplication of a genomic region containing the Cdc2L1-2 and MMP21-22 genes on human chromosome 1p36.3 and their linkage to D1Z2.* Genome research, 1998. **8**(9): p. 929-39.
10. Xiang, J., et al., *Molecular cloning and expression of alternatively spliced PITSLRE protein kinase isoforms.* The Journal of biological chemistry, 1994. **269**(22): p. 15786-94.
11. Gururajan, R., et al., *Isolation and characterization of two novel metalloproteinase genes linked to the Cdc2L locus on human chromosome 1p36.3.* Genomics, 1998. **52**(1): p. 101-6.
12. Puente, X.S., et al., *Comparative genomic analysis of human and chimpanzee proteases.* Genomics, 2005. **86**(6): p. 638-47.
13. Tischler, J., et al., *Combinatorial RNA interference in Caenorhabditis elegans reveals that redundancy between gene duplicates can be maintained for more than 80 million years of evolution.* Genome biology, 2006. **7**(8): p. R69.
14. Feng, Y., A.C. Goulet, and M.A. Nelson, *Identification and characterization of the human Cdc2l2 gene promoter.* Gene, 2004. **330**: p. 75-84.
15. Kahle, A., Y. Feng, and M. A. Nelson, *Isolation and characterization of the human Cdc2L1 gene promoter.* Gene, 2005. **344**: p. 53-60.
16. Feng, Y., A.-C. Goulet, and M.A. Nelson, *Identification and characterization of the human Cdc2l2 gene promoter.* Gene, 2004. **330**: p. 75-84.
17. Trembley, J.H., et al., *Cyclin dependent kinase 11 in RNA transcription and splicing.* Progress in nucleic acid research and molecular biology, 2004. **77**: p. 263-88.
18. *https://*http://www.ncbi.nlm.nih.gov/gene/984. [cited 2016.
19. Kidd, V.J., et al., *Regulated expression of a cell division control-related protein kinase during development.* Cell growth & differentiation : the

molecular biology journal of the American Association for Cancer Research, 1991. **2**(2): p. 85-93.
20. Bunnell, B.A., D.E. Adams, and V.J. Kidd, *Transient expression of a p58 protein kinase cDNA enhances mammalian glycosyltransferase activity.* Biochemical and biophysical research communications, 1990. **171**(1): p. 196-203.
21. Cornelis, S., et al., *Identification and Characterization of a Novel Cell Cycle–Regulated Internal Ribosome Entry Site.* Molecular Cell, 2000. **5**: p. 597-605.
22. Hu, D., et al., *CDK11 complexes promote pre-mRNA splicing.* The Journal of biological chemistry, 2003. **278**(10): p. 8623-9.
23. Trembley, J.H., et al., *PITSLRE p110 protein kinases associate with transcription complexes and affect their activity.* The Journal of biological chemistry, 2002. **277**(4): p. 2589-96.
24. Bunnell, B.A., et al., *Increased expression of a 58-kDa protein kinase leads to changes in the CHO cell cycle.* Proceedings of the National Academy of Sciences of the United States of America, 1990. **87**(19): p. 7467-71.
25. Petretti, C., et al., *The PITSLRE/CDK11p58 protein kinase promotes centrosome maturation and bipolar spindle formation.* EMBO reports, 2006. **7**(4): p. 418-24.
26. Beyaert, R., et al., *Cleavage of PITSLRE kinases by ICE/CASP-1 and CPP32/CASP-3 during apoptosis induced by tumor necrosis factor.* The Journal of biological chemistry, 1997. **272**(18): p. 11694-7.
27. Chen, K. and N. Rajewsky, *The evolution of gene regulation by transcription factors and microRNAs.* Nature reviews. Genetics, 2007. **8**(2): p. 93-103.
28. Saunders, A., L.J. Core, and J.T. Lis, *Breaking barriers to transcription elongation.* Nature reviews. Molecular cell biology, 2006. **7**(8): p. 557-67.
29. Bentley, D.L., *Coupling mRNA processing with transcription in time and space.* Nature reviews. Genetics, 2014. **15**(3): p. 163-75.
30. Mapendano, C.K., et al., *Crosstalk between mRNA 3' end processing and transcription initiation.* Molecular cell, 2010. **40**(3): p. 410-22.
31. Shandilya, J. and S.G. Roberts, *The transcription cycle in eukaryotes: from productive initiation to RNA polymerase II recycling.* Biochimica et biophysica acta, 2012. **1819**(5): p. 391-400.
32. Bose, T. and J.L. Gerton, *Cohesinopathies, gene expression, and chromatin organization.* The Journal of cell biology, 2010. **189**(2): p. 201-10.
33. Murakami, K., et al., *Architecture of an RNA polymerase II transcription pre-initiation complex.* Science, 2013. **342**(6159): p. 1238724.
34. Hsin, J.P. and J.L. Manley, *The RNA polymerase II CTD coordinates transcription and RNA processing.* Genes & development, 2012. **26**(19): p. 2119-37.
35. Li, B., et al., *Analyses of promoter-proximal pausing by RNA polymerase II on the hsp70 heat shock gene promoter in a Drosophila nuclear extract.* Molecular and cellular biology, 1996. **16**(10): p. 5433-43.
36. Fay, A., et al., *Cohesin selectively binds and regulates genes with paused RNA polymerase.* Current biology : CB, 2011. **21**(19): p. 1624-34.
37. de la Mata, M., et al., *A slow RNA polymerase II affects alternative splicing in vivo.* Molecular cell, 2003. **12**(2): p. 525-32.

38. Matera, A.G. and Z. Wang, *A day in the life of the spliceosome.* Nature reviews. Molecular cell biology, 2014. **15**(2): p. 108-21.
39. Will, C.L. and R. Luhrmann, *Spliceosome structure and function.* Cold Spring Harbor perspectives in biology, 2011. **3**(7).
40. Shepard, P.J. and K.J. Hertel, *The SR protein family.* Genome biology, 2009. **10**(10): p. 242.
41. Loyer, P., et al., *The RNP protein, RNPS1, associates with specific isoforms of the p34cdc2-related PITSLRE protein kinase in vivo.* Journal of cell science, 1998. **111 (Pt 11)**: p. 1495-506.
42. Fu, X.D., *The superfamily of arginine/serine-rich splicing factors.* RNA, 1995. **1**(7): p. 663-80.
43. Conaway, J.W., et al., *Control of elongation by RNA polymerase II.* Trends in biochemical sciences, 2000. **25**(8): p. 375-80.
44. Dickinson, L.A., et al., *Cyclin L is an RS domain protein involved in pre-mRNA splicing.* The Journal of biological chemistry, 2002. **277**(28): p. 25465-73.
45. Trembley, J.H., et al., *Casein kinase 2 interacts with cyclin-dependent kinase 11 (CDK11) in vivo and phosphorylates both the RNA polymerase II carboxyl-terminal domain and CDK11 in vitro.* The Journal of biological chemistry, 2003. **278**(4): p. 2265-70.
46. Sachs, N.A. and R.R. Vaillancourt, *Cyclin-dependent kinase 11p110 activity in the absence of CK2.* Biochimica et Biophysica Acta (BBA) - General Subjects, 2003. **1624**(1-3): p. 98-108.
47. Malek, S.N. and S. Desiderio, *A cyclin-dependent kinase homologue, p130PITSLRE is a phosphotyrosine-independent SH2 ligand.* The Journal of biological chemistry, 1994. **269**(52): p. 33009-20.
48. Swartz, J.E., et al., *The shuttling SR protein 9G8 plays a role in translation of unspliced mRNA containing a constitutive transport element.* The Journal of biological chemistry, 2007. **282**(27): p. 19844-53.
49. Valente, S.T., et al., *HIV-1 mRNA 3' end processing is distinctively regulated by eIF3f, CDK11, and splice factor 9G8.* Molecular cell, 2009. **36**(2): p. 279-89.
50. Shi, J., et al., *The p34cdc2-related cyclin-dependent kinase 11 interacts with the p47 subunit of eukaryotic initiation factor 3 during apoptosis.* The Journal of biological chemistry, 2003. **278**(7): p. 5062-71.
51. Yu, W., et al., *Cyclin T1-dependent genes in activated CD4 T and macrophage cell lines appear enriched in HIV-1 co-factors.* PloS one, 2008. **3**(9): p. e3146.
52. Berke, J.D., et al., *Dopamine and glutamate induce distinct striatal splice forms of Ania-6, an RNA polymerase II-associated cyclin.* Neuron, 2001. **32**(2): p. 277-87.
53. de Graaf, K., et al., *Characterization of cyclin L2, a novel cyclin with an arginine/serine-rich domain: phosphorylation by DYRK1A and colocalization with splicing factors.* The Journal of biological chemistry, 2004. **279**(6): p. 4612-24.
54. Yang, L., et al., *Cyclin L2, a novel RNA polymerase II-associated cyclin, is involved in pre-mRNA splicing and induces apoptosis of human hepatocellular carcinoma cells.* The Journal of biological chemistry, 2004. **279**(12): p. 11639-48.

55. Loyer, P., et al., *Characterization of cyclin L1 and L2 interactions with CDK11 and splicing factors: influence of cyclin L isoforms on splice site selection.* The Journal of biological chemistry, 2008. **283**(12): p. 7721-32.
56. Herrmann, A., et al., *Characterization of cyclin L1 as an immobile component of the splicing factor compartment.* FASEB journal : official publication of the Federation of American Societies for Experimental Biology, 2007. **21**(12): p. 3142-52.
57. Altafaj, X., et al., *Neurodevelopmental delay, motor abnormalities and cognitive deficits in transgenic mice overexpressing Dyrk1A (minibrain), a murine model of Down's syndrome.* Human molecular genetics, 2001. **10**(18): p. 1915-23.
58. Courcet, J.B., et al., *The DYRK1A gene is a cause of syndromic intellectual disability with severe microcephaly and epilepsy.* Journal of medical genetics, 2012. **49**(12): p. 731-6.
59. Loyer, P., et al., *The RNA Binding Motif Protein 15B (RBM15B/OTT3) Is a Functional Competitor of Serine-Arginine (SR) Proteins and Antagonizes the Positive Effect of the CDK11p110-Cyclin L2 Complex on Splicing.* Journal of Biological Chemistry, 2010. **286**(1): p. 147-159.
60. Choi, H.H., et al., *CHK2 kinase promotes pre-mRNA splicing via phosphorylating CDK11(p110).* Oncogene, 2014. **33**(1): p. 108-15.
61. Chi, Y., et al., *Thr-370 is responsible for CDK11(p58) autophosphorylation, dimerization, and kinase activity.* The Journal of biological chemistry, 2011. **286**(3): p. 1748-57.
62. Drogat, J., et al., *Cdk11-cyclinL controls the assembly of the RNA polymerase II mediator complex.* Cell reports, 2012. **2**(5): p. 1068-76.
63. Zong, H., et al., *Cyclin-dependent kinase 11(p58) interacts with HBO1 and enhances its histone acetyltransferase activity.* FEBS letters, 2005. **579**(17): p. 3579-88.
64. Chi, Y., et al., *CDK11p58 represses vitamin D receptor-mediated transcriptional activation through promoting its ubiquitin–proteasome degradation.* Biochemical and biophysical research communications, 2009. **386**(3): p. 493-498.
65. Wang, Y., et al., *Repression of estrogen receptor alpha by CDK11p58 through promoting its ubiquitin-proteasome degradation.* Journal of biochemistry, 2009. **145**(3): p. 331-43.
66. Zong, H., et al., *Cyclin D3/CDK11p58 complex is involved in the repression of androgen receptor.* Molecular and cellular biology, 2007. **27**(20): p. 7125-42.
67. Duijf, P.H. and R. Benezra, *The cancer biology of whole-chromosome instability.* Oncogene, 2013. **32**(40): p. 4727-36.
68. Kops, G.J., B.A. Weaver, and D.W. Cleveland, *On the road to cancer: aneuploidy and the mitotic checkpoint.* Nature reviews. Cancer, 2005. **5**(10): p. 773-85.
69. Musacchio, A. and E.D. Salmon, *The spindle-assembly checkpoint in space and time.* Nature reviews. Molecular cell biology, 2007. **8**(5): p. 379-93.
70. Mierzwa, B. and D.W. Gerlich, *Cytokinetic abscission: molecular mechanisms and temporal control.* Developmental cell, 2014. **31**(5): p. 525-38.
71. Miller, A.L. and W.M. Bement, *Regulation of cytokinesis by Rho GTPase flux.* Nature cell biology, 2009. **11**(1): p. 71-7.

72. Lahti, J.M., et al., *PITSLRE protein kinase activity is associated with apoptosis.* Molecular and cellular biology, 1995. **15**(1): p. 1-11.
73. Schepens, B., et al., *A role for hnRNP C1/C2 and Unr in internal initiation of translation during mitosis.* The EMBO journal, 2007. **26**(1): p. 158-69.
74. Tinton, S.A., et al., *Regulation of the cell-cycle-dependent internal ribosome entry site of the PITSLRE protein kinase: roles of Unr (upstream of N-ras) protein and phosphorylated translation initiation factor eIF-2alpha.* The Biochemical journal, 2005. **385**(Pt 1): p. 155-63.
75. Cornelis, S., et al., *UNR translation can be driven by an IRES element that is negatively regulated by polypyrimidine tract binding protein.* Nucleic acids research, 2005. **33**(10): p. 3095-108.
76. Ohno, S., et al., *Polypyrimidine tract-binding protein regulates the cell cycle through IRES-dependent translation of CDK11(p58) in mouse embryonic stem cells.* Cell Cycle, 2011. **10**(21): p. 3706-13.
77. Spriggs, K.A., M. Bushell, and A.E. Willis, *Translational regulation of gene expression during conditions of cell stress.* Molecular cell, 2010. **40**(2): p. 228-37.
78. Komar, A.A. and M. Hatzoglou, *Cellular IRES-mediated translation: The war of ITAFs in pathophysiological states.* Cell Cycle, 2011. **10**(2): p. 229-240.
79. Barna, M., et al., *Suppression of Myc oncogenic activity by ribosomal protein haploinsufficiency.* Nature, 2008. **456**(7224): p. 971-5.
80. Wilker, E.W., et al., *14-3-3sigma controls mitotic translation to facilitate cytokinesis.* Nature, 2007. **446**(7133): p. 329-32.
81. Li, T., et al., *Failure To Proliferate and Mitotic Arrest of CDK11p110/p58-Null Mutant Mice at the Blastocyst Stage of Embryonic Cell Development.* Molecular and cellular biology, 2004. **24**(8): p. 3188-3197.
82. Feng, Y., et al., *The cyclin-dependent kinase 11 interacts with 14-3-3 proteins.* Biochemical and biophysical research communications, 2005. **331**(4): p. 1503-9.
83. Hotchin, N.A., et al., *CDK11p58 Is Required for Centriole Duplication and Plk4 Recruitment to Mitotic Centrosomes.* PloS one, 2011. **6**(1): p. e14600.
84. Yokoyama, H., et al., *Cdk11 is a RanGTP-dependent microtubule stabilization factor that regulates spindle assembly rate.* The Journal of cell biology, 2008. **180**(5): p. 867-75.
85. Ishiguro, K. and Y. Watanabe, *Chromosome cohesion in mitosis and meiosis.* Journal of cell science, 2007. **120**(Pt 3): p. 367-9.
86. Peters, J.M., A. Tedeschi, and J. Schmitz, *The cohesin complex and its roles in chromosome biology.* Genes & development, 2008. **22**(22): p. 3089-114.
87. Hu, D., et al., *CDK11(p58) is required for the maintenance of sister chromatid cohesion.* Journal of cell science, 2007. **120**(Pt 14): p. 2424-34.
88. Rakkaa, T., et al., *CDK11(p58) kinase activity is required to protect sister chromatid cohesion at centromeres in mitosis.* Chromosome research : an international journal on the molecular, supramolecular and evolutionary aspects of chromosome biology, 2014. **22**(3): p. 267-76.
89. Kong, X., et al., *CDK11p58 phosphorylation of PAK1 Ser174 promotes DLC2 binding and roles on cell cycle progression.* Journal of biochemistry, 2009. **146**(3): p. 417-27.

90. Chen, S., et al., *The C-terminal kinase domain of the p34cdc2-related PITSLRE protein kinase (p110C) associates with p21-activated kinase 1 and inhibits its activity during anoikis.* The Journal of biological chemistry, 2003. **278**(22): p. 20029-36.
91. Zhang, S., et al., *Interaction of p58(PITSLRE), a G2/M-specific protein kinase, with cyclin D3.* The Journal of biological chemistry, 2002. **277**(38): p. 35314-22.
92. Zheng, T., et al., *CDKG1 protein kinase is essential for synapsis and male meiosis at high ambient temperature in Arabidopsis thaliana.* Proceedings of the National Academy of Sciences of the United States of America, 2014. **111**(6): p. 2182-7.
93. Biswas, U., et al., *Meiotic cohesin SMC1beta provides prophase I centromeric cohesion and is required for multiple synapsis-associated functions.* PLoS genetics, 2013. **9**(12): p. e1003985.
94. Revenkova, E. and R. Jessberger, *Shaping meiotic prophase chromosomes: cohesins and synaptonemal complex proteins.* Chromosoma, 2006. **115**(3): p. 235-40.
95. Francone, V.P. and J. Mezquita, *Diversification of CDK11 transcripts during chicken testis development and regression.* Molecular reproduction and development, 2005. **72**(3): p. 273-80.
96. Niu, Z., et al., *Protein expression pattern of CDK11(p58) during testicular development in the mouse.* Molecular and cellular biochemistry, 2005. **270**(1-2): p. 99-106.
97. Jehan, Z., et al., *Novel noncoding RNA from human Y distal heterochromatic block (Yq12) generates testis-specific chimeric CDC2L2.* Genome research, 2007. **17**(4): p. 433-40.
98. Rangarajan, R., et al., *Pbcrk-1, the Plasmodium berghei orthologue of P. falciparum cdc-2 related kinase-1 (Pfcrk-1), is essential for completion of the intraerythrocytic asexual cycle.* Experimental parasitology, 2006. **112**(3): p. 202-7.
99. Hussein, M.R., A.K. Haemel, and G.S. Wood, *Apoptosis and melanoma: molecular mechanisms.* The Journal of pathology, 2003. **199**(3): p. 275-88.
100. Lowe, S.W. and A.W. Lin, *Apoptosis in cancer.* Carcinogenesis, 2000. **21**(3): p. 485-95.
101. Tang, D., R. Gururajan, and V.J. Kidd, *Phosphorylation of PITSLRE p110 isoforms accompanies their processing by caspases during Fas-mediated cell death.* The Journal of biological chemistry, 1998. **273**(26): p. 16601-7.
102. Chun, H.S., et al., *Dopaminergic cell death induced by MPP(+), oxidant and specific neurotoxicants shares the common molecular mechanism.* Journal of neurochemistry, 2001. **76**(4): p. 1010-21.
103. Ariza, M.E., et al., *Fas-induced apoptosis in human malignant melanoma cell lines is associated with the activation of the p34(cdc2)-related PITSLRE protein kinases.* The Journal of biological chemistry, 1999. **274**(40): p. 28505-13.
104. Mikolajczyk, M. and M.A. Nelson, *Regulation of stability of cyclin-dependent kinase CDK11p110 and a caspase-processed form, CDK11p46, by Hsp90.* Journal of Biochemistry, 2004. **384**: p. 461-467.
105. Cimini, D., et al., *Merotelic kinetochore orientation occurs frequently during early mitosis in mammalian tissue cells and error correction is*

achieved by two different mechanisms. Journal of cell science, 2003. **116**(Pt 20): p. 4213-25.
106. Shi, J., J.W. Hershey, and M.A. Nelson, *Phosphorylation of the eukaryotic initiation factor 3f by cyclin-dependent kinase 11 during apoptosis.* FEBS letters, 2009. **583**(6): p. 971-7.
107. Shi, J. and M.A. Nelson, *The cyclin-dependent kinase 11 interacts with NOT2.* Biochemical and biophysical research communications, 2005. **334**(4): p. 1310-6.
108. Mikolajczyk, M., et al., *The cyclin-dependent kinase 11(p46) isoform interacts with RanBPM.* Biochemical and biophysical research communications, 2003. **310**(1): p. 14-8.
109. Denis, C.L. and J. Chen, *The CCR4-NOT complex plays diverse roles in mRNA metabolism.* Progress in nucleic acid research and molecular biology, 2003. **73**: p. 221-50.
110. Jayne, S., et al., *Involvement of the SMRT/NCoR-HDAC3 complex in transcriptional repression by the CNOT2 subunit of the human Ccr4-Not complex.* The Biochemical journal, 2006. **398**(3): p. 461-7.
111. Li, Z., et al., *Downregulation of β1,4-galactosyltransferase 1 inhibits CDK11p58-mediated apoptosis induced by cycloheximide.* Biochemical and biophysical research communications, 2005. **327**(2): p. 628-636.
112. Zhang, S.W., et al., *Effect of p58GTA on beta-1,4-galactosyltransferase 1 activity and cell-cycle in human hepatocarcinoma cells.* Molecular and cellular biochemistry, 2001. **221**(1-2): p. 161-8.
113. Feng, Y., et al., *Death-signal-induced relocalization of cyclin-dependent kinase 11 to mitochondria.* The Biochemical journal, 2005. **392**(Pt 1): p. 65-73.
114. Chen, C., et al., *Induction of apoptosis by p110C requires mitochondrial translocation of the proapoptotic BCL-2 family member BAD.* FEBS letters, 2006. **580**(3): p. 813-21.
115. Yun, X., et al., *CDK11(p58) protein kinase activity is associated with Bcl-2 down-regulation in pro-apoptosis pathway.* Molecular and cellular biochemistry, 2007. **304**(1-2): p. 213-8.
116. Liu, X., et al., *CDK11(p58) promotes rat astrocyte inflammatory response via activating p38 and JNK pathways induced by lipopolysaccharide.* Neurochemical research, 2012. **37**(3): p. 563-73.
117. Dave, B.J., et al., *Deletion of cell division cycle 2-like 1 gene locus on 1p36 in non-Hodgkin lymphoma.* Cancer genetics and cytogenetics, 1999. **108**(2): p. 120-6.
118. Kiechle, M., et al., *Genetic imbalances in precursor lesions of endometrial cancer detected by comparative genomic hybridization.* The American journal of pathology, 2000. **156**(6): p. 1827-33.
119. Lahti, J.M., et al., *Alterations in the PITSLRE protein kinase gene complex on chromosome 1p36 in childhood neuroblastoma.* Nature genetics, 1994. **7**(3): p. 370-5.
120. Nelson, M.A., et al., *Abnormalities in the p34cdc2-related PITSLRE protein kinase gene complex (CDC2L) on chromosome band 1p36 in melanoma.* Cancer genetics and cytogenetics, 1999. **108**(2): p. 91-9.
121. White, P.S., et al., *A region of consistent deletion in neuroblastoma maps within human chromosome lp36.2-36.3.* Proceedings of the National

Academy of Sciences of the United States of America, 1995. **92**: p. 5520-5524.
122. Zehnbauer, B.A., et al., *Characterization of N-myc amplification units in human neuroblastoma cells.* Molecular and cellular biology, 1988. **8**(2): p. 522-30.
123. Martinsson, T., et al., *Delimitation of a critical tumour suppressor region at distal 1p in neuroblastoma tumours.* European journal of cancer, 1997. **33**(12): p. 1997-2001.
124. Feng, Y., et al., *Analysis of mutations and identification of several polymorphisms in the putative promoter region of the P34CDC2-related CDC2L1 gene located at 1P36 in melanoma cell lines and melanoma families.* International journal of cancer. Journal international du cancer, 2002. **99**(6): p. 834-8.
125. Poetsch, M., T. Dittberner, and C. Woenckhaus, *Microsatellite analysis at 1p36.3 in malignant melanoma of the skin: fine mapping in search of a possible tumour suppressor gene region.* Melanoma research, 2003. **13**(1): p. 29-33.
126. Poetsch, M., T. Dittberner, and C. Woenckhaus, *Does the PITSLRE gene complex contribute to the pathogenesis of malignant melanoma of the skin? A study of patient-derived tumor samples?* Cancer genetics and cytogenetics, 2001. **128**(2): p. 181-2.
127. Chandramouli, A., et al., *Haploinsufficiency of the cdc2l gene contributes to skin cancer development in mice.* Carcinogenesis, 2007. **28**(9): p. 2028-35.
128. Naik, S., et al., *Vascular Endothelial Growth Factor Receptor-1 Is Synthetic Lethal to Aberrant {beta}-Catenin Activation in Colon Cancer.* Clinical cancer research : an official journal of the American Association for Cancer Research, 2009. **15**(24): p. 7529-7537.
129. Polakis, P., *Wnt signaling and cancer.* Genes & development, 2000. **14**(15): p. 1837-51.
130. Tiedemann, R.E., et al., *Identification of molecular vulnerabilities in human multiple myeloma cells by RNA interference lethality screening of the druggable genome.* Cancer research, 2012. **72**(3): p. 757-68.
131. Tiedemann, R.E., et al., *Kinome-wide RNAi studies in human multiple myeloma identify vulnerable kinase targets, including a lymphoid-restricted kinase, GRK6.* Blood, 2010. **115**(8): p. 1594-604.
132. Duan, Z., et al., *Systematic Kinome shRNA Screening Identifies CDK11 (PITSLRE) Kinase Expression Is Critical for Osteosarcoma Cell Growth and Proliferation.* Clinical cancer research : an official journal of the American Association for Cancer Research, 2012.
133. Bajic, V.P., et al., *Mislocalization of CDK11/PITSLRE, a regulator of the G2/M phase of the cell cycle, in Alzheimer disease.* Cellular & molecular biology letters, 2011. **16**(3): p. 359-72.
134. Li, Y., et al., *Genetic variations of the CDC2L2 gene are associated with type 2 diabetes in a Han Chinese cohort.* Diabetes/metabolism research and reviews, 2007. **23**(6): p. 455-61.
135. Zhang, G., et al., *Analyses of CDC2L1 gene mutations in keloid tissue.* Clinical and experimental dermatology, 2012. **37**(3): p. 277-83.
136. Liu, X., et al., *LPS-stimulating astrocyte-conditioned medium causes neuronal apoptosis via increasing CDK11(p58) expression in PC12 cells*

through downregulating AKT pathway. Cellular and molecular neurobiology, 2013. **33**(6): p. 779-87.
137. Shapira, S.K., et al., *Chromosome 1p36 deletions: the clinical phenotype and molecular characterization of a common newly delineated syndrome.* American journal of human genetics, 1997. **61**(3): p. 642-50.
138. Rosenfeld, J.A., et al., *Refinement of causative genes in monosomy 1p36 through clinical and molecular cytogenetic characterization of small interstitial deletions.* American journal of medical genetics. Part A, 2010. **152A**(8): p. 1951-9.
139. Luciano, M., et al., *A genome-wide association study for reading and language abilities in two population cohorts.* Genes, brain, and behavior, 2013. **12**(6): p. 645-52.
140. Evangelista, M., et al., *Kinome siRNA screen identifies regulators of ciliogenesis and hedgehog signal transduction.* Science signaling, 2008. **1**(39): p. ra7.
141. Nybakken, K., et al., *A genome-wide RNA interference screen in Drosophila melanogaster cells for new components of the Hh signaling pathway.* Nature genetics, 2005. **37**(12): p. 1323-32.
142. Robbins, D.J., D.L. Fei, and N.A. Riobo, *The Hedgehog signal transduction network.* Science signaling, 2012. **5**(246): p. re6.
143. Cheng, S.Y. and J.M. Bishop, *Suppressor of Fused represses Gli-mediated transcription by recruiting the SAP18-mSin3 corepressor complex.* Proceedings of the National Academy of Sciences of the United States of America, 2002. **99**(8): p. 5442-7.
144. Gregory, S.L., et al., *A Drosophila overexpression screen for modifiers of Rho signalling in cytokinesis.* Fly, 2007. **1**(1): p. 13-22.
145. Duan, Y., et al., *Cyclin D3/CDK11(p58) complex involved in Schwann cells proliferation repression caused by lipopolysaccharide.* Inflammation, 2010. **33**(3): p. 189-99.
146. Liu, X., et al., *The Functional Interaction Between CDK11p58 and β-1,4-Galactosyltransferase I Involved in Astrocyte Activation Caused by Lipopolysaccharide.* Inflammation, 2012. **35**(4): p. 1365-1377.
147. Liu, X., et al., *CDK11p58 Promotes Rat Astrocyte Inflammatory Response via Activating p38 and JNK Pathways Induced by Lipopolysaccharide.* Neurochemical research, 2011. **37**(3): p. 563-573.
148. Ji, Y., et al., *Increased expression of CDK11p58 and cyclin D3 following spinal cord injury in rats.* Molecular and cellular biochemistry, 2008. **309**(1-2): p. 49-60.
149. Wilkinson, S., et al., *The cyclin-dependent kinase PITSLRE/CDK11 is required for successful autophagy.* Autophagy, 2011. **7**(11): p. 1295-301.
150. Mizushima, N., *Autophagy: process and function.* Genes & development, 2007. **21**(22): p. 2861-73.
151. Chen, N. and V. Karantza-Wadsworth, *Role and regulation of autophagy in cancer.* Biochimica et biophysica acta, 2009. **1793**(9): p. 1516-23.
152. Wilkinson, S. and K.M. Ryan, *Autophagy: an adaptable modifier of tumourigenesis.* Current opinion in genetics & development, 2010. **20**(1): p. 57-64.
153. Mizushima, N., et al., *Autophagy fights disease through cellular self-digestion.* Nature, 2008. **451**(7182): p. 1069-75.

154. Hoyer-Hansen, M. and M. Jaattela, *Autophagy: an emerging target for cancer therapy.* Autophagy, 2008. **4**(5): p. 574-80.
155. Mathew, R., et al., *Autophagy suppresses tumor progression by limiting chromosomal instability.* Genes & development, 2007. **21**(11): p. 1367-81.
156. Aita, V.M., et al., *Cloning and genomic organization of beclin 1, a candidate tumor suppressor gene on chromosome 17q21.* Genomics, 1999. **59**(1): p. 59-65.
157. Liang, X.H., et al., *Induction of autophagy and inhibition of tumorigenesis by beclin 1.* Nature, 1999. **402**: p. 672-676.
158. Kabeya, Y., et al., *LC3, a mammalian homologue of yeast Apg8p, is localised in autophagasome membranes after processing.* The EMBO journal, 2000. **19**(21): p. 5720-5728.
159. Noda, N.N., Y. Ohsumi, and F. Inagaki, *Atg8-family interacting motif crucial for selective autophagy.* FEBS letters, 2010. **584**(7): p. 1379-85.
160. Klionsky, D.J., et al., *Guidelines for the use and interpretation of assays for monitoring autophagy.* Autophagy, 2012. **8**(4): p. 445-544.
161. Kirkin, V., et al., *A role for ubiquitin in selective autophagy.* Molecular cell, 2009. **34**(3): p. 259-69.
162. Kirkin, V., et al., *A role for NBR1 in autophagosomal degradation of ubiquitinated substrates.* Molecular cell, 2009. **33**(4): p. 505-16.
163. Ichimura, Y., et al., *Structural basis for sorting mechanism of p62 in selective autophagy.* The Journal of biological chemistry, 2008. **283**(33): p. 22847-57.
164. Rajagopalan, H. and C. Lengauer, *Aneuploidy and cancer.* Nature, 2004. **432**: p. 338-341.
165. Pavelka, N., et al., *Aneuploidy confers quantitative proteome changes and phenotypic variation in budding yeast.* Nature, 2010. **468**(7321): p. 321-5.
166. Uetake, Y. and G. Sluder, *Prolonged prometaphase blocks daughter cell proliferation despite normal completion of mitosis.* Current biology : CB, 2010. **20**(18): p. 1666-71.
167. Thompson, S.L. and D.A. Compton, *Proliferation of aneuploid human cells is limited by a p53-dependent mechanism.* The Journal of cell biology, 2010. **188**(3): p. 369-81.
168. Thompson, S.L. and D.A. Compton, *Examining the link between chromosomal instability and aneuploidy in human cells.* The Journal of cell biology, 2008. **180**(4): p. 665-72.
169. Vitre, B.D. and D.W. Cleveland, *Centrosomes, chromosome instability (CIN) and aneuploidy.* Current opinion in cell biology, 2012. **24**(6): p. 809-15.
170. Williams, B.R., et al., *Aneuploidy Affects Proliferation and Spontaneous Immortalization in Mammalian Cells.* Science, 2008. **322**: p. 703-709.
171. Manchado, E. and M. Malumbres, *Targeting aneuploidy for cancer therapy.* Cell, 2011. **144**(4): p. 465-6.
172. Torres, E.M., et al., *Identification of aneuploidy-tolerating mutations.* Cell, 2010. **143**(1): p. 71-83.
173. Yue, Z., et al., *Beclin 1, an autophagy gene essential for early embryonic development, is a haploinsufficient tumor suppressor.* Proceedings of the National Academy of Sciences of the United States of America, 2003. **100**(25): p. 15077-82.

174. Young, A.R., et al., *Autophagy mediates the mitotic senescence transition.* Genes & development, 2009. **23**(7): p. 798-803.
175. Katsuragi, Y., Y. Ichimura, and M. Komatsu, *p62/SQSTM1 functions as a signaling hub and an autophagy adaptor.* The FEBS journal, 2015. **282**(24): p. 4672-8.
176. Moscat, J. and M.T. Diaz-Meco, *p62 at the crossroads of autophagy, apoptosis, and cancer.* Cell, 2009. **137**(6): p. 1001-4.
177. Mizushima, N., *Methods for monitoring autophagy.* The international journal of biochemistry & cell biology, 2004. **36**(12): p. 2491-502.
178. Eskelinen, E., et al., *Inhibition of Autophagy in Mitotic Animal Cells.* Traffic, 2002. **3**: p. 878-893.
179. Barth, S., D. Glick, and K.F. Macleod, *Autophagy: assays and artifacts.* The Journal of pathology, 2010. **221**(2): p. 117-24.
180. Mizushima, N., T. Yoshimori, and B. Levine, *Methods in mammalian autophagy research.* Cell, 2010. **140**(3): p. 313-26.
181. Kroemer, G. and B. Levine, *Autophagic cell death: the story of a misnomer.* Nature reviews. Molecular cell biology, 2008. **9**(12): p. 1004-10.
182. Levine, B. and J. Yuan, *Autophagy in cell death: an innocent convict?* The Journal of clinical investigation, 2005. **115**(10): p. 2679-88.
183. van Vugt, M.A. and R.H. Medema, *Getting in and out of mitosis with Polo-like kinase-1.* Oncogene, 2005. **24**(17): p. 2844-59.
184. Kishi, K., et al., *Functional dynamics of Polo-like kinase 1 at the centrosome.* Molecular and cellular biology, 2009. **29**(11): p. 3134-50.
185. Lee, K. and K. Rhee, *PLK1 phosphorylation of pericentrin initiates centrosome maturation at the onset of mitosis.* The Journal of cell biology, 2011. **195**(7): p. 1093-101.
186. Sumara, I., et al., *Roles of Polo-like Kinase 1 in the Assembly of Functional Mitotic Spindles.* Current Biology, 2004. **14**(19): p. 1712-1722.
187. Lenart, P., et al., *The small-molecule inhibitor BI 2536 reveals novel insights into mitotic roles of polo-like kinase 1.* Current biology : CB, 2007. **17**(4): p. 304-15.
188. Steegmaier, M., et al., *BI 2536, a potent and selective inhibitor of polo-like kinase 1, inhibits tumor growth in vivo.* Current biology : CB, 2007. **17**(4): p. 316-22.
189. Tinevez, J.Y., et al., *A quantitative method for measuring phototoxicity of a live cell imaging microscope.* Methods in enzymology, 2012. **506**: p. 291-309.
190. Durrbaum, M., et al., *Unique features of the transcriptional response to model aneuploidy in human cells.* BMC genomics, 2014. **15**: p. 139.
191. Stingele, S., et al., *Global analysis of genome, transcriptome and proteome reveals the response to aneuploidy in human cells.* Molecular systems biology, 2012. **8**: p. 608.
192. Tang, Y.-C., et al., *Identification of Aneuploidy-Selective Antiproliferation Compounds.* Cell, 2011. **144**(4): p. 499-512.
193. Vitale, I., et al., *Multipolar mitosis of tetraploid cells: inhibition by p53 and dependency on Mos.* The EMBO journal, 2010. **29**(7): p. 1272-84.
194. Thompson, S.L. and D.A. Compton, *Chromosome missegregation in human cells arises through specific types of kinetochore-microtubule attachment errors.* Proceedings of the National Academy of Sciences of the United States of America, 2011. **108**(44): p. 17974-8.

195. Maliga, Z., T.M. Kapoor, and T.J. Mitchison, *Evidence that monastrol is an allosteric inhibitor of the mitotic kinesin Eg5.* Chemistry & biology, 2002. **9**(9): p. 989-96.
196. Cochran, J.C., et al., *Monastrol inhibition of the mitotic kinesin Eg5.* The Journal of biological chemistry, 2005. **280**(13): p. 12658-67.
197. King, J.S., D.M. Veltman, and R.H. Insall, *The induction of autophagy by mechanical stress.* Autophagy, 2011. **7**(12): p. 1490-9.
198. Song, Y.M., et al., *Dimethyl sulfoxide reduces hepatocellular lipid accumulation through autophagy induction.* Autophagy, 2012. **8**(7): p. 1085-97.
199. Tang, Y.C., et al., *Identification of aneuploidy-selective antiproliferation compounds.* Cell, 2011. **144**(4): p. 499-512.
200. Bunz, F., et al., *Requirement for p53 and p21 to sustain G2 arrest after DNA damage.* Science, 1998. **282**(5393): p. 1497-501.
201. Matsui, A., Y. Kamada, and A. Matsuura, *The role of autophagy in genome stability through suppression of abnormal mitosis under starvation.* PLoS genetics, 2013. **9**(1): p. e1003245.
202. Wu, W.K., et al., *The autophagic paradox in cancer therapy.* Oncogene, 2012. **31**(8): p. 939-53.
203. Bunz, F., et al., *Targeted Inactivation of p53 in Human Cells Does Not Result in Aneuploidy.* Cancer Research, 2002. **62**: p. 1129-1133.
204. Erenpreisa, J., et al., *Polyploid tumour cells elicit paradiploid progeny through depolyploidizing divisions and regulated autophagic degradation.* Cell biology international, 2011. **35**(7): p. 687-95.
205. Yang, Z.J., et al., *The role of autophagy in cancer: therapeutic implications.* Molecular cancer therapeutics, 2011. **10**(9): p. 1533-41.
206. Santaguida, S., et al., *Aneuploidy-induced cellular stresses limit autophagic degradation.* Genes & development, 2015. **29**(19): p. 2010-21.
207. Liu, D., et al., *Autophagy regulates the survival of cells with chromosomal instability.* Oncotarget, 2016. **7**(39): p. 63913-63923.
208. Tasdemir, E., et al., *Regulation of autophagy by cytoplasmic p53.* Nature cell biology, 2008. **10**(6): p. 676-87.
209. Scherz-Shouval, R., et al., *p53-dependent regulation of autophagy protein LC3 supports cancer cell survival under prolonged starvation.* Proceedings of the National Academy of Sciences of the United States of America, 2010. **107**(43): p. 18511-6.
210. Levine, B. and J. Abrams, *p53: The Janus of autophagy?* Nature cell biology, 2008. **10**(6): p. 637-9.
211. Lee, I.H., et al., *Atg7 modulates p53 activity to regulate cell cycle and survival during metabolic stress.* Science, 2012. **336**(6078): p. 225-8.
212. Rosenfeldt, M.T., et al., *p53 status determines the role of autophagy in pancreatic tumour development.* Nature, 2013. **504**(7479): p. 296-300.
213. Rancati, G., et al., *Aneuploidy underlies rapid adaptive evolution of yeast cells deprived of a conserved cytokinesis motor.* Cell, 2008. **135**(5): p. 879-93.
214. Theveneau, E. and R. Mayor, *Collective cell migration of epithelial and mesenchymal cells.* Cellular and molecular life sciences : CMLS, 2013. **70**(19): p. 3481-92.

215. Sanz-Moreno, V. and C.J. Marshall, *The plasticity of cytoskeletal dynamics underlying neoplastic cell migration.* Current opinion in cell biology, 2010. **22**(5): p. 690-6.
216. Bokel, C. and N.H. Brown, *Integrins in development: moving on, responding to, and sticking to the extracellular matrix.* Developmental cell, 2002. **3**(3): p. 311-21.
217. Vicente-Manzanares, M., C.K. Choi, and A.R. Horwitz, *Integrins in cell migration--the actin connection.* Journal of cell science, 2009. **122**(Pt 2): p. 199-206.
218. Wozniak, M.A., et al., *Focal adhesion regulation of cell behavior.* Biochimica et biophysica acta, 2004. **1692**(2-3): p. 103-19.
219. Blystone, S.D., *Integrating an integrin: a direct route to actin.* Biochimica et biophysica acta, 2004. **1692**(2-3): p. 47-54.
220. Mitra, S.K., D.A. Hanson, and D.D. Schlaepfer, *Focal adhesion kinase: in command and control of cell motility.* Nature reviews. Molecular cell biology, 2005. **6**(1): p. 56-68.
221. Tomar, A., et al., *A FAK-p120RasGAP-p190RhoGAP complex regulates polarity in migrating cells.* Journal of cell science, 2009. **122**(Pt 11): p. 1852-62.
222. Westhoff, M.A., et al., *SRC-mediated phosphorylation of focal adhesion kinase couples actin and adhesion dynamics to survival signaling.* Molecular and cellular biology, 2004. **24**(18): p. 8113-33.
223. McLean, G.W., et al., *The role of focal-adhesion kinase in cancer - a new therapeutic opportunity.* Nature reviews. Cancer, 2005. **5**(7): p. 505-15.
224. Etienne-Manneville, S., *Polarity proteins in migration and invasion.* Oncogene, 2008. **27**(55): p. 6970-80.
225. Ridley, A.J., et al., *Cell migration: integrating signals from front to back.* Science, 2003. **302**(5651): p. 1704-9.
226. Gomes, E.R., S. Jani, and G.G. Gundersen, *Nuclear movement regulated by Cdc42, MRCK, myosin, and actin flow establishes MTOC polarization in migrating cells.* Cell, 2005. **121**(3): p. 451-63.
227. Bornens, M., *The centrosome in cells and organisms.* Science, 2012. **335**(6067): p. 422-6.
228. Rios, R.M., *The centrosome-Golgi apparatus nexus.* Philosophical transactions of the Royal Society of London. Series B, Biological sciences, 2014. **369**(1650).
229. Sadok, A. and C.J. Marshall, *Rho GTPases: masters of cell migration.* Small GTPases, 2014. **5**: p. e29710.
230. Simpson, K.J., et al., *Identification of genes that regulate epithelial cell migration using an siRNA screening approach.* Nature cell biology, 2008. **10**(9): p. 1027-38.
231. Li, Z., et al., *Downregulation of beta1,4-galactosyltransferase 1 inhibits CDK11(p58)-mediated apoptosis induced by cycloheximide.* Biochemical and biophysical research communications, 2005. **327**(2): p. 628-36.
232. Jonkman, J.E., et al., *An introduction to the wound healing assay using live-cell microscopy.* Cell adhesion & migration, 2014. **8**(5): p. 440-51.
233. Hulkower, K.I. and R.L. Herber, *Cell migration and invasion assays as tools for drug discovery.* Pharmaceutics, 2011. **3**(1): p. 107-24.

234. Chi, Y., et al., *CDK11p58 inhibits ERalpha-positive breast cancer invasion by targeting integrin beta3 via the repression of ERalpha signaling.* BMC cancer, 2014. **14**: p. 577.
235. Liang, C.C., A.Y. Park, and J.L. Guan, *In vitro scratch assay: a convenient and inexpensive method for analysis of cell migration in vitro.* Nature protocols, 2007. **2**(2): p. 329-33.
236. Bijnsdorp, I.V., et al., *Increased migration by stimulation of thymidine phosphorylase in endothelial cells of different origin.* Nucleosides, nucleotides & nucleic acids, 2010. **29**(4-6): p. 482-7.
237. Petrie, R.J., A.D. Doyle, and K.M. Yamada, *Random versus directionally persistent cell migration.* Nature reviews. Molecular cell biology, 2009. **10**(8): p. 538-49.
238. Cory, G., *Scratch-wound assay.* Methods in molecular biology, 2011. **769**: p. 25-30.
239. Etienne-Manneville, S. and A. Hall, *Integrin-mediated activation of Cdc42 controls cell polarity in migrating astrocytes through PKCzeta.* Cell, 2001. **106**(4): p. 489-98.
240. Magdalena, J., et al., *Involvement of the Arp2/3 complex and Scar2 in Golgi polarity in scratch wound models.* Molecular biology of the cell, 2003. **14**(2): p. 670-84.
241. Tamura, R.E., et al., *GADD45alpha and gamma interaction with CDK11p58 regulates SPDEF protein stability and SPDEF-mediated effects on cancer cell migration.* Oncotarget, 2016. **7**(12): p. 13865-79.
242. Budayeva, H.G. and I.M. Cristea, *A mass spectrometry view of stable and transient protein interactions.* Advances in experimental medicine and biology, 2014. **806**: p. 263-82.
243. *https://*http://www.ncbi.nlm.nih.gov/gene/728642.
244. *https://*http://www.ncbi.nlm.nih.gov/gene/984.
245. Mikolajczyk, M. and M.A. Nelson, *Regulation of stability of cyclin-dependent kinase CDK11p110 and a caspase-processed form, CDK11p46, by Hsp90.* The Biochemical journal, 2004. **384**(Pt 3): p. 461-7.
246. Hao, Y., et al., *CDK11p46 and RPS8 associate with each other and suppress translation in a synergistic manner.* Biochemical and biophysical research communications, 2011. **407**(1): p. 169-74.
247. Rao, V.S., et al., *Protein-protein interaction detection: methods and analysis.* International journal of proteomics, 2014. **2014**: p. 147648.
248. Suratanee, A., et al., *Characterizing protein interactions employing a genome-wide siRNA cellular phenotyping screen.* PLoS computational biology, 2014. **10**(9): p. e1003814.
249. Steckel, M., et al., *Determination of synthetic lethal interactions in KRAS oncogene-dependent cancer cells reveals novel therapeutic targeting strategies.* Cell research, 2012. **22**(8): p. 1227-45.
250. Estojak, J., R. Brent, and E.A. Golemis, *Correlation of two-hybrid affinity data with in vitro measurements.* Molecular and cellular biology, 1995. **15**(10): p. 5820-9.
251. Vikis, H.G. and K.L. Guan, *Glutathione-S-transferase (GST)-fusion based assays for studying protein-protein interactions.* Methods in molecular biology, 2015. **1278**: p. 353-64.

252. Brymora, A., V.A. Valova, and P.J. Robinson, *Protein-protein interactions identified by pull-down experiments and mass spectrometry.* Current protocols in cell biology, 2004. **Chapter 17**: p. Unit 17 5.
253. Free, R.B., L.A. Hazelwood, and D.R. Sibley, *Identifying novel protein-protein interactions using co-immunoprecipitation and mass spectroscopy.* Current protocols in neuroscience, 2009. **Chapter 5**: p. Unit 5 28.
254. Markham, K., Y. Bai, and G. Schmitt-Ulms, *Co-immunoprecipitations revisited: an update on experimental concepts and their implementation for sensitive interactome investigations of endogenous proteins.* Analytical and bioanalytical chemistry, 2007. **389**(2): p. 461-73.
255. Ha, S.H., S.Y. Kim, and J.E. Ferrell, Jr., *The Prozone Effect Accounts for the Paradoxical Function of the Cdk-Binding Protein Suc1/Cks.* Cell reports, 2016. **14**(6): p. 1408-21.
256. Kaiser, P., et al., *Tandem affinity purification combined with mass spectrometry to identify components of protein complexes.* Methods in molecular biology, 2008. **439**: p. 309-26.
257. Berggard, T., S. Linse, and P. James, *Methods for the detection and analysis of protein-protein interactions.* Proteomics, 2007. **7**(16): p. 2833-42.
258. von Mering, C., et al., *Comparative assessment of large-scale data sets of protein-protein interactions.* Nature, 2002. **417**(6887): p. 399-403.
259. Mrowka, R., A. Patzak, and H. Herzel, *Is there a bias in proteome research?* Genome research, 2001. **11**(12): p. 1971-3.
260. Trinkle-Mulcahy, L., et al., *Identifying specific protein interaction partners using quantitative mass spectrometry and bead proteomes.* The Journal of cell biology, 2008. **183**(2): p. 223-39.
261. Mellacheruvu, D., et al., *The CRAPome: a contaminant repository for affinity purification-mass spectrometry data.* Nature methods, 2013. **10**(8): p. 730-6.
262. Han, X., A. Aslanian, and J.R. Yates, 3rd, *Mass spectrometry for proteomics.* Current opinion in chemical biology, 2008. **12**(5): p. 483-90.
263. Zhu, W., J.W. Smith, and C.M. Huang, *Mass spectrometry-based label-free quantitative proteomics.* Journal of biomedicine & biotechnology, 2010. **2010**: p. 840518.
264. Patel, V.J., et al., *A comparison of labeling and label-free mass spectrometry-based proteomics approaches.* Journal of proteome research, 2009. **8**(7): p. 3752-9.
265. Turriziani, B., et al., *On-beads digestion in conjunction with data-dependent mass spectrometry: a shortcut to quantitative and dynamic interaction proteomics.* Biology, 2014. **3**(2): p. 320-32.
266. Gingras, A.C., et al., *Analysis of protein complexes using mass spectrometry.* Nature reviews. Molecular cell biology, 2007. **8**(8): p. 645-54.
267. Deane, C.M., et al., *Protein interactions: two methods for assessment of the reliability of high throughput observations.* Molecular & cellular proteomics : MCP, 2002. **1**(5): p. 349-56.
268. Hornick, J.E., et al., *Kinesins to the core: The role of microtubule-based motor proteins in building the mitotic spindle midzone.* Seminars in cell & developmental biology, 2010. **21**(3): p. 290-9.

269. Gruneberg, U., et al., *KIF14 and citron kinase act together to promote efficient cytokinesis.* The Journal of cell biology, 2006. **172**(3): p. 363-72.
270. Carleton, M., et al., *RNA interference-mediated silencing of mitotic kinesin KIF14 disrupts cell cycle progression and induces cytokinesis failure.* Molecular and cellular biology, 2006. **26**(10): p. 3853-63.
271. Xiang, J., J.M. Lahti, and V.J. Kidd, *2-Aminopurine overrides a late telophase delay created by ectopic expression of the PITSLRE beta 1 protein kinase.* Biochemical and biophysical research communications, 1994. **199**(3): p. 1167-73.
272. Okada, M., *Regulation of the SRC family kinases by Csk.* International journal of biological sciences, 2012. **8**(10): p. 1385-97.
273. Nakayama, Y., et al., *Cytokinesis Failure Leading to Chromosome Instability in v-Src-Induced Oncogenesis.* International journal of molecular sciences, 2017. **18**(4).
274. Yeatman, T.J., *A renaissance for SRC.* Nature reviews. Cancer, 2004. **4**(6): p. 470-80.
275. Nakayama, Y., et al., *c-Src but not Fyn promotes proper spindle orientation in early prometaphase.* The Journal of biological chemistry, 2012. **287**(30): p. 24905-15.
276. Cloutier, J.F. and A. Veillette, *Association of inhibitory tyrosine protein kinase p50csk with protein tyrosine phosphatase PEP in T cells and other hemopoietic cells.* The EMBO journal, 1996. **15**(18): p. 4909-18.
277. Chu, I., et al., *p27 phosphorylation by Src regulates inhibition of cyclin E-Cdk2.* Cell, 2007. **128**(2): p. 281-94.
278. Kasahara, K., et al., *Src signaling regulates completion of abscission in cytokinesis through ERK/MAPK activation at the midbody.* The Journal of biological chemistry, 2007. **282**(8): p. 5327-39.
279. Kimple, M.E., A.L. Brill, and R.L. Pasker, *Overview of affinity tags for protein purification.* Current protocols in protein science, 2013. **73**: p. Unit 9 9.
280. Hofmann, J.C., A. Husedzinovic, and O.J. Gruss, *The function of spliceosome components in open mitosis.* Nucleus, 2010. **1**(6): p. 447-59.
281. Hofmann, J.C., et al., *The Prp19 complex directly functions in mitotic spindle assembly.* PloS one, 2013. **8**(9): p. e74851.
282. Fujiyama-Nakamura, S., et al., *Parvulin (Par14), a peptidyl-prolyl cis-trans isomerase, is a novel rRNA processing factor that evolved in the metazoan lineage.* Molecular & cellular proteomics : MCP, 2009. **8**(7): p. 1552-65.
283. Ting, L., et al., *Normalization and statistical analysis of quantitative proteomics data generated by metabolic labeling.* Molecular & cellular proteomics : MCP, 2009. **8**(10): p. 2227-42.
284. Zieve, G.W., et al., *Production of large numbers of mitotic mammalian cells by use of the reversible microtubule inhibitor nocodazole. Nocodazole accumulated mitotic cells.* Experimental cell research, 1980. **126**(2): p. 397-405.
285. Matsui, Y., et al., *Enrichment of cell populations in metaphase, anaphase, and telophase by synchronization using nocodazole and blebbistatin: a novel method suitable for examining dynamic changes in proteins during mitotic progression.* European journal of cell biology, 2012. **91**(5): p. 413-9.

286. Meek, S.E., W.S. Lane, and H. Piwnica-Worms, *Comprehensive proteomic analysis of interphase and mitotic 14-3-3-binding proteins.* The Journal of biological chemistry, 2004. **279**(31): p. 32046-54.
287. Kahle, A., Y. Feng, and A.N. M, *Isolation and characterization of the human Cdc2L1 gene promoter.* Gene, 2005. **344**: p. 53-60.
288. Liu, J. and I.D. Krantz, *Cornelia de Lange syndrome, cohesin, and beyond.* Clinical genetics, 2009. **76**(4): p. 303-14.
289. Deardorff, M.A., S.E. Noon, and I.D. Krantz, *Cornelia de Lange Syndrome*, in *GeneReviews(R)*, R.A. Pagon, et al., Editors. 1993: Seattle (WA).
290. Mannini, L., et al., *Mutation spectrum and genotype-phenotype correlation in Cornelia de Lange syndrome.* Human mutation, 2013. **34**(12): p. 1589-96.
291. Krantz, I.D., et al., *Cornelia de Lange syndrome is caused by mutations in NIPBL, the human homolog of Drosophila melanogaster Nipped-B.* Nature genetics, 2004. **36**(6): p. 631-5.
292. Gillis, L.A., et al., *NIPBL mutational analysis in 120 individuals with Cornelia de Lange syndrome and evaluation of genotype-phenotype correlations.* American journal of human genetics, 2004. **75**(4): p. 610-23.
293. Huisman, S.A., et al., *High rate of mosaicism in individuals with Cornelia de Lange syndrome.* Journal of medical genetics, 2013. **50**(5): p. 339-44.
294. Deardorff, M.A., et al., *HDAC8 mutations in Cornelia de Lange syndrome affect the cohesin acetylation cycle.* Nature, 2012. **489**(7415): p. 313-7.
295. Kaiser, F.J., et al., *Loss-of-function HDAC8 mutations cause a phenotypic spectrum of Cornelia de Lange syndrome-like features, ocular hypertelorism, large fontanelle and X-linked inheritance.* Human molecular genetics, 2014. **23**(11): p. 2888-900.
296. Singh, V.P. and J.L. Gerton, *Cohesin and human disease: lessons from mouse models.* Current opinion in cell biology, 2015. **37**: p. 9-17.
297. Kaur, M., et al., *Precocious sister chromatid separation (PSCS) in Cornelia de Lange syndrome.* American journal of medical genetics. Part A, 2005. **138**(1): p. 27-31.
298. Castronovo, P., et al., *Premature chromatid separation is not a useful diagnostic marker for Cornelia de Lange syndrome.* Chromosome research : an international journal on the molecular, supramolecular and evolutionary aspects of chromosome biology, 2009. **17**(6): p. 763-71.
299. Liu, J., et al., *Transcriptional dysregulation in NIPBL and cohesin mutant human cells.* PLoS biology, 2009. **7**(5): p. e1000119.
300. Schaaf, C.A., et al., *Genome-wide control of RNA polymerase II activity by cohesin.* PLoS genetics, 2013. **9**(3): p. e1003382.
301. Zakari, M., K. Yuen, and J.L. Gerton, *Etiology and pathogenesis of the cohesinopathies.* Wiley interdisciplinary reviews. Developmental biology, 2015. **4**(5): p. 489-504.
302. Whelan, G., et al., *Cohesin acetyltransferase Esco2 is a cell viability factor and is required for cohesion in pericentric heterochromatin.* The EMBO journal, 2012. **31**(1): p. 71-82.
303. Nolen, L.D., et al., *Regional chromatin decompaction in Cornelia de Lange syndrome associated with NIPBL disruption can be uncoupled from cohesin and CTCF.* Human molecular genetics, 2013. **22**(20): p. 4180-93.

304. Zuin, J., et al., *A cohesin-independent role for NIPBL at promoters provides insights in CdLS.* PLoS genetics, 2014. **10**(2): p. e1004153.
305. Hamilton, A., et al., *Concordance between whole-exome sequencing and clinical Sanger sequencing: implications for patient care.* Molecular genetics & genomic medicine, 2016. **4**(5): p. 504-12.
306. Anand, S., et al., *Next Generation Sequencing of Pooled Samples: Guideline for Variants' Filtering.* Scientific reports, 2016. **6**: p. 33735.
307. Schenkel, L.C., et al., *Clinical Next-Generation Sequencing Pipeline Outperforms a Combined Approach Using Sanger Sequencing and Multiplex Ligation-Dependent Probe Amplification in Targeted Gene Panel Analysis.* The Journal of molecular diagnostics : JMD, 2016. **18**(5): p. 657-67.
308. Merriman, B. and J.M. Rothberg, *Progress in ion torrent semiconductor chip based sequencing.* Electrophoresis, 2012. **33**(23): p. 3397-417.
309. Gordillo, M., H. Vega, and E.W. Jabs, *Roberts Syndrome*, in *GeneReviews(R)*, R.A. Pagon, et al., Editors. 1993: Seattle (WA).
310. Rainger, J., et al., *Miller (Genee-Wiedemann) syndrome represents a clinically and biochemically distinct subgroup of postaxial acrofacial dysostosis associated with partial deficiency of DHODH.* Human molecular genetics, 2012. **21**(18): p. 3969-83.
311. Rosado-Lugo, J.D. and M. Hampsey, *The Ssu72 phosphatase mediates the RNA polymerase II initiation-elongation transition.* The Journal of biological chemistry, 2014. **289**(49): p. 33916-26.
312. Kim, H.S., et al., *The hsSsu72 phosphatase is a cohesin-binding protein that regulates the resolution of sister chromatid arm cohesion.* The EMBO journal, 2010. **29**(20): p. 3544-57.
313. Shimada, S., et al., *Microarray analysis of 50 patients reveals the critical chromosomal regions responsible for 1p36 deletion syndrome-related complications.* Brain & development, 2015. **37**(5): p. 515-26.
314. Battaglia, A., *1p36 Deletion Syndrome*, in *GeneReviews(R)*, R.A. Pagon, et al., Editors. 1993: Seattle (WA).
315. Gervasini, C., et al., *Genomic imbalances in patients with a clinical presentation in the spectrum of Cornelia de Lange syndrome.* BMC medical genetics, 2013. **14**: p. 41.
316. Zhou, Y., et al., *The emerging roles and therapeutic potential of cyclin-dependent kinase 11 (CDK11) in human cancer.* Oncotarget, 2016. **7**(26): p. 40846-40859.
317. Zhou, Y., et al., *Cyclin-dependent kinase 11(p110) (CDK11(p110)) is crucial for human breast cancer cell proliferation and growth.* Scientific reports, 2015. **5**: p. 10433.
318. Duan, Z., et al., *Systematic kinome shRNA screening identifies CDK11 (PITSLRE) kinase expression is critical for osteosarcoma cell growth and proliferation.* Clinical cancer research : an official journal of the American Association for Cancer Research, 2012. **18**(17): p. 4580-8.
319. Alves, S., et al., *Colorectal cancer-related mutant KRAS alleles function as positive regulators of autophagy.* Oncotarget, 2015. **6**(31): p. 30787-802.
320. Quidville, V., et al., *Targeting the deregulated spliceosome core machinery in cancer cells triggers mTOR blockade and autophagy.* Cancer research, 2013. **73**(7): p. 2247-58.

321. Vitale, I., et al., *Mitotic catastrophe: a mechanism for avoiding genomic instability.* Nature reviews. Molecular cell biology, 2011. **12**(6): p. 385-92.
322. Santaguida, S. and A. Amon, *Short- and long-term effects of chromosome mis-segregation and aneuploidy.* Nature reviews. Molecular cell biology, 2015. **16**(8): p. 473-85.
323. Wang, C.Y., L.N. Liu, and Z.B. Zhao, *The role of ROS toxicity in spontaneous aneuploidy in cultured cells.* Tissue & cell, 2013. **45**(1): p. 47-53.
324. Gordon, D.J., B. Resio, and D. Pellman, *Causes and consequences of aneuploidy in cancer.* Nature reviews. Genetics, 2012. **13**(3): p. 189-203.
325. Maskey, D., et al., *ATG5 is induced by DNA-damaging agents and promotes mitotic catastrophe independent of autophagy.* Nature communications, 2013. **4**: p. 2130.
326. Tripathi, B.K. and P.S. Zelenka, *Cdk5: A regulator of epithelial cell adhesion and migration.* Cell adhesion & migration, 2010. **4**(3): p. 333-6.
327. Ghigna, C., et al., *Cell motility is controlled by SF2/ASF through alternative splicing of the Ron protooncogene.* Molecular cell, 2005. **20**(6): p. 881-90.
328. David, C.J. and J.L. Manley, *Alternative pre-mRNA splicing regulation in cancer: pathways and programs unhinged.* Genes & development, 2010. **24**(21): p. 2343-64.

Appendix

Table S1

Protein significantly enriched in GFP.CDK11p58 Nuc (Asynchronous) Co-immunoprecipitate			
Protein Name	**Gene Name**	**Fold Enrichment**	**Significance (p)**
Cyclin-dependent kinase 11B	CDK11B	9.04E+02	8.29E-06
Heat shock protein HSP 90-beta	HSP90AB1	4.79E+00	8.19E-08
Hsp90 co-chaperone Cdc37	CDC37	4.76E+01	1.77E-05
SAP30 Binding Protein	SAP30BP	4.45E+02	2.54E-04
Heat shock protein HSP 90-alpha	HSP90AA1	7.32E+00	4.16E-07
Cyclin-L1	CCNL1	9.62E+02	1.03E-06
Peptidyl-prolyl cis-trans isomerase FKBP5	FKBP5	1.88E+01	7.80E-04
Cyclin-L2	CCNL2	2.19E+02	2.78E-04
Serine/arginine repetitive matrix protein 2	SRRM2	2.29E+00	2.43E-05
Cellular nucleic acid-binding protein	CNBP	2.44E+00	1.16E-02
Pinin	PNN	1.09E+01	3.08E-02
Histone deacetylase complex subunit SAP18	SAP18	2.93E+00	1.98E-02
Mitochondrial import inner membrane translocase subunit TIM16	PAM16	3.99E+00	2.85E-06
Serine/arginine-rich splicing factor 6	SRSF6	3.21E+00	2.60E-03
CREB-binding protein	CREBBP	2.01E+00	1.81E-02
Serine/arginine-rich splicing factor 1	SRSF1	2.21E+00	6.27E-03
Translocon-associated protein subunit gamma	SSR3	2.32E+00	3.84E-05

BAG family molecular chaperone regulator 2	BAG2	2.56E+00	1.50E-03
RNA-binding protein 8A	RBM8A	4.60E+00	1.87E-02
26S proteasome non-ATPase regulatory subunit 14	PSMD14	2.07E+00	2.59E-02
RNA-binding protein with serine-rich domain 1	RNPS1	3.47E+00	3.36E-02
Transformer-2 protein homolog beta	TRA2B	3.84E+00	1.59E-02
Survival of motor neuron-related-splicing factor 30	SMNDC1	2.50E+00	1.51E-02
Zinc finger protein 638	ZNF638	2.06E+00	1.70E-03
Myosin-11	MYH11	3.43E+08	1.06E-05
1-phosphatidylinositol 4,5-bisphosphate phosphodiesterase beta-3	PLCB3	2.15E+00	3.14E-03
Myeloid leukemia factor 2	MLF2	3.67E+00	1.22E-03
Serine/arginine-rich splicing factor 10	SRSF10	2.25E+00	1.54E-02
Ras-related protein Rab-1B	RAB1B	2.70E+00	2.57E-03
Protein Name	**Gene Name**	**Fold Enrichment**	**Significance (p)**
SERPINE1 mRNA Binding Protein	SERBP1	3.13E+00	2.69E-02
Nibrin	NBN	2.03E+00	2.95E-03
Prefoldin subunit 3	VBP1	2.50E+00	4.95E-02
Serine/threonine-protein phosphatase 5	PPP5C	2.13E+00	1.11E-03
Envoplakin	EVPL	3.75E+00	4.39E-02
Protein NPAT	NPAT	5.68E+00	1.50E-02
AN1-type zinc finger protein 3	ZFAND3	2.53E+00	3.50E-02
DnaJ homolog subfamily B member 6	DNAJB6	2.26E+00	7.13E-03
Phospholipase A-2-activating protein	PLAA	2.21E+00	2.40E-02

Serine/threonine-protein kinase 38	STK38	4.47E+00	2.40E-02
Tripartite motif-containing protein 38	TRIM38	2.01E+00	3.13E-02
Caspase-3	CASP3	2.73E+00	1.98E-02
Transformer-2 protein homolog alpha	TRA2A	4.34E+00	3.83E-02
Protein YIF1A	YIF1A	3.78E+00	3.38E-03
Tubulin alpha-4A chain	TUBA4A	2.49E+00	1.61E-02
Cell division cycle protein 20 homolog	CDC20	2.12E+00	1.94E-05
Adenylate kinase isoenzyme 6	TAF9	3.54E+00	4.37E-02
Apolipoprotein D	APOD	5.03E+00	1.08E-04
DNA-binding protein inhibitor ID-1	ID1	3.25E+00	8.43E-03
Diphosphomevalonate decarboxylase	MVD	2.21E+00	6.47E-03
Inositol-tetrakisphosphate 1-kinase	ITPK1	5.50E+00	8.56E-03
Signal peptidase complex subunit 3	SPCS3	3.20E+00	7.32E-03
Transmembrane protein 11, mitochondrial	TMEM11	2.34E+00	1.55E-02
ERO1-like protein alpha	ERO1L	2.03E+00	1.04E-02
RNA polymerase II subunit A C-terminal domain phosphatase	CTDP1	2.34E+00	2.22E-02
Proteasome subunit beta type-7	PSMB7	3.07E+00	4.38E-03
Pachytene checkpoint protein 2 homolog	TRIP13	3.17E+07	1.45E-02
Peptide chain release factor 1, mitochondrial	MTRF1	1.36E+01	2.34E-02
Calcium-binding mitochondrial carrier protein SCaMC-2	SLC25A25	3.36E+00	4.07E-02
Tumor protein p53-inducible protein 11	TP53I11	2.63E+00	1.96E-03
YLP motif-containing protein 1	YLPM1	2.26E+00	1.05E-03
Inactive tyrosine-protein kinase 7	PTK7	2.13E+00	4.79E-02
Receptor expression-enhancing protein 5	REEP5	2.35E+00	2.43E-02

Aurora kinase B	AURKB	7.02E+00	8.82E-03
Cleft lip and palate transmembrane protein 1	CLPTM1	3.03E+00	2.73E-02
Amine oxidase [flavin-containing] B	MAOB	2.05E+00	1.05E-04
SEC23-interacting protein	SEC23IP	5.68E+00	1.61E-02
Protein Name	**Gene Name**	**Fold Enrichment**	**Significance (p)**
Pre-mRNA-splicing factor CWC22 homolog	CWC22	2.44E+00	4.02E-02
Syntaxin-18	STX18	2.04E+00	1.87E-02
E3 ubiquitin-protein ligase LRSAM1	LRSAM1	3.71E+00	5.08E-04
Protein FAM60A	FAM60A	3.21E+00	3.42E-03
A-kinase anchor protein 8	AKAP8	2.73E+00	2.17E-02
Forkhead box protein K2	FOXK2	6.54E+00	4.57E-02
Nitrilase homolog 1	NIT1	1.43E+01	1.45E-02
UPF0510 protein INM02	C19orf63	2.50E+00	1.04E-02
FAST kinase domain-containing protein 5	FASTKD5	5.96E+00	6.17E-04
Neurogranin;NEUG(55-78)	NRGN	6.08E+00	3.21E-04
Ferritin heavy chain;Ferritin	FTH1	2.44E+01	8.03E-05
Sperm-associated antigen 7	SPAG7	2.65E+07	1.49E-02
Melanoma-associated antigen G1	NDNL2	2.68E+00	3.23E-02
Ribonucleoprotein PTB-binding 2	RAVER2	2.21E+00	2.84E-02
AP-1 complex-associated regulatory protein	AP1AR	2.67E+00	2.42E-02
DnaJ homolog subfamily B member 14	DNAJB14	4.36E+00	9.94E-07
Serine/threonine-protein phosphatase 6 regulatory subunit 3	PPP6R3	1.01E+01	5.34E-03
NADH dehydrogenase [ubiquinone] 1	NDUFB3	2.20E+00	1.16E-03

beta subcomplex subunit 3			
Fanconi anemia group D2 protein	FANCD2	3.22E+00	2.27E-04
Mitochondrial carnitine/acylcarnitine carrier protein CACL	SLC25A29	4.49E+00	3.04E-02
Kelch-like protein 11	KLHL11	6.91E+00	4.31E-02
Histone H2B type 3-B	HIST3H2BB	3.36E+00	1.48E-03
ATP synthase subunit s-like protein	ATP5SL	3.24E+00	6.89E-03
ADP-ribose pyrophosphatase, mitochondrial	NUDT9	2.06E+00	1.50E-02
Chitobiosyldiphosphodolichol beta-mannosyltransferase	ALG1	3.85E+07	9.66E-04
Probable tRNA pseudouridine synthase 1	TRUB1	5.52E+00	2.05E-03
Nuclear pore glycoprotein p62	NUP62	6.85E+00	1.31E-02
Oxysterol-binding protein-related protein 9	OSBPL9	3.55E+00	6.97E-03
Polymerase delta-interacting protein 2	POLDIP2	2.90E+00	1.00E-02
GPN-loop GTPase 1	GPN1	2.27E+00	1.69E-04
Protein bicaudal D homolog 2	BICD2	6.94E+00	3.41E-03
Serine/threonine-protein phosphatase 6 regulatory subunit 1	PPP6R1	6.61E+00	4.47E-02
Protein Name	**Gene Name**	**Fold Enrichment**	**Significance (p)**
Spindle and kinetochore-associated protein 3	SKA3	1.55E+07	1.28E-02
Ankyrin repeat domain-containing protein 27	ANKRD27	3.47E+00	9.44E-03
52 kDa repressor of the inhibitor of the protein kinase	PRKRIR	9.32E+00	9.62E-05
Ubiquitin carboxyl-terminal hydrolase isozyme L5	UCHL5	2.23E+00	1.82E-02

Ester hydrolase C11orf54	C11orf54	1.21E+07	2.21E-02
Ankyrin repeat domain-containing protein 10	ANKRD10	1.87E+01	1.27E-02
Fanconi anemia group I protein	FANCI	2.29E+00	9.47E-03
Cell division control protein 45 homolog	CDC45	1.16E+01	1.98E-02
CTTNBP2 N-terminal-like protein	CTTNBP2NL	2.50E+00	4.08E-02
Protein-tyrosine phosphatase mitochondrial 1	PTPMT1	8.04E+00	4.93E-02
LysM and putative peptidoglycan-binding domain-containing protein 2	LYSMD2	6.75E+00	1.61E-02
Tubulin--tyrosine ligase	TTL	2.23E+00	3.97E-02
Junction Plakoglobin	JUP	5.30E+00	2.48E-02
Calmodulin-regulated spectrin-associated protein 1	CAMSAP1	2.36E+00	6.83E-03
Nucleoside diphosphate kinase 6;Nucleoside diphosphate kinase	NME6	2.37E+00	1.02E-02
Peroxisomal membrane protein PEX14	PEX14	4.26E+00	4.11E-03
Box C/D snoRNA protein 1	ZNHIT6	3.71E+00	1.07E-03
Syntaxin-17	STX17	2.18E+00	8.08E-03
Neuroblastoma-amplified sequence	NBAS	2.80E+00	4.24E-02
Nuclear pore complex protein Nup214	NUP214	2.10E+00	4.08E-02
DNA polymerase subunit gamma-1	POLG	3.74E+00	4.83E-03
Mitochondrial import inner membrane translocase subunit Tim17-A	TIMM17A	2.31E+00	1.35E-03
H(+)/Cl(-) exchange transporter 3	CLCN3	2.22E+00	3.86E-02
Sentrin-specific protease 5	SENP5	3.24E+00	1.24E-02
Required for meiotic nuclear division protein 1 homolog	RMND1	6.34E+00	1.14E-02
Protein Hook homolog 1	HOOK1	2.24E+00	5.57E-03

Serine/arginine-rich splicing factor 8	SRSF8	4.83E+00	4.44E-02
Neurotensin receptor type 1	NTSR1	2.24E+00	1.59E-03
Heat shock 70 kDa protein 12A	HSPA12A	7.04E+00	3.88E-05
Exonuclease 1	EXO1	3.94E+00	2.34E-02
Presenilin-1	PSEN1	5.39E+06	4.94E-02
Protein Name	**Gene Name**	**Fold Enrichment**	**Significance (p)**
Protein transport protein Sec61 subunit gamma	SEC61G	2.84E+00	3.26E-02
SWI/SNF-related matrix-associated actin-dependent regulator of chromatin subfamily E member 1-related	HMG20B	1.41E+01	3.70E-04
Unconventional prefoldin RPB5 interactor 1	URI1	3.51E+00	2.96E-04
Prostate tumor-overexpressed gene 1 protein	PTOV1	3.08E+00	3.65E-02
POU domain, class 2, transcription factor 1	POU2F1	4.32E+00	1.76E-02
5-3 exoribonuclease 1	XRN1	2.37E+00	3.82E-02
SH3 domain-binding protein 1	SH3BP1	5.57E+00	2.40E-03
Solute carrier family 25 member 46	SLC25A46	1.02E+01	9.53E-03
Peroxisomal acyl-coenzyme A oxidase 3	ACOX3	5.39E+00	3.26E-02
COMM domain-containing protein 6	COMMD6	5.26E+06	1.17E-03
Iron-sulfur protein NUBPL	NUBPL	2.38E+00	1.06E-02
Absent in melanoma 1 protein	AIM1	4.64E+00	2.05E-02
Zinc finger protein 8	ZNF8	1.09E+01	2.77E-06
Forkhead-associated domain-containing protein 1	FHAD1	2.00E+06	1.13E-02
Protein FAM168B	FAM168B	2.91E+07	2.47E-02

Afadin	MLLT4	3.13E+00	3.07E-02
Transmembrane protein 9	TMEM9	8.90E+00	2.42E-02
Bifunctional arginine demethylase and lysyl-hydroxylase JMJD6	JMJD6	1.09E+07	1.16E-03
Squalene monooxygenase	SQLE	3.83E+06	1.30E-02
R3H domain-containing protein 1	R3HDM1	8.25E+00	3.26E-02
Kinase D-interacting substrate of 220 kDa	KIDINS220	9.36E+06	1.36E-02
Meiosis arrest female protein 1	KIAA0430	5.40E+06	1.29E-02
Transmembrane protein 85	TMEM85	2.09E+07	1.04E-02
Dermal papilla-derived protein 6	DERP6	5.72E+06	8.42E-04
Derlin-2	DERL2	1.18E+07	8.15E-04
Zinc finger CCHC domain-containing protein 10	ZCCHC10	7.69E+00	4.89E-02

Table S2

Protein significantly enriched in GFP.CDK11p110 Nuc (Asynchronous) Co-immunoprecipitate			
Protein Name	**Gene Name**	**Fold Enrichment**	**Significance (p)**
Cyclin-dependent kinase 11B	CDK11B	1.62E+02	2.07E-04
Hsp90 co-chaperone Cdc37	CDC37	2.38E+00	4.79E-03
SAP30 Binding Protein	SAP30BP	9.39E+01	2.20E-03
Cyclin-L1	CCNL1	1.15E+02	2.22E-04
Cyclin-L2	CCNL2	7.93E+01	7.71E-03
Cellular nucleic acid-binding protein	CNBP	2.58E+00	5.64E-03
Pinin	PNN	2.15E+00	3.85E-02
Mediator of RNA polymerase II transcription subunit 23	MED23	2.17E+00	3.16E-02
Major vault protein	MVP	8.67E+00	3.93E-02
Retinoblastoma-associated protein	RB1	2.37E+00	3.78E-02
Translocon-associated protein subunit gamma	SSR3	2.49E+00	1.56E-02
Negative elongation factor E	RDBP	2.24E+00	1.31E-05
Myosin-11	MYH11	4.33E+08	1.32E-02
1-phosphatidylinositol 4,5-bisphosphate phosphodiesterase beta-3	PLCB3	2.23E+00	7.69E-03
Glycerol-3-phosphate dehydrogenase, mitochondrial	GPD2	2.34E+00	1.55E-02
Casein kinase II subunit alpha	CSNK2A1	1.06E+01	1.04E-02
Mitotic checkpoint serine/threonine-protein kinase BUB1 beta	BUB1B	2.20E+00	5.68E-03
Peptidyl-prolyl cis-trans isomerase D	PPID	2.13E+00	2.87E-02
Ras-related protein Rab-1B	RAB1B	2.99E+00	3.30E-03

SERPINE1 mRNA Binding Protein	SERBP1	2.68E+00	1.98E-02
Pumilio homolog 2	PUM2	2.90E+00	1.85E-02
Etoposide-induced protein 2.4 homolog	EI24	2.26E+00	9.82E-03
Uncharacterized protein C19orf43	C19orf43	2.03E+00	3.33E-02
Prefoldin subunit 3	VBP1	2.50E+00	1.03E-04
Pseudouridine synthase	PUS1	2.37E+00	1.56E-02
Serine/threonine-protein kinase mTOR	MTOR	2.01E+00	1.44E-04
Cleavage and polyadenylation specificity factor subunit 4	CPSF4	2.82E+00	4.81E-02
AN1-type zinc finger protein 3	ZFAND3	2.52E+00	1.74E-02
DnaJ homolog subfamily B member 6	DNAJB6	2.13E+00	2.20E-02
Phospholipase A-2-activating protein	PLAA	2.65E+00	8.21E-03
Small acidic protein	SMAP	2.14E+00	6.33E-04
Espin	ESPN	2.19E+00	1.05E-02
Protein Name	**Gene Name**	**Fold Enrichment**	**Significance (p)**
StAR-related lipid transfer protein 7, mitochondrial	STARD7	2.22E+00	2.48E-02
Mediator of RNA polymerase II transcription subunit 27	MED27	3.15E+00	8.20E-03
Tripartite motif-containing protein 38	TRIM38	2.19E+00	7.16E-03
Poly [ADP-ribose] polymerase 4	PARP4	3.17E+00	1.40E-02
Caspase-3;Caspase-3 subunit p17;Caspase-3 subunit p12	CASP3	2.79E+00	2.51E-04
Tyrosine-protein kinase Fer	FER	2.18E+00	1.06E-02
Dolichyl-phosphate beta-glucosyltransferase	ALG5	2.01E+00	3.39E-02
Cell division cycle protein 20 homolog	CDC20	2.25E+00	3.54E-03

Aurora kinase A	AURKA	2.19E+00	8.35E-04
Adenylate kinase isoenzyme 6	TAF9	3.94E+00	3.48E-02
Interferon regulatory factor 3	IRF3	8.92E+00	1.38E-02
Golgi resident protein GCP60	ACBD3	2.29E+00	2.81E-02
Exosome complex component RRP43	EXOSC8	2.42E+00	2.77E-02
DNA-binding protein inhibitor ID-1	ID1	3.27E+00	2.17E-03
Potential tRNA (adenine(58)-N(1))-methyltransferase subunit TRMT61B	TRMT61B	2.39E+00	1.61E-02
Ubiquitin-associated domain-containing protein 2	UBAC2	2.76E+00	4.04E-02
Thymopoietin	TMPO	2.03E+00	1.25E-02
Diphosphomevalonate decarboxylase	MVD	2.53E+00	1.55E-03
Lupus La protein	SSB	2.27E+00	1.84E-03
Inositol-tetrakisphosphate 1-kinase	ITPK1	5.62E+00	4.04E-02
Ubiquitin-conjugating enzyme E2 H	UBE2H	2.78E+00	3.99E-02
Tyrosine—tRNA ligase, cytoplasmic	YARS	3.28E+00	4.06E-02
Signal peptidase complex subunit 3	SPCS3	2.45E+00	1.84E-02
Transmembrane protein 11, mitochondrial	TMEM11	2.05E+00	2.33E-02
Proteasome subunit beta type-7	PSMB7	2.77E+00	2.25E-02
Type I inositol 3,4-bisphosphate 4-phosphatase	INPP4A	2.54E+00	5.38E-03
Peptide chain release factor 1, mitochondrial	MTRF1	1.00E+01	4.81E-04
Protein NDRG1	NDRG1	2.86E+00	3.33E-03
Tumor protein p53-inducible protein 11	TP53I11	2.33E+00	1.04E-02
Translation initiation factor eIF-2B subunit beta	EIF2B2	2.05E+00	4.39E-02
RNMT-activating mini protein	FAM103A1	2.06E+00	7.85E-03

Zinc finger protein 217	ZNF217	2.48E+00	1.17E-02
Protein Name	**Gene Name**	**Fold Enrichment**	**Significance (p)**
Receptor expression-enhancing protein 5	REEP5	2.55E+00	1.13E-02
Aurora kinase B	AURKB	3.75E+00	6.17E-03
FERM domain-containing protein 8	FRMD8	2.23E+00	3.83E-03
Cyclin-G-associated kinase	GAK	2.04E+00	4.75E-03
SEC23-interacting protein	SEC23IP	5.92E+00	6.56E-03
Pre-mRNA-splicing factor CWC22 homolog	CWC22	2.60E+00	1.74E-03
Receptor-interacting serine/threonine-protein kinase 2	RIPK2	2.60E+00	4.94E-03
Syntaxin-18	STX18	2.39E+00	8.93E-03
39S ribosomal protein L52, mitochondrial	MRPL52	2.28E+00	4.34E-03
Cytochrome c oxidase subunit 6B1	COX6B1	2.27E+00	3.79E-02
FAST kinase domain-containing protein 5	FASTKD5	8.15E+00	7.21E-05
ETS-related transcription factor Elf-2	ELF2	3.94E+00	2.49E-03
Bystin	BYSL	2.03E+00	1.66E-02
Selenoprotein O	SELO	3.06E+00	3.43E-02
Casein kinase II subunit alpha	CSNK2A2	1.04E+01	1.76E-02
Cyclin-T2	CCNT2	2.15E+00	4.22E-03
ZW10 interactor	ZWINT	3.72E+00	3.41E-03
Ribonucleoprotein PTB-binding 2	RAVER2	3.19E+00	1.27E-02
AP-1 complex-associated regulatory protein	AP1AR	2.39E+00	2.56E-02
DnaJ homolog subfamily B member 14	DNAJB14	5.09E+00	2.73E-02

Coatomer subunit gamma-2	COPG2	2.64E+00	7.83E-03
Adenylyltransferase and sulfurtransferase MOCS3	MOCS3	2.51E+00	3.53E-02
Ankyrin repeat and KH domain-containing protein 1	ANKHD1	2.14E+00	1.75E-03
Serine/threonine-protein phosphatase 6 regulatory subunit 3	PPP6R3	5.53E+00	3.41E-02
Protein PRR14L	PRR14L	2.02E+00	2.82E-02
DnaJ homolog subfamily C member 17	DNAJC17	3.29E+00	7.34E-03
Fanconi anemia group D2 protein	FANCD2	2.88E+00	1.67E-03
Kelch-like protein 11	KLHL11	6.53E+00	2.37E-02
ATP synthase subunit s-like protein	ATP5SL	3.41E+00	5.09E-03
ADP-ribose pyrophosphatase, mitochondrial	NUDT9	2.33E+00	1.02E-02
Decaprenyl-diphosphate synthase subunit 2	PDSS2	2.01E+07	2.42E-03
Actin-binding LIM protein 1	ABLIM1	2.24E+00	3.43E-02
Protein Name	**Gene Name**	**Fold Enrichment**	**Significance (p)**
Leucine-rich repeat-containing protein 41	LRRC41	2.17E+00	3.11E-03
Probable tRNA pseudouridine synthase 1	TRUB1	6.54E+00	1.98E-03
Nuclear pore glycoprotein p62	NUP62	7.37E+00	8.06E-03
Uncharacterized protein C18orf25	C18orf25	4.70E+00	3.54E-03
Origin recognition complex subunit 6	ORC6	2.13E+00	4.20E-03
Eyes absent homolog 3	EYA3	2.02E+00	1.73E-03
Oxysterol-binding protein;Oxysterol-binding protein-related protein 9	OSBPL9	2.97E+00	3.96E-03
Serine—tRNA ligase, mitochondrial	FBXO17	2.74E+00	1.39E-02

Protein FAM169A	FAM169A	2.33E+00	4.16E-02
Microtubule-associated protein RP/EB family member 2	MAPRE2	3.72E+00	3.99E-02
D-beta-hydroxybutyrate dehydrogenase, mitochondrial	BDH1	2.03E+00	2.64E-02
Transcription factor 12	TCF12	2.57E+00	1.44E-03
Protein bicaudal D homolog 2	BICD2	4.23E+00	1.54E-02
Serine/threonine-protein phosphatase 6 regulatory subunit 1	PPP6R1	7.19E+00	9.09E-03
Ubiquinol-cytochrome c reductase complex chaperone CBP3 homolog	UQCC	7.73E+00	1.05E-03
Lysophosphatidylcholine acyltransferase 1	LPCAT1	2.08E+00	2.41E-02
WD repeat-containing protein 70	WDR70	2.82E+00	2.65E-02
Long-chain-fatty-acid—CoA ligase 1	ACSL1	2.93E+00	8.58E-03
UPF0760 protein C2orf29	C2orf29	2.17E+00	1.17E-02
Syntaxin-4	STX4	2.32E+00	1.25E-02
Bifunctional ATP-dependent dihydroxyacetone kinase/FAD-AMP lyase	DAK	2.22E+00	1.27E-03
Mitochondrial tRNA-specific 2-thiouridylase 1	TRMU	2.13E+00	4.02E-02
Pseudouridylate synthase 7 homolog	PUS7	6.17E+00	1.79E-03
Tripartite motif-containing protein 26	TRIM26	6.16E+00	1.76E-04
Ester hydrolase C11orf54	C11orf54	1.40E+07	3.62E-03
Unconventional myosin-IXb	MYO9B	2.98E+00	4.51E-02
Fanconi anemia group I protein	FANCI	2.34E+00	6.89E-03
Cell division control protein 45 homolog	CDC45	1.06E+01	7.66E-03
Alpha-1,3/1,6-mannosyltransferase ALG2	ALG2	3.86E+00	3.62E-02

CTTNBP2 N-terminal-like protein	CTTNBP2NL	2.10E+00	2.53E-02
Protein-tyrosine phosphatase mitochondrial 1	PTPMT1	6.21E+00	4.42E-02
Protein Name	**Gene Name**	**Fold Enrichment**	**Significance (p)**
DNA primase;DNA primase small subunit	PRIM1	5.01E+00	4.58E-03
Golgin subfamily A member 4	GOLGA4	3.35E+00	4.44E-03
Probable asparagine—tRNA ligase, mitochondrial	NARS2	2.38E+00	2.38E-02
UPF0544 protein C5orf45	C5orf45	2.03E+00	2.80E-03
Tubulin-specific chaperone D	TBCD	2.12E+00	3.73E-02
Cysteine protease ATG4B	ATG4B	2.24E+00	7.56E-03
Pantothenate kinase 4	PANK4	3.02E+00	1.47E-02
Calmodulin-regulated spectrin-associated protein 1	CAMSAP1	2.41E+00	5.24E-03
Ephexin-1	NGEF	7.02E+00	3.77E-02
Nucleoside diphosphate kinase 6	NME6	2.04E+00	7.12E-03
Peroxisomal membrane protein PEX14	PEX14	3.53E+00	4.33E-02
G patch domain-containing protein 8	GPATCH8	2.27E+00	1.39E-02
Box C/D snoRNA protein 1	ZNHIT6	3.37E+00	8.13E-03
Syntaxin-17	STX17	2.64E+00	4.08E-03
Neuroblastoma-amplified sequence	NBAS	5.89E+00	3.02E-03
Solute carrier family 12 member 2	SLC12A2	4.13E+00	1.97E-04
Integrin alpha-6;Integrin alpha-6 heavy chain	ITGA6	3.65E+00	9.99E-03
6-phosphofructo-2-kinase	PFKFB4	6.51E+00	3.11E-02
E3 ubiquitin-protein ligase UBR3	UBR3	2.21E+00	3.20E-02

Fragile X mental retardation protein 1	FMR1	3.03E+00	1.30E-02
Eukaryotic translation initiation factor 2D	EIF2D	1.33E+07	4.20E-02
Eukaryotic translation initiation factor 3 subunit M	EIF3M	2.34E+00	4.81E-02
Protein NEDD1	NEDD1	2.06E+00	4.01E-02
Transmembrane protein 209	TMEM209	5.59E+00	2.26E-02
Arginine-glutamic acid dipeptide repeats protein	RERE	3.66E+07	8.35E-04
A/G-specific adenine DNA glycosylase	MUTYH	2.22E+00	6.78E-03
Neurotensin receptor type 1	NTSR1	2.44E+00	3.63E-03
Heat shock 70 kDa protein 12A	HSPA12A	5.75E+00	4.28E-02
Exonuclease 1	EXO1	6.49E+00	7.47E-04
Presenilin-1	PSEN1	9.13E+06	1.62E-03
Coiled-coil-helix-coiled-coil-helix domain-containing protein 8	CHCHD8	5.63E+00	4.43E-03
Protein Name	**Gene Name**	**Fold Enrichment**	**Significance (p)**
Enoyl-CoA delta isomerase 1, mitochondrial	ECI1	3.03E+00	4.61E-02
SWI/SNF-related matrix-associated actin-dependent regulator of chromatin	HMG20B	9.25E+00	4.00E-02
Prostate tumor-overexpressed gene 1 protein	PTOV1	4.07E+00	2.20E-02
Guanine nucleotide-binding protein G(I)/G(S)/G(O) subunit gamma-7	GNG7	5.80E+00	3.93E-03
YY1-associated factor 2	YAF2	5.29E+00	5.02E-03
POU domain, class 2, transcription factor 1	POU2F1	3.67E+00	1.12E-02
5-3 exoribonuclease 1	XRN1	2.48E+00	2.94E-02

SH3 domain-binding protein 1	SH3BP1	4.81E+00	1.45E-02
Solute carrier family 25 member 46	SLC25A46	6.53E+00	4.93E-02
MAP7 domain-containing protein 1	MAP7D1	2.40E+00	2.36E-02
Peroxisomal acyl-coenzyme A oxidase 3	ACOX3	5.48E+00	1.66E-02
Frizzled-6	FZD6	2.49E+00	3.20E-02
Protein C10	C12orf57	2.69E+00	3.26E-02
COMM domain-containing protein 6	COMMD6	7.28E+06	4.56E-03
Zinc transporter ZIP10	SLC39A10	2.01E+00	9.41E-03
Cation-independent mannose-6-phosphate receptor	IGF2R	3.33E+06	1.25E-02
Exocyst complex component 6	EXOC6	7.23E+00	3.72E-02
Transmembrane emp24 domain-containing protein 1	TMED1	3.07E+00	3.21E-02
Galectin-3-binding protein	LGALS3BP	2.73E+00	2.37E-02
Protein RUFY3	RUFY3	7.36E+06	1.09E-02
Pre-B-cell leukemia transcription factor-interacting protein 1	PBXIP1	2.21E+00	9.77E-03
UPF0554 protein C2orf43	C2orf43	3.96E+00	3.26E-02
Armadillo repeat protein deleted in velo-cardio-facial syndrome	ARVCF	3.26E+00	3.87E-02
Apolipoprotein A2	APOA2	3.81E+00	4.59E-02
Coxsackievirus and adenovirus receptor	CXADR	3.10E+00	4.94E-02
Vacuolar protein sorting-associated protein VTA1 homolog	VTA1	2.85E+00	1.37E-02
R3H domain-containing protein 1	R3HDM1	1.54E+01	9.08E-05
Gephyrin	GPHN	2.84E+00	3.85E-03
Vacuole membrane protein 1	VMP1	9.30E+06	1.78E-02
Thrombospondin-2	THBS2	1.63E+07	2.23E-02

Zinc fingers and homeoboxes protein 2	ZHX2	4.75E+00	2.94E-02
Dermal papilla-derived protein 6	DERP6	7.22E+06	3.62E-07
Protein Name	**Gene Name**	**Fold Enrichment**	**Significance (p)**
Derlin-2	DERL2	1.31E+07	1.88E-06
Zinc finger protein 292	ZNF292	8.66E+00	3.99E-02
Signal transducing adapter molecule 2	STAM2	4.56E+00	3.78E-03
Serine/threonine-protein kinase Chk2	CHEK2	6.56E+00	2.65E-04
Glutathione peroxidase 1	GPX1	2.45E+00	1.70E-02
Pyruvate carboxylase, mitochondrial	PC	2.41E+00	1.17E-02
Kinesin-like protein KIF7	KIF7	2.96E+00	3.30E-03
Transcription factor Sp6	SP6	3.09E+00	1.31E-02
Tight junction-associated protein 1	TJAP1	5.65E+00	4.88E-02
Probable alpha-ketoglutarate-dependent dioxygenase ABH5	ALKBH5	4.07E+00	3.36E-03
Fidgetin-like protein 1	FIGNL1	2.53E+06	4.99E-02
Protein phosphatase 1 reg. subunit 21	PPP1R21	5.28E+00	1.42E-02
Poly(ADP-ribose) glycohydrolase	PARG	3.06E+00	8.64E-03
Neuron navigator 1	NAV1	1.32E+01	1.72E-02
F-box only protein 30	FBXO30	3.50E+06	3.19E-03
Zinc finger CCHC domain-containing protein 10	ZCCHC10	1.27E+01	1.24E-02
WD repeat-containing protein C2orf44	C2orf44	1.57E+09	6.06E-04
Charged multivesicular body protein 5	CHMP5	3.14E+00	3.88E-02

Table S3

Protein significantly enriched in GFP.CDK11p58 Mit (Synchronised Mitosis) Co-immunoprecipitate			
Protein Name	**Gene Name**	**Fold Enrichment**	**Significance (p)**
Cyclin-dependent kinase 11B	CDK11B	1.89E+03	3.16E-04
Heat shock protein HSP 90-beta	HSP90AB1	1.87E+01	1.96E-06
Hsp90 co-chaperone Cdc37	CDC37	5.45E+01	3.76E-04
SAP30 Binding Protein	SAP30BP	3.76E+02	1.96E-03
Tubulin beta-4B chain	TUBB4B	2.65E+00	2.30E-02
Tubulin alpha-1B chain	TUBA1B	2.72E+00	4.05E-02
Heat shock cognate 71 kDa protein	HSPA8	3.25E+00	1.40E-02
Heat shock protein HSP 90-alpha	HSP90AA1	4.40E+01	1.42E-05
Cyclin-L1	CCNL1	1.78E+03	1.93E-03
78 kDa glucose-regulated protein	HSPA5	3.58E+00	2.76E-03
RuvB-like 2	RUVBL2	2.53E+00	2.50E-02
Tubulin beta chain	TUBB	3.01E+00	2.77E-02
RuvB-like 1	RUVBL1	2.90E+00	4.35E-02
Peptidyl-prolyl cis-trans isomerase FKBP5	FKBP5	1.28E+02	7.31E-03
Eukaryotic initiation factor 4A-III	EIF4A3	6.37E+00	4.58E-02
Cyclin-L2	CCNL2	9.99E+02	1.00E-02
60S ribosomal protein L38	RPL38	2.44E+00	1.61E-02
Heat shock 70 kDa protein 1A/1B	HSPA1B	4.39E+00	3.58E-02
Ribosomal Protein L10	RPL10	2.81E+00	4.11E-02
Translational activator GCN1	GCN1L1	2.08E+00	3.00E-02

Serine/arginine-rich splicing factor 3	SRSF3	3.63E+00	3.94E-02
Polyadenylate-binding protein 1	PABPC1	3.42E+00	1.97E-03
60S acidic ribosomal protein P2	RPLP2	2.65E+00	4.42E-02
Cyclin-dependent kinase 1	CDK1	2.15E+00	2.91E-02
Long-chain-fatty-acid--CoA ligase 5	ACSL5	2.21E+00	4.87E-03
Ras-related protein Rab-14	RAB14	2.64E+00	4.27E-02
Trans-2,3-enoyl-CoA reductase	TECR	5.00E+00	3.95E-02
Exportin-1	XPO1	3.61E+00	4.22E-03
Complement component 1 Q subcomponent-binding protein	C1QBP	5.37E+00	1.52E-02
DnaJ homolog subfamily A member 1	DNAJA1	3.96E+00	2.82E-02
Translocon-associated protein subunit delta	SSR4	2.23E+00	4.05E-02
60S ribosomal protein L39	RPL39	2.97E+00	2.87E-02
Ras-related protein Rab-11B	RAB11B	2.15E+00	3.85E-02
U5 small nuclear ribonucleoprotein 200 kDa helicase	SNRNP200	2.78E+00	3.66E-02
Protein Name	**Gene Name**	**Fold Enrichment**	**Significance (p)**
Mitochondrial import inner membrane translocase subunit TIM44	TIMM44	2.50E+00	4.57E-02
Heterogeneous nuclear ribonucleoprotein L	HNRNPL	4.85E+00	4.59E-02
DNA topoisomerase 1	TOP1	2.36E+00	3.37E-02
40S ribosomal protein S26	RPS26	2.94E+00	3.94E-02
Thyroid hormone receptor-associated protein 3	THRAP3	6.06E+00	4.87E-03
THO complex subunit 4	ALYREF	3.31E+00	2.73E-02
Emerin	EMD	2.45E+00	4.57E-02

26S protease regulatory subunit 10B	PSMC6	3.37E+00	3.39E-02
Perilipin-3	PLIN3	2.04E+00	4.18E-02
Bcl-2-associated transcription factor 1	BCLAF1	5.28E+00	8.15E-04
Mitochondrial import inner membrane translocase subunit TIM16	PAM16	9.99E+00	1.51E-03
26S protease regulatory subunit 6B	PSMC4	3.19E+00	4.85E-02
Putative pre-mRNA-splicing factor ATP-dependent RNA helicase DHX15	DHX15	3.51E+00	1.72E-02
Serine/arginine-rich splicing factor 6	SRSF6	4.45E+00	2.08E-02
Hemoglobin subunit alpha	HBA1	4.10E+00	1.82E-02
Nuclear pore complex protein Nup93	NUP93	2.43E+00	3.46E-02
Serine/arginine-rich splicing factor 1	SRSF1	7.07E+00	1.64E-02
Polyadenylate-binding protein 4	PABPC4	3.53E+00	1.51E-03
Heterogeneous nuclear ribonucleoproteins C1/C2	HNRNPC	4.31E+00	9.32E-03
Calnexin	CANX	2.50E+00	2.69E-02
Methionine--tRNA ligase, cytoplasmic	MARS	2.25E+00	3.09E-02
RNA-binding motif protein, X	RBMX	2.72E+00	2.72E-02
Exportin-2	CSE1L	2.10E+00	2.93E-02
Pre-mRNA-processing-splicing factor 8	PRPF8	2.72E+00	2.05E-02
Proteasome subunit beta type-2	PSMB2	2.19E+00	3.31E-02
Enhancer of rudimentary homolog	ERH	5.10E+00	2.86E-03
26S protease regulatory subunit 6A	PSMC3	2.79E+00	4.26E-02
U5 small nuclear ribonucleoprotein 40 kDa protein	SNRNP40	4.31E+00	3.02E-02
26S proteasome non-ATPase regulatory subunit 11	PSMD11	4.91E+00	3.65E-02
Aspartyl/asparaginyl beta-hydroxylase	ASPH	2.76E+00	2.96E-02

Serine/arginine-rich splicing factor 7	SRSF7	6.86E+00	1.23E-02
Cell division cycle 5-like protein	CDC5L	3.33E+00	3.07E-02
Cytoskeleton-associated protein 5	CKAP5	2.59E+00	4.23E-02
Protein Name	**Gene Name**	**Fold Enrichment**	**Significance (p)**
26S proteasome non-ATPase regulatory subunit 14	PSMD14	3.64E+00	4.72E-02
Signal recognition particle receptor subunit alpha	SRPR	2.12E+00	4.70E-03
RNA-binding protein with serine-rich domain 1	RNPS1	7.72E+00	2.26E-02
TFIIH basal transcription factor complex helicase XPD subunit	ERCC2	2.63E+00	6.39E-03
4F2 cell-surface antigen heavy chain	SLC3A2	2.91E+00	4.01E-02
Serine/arginine-rich splicing factor 4	SRSF4	3.07E+00	2.84E-02
Tyrosine-protein phosphatase non-receptor type 1	PTPN1	2.71E+00	4.15E-02
Aldehyde dehydrogenase X, mitochondrial	ALDH1B1	2.21E+00	2.52E-02
Proteasome activator complex subunit 3	PSME3	2.93E+00	4.46E-02
Pre-mRNA-processing factor 19	PRPF19	2.43E+00	2.97E-02
Uncharacterized protein C12orf50	C12orf50	5.41E+01	4.41E-02
1-acyl-sn-glycerol-3-phosphate acyltransferase epsilon	AGPAT5	3.05E+00	1.59E-02
Ubiquitin carboxyl-terminal hydrolase L5	UCHL5	2.97E+00	4.62E-02
Zinc finger protein 638	ZNF638	2.23E+00	4.82E-02

Phosphatidylserine decarboxylase proenzyme;Phosphatidylserine decarboxylase alpha chain;Phosphatidylserine decarboxylase beta chain	PISD	2.69E+00	3.60E-02
Lysine--tRNA ligase	KARS	2.19E+00	3.79E-02
RNA-binding protein 39	RBM39	2.19E+00	3.54E-02
Leucine-zipper-like transcriptional regulator 1	LZTR1	1.84E+01	2.87E-02
NADH dehydrogenase [ubiquinone] iron-sulfur protein 7, mitochondrial	NDUFS7	2.21E+00	4.88E-02
Histone acetyltransferase KAT8	KAT8	7.34E+00	1.76E-02
Casein kinase II subunit alpha	CSNK2A1	5.60E+00	2.77E-02
HIG1 domain family member 1A	HIGD1A	2.57E+00	2.42E-02
Abl interactor 2	ABI2	2.37E+01	2.15E-02
Apoptotic chromatin condensation inducer in the nucleus	ACIN1	7.65E+00	2.15E-02
Myeloid leukemia factor 2	MLF2	2.35E+00	6.76E-03
Serine/arginine-rich splicing factor 10	SRSF10	7.73E+00	1.74E-02
Protein Name	**Gene Name**	**Fold Enrichment**	**Significance (p)**
Suppressor of tumorigenicity 14 protein	ST14	2.14E+00	3.77E-02
Growth arrest and DNA damage-inducible proteins-interacting protein 1	GADD45GIP1	3.07E+00	4.15E-02
Serine/arginine-rich splicing factor 9	SRSF9	7.62E+00	1.02E-02
Prostaglandin E synthase 2	PTGES2	2.14E+00	4.24E-03
Tumour Protein D52	TPD52	2.02E+00	2.30E-03
Syntaxin-binding protein 3	STXBP3	2.33E+00	3.37E-02
Myb-binding protein 1A	MYBBP1A	2.28E+00	4.07E-02

Sodium-coupled neutral amino acid transporter 2	SLC38A2	3.04E+00	4.78E-02
Integrator complex subunit 1	INTS1	2.29E+00	3.32E-02
Origin recognition complex subunit 3	ORC3	5.16E+00	3.10E-02
Cleavage and polyadenylation specificity factor subunit 2	CPSF2	4.12E+00	4.36E-02
U1 small nuclear ribonucleoprotein 70 kDa	SNRNP70	3.62E+00	4.53E-02
Stromal interaction molecule 2	STIM2	3.32E+00	2.13E-02
Coiled-coil domain-containing protein 51	CCDC51	3.71E+00	2.66E-02
DnaJ homolog subfamily A member 2	DNAJA2	4.33E+00	2.91E-02
Uncharacterized protein C2orf47, mitochondrial	C2orf47	2.88E+00	9.16E-03
26S proteasome non-ATPase regulatory subunit 13	PSMD13	3.42E+00	2.79E-02
Matrin-3	MATR3	2.37E+00	4.99E-02
TATA-binding protein-associated factor 172	BTAF1	2.86E+00	2.37E-02
Multidrug resistance-associated protein 1	ABCC1	3.28E+00	2.96E-02
Serine/threonine-protein kinase PLK1	PLK1	2.31E+00	2.95E-02
Serine/threonine-protein phosphatase 5	PPP5C	5.39E+00	1.90E-02
60 kDa SS-A/Ro ribonucleoprotein	TROVE2	3.68E+00	2.24E-02
Zinc transporter SLC39A7	SLC39A7	1.28E+01	7.59E-03
Stromal cell-derived factor 2-like protein 1	SDF2L1	4.28E+00	4.56E-02
Ras-related protein Rab-21	RAB21	2.50E+00	2.05E-02
Proteasome activator complex subunit 1	PSME1	2.83E+00	2.18E-02

Tubulin beta-2A chain	TUBB2A	2.19E+00	3.78E-02
Ubiquilin-1	UBQLN1	2.40E+00	3.04E-04
Protein Name	**Gene Name**	**Fold Enrichment**	**Significance (p)**
Pre-mRNA-processing factor 40 homolog A	PRPF40A	4.09E+00	2.11E-02
Activating signal cointegrator 1 complex subunit 3	ASCC3	2.11E+00	4.54E-02
Calcium-transporting ATPase type 2C member 1	ATP2C1	2.06E+00	3.90E-02
Pre-mRNA-splicing factor SPF27	BCAS2	2.91E+00	2.88E-02
Reticulon-4	RTN4	3.22E+00	4.59E-04
Protein LLP homolog	LLPH	7.29E+00	1.28E-02
Mitotic spindle-associated MMXD complex subunit MIP18	FAM96B	2.28E+00	2.13E-02
Alpha-globin transcription factor CP2	TFCP2	2.92E+00	2.07E-02
Suppressor of G2 allele of SKP1 homolog	SUGT1	3.66E+00	1.87E-02
3-beta-hydroxysteroid-Delta(8),Delta(7)-isomerase	EBP	3.66E+00	2.26E-03
Heterogeneous nuclear ribonucleoprotein U-like protein 2	HNRNPUL2	5.35E+00	3.98E-02
Multiple myeloma tumor-associated protein 2	MMTAG2	2.47E+00	2.89E-02
Cleavage and polyadenylation specificity factor subunit 3	CPSF3	7.01E+00	3.94E-02
Transformer-2 protein homolog alpha	TRA2A	1.40E+01	2.13E-02
RNA-binding protein Raly	RALY	2.54E+00	1.91E-02
Programmed cell death protein 6	PDCD6	6.60E+00	3.23E-02
SRSF protein kinase 1	SRPK1	2.77E+00	4.22E-02

Importin-5	IPO5	3.28E+00	2.75E-02
Ras-related protein Rab-6A	RAB6A	4.69E+00	3.17E-02
Protein mago nashi homolog 2	MAGOHB	5.11E+01	2.25E-02
Acetolactate synthase-like protein	ILVBL	2.06E+00	3.30E-02
Lysine-specific histone demethylase 1A	KDM1A	2.31E+01	3.14E-02
LanC-like protein 2	LANCL2	9.96E+00	4.66E-02
Uridine-cytidine kinase 2	UCK2	2.26E+00	4.81E-02
ADP-ribosylation factor 5	ARF5	4.27E+00	1.22E-02
Ceroid-lipofuscinosis neuronal protein 6	CLN6	1.10E+01	9.00E-03
Microsomal glutathione S-transferase 1	MGST1	1.61E+01	1.04E-02
Splicing factor 3B subunit 4	SF3B4	4.12E+00	3.41E-02
Zinc finger and BTB domain-containing protein 7A	ZBTB7A	7.32E+00	1.96E-02
Phenylalanine--tRNA ligase, mitochondrial	FARS2	3.85E+00	4.72E-02
Protein Name	**Gene Name**	**Fold Enrichment**	**Significance (p)**
Glutaryl-CoA dehydrogenase, mitochondrial	GCDH	2.28E+00	3.88E-02
Nuclear receptor subfamily 2 group F member 6	NR2F6	3.93E+01	2.51E-02
E3 ubiquitin-protein ligase UBR4	UBR4	3.83E+00	3.33E-02
Ceramide synthase 2	CERS2	2.02E+00	1.85E-02
Mortality factor 4-like protein 1	MORF4L1	4.28E+00	4.79E-02
FAST kinase domain-containing protein 5	FASTKD5	2.89E+00	4.64E-02
Methyltransferase-like protein 7B	METTL7B	3.73E+00	2.64E-03
Ferritin heavy chain;Ferritin	FTH1	5.38E+01	2.16E-02

Thioredoxin-related transmembrane protein 2	TMX2	3.43E+00	7.04E-03
Ubiquitin-like protein 4A	UBL4A	3.16E+00	2.28E-02
N-acetyltransferase 14	NAT14	8.30E+00	1.69E-02
Guanine nucleotide-binding protein-like 3-like protein	GNL3L	2.86E+00	4.62E-02
G2/mitotic-specific cyclin-B1	CCNB1	2.86E+00	2.88E-02
Cyclin-dependent kinase 4	CDK4	7.63E+00	1.38E-02
Microtubule-associated protein RP/EB family member 2	MAPRE2	1.01E+01	2.35E-02
D-beta-hydroxybutyrate dehydrogenase, mitochondrial	BDH1	3.42E+00	1.56E-03
Serine hydroxymethyltransferase	SHMT1	1.34E+01	3.47E-02
Protein bicaudal D homolog 2	BICD2	6.52E+00	1.07E-02
Periphilin-1	PPHLN1	3.05E+00	3.47E-02
Transmembrane protein 245	TMEM245	5.64E+00	2.29E-02
Bifunctional ATP-dependent dihydroxyacetone kinase/FAD-AMP lyase	DAK	2.53E+00	2.93E-02
WD40 repeat-containing protein SMU1	SMU1	8.67E+00	3.79E-02
Translation initiation factor eIF-2B subunit delta	EIF2B4	2.53E+00	2.73E-04
Serine/threonine-protein phosphatase 4 catalytic subunit	PPP4C	3.41E+00	4.08E-02
Bcl-2-like protein 1	BCL2L1	5.20E+01	8.92E-04
Bifunctional protein NCOAT	MGEA5	5.84E+00	4.07E-02
ADP-ribosylation factor-like protein 1	ARL1	1.68E+01	2.52E-02
Ephexin-1	NGEF	6.35E+00	3.63E-02
Cirhin	CIRH1A	4.48E+00	4.15E-02
COBW domain-containing protein 6	CBWD6	2.79E+00	1.49E-02

Protein Name	Gene Name	Fold Enrichment	Significance (p)
HLA class I histocompatibility antigen, Cw-18 alpha chain	HLA-C	3.46E+07	3.30E-03
AP-2 complex subunit sigma	AP2S1	1.08E+01	3.71E-02
HLA class I histocompatibility antigen, B-37 alpha chain;HLA class I histocompatibility antigen, B-48 alpha chain	HLA-B	1.59E+01	1.79E-03
Transmembrane protein 201	TMEM201	2.30E+00	6.49E-04
Ubiquitin carboxyl-terminal hydrolase 15;Ubiquitin carboxyl-terminal hydrolase	USP15	3.24E+07	1.93E-02
Multidrug resistance-associated protein 4	ABCC4	5.31E+00	1.28E-02
TBC1 domain family member 15	TBC1D15	3.21E+00	1.74E-03
Atlastin-3	ATL3	3.98E+00	1.22E-02
Fragile X mental retardation protein 1	FMR1	2.71E+00	4.11E-02
NF-kappa-B inhibitor-interacting Ras-like protein 1	NKIRAS1	7.77E+00	3.56E-02
BCL2 Associated Transcription Factor	BCLAF1	7.26E+01	3.06E-02
Sorting nexin-4	SNX4	1.24E+07	6.27E-03
Transmembrane emp24 domain-containing protein 1	TMED1	6.64E+00	3.16E-02
Bifunctional arginine demethylase and lysyl-hydroxylase JMJD6	JMJD6	5.59E+07	6.78E-03
UPF0554 protein C2orf43	C2orf43	4.98E+00	5.04E-03
Gasdermin-D	GSDMD	4.55E+07	1.86E-02
Rho-related GTP-binding protein RhoC	RHOC	3.55E+00	2.14E-02
Paraoxinase 2	PON2	2.79E+00	1.67E-02

Importin-8	IPO8	2.65E+00	4.80E-02
Carboxypeptidase D	CPD	2.93E+00	3.07E-02
GTPase NRas	NRAS	4.80E+00	1.40E-02
Kit ligand;Soluble KIT ligand	KITLG	4.27E+00	1.67E-02
rRNA maturation factor homolog	YBEY	9.34E+00	1.60E-02
Periodic tryptophan protein 2 homolog	PWP2	3.30E+00	4.91E-02
Ribosomal RNA-processing protein 7 homolog A	RRP7A	2.97E+07	5.16E-03

Table S4

Protein significantly enriched in GFP.CDK11p110 Mit (Synchronised Mitosis) Co-immunoprecipitate			
Protein Name	Gene Name	Fold Enrichment	Significance (p)
Cyclin-dependent kinase 11B	CDK11B	2.61E+02	1.98E-05
Hsp90 co-chaperone Cdc37	CDC37	3.40E+00	6.23E-04
SAP30 Binding Protein	SAP30BP	1.34E+02	1.92E-04
Cyclin-L1	CCNL1	4.72E+02	4.07E-05
40S ribosomal protein S6	RPS6	2.16E+00	3.60E-02
Peptidyl-prolyl cis-trans isomerase FKBP5	FKBP5	2.85E+00	7.17E-03
Cyclin-L2	CCNL2	3.22E+02	2.56E-03
60S ribosomal protein L27	RPL27	2.27E+00	1.56E-02
60S ribosomal protein L35	RPL35	2.69E+00	9.76E-03
60S ribosomal protein L18	RPL18	2.15E+00	4.63E-02
60S ribosomal protein L38	RPL38	2.38E+00	1.01E-02
60S ribosomal protein L23a	RPL23A	2.16E+00	1.01E-02
60S ribosomal protein L10	RPL10	2.49E+00	8.58E-03
60S ribosomal protein L10a	RPL10A	2.90E+00	2.06E-02
Serine/arginine-rich splicing factor 3	SRSF3	2.59E+00	3.91E-02
60S ribosomal protein L31	RPL31	2.05E+00	4.12E-03
Albumin	ALB	2.13E+00	3.99E-02
60S acidic ribosomal protein P2	RPLP2	2.42E+00	1.81E-02
60S ribosomal protein L36	RPL36	2.72E+00	3.82E-02
60S ribosomal protein L32	RPL32	2.65E+00	4.37E-02

SWI/SNF-related matrix-associated actin-dependent regulator of chromatin subfamily E member 1	SMARCE1	2.89E+00	3.88E-02
Exportin-1	XPO1	2.51E+00	1.75E-02
Complement component 1 Q subcomponent-binding protein	C1QBP	4.92E+00	1.71E-02
60S ribosomal protein L22-like 1	RPL22L1	2.26E+00	3.38E-02
40S ribosomal protein S7	RPS7	4.98E+00	1.15E-02
U5 small nuclear ribonucleoprotein 200 kDa helicase	SNRNP200	2.55E+00	3.13E-02
Pinin	PNN	2.45E+00	2.08E-03
DNA topoisomerase 1	TOP1	2.87E+00	3.57E-03
Nucleolar RNA helicase 2	DDX21	2.75E+00	1.76E-02
FACT complex subunit SPT16	SUPT16H	2.86E+00	4.44E-02
40S ribosomal protein S26	RPS26	3.16E+00	2.49E-02
Thyroid hormone receptor-associated protein 3	THRAP3	2.91E+00	6.34E-03
Protein Name	**Gene Name**	**Fold Enrichment**	**Significance (p)**
THO complex subunit 4	ALYREF	2.10E+00	9.28E-03
Histone deacetylase complex subunit SAP18	SAP18	2.76E+00	3.11E-02
Bcl-2-associated transcription factor 1	BCLAF1	2.11E+00	3.30E-03
Serine/arginine-rich splicing factor 6	SRSF6	2.50E+00	2.22E-03
Major vault protein	MVP	4.68E+00	8.60E-05
Eukaryotic translation initiation factor 2 subunit 2	EIF2S2	3.53E+00	3.78E-02
Serine/arginine-rich splicing factor 1	SRSF1	4.18E+00	8.48E-03
Heterogeneous nuclear ribonucleoproteins C1/C2	HNRNPC	3.01E+00	3.92E-02

Calnexin	CANX	2.07E+00	3.98E-02
RNA-binding motif protein, X chromosome	RBMX	2.10E+00	2.71E-02
40S ribosomal protein S30	FAU	3.14E+00	1.11E-02
Pre-mRNA-processing-splicing factor 8	PRPF8	2.71E+00	2.30E-02
39S ribosomal protein L15, mitochondrial	MRPL15	2.31E+00	1.35E-02
Enhancer of rudimentary homolog	ERH	3.05E+00	1.87E-03
ATPase inhibitor, mitochondrial	ATPIF1	2.49E+00	4.52E-02
U5 small nuclear ribonucleoprotein 40 kDa protein	SNRNP40	2.92E+00	4.54E-02
Serine/arginine-rich splicing factor 7	SRSF7	4.32E+00	4.49E-02
Cell division cycle 5-like protein	CDC5L	3.49E+00	4.81E-03
RNA-binding protein 8A	RBM8A	2.74E+00	4.57E-03
Transcription factor A, mitochondrial	TFAM	2.91E+00	4.18E-02
RNA-binding protein with serine-rich domain 1	RNPS1	3.13E+00	9.87E-03
ATP-binding cassette sub-family D member 3	ABCD3	2.66E+00	1.42E-02
U4/U6.U5 tri-snRNP-associated protein 1	SART1	2.35E+00	2.79E-02
Transformer-2 protein homolog beta	TRA2B	2.97E+00	1.85E-02
General transcription factor 3C polypeptide 4	GTF3C4	2.85E+00	3.65E-02
Eukaryotic translation initiation factor 2 subunit 1	EIF2S1	2.86E+00	4.66E-02
Proteasome activator complex subunit 3	PSME3	2.00E+00	3.59E-02
Pre-mRNA-processing factor 19	PRPF19	2.24E+00	7.09E-03
Uncharacterized protein C12orf50	C12orf50	1.87E+01	4.53E-02

40S ribosomal protein S27-like	RPS27L	2.15E+00	2.52E-02
Protein Name	**Gene Name**	**Fold Enrichment**	**Significance (p)**
Cytochrome c oxidase protein 20 homolog	COX20	2.88E+00	3.51E-02
Serine/arginine-rich splicing factor 2	SRSF2	2.97E+00	4.04E-02
Ubiquitin carboxyl-terminal hydrolase isozyme L5	UCHL5	2.15E+00	3.88E-02
Nucleolar GTP-binding protein 1	GTPBP4	2.01E+00	4.17E-03
AP-3 complex subunit delta-1	AP3D1	2.75E+00	4.32E-02
Signal recognition particle 14 kDa protein	SRP14	2.61E+00	4.86E-03
BAG family molecular chaperone regulator 3	BAG3	2.06E+00	2.76E-02
Probable ATP-dependent RNA helicase DDX23	DDX23	2.58E+00	3.18E-02
Histone acetyltransferase KAT8	KAT8	4.58E+00	2.85E-03
PC4 and SFRS1-interacting protein	PSIP1	3.35E+00	4.94E-02
Casein kinase II subunit alpha	CSNK2A1	3.17E+02	4.68E-04
Apoptotic chromatin condensation inducer in the nucleus	ACIN1	2.55E+00	9.10E-04
Serine/arginine-rich splicing factor 10	SRSF10	3.55E+00	2.69E-02
Suppressor of tumorigenicity 14 protein	ST14	2.15E+00	2.25E-02
High mobility group protein HMG-I/HMG-Y	HMGA1	3.80E+00	1.87E-02
Squamous cell carcinoma antigen recognized by T-cells 3	SART3	2.25E+00	4.12E-02
Casein kinase II subunit beta	CSNK2B	5.40E+00	9.56E-03

Growth arrest and DNA damage-inducible proteins-interacting protein 1	GADD45GIP1	2.46E+00	1.91E-02
Heterochromatin protein 1-binding protein 3	HP1BP3	2.18E+00	4.92E-02
Serine/arginine-rich splicing factor 9	SRSF9	4.66E+00	1.17E-02
Cyclin-T1	CCNT1	2.07E+00	3.04E-02
Sodium-coupled neutral amino acid transporter 2	SLC38A2	2.77E+00	2.65E-02
U1 small nuclear ribonucleoprotein 70 kDa	SNRNP70	2.51E+00	3.06E-02
39S ribosomal protein L27, mitochondrial	MRPL27	2.66E+00	4.08E-02
Pleiotropic regulator 1	PLRG1	4.01E+00	2.11E-02
TATA-binding protein-associated factor 172	BTAF1	2.70E+00	3.83E-03
Multidrug resistance-associated protein 1	ABCC1	2.40E+00	4.47E-02
NADH dehydrogenase [ubiquinone] iron-sulfur protein 4, mitochondrial	NDUFS4	2.40E+00	3.61E-02
60S ribosomal protein L26-like 1	RPL26L1	2.39E+00	1.76E-02
Programmed cell death protein 2-like	PDCD2L	2.11E+00	5.92E-03
RNA-binding protein 25	RBM25	4.72E+00	7.24E-03
39S ribosomal protein L55, mitochondrial	MRPL55	2.72E+00	2.11E-03
7SK snRNA methylphosphate capping enzyme	MEPCE	3.04E+00	1.68E-02
LBH Domain containing 1	C11orf48	3.11E+00	1.58E-03
39S ribosomal protein L48, mitochondrial	MRPL48	3.11E+00	4.03E-02
Pre-mRNA-processing factor 40 homolog A	PRPF40A	4.22E+00	2.71E-03

Pre-mRNA-splicing factor SPF27	BCAS2	4.31E+00	2.53E-02
Reticulon-4	RTN4	2.25E+00	9.37E-05
Lipoamide acyltransferase component of branched-chain alpha-keto acid dehydrogenase complex, mitochondrial	DBT	4.40E+00	3.38E-02
Protein LLP homolog	LLPH	6.61E+00	1.56E-02
Protein DEK	DEK	7.92E+00	4.17E-02
Alpha-globin transcription factor CP2	TFCP2	2.85E+00	3.99E-02
Putative methyltransferase NSUN4	NSUN4	4.05E+00	2.58E-02
Vacuolar protein sorting-associated protein 28 homolog	VPS28	2.45E+00	2.27E-02
Sideroflexin-4	SFXN4	3.60E+00	2.51E-02
Suppressor of G2 allele of SKP1 homolog	SUGT1	3.40E+00	1.09E-02
ATP-dependent RNA helicase DDX18	DDX18	3.28E+00	3.50E-02
Zinc finger CCCH domain-containing protein 18	ZC3H18	3.79E+00	1.04E-05
3-beta-hydroxysteroid-Delta(8),Delta(7)-isomerase	EBP	4.56E+00	2.96E-02
Nucleolar protein 14	NOP14	2.81E+00	4.70E-02
Heterogeneous nuclear ribonucleoprotein U-like protein 2	HNRNPUL2	3.36E+00	1.84E-02
Nucleolar protein 56	NOP56	2.32E+00	2.83E-02
Transformer-2 protein homolog alpha	TRA2A	5.08E+00	1.33E-03
Basic Transcription Factor 3	BTF3	4.78E+00	4.73E-02
SRSF protein kinase 1	SRPK1	3.63E+00	2.42E-02
Importin-5	IPO5	2.45E+00	4.77E-02
Bloom syndrome protein	BLM	2.36E+00	3.50E-02

Protein Name	Gene Name	Fold Enrichment	Significance (p)
Nucleoporin NDC1	TMEM48	2.09E+00	3.94E-02
Lysine-specific histone demethylase 1A	KDM1A	1.41E+01	6.19E-03
cAMP-dependent protein kinase type II-alpha regulatory subunit	PRKAR2A	2.55E+00	4.88E-02
Thyroid Hormone Receptor Interactor 12	TRIP12	1.60E+01	4.42E-02
Pre-mRNA-splicing factor SYF2	SYF2	4.64E+00	4.86E-03
ESF1 homolog	ESF1	4.27E+00	3.44E-02
Tripeptidyl-peptidase 1	TPP1	4.93E+00	3.34E-03
Eukaryotic translation initiation factor 1A, X-chromosomal	EIF1AX	7.92E+00	3.57E-02
Protein SON	SON	2.59E+00	1.26E-03
Translation initiation factor eIF-2B subunit beta	EIF2B2	2.34E+00	3.88E-02
Coiled-coil domain-containing protein 12	CCDC12	7.23E+07	1.53E-02
Intron-binding protein aquarius	AQR	7.33E+00	9.20E-03
Zinc finger and BTB domain-containing protein 7A	ZBTB7A	8.76E+00	1.88E-02
Probable ATP-dependent RNA helicase DDX47	DDX47	3.80E+00	4.25E-02
Protein FAM92A1	FAM92A1	6.04E+00	2.33E-02
Exosome complex component RRP45	EXOSC9	2.01E+00	2.53E-02
Receptor-type tyrosine-protein phosphatase gamma	PTPRG	7.08E+00	2.88E-02
Ferritin heavy chain;Ferritin	FTH1	9.37E+00	4.63E-03
Casein kinase II subunit alpha	CSNK2A2	7.64E+01	2.46E-04

Thioredoxin-related transmembrane protein 2	TMX2	3.49E+00	2.92E-02
Zinc finger protein 691	ZNF691	2.37E+00	4.44E-02
Clathrin interactor 1	CLINT1	2.00E+00	1.44E-02
Coatomer subunit gamma-2	COPG2	4.42E+00	2.11E-02
Transcription initiation factor TFIID subunit 10	TAF10	2.60E+00	2.59E-02
mRNA turnover protein 4 homolog	MRTO4	6.67E+00	2.69E-02
Serine/threonine-protein kinase PRP4 homolog	PRPF4B	7.81E+00	3.47E-02
G2/mitotic-specific cyclin-B1	CCNB1	2.53E+00	2.12E-03
Uncharacterized protein C18orf25	C18orf25	5.42E+00	4.77E-03
ATP-dependent RNA helicase DDX50	DDX50	5.33E+00	3.94E-02
RNA methyltransferase-like protein 1	RNMTL1	5.24E+00	2.63E-02
UPF0449 protein C19orf25	C19orf25	2.29E+00	2.73E-02
Protein Name	**Gene Name**	**Fold Enrichment**	**Significance (p)**
Microtubule-associated protein RP/EB family member 2	MAPRE2	6.56E+00	3.65E-02
D-beta-hydroxybutyrate dehydrogenase, mitochondrial	BDH1	2.47E+00	1.27E-02
Zinc finger CCHC domain-containing protein 8	ZCCHC8	2.51E+00	1.79E-02
Periphilin-1	PPHLN1	2.73E+00	3.82E-02
WD40 repeat-containing protein SMU1	SMU1	5.65E+00	7.34E-03
Serine/threonine-protein phosphatase 4 catalytic subunit	PPP4C	2.75E+00	4.99E-02
EF-hand domain-containing family member A1	EFHA1	9.66E+06	3.99E-02
Ninein	NIN	5.27E+00	4.03E-02

60S acidic ribosomal protein P1	RPLP1	7.15E+00	8.87E-03
Bcl-2-like protein 1	BCL2L1	3.02E+01	1.84E-02
AP-2 complex subunit sigma	AP2S1	9.42E+00	4.74E-02
HLA class I histocompatibility antigen, B-37 alpha chain	HLA-B	1.73E+01	1.16E-02
Myelin basic protein	MBP	3.80E+00	3.03E-02
Arginine-glutamic acid dipeptide repeats protein	RERE	1.21E+08	2.41E-05
NF-kappa-B inhibitor-interacting Ras-like protein 1	NKIRAS1	5.88E+00	4.47E-02
Protein ELYS	AHCTF1	2.97E+00	3.79E-02
Unconventional prefoldin RPB5 interactor 1	URI1	3.41E+00	6.29E-03
HEAT repeat-containing protein 7A	HEATR7A	4.70E+06	4.68E-02
Sorting nexin-4	SNX4	9.50E+06	3.42E-02
Forkhead-associated domain-containing protein 1	FHAD1	4.55E+00	1.00E-02
MKI67 FHA domain-interacting nucleolar phosphoprotein	MKI67IP	8.54E+00	3.45E-02
Apolipoprotein A2	APOA2	3.19E+00	1.06E-03
Nucleolar and spindle-associated protein 1	NUSAP1	2.95E+00	6.28E-03
Lanosterol 14-alpha demethylase	CYP51A1	6.20E+06	3.61E-02
Insulin-like growth factor-binding protein 6	IGFBP6	1.21E+07	3.59E-02
Tubulin alpha-1A chain	TUBA1A	3.44E+01	4.36E-02
Zinc finger and BTB domain-containing protein 10	ZBTB10	9.76E+00	4.82E-02
Cell surface glycoprotein MUC18	MCAM	4.91E+00	1.81E-02

Protein Name	Gene Name	Fold Enrichment	Significance (p)
Arfaptin-2	ARFIP2	2.34E+00	4.34E-02
Activating signal cointegrator 1	TRIP4	6.87E+00	3.15E-02
Band 4.1-like protein 1	EPB41L1	6.69E+00	1.75E-03
WD repeat-containing protein C2orf44	C2orf44	3.53E+00	1.18E-02
Splicing factor, arginine/serine-rich 19	SCAF1	4.67E+00	2.62E-03